



Université de Liège

Faculté des Sciences Appliquées

Collège de doctorat en Électricité,
électronique et informatique

Finite-Element Modeling of Thin Wires Including Skin- and Proximity Effects

Doctoral Dissertation presented by

Jonathan VELASCO

Submitted in partial fulfillment of the requirements for the degree of
Doctor of Philosophy in Engineering Sciences

January 2022

Thesis committee:

Fabrice FREBEL (Université de Liège), President
Christophe GEUZAINÉ (Université de Liège), Supervisor
François HENROTTE (UCLouvain - Université de Liège)
André NICOLET (Aix-Marseille Université)
Ruth VAZQUEZ SABARIEGO (KU Leuven)

Author contact information:

Jonathan Velasco

ACE - Applied and Computational Electromagnetics,
Dept. of Electrical Engineering and Computer Science,
University of Liège

Montefiore Institute B28,
Quartier Polytech 1,
Allée de la Découverte 10,
4000 Liège, Belgium

Email: jonathan.velasco@uliege.be

Funding:

This work was supported in part by grant PIT7508 (ATAC-HP).

Computational resources have been provided by the Consortium des Équipements de Calcul Intensif (CÉCI), funded by the Fonds de la Recherche Scientifique de Belgique (F.R.S.-FNRS) under Grant No. 2.5020.11.

Abstract

This thesis presents an accurate and inexpensive treatment of thin conducting wires in finite element (FE) models for the magnetic vector potential magnetodynamics formulation in frequency domain. The idea of the proposed technique, called Semi-Analytical (SA) method, is three-fold. Real conductors are represented in the FE model by idealized thin wires with vanishing radius. The implied modelling error is then canceled by means of a field truncation based on the solution of a small auxiliary FE problem. Finally, analytical results are invoked to reconstruct the local field solution and to accurately evaluate the losses and impedances. The SA method is first demonstrated and then systematically compared against the results of a conventional fully discretized finite element model (FM) in case of a single conductor and of multiple parallel conductors. The method's accuracy at a broad range of frequencies is studied, particularly emphasizing the impact of spacing between conductors. Lastly, the formulation is extended to include excitation sources (e.g., voltage, current) and analytical expressions accounting for frequency-dependent effects on the inductance and resistance of multi-turn coils.



Contents

| | |
|------------------------------------------------------------------------------|-----------|
| Contents | i |
| List of Figures | v |
| List of Tables | ix |
| List of Symbols | xi |
| Introduction | 1 |
| Context and Motivations | 1 |
| State of the Art | 2 |
| Dissertation goals | 2 |
| Dissertation outline | 3 |
| Original contributions | 4 |
| Chapter 1 Magnetoquasistatics | 5 |
| 1.1 Maxwell’s Equations in Macroscopic Media | 5 |
| 1.2 Maxwell’s Model in Frequency Domain | 6 |
| 1.3 Magnetoquasistatic Approximation | 6 |
| 1.4 Constitutive Laws for the Magnetoquasistatic Approximation | 7 |
| 1.4.1 Ohm’s Law and Conductors | 8 |
| 1.4.2 Magnetization | 8 |
| 1.5 General Remarks | 9 |
| 1.6 $\mathbf{a} - v$ formulation with classical massive conductors | 10 |
| Chapter 2 Semi-Analytical Modeling of the Skin Effect in Thin Wires | 13 |
| 2.1 Biot-Savart Law: Modeling of Thin Wires | 14 |
| 2.2 The $\mathbf{a} - v$ Thin Wire Idealization | 15 |
| 2.3 Field Truncation | 17 |
| 2.4 Semi-analytical Modeling of Thin Wires | 19 |

| | | |
|-------------------------------------------------------------------------------------|------------------------------------------------------------------------------------------|-----------|
| 2.5 | Analytical Solution of a Wire in Isolation - Skin Effect | 21 |
| 2.6 | Limitation and Proximity Effect | 28 |
| 2.7 | Semi-Analytical Modeling of the Skin Effect in Thin Wires - A Summary | 30 |
| 2.8 | Numerical Tests: Three Parallel Wires | 31 |
| 2.8.1 | Local Agreement - Magnetic Vector Potential | 33 |
| 2.8.1.1 | Frequency 1Hz and conductor spacing of 8mm | 34 |
| 2.8.1.2 | Frequency 1MHz and conductor spacing of 8mm | 37 |
| 2.8.1.3 | Frequency 1Hz and conductor spacing of 2.05mm | 40 |
| 2.8.1.4 | Frequency 1MHz and conductor spacing of 2.05mm | 43 |
| 2.8.1.5 | Conclusion - Local Agreement | 46 |
| 2.8.2 | Global Agreement - Inductance Matrix | 47 |
| 2.8.2.1 | Self-Inductance | 47 |
| 2.8.2.2 | Mutual-Inductance | 55 |
| 2.8.3 | Conclusions | 62 |
| Chapter 3 Semi-Analytical Modeling of the Proximity Effect in Thin Wires | | 63 |
| 3.1 | Analytical Modelling of a Wire Subjected to an External Magnetic Field | 64 |
| 3.2 | Semi-Analytical Modeling of Thin Wires Accounting for Proximity Effects | 70 |
| 3.3 | Numerical Results | 73 |
| 3.3.1 | Frequency 1Hz and conductor spacing of 8mm | 74 |
| 3.3.2 | Frequency 1MHz and conductor spacing of 8mm | 77 |
| 3.3.3 | Frequency 1Hz and conductor spacing of 2.05mm | 80 |
| 3.3.4 | Frequency 1MHz and conductor spacing of 2.05mm | 83 |
| 3.4 | Highlights and Remarks | 86 |
| Chapter 4 Efficient Modeling of Multi-turn Coils | | 87 |
| 4.1 | Global Quantities for thin wires | 88 |
| 4.2 | Joule losses | 90 |
| 4.2.1 | Joule losses P_{skin} in the Skin effect analytical solution | 90 |
| 4.2.2 | Joule losses P_{prox} in the proximity effect analytical solution | 92 |
| 4.3 | Numerical Tests | 93 |
| 4.3.1 | 5-Turn Coil | 95 |
| 4.3.1.1 | Impedance vs. inter-turn spacing at 1Hz and 1MHz | 95 |
| 4.3.1.2 | Impedance at a broad range of frequencies at a inter-turn spacing of 8mm | 98 |
| 4.3.1.3 | Impedance at a broad range of frequencies at a inter-turn spacing of 2.05mm | 103 |
| 4.3.2 | 10-Turn Coil | 108 |
| 4.3.2.1 | Impedance vs. inter-turn spacing at 1Hz and 1MHz | 108 |
| 4.3.2.2 | Impedance at a broad range of frequencies at a inter-turn spacing of 8mm | 111 |

| | | |
|------------------------------------------|------------------------------------------------------------------------------------------|------------|
| 4.3.2.3 | Impedance at a broad range of frequencies at a inter-turn spacing of 2.05mm | 116 |
| 4.3.3 | 15-Turn Coil | 121 |
| 4.3.3.1 | Impedance vs. inter-turn spacing at 1Hz and 1MHz | 121 |
| 4.3.3.2 | Impedance at a broad range of frequencies at a inter-turn spacing of 8mm | 124 |
| 4.3.3.3 | Impedance at a broad range of frequencies at a inter-turn spacing of 2.05mm | 129 |
| 4.3.4 | Highlights and Remarks | 134 |
| Main Achievements and Conclusions | | 135 |
| | Future Work | 136 |
| Bibliography | | 137 |

List of Figures

| | | |
|------|--------------------------------------------------------------------------------------------------------------------------------------------------------------------------------------------------------------------------------------------------------------------------------------------------------------------------------------------------------------------------------------------------------------------------------------|----|
| 2.1 | Current density in Full Model (Left) and Thin Wire Approximation (Right) | 13 |
| 2.2 | Elemental magnetic induction $d\mathbf{b}$ due to current element $I d\mathbf{l}$ | 14 |
| 2.3 | Magnetic vector potential along the r-axis at 1Hz, showing the non-physical mesh-related overestimation of the peak \mathbf{a} -field due to the thin wire idealization compared to the physical solution obtained with the Full model. | 16 |
| 2.4 | Top: Mesh with explicit discretization of the real round conductor Ω_{c_i} highlighted. Bottom: Mesh around the idealized (pointwise) thin conductor Ω_{LR_i} with a fine (Left) or a coarser (Right) discretization, and with highlighted mesh dependent sleeve Ω_{SL_i} . | 17 |
| 2.5 | Domain of analysis of the initial problem (Left), and of the auxiliary problem (Right). | 18 |
| 2.6 | Solution \mathbf{a}^w of the auxiliary problem, and cut-view of truncated field $\mathbf{a}^c - \mathbf{a}^w$. | 18 |
| 2.7 | Sleeve in a Finite-Element Mesh: Structured (Left) and Unstructured (Right). | 19 |
| 2.8 | Graphical representation of the local correction of the magnetic vector potential \mathbf{a} as of (2.5), for a single round conductor of radius $R = 1\text{mm}$ and a structured sleeve of radius $r_{SL} = 3\text{mm}$. The term \mathbf{a}^c represents the solution in the whole domain, $\mathbf{a}^c - \mathbf{a}^w$ the truncation of the field solution, and \mathbf{a}_{corr} the analytical correction as of (2.6) | 20 |
| 2.9 | Comparative view of the magnetic vector potential \mathbf{a} along the r-axis for a single wire at 1Hz (Top) and 1MHz (Bottom). | 21 |
| 2.10 | Comparative view of the flux (2.7) vs frequency characteristic, computed with the thin wire approach and with the conventional FE method for a single wire. | 22 |
| 2.11 | Static (DC - Left) and Dynamic (AC - Right) Current Density Distribution. | 24 |
| 2.12 | Color map of the current density distribution within the cross section of a round wire at 1Hz: Real(Left), Imaginary(Right) | 24 |

| | | |
|------|----------------------------------------------------------------------------------------------------------------------------------------------------------------------------------------------------------------------|----|
| 2.13 | Line plot of the current density distribution within the cross section of a round wire due to skin-excitation at 1Hz and relative error: Real(Left), Imaginary(Right) | 25 |
| 2.14 | Color map of the current density distribution within the cross section of a round wire at 1MHz: Real(Left), Imaginary(Right) | 26 |
| 2.15 | Line plot of the current density distribution within the cross section of a round wire due to skin-excitation at 1MHz and relative error : Real(Left), Imaginary(Right) | 26 |
| 2.16 | Single wire in Isolation | 27 |
| 2.17 | Different components of the corrected field \mathbf{a} as of (2.5) with three wires at 1MHz (Top), and comparative view of the computed \mathbf{a} field focused on the rightmost wire (Bottom). | 29 |
| 2.18 | Three parallel wires model description with current excitation I and conductor spacing d . Top figure represents the fully discretized model and bottom model represents the analogous semi-analytical model . . | 32 |
| 2.19 | Small conductor spacing (2.05mm): Structured Sleeve 1mm (Left), Unstructured Sleeve 3mm (Right) | 33 |
| 2.20 | Real part of \mathbf{a} in three parallel wires at 1Hz with conductor spacing of 8mm: Structured Sleeves (Left) and Unstructured Sleeves (Right) . . | 35 |
| 2.21 | Imaginary part of \mathbf{a} in three parallel wires at 1Hz with conductor spacing of 8mm: Structured Sleeves (Left) and Unstructured Sleeves (Right) | 36 |
| 2.22 | Real part of \mathbf{a} in three parallel wires at 1MHz with conductor spacing of 8mm: Structured Sleeves (Left) and Unstructured Sleeves (Right) . | 38 |
| 2.23 | Imaginary part of \mathbf{a} in three parallel wires at 1Hz with conductor spacing of 8mm: Structured Sleeves (Left) and Unstructured Sleeves (Right) | 39 |
| 2.24 | Real part of \mathbf{a} in three parallel wires at 1Hz with conductor spacing of 2.05mm: Structured Sleeves (Left) and Unstructured Sleeves (Right) . | 41 |
| 2.25 | Imaginary part of \mathbf{a} in three parallel wires at 1Hz with conductor spacing of 2.05mm: Structured Sleeves (Left) and Unstructured Sleeves (Right) | 42 |
| 2.26 | Real part of \mathbf{a} in three parallel wires at 1MHz with conductor spacing of 2.05mm: Structured Sleeves (Left) and Unstructured Sleeves (Right) | 44 |
| 2.27 | Imaginary part of \mathbf{a} in three parallel wires at 1MHz with conductor spacing of 2.05mm: Structured Sleeves (Left) and Unstructured Sleeves (Right) | 45 |
| 2.28 | Self inductance with conductor spacing of 8mm using sleeve parameter of 1mm: Structured Sleeves (Left) and Unstructured Sleeves (Right) . | 49 |
| 2.29 | Self inductance with conductor spacing of 8mm using sleeve parameter of 0.5mm: Structured Sleeves (Left) and Unstructured Sleeves (Right) | 50 |
| 2.30 | Self inductance with conductor spacing of 8mm using sleeve parameter of 3mm: Structured Sleeves (Left) and Unstructured Sleeves (Right) . | 51 |
| 2.31 | Self inductance with conductor spacing of 2.05mm using sleeve parameter of 1mm: Structured Sleeves (Left) and Unstructured Sleeves (Right) | 53 |
| 2.32 | Self inductance with conductor spacing of 2.05mm using sleeve parameter of 0.5mm: Structured Sleeves (Left) and Unstructured Sleeves (Right) | 54 |

| | | |
|------|--------------------------------------------------------------------------------------------------------------------------------------------------------------------------------------------------------------|----|
| 2.33 | Self inductance with conductor spacing of 8mm using sleeve parameter of 1mm: Structured Sleeves (Left) and Unstructured Sleeves (Right) . | 56 |
| 2.34 | Self inductance with conductor spacing of 8mm using sleeve parameter of 0.5mm: Structured Sleeves (Left) and Unstructured Sleeves (Right) | 57 |
| 2.35 | Self inductance with conductor spacing of 8mm using sleeve parameter of 3mm: Structured Sleeves (Left) and Unstructured Sleeves (Right) . | 58 |
| 2.36 | Self inductance with conductor spacing of 2.05mm using sleeve parameter of 1mm: Structured Sleeves (Left) and Unstructured Sleeves (Right) | 60 |
| 2.37 | Self inductance with conductor spacing of 2.05mm using sleeve parameter of 0.5mm: Structured Sleeves (Left) and Unstructured Sleeves (Right) | 61 |
| 3.1 | Proximity excitation. | 63 |
| 3.2 | Current density distribution due to proximity-effect excitation: Real(Left), Imaginary(Right) at 1Hz | 67 |
| 3.3 | Current Density Distribution within the Cross Section of a Round Wire due to proximity-excitation at 1Hz | 68 |
| 3.4 | Current density distribution due to proximity-effect excitation: Real(Left), Imaginary(Right) at 1MHz | 68 |
| 3.5 | Current Density Distribution within the Cross Section of a Round Wire due to proximity-excitation at 1MHz | 69 |
| 3.6 | Different components of the corrected field \mathbf{a} as of (2.5) with three wires at 1MHz (Top), and comparative view of the computed \mathbf{a} field focused on the rightmost wire (Bottom). | 72 |
| 3.7 | Real part of \mathbf{a} in three parallel wires at 1Hz with conductor spacing of 8mm: Structured Sleeves (Left) and Unstructured Sleeves (Right) . . | 75 |
| 3.8 | Imaginary part of \mathbf{a} in three parallel wires at 1Hz with conductor spacing of 8mm: Structured Sleeves (Left) and Unstructured Sleeves (Right) | 76 |
| 3.9 | Real part of \mathbf{a} in three parallel wires at 1MHz with conductor spacing of 8mm: Structured Sleeves (Left) and Unstructured Sleeves (Right) . | 78 |
| 3.10 | Imaginary part of \mathbf{a} in three parallel wires at 1MHz with conductor spacing of 8mm: Structured Sleeves (Left) and Unstructured Sleeves (Right) | 79 |
| 3.11 | Real part of \mathbf{a} in three parallel wires at 1Hz with conductor spacing of 2.05mm: Structured Sleeves (Left) and Unstructured Sleeves (Right) . | 81 |
| 3.12 | Imaginary part of \mathbf{a} in three parallel wires at 1Hz with conductor spacing of 2.05mm: Structured Sleeves (Left) and Unstructured Sleeves (Right) | 82 |
| 3.13 | Real part of \mathbf{a} in three parallel wires at 1MHz with conductor spacing of 2.05mm: Structured Sleeves (Left) and Unstructured Sleeves (Right) | 84 |
| 3.14 | Imaginary part of \mathbf{a} in three parallel wires at 1Hz with conductor spacing of 2.05mm: Structured Sleeves (Left) and Unstructured Sleeves (Right) | 85 |
| 4.1 | Current density in Full Model FM (Left) and Semi-Analytical SA (Right) in a 5 Turn Coil. | 87 |

| | | |
|------|--------------------------------------------------------------------------------------------------------------------------------------------------------------------|-----|
| 4.2 | Voltage Driven Multi-turn coil | 88 |
| 4.3 | Comparison between multi-turn inductors and massive inductors | 88 |
| 4.4 | Multi-turn coil in FE model | 89 |
| 4.5 | Application cases with geometrical description and connection order: Symmetrical-half in the case of 5-turn winding (Left), 15-turn winding (Right). | 93 |
| 4.6 | Geometrical representation of a 15-turn coil with an inter-turn distance of: 8mm (left) and 2.05mm (right) | 94 |
| 4.7 | Impact of Inter-turn spacing on Impedance of a 5-turn multi-turn coil at 1Hz: Resistance (Left), Inductance (Right) | 96 |
| 4.8 | Impact of Inter-turn spacing on Impedance of a 5-turn multi-turn coil at 1MHz: Resistance (Left), Inductance (Right) | 97 |
| 4.9 | Impedance at a broad range of frequencies with large inter-turn spacing on a 5-Turn coil: Resistance (Left), Inductance (Right) | 99 |
| 4.10 | Impedance at a broad range of frequencies with small inter-turn spacing on a 5-Turn coil: Resistance (Left), Inductance (Right) | 104 |
| 4.11 | Impact of Inter-turn spacing on Impedance of a 10-turn multi-turn coil at 1Hz: Resistance (Left), Inductance (Right) | 109 |
| 4.12 | Impact of Inter-turn spacing on Impedance of a 10-turn multi-turn coil at 1MHz: Resistance (Left), Inductance (Right) | 110 |
| 4.13 | Impedance at a broad range of frequencies with large inter-turn spacing on a 10-Turn coil: Resistance (Left), Inductance (Right) | 112 |
| 4.14 | Impedance at a broad range of frequencies with small inter-turn spacing on a 10-Turn coil: Resistance (Left), Inductance (Right) | 117 |
| 4.15 | Impact of Inter-turn spacing on Impedance of a 15-turn multi-turn coil at 1Hz: Resistance (Left), Inductance (Right) | 122 |
| 4.16 | Impact of Inter-turn spacing on Impedance of a 15-turn multi-turn coil at 1MHz: Resistance (Left), Inductance (Right) | 123 |
| 4.17 | Impedance at a broad range of frequencies with large inter-turn spacing on a 15-Turn coil: Resistance (Left), Inductance (Right) | 125 |
| 4.18 | Impedance at a broad range of frequencies with large inter-turn spacing on a 15-Turn coil: Resistance (Left), Inductance (Right) | 130 |



List of Tables

| | | |
|-----|-------------------------------------------------------------------------------------------------------------------------------------------------------------------------------------------------------------------------------------------------------------------------------------|-----|
| 4.1 | Relative difference between Degrees-of-Freedom used in Full-Model and Semi-analytical Model versus the relative error in the solution of the impedance at a broad range of frequencies for a 5-turn winding with 8mm of inter-turn distance and a sleeve size of 1mm | 100 |
| 4.2 | Relative difference between Degrees-of-Freedom used in Full-Model and Semi-analytical Model versus the relative error in the solution of the impedance at a broad range of frequencies for a 5-turn winding with 8mm of inter-turn distance and a sleeve size of 0.5mm | 101 |
| 4.3 | Relative difference between Degrees-of-Freedom used in Full-Model and Semi-analytical Model versus the relative error in the solution of the impedance at a broad range of frequencies for a 5-turn winding with 8mm of inter-turn distance and a sleeve size of 0.5mm | 102 |
| 4.4 | Relative difference between Degrees-of-Freedom used in Full-Model and Semi-analytical Model versus the relative error in the solution of the impedance at a broad range of frequencies for a 5-turn winding with 2.05mm of inter-turn distance and a sleeve size of 1mm | 105 |
| 4.5 | Relative difference between Degrees-of-Freedom used in Full-Model and Semi-analytical Model versus the relative error in the solution of the impedance at a broad range of frequencies for a 5-turn winding with 2.05mm of inter-turn distance and a sleeve size of 0.5mm | 106 |
| 4.6 | Relative difference between Degrees-of-Freedom used in Full-Model and Semi-analytical Model versus the relative error in the solution of the impedance at a broad range of frequencies for a 5-turn winding with 2.05mm of inter-turn distance and a sleeve size of 3mm | 107 |
| 4.7 | Relative difference between Degrees-of-Freedom used in Full-Model and Semi-analytical Model versus the relative error in the solution of the impedance at a broad range of frequencies for a 10-turn winding with 8mm of inter-turn distance and a sleeve size of 1mm | 113 |

| | | |
|------|--------------------------------------------------------------------------------------------------------------------------------------------------------------------------------------------------------------------------------------------------------------------------------------|-----|
| 4.8 | Relative difference between Degrees-of-Freedom used in Full-Model and Semi-analytical Model versus the relative error in the solution of the impedance at a broad range of frequencies for a 10-turn winding with 8mm of inter-turn distance and a sleeve size of 0.5mm | 114 |
| 4.9 | Relative difference between Degrees-of-Freedom used in Full-Model and Semi-analytical Model versus the relative error in the solution of the impedance at a broad range of frequencies for a 10-turn winding with 8mm of inter-turn distance and a sleeve size of 3mm | 115 |
| 4.10 | Relative difference between Degrees-of-Freedom used in Full-Model and Semi-analytical Model versus the relative error in the solution of the impedance at a broad range of frequencies for a 10-turn winding with 2.05mm of inter-turn distance and a sleeve size of 1mm | 118 |
| 4.11 | Relative difference between Degrees-of-Freedom used in Full-Model and Semi-analytical Model versus the relative error in the solution of the impedance at a broad range of frequencies for a 10-turn winding with 2.05mm of inter-turn distance and a sleeve size of 0.5mm | 119 |
| 4.12 | Relative difference between Degrees-of-Freedom used in Full-Model and Semi-analytical Model versus the relative error in the solution of the impedance at a broad range of frequencies for a 10-turn winding with 2.05mm of inter-turn distance and a sleeve size of 3mm | 120 |
| 4.13 | Relative difference between Degrees-of-Freedom used in Full-Model and Semi-analytical Model versus the relative error in the solution of the impedance at a broad range of frequencies for a 15-turn winding with 8mm of inter-turn distance and a sleeve size of 1mm | 126 |
| 4.14 | Relative difference between Degrees-of-Freedom used in Full-Model and Semi-analytical Model versus the relative error in the solution of the impedance at a broad range of frequencies for a 15-turn winding with 8mm of inter-turn distance and a sleeve size of 0.5mm | 127 |
| 4.15 | Relative difference between Degrees-of-Freedom used in Full-Model and Semi-analytical Model versus the relative error in the solution of the impedance at a broad range of frequencies for a 15-turn winding with 8mm of inter-turn distance and a sleeve size of 3mm | 128 |
| 4.16 | Relative difference between Degrees-of-Freedom used in Full-Model and Semi-analytical Model versus the relative error in the solution of the impedance at a broad range of frequencies for a 15-turn winding with 2.05mm of inter-turn distance and a sleeve size of 1mm | 131 |
| 4.17 | Relative difference between Degrees-of-Freedom used in Full-Model and Semi-analytical Model versus the relative error in the solution of the impedance at a broad range of frequencies for a 15-turn winding with 2.05mm of inter-turn distance and a sleeve size of 0.5mm | 132 |
| 4.18 | Relative difference between Degrees-of-Freedom used in Full-Model and Semi-analytical Model versus the relative error in the solution of the impedance at a broad range of frequencies for a 15-turn winding with 2.05mm of inter-turn distance and a sleeve size of 3mm | 133 |



List of Symbols

Alphanumeric symbols

| | |
|----------------|---------------------------------------------|
| a | Magnetic vector potential (Wb/m) |
| b | Magnetic flux density (T) |
| d | Electric flux density (C/m ²) |
| e | Electric field (V/m) |
| \mathbb{E}^3 | Three-dimensional oriented Euclidean space |
| h | Magnetic field (A/m) |
| j | Current density (A/m ²) |
| J | Magnetic polarization (T) |
| m | Magnetization (A/m) |
| <i>n</i> | Time step |
| p | Electric polarization (C/m ²) |
| <i>q</i> | Electric charge density (C/m ³) |
| <i>t</i> | Time instant |
| <i>v</i> | Electric scalar potential (V) |
| x | Point (<i>x, y, z</i>) |

Greek symbols

| | |
|--------------|----------------------------------------------------------------------------|
| Ω | Bounded open set of E^3 |
| ϕ | Magnetic scalar potential (A) |
| σ | Electric conductivity (S/m) |
| μ | Magnetic permeability (H/m) |
| μ_0 | Magnetic permeability of vacuum ($= 4\pi \times 10^{-7}$ H/m) |
| μ_r | Relative magnetic permeability ($= \mu/\mu_0$) |
| χ | Magnetic susceptibility |
| χ_r | Relative magnetic susceptibility ($= \chi/\mu_0$) |
| ϵ | Electric permittivity (F/m) |
| ϵ_0 | Electric permittivity of vacuum ($\simeq 8.854187817 \cdot 10^{-12}$ F/m) |
| ϵ_r | Relative electric permittivity ($= \epsilon/\epsilon_0$) |

Abbreviations

| | |
|-----|-------------------------|
| 1D | One-dimensional |
| 2D | Two-dimensional |
| 3D | Three-dimensional |
| CPU | Central Processing Unit |
| DC | Direct Current |
| DoF | Degree of Freedom |
| FE | Finite-Element |

Operators

| | |
|------------|-------------------|
| ∂ | Boundary operator |
| C | Complement |

-
- $\partial_{x,y,z}$ Space derivatives in cartesian coordinates
 $\partial_{r,\phi,z}$ Space derivatives in cylindrical coordinates
 ∂_t Time derivative
curl Curl
div Divergence
grad Gradient
 \cdot Scalar product
 \times Vector product



Introduction

Context and Motivations

Electric conductors are essential components in any electromagnetic system. Their role is to transfer power from the supply to the system and, when wound into a set of coils, to shape the magnetic field to ensure the proper and efficient operation of the device.

Alternative current (AC) carrying conductors are subjected to skin effect and proximity effect. Skin effect repels charge carriers towards the surface of the conductor, whereas proximity effect repels them towards the region of the conductor the farthest from a neighboring current carrying conductor. Both effects yield a complex inhomogeneous distribution of the current density over conducting cross sections, with sharp gradients, and that impacts significantly the impedance of the conductor seen from the supply.

A careful consideration of the impact of skin- and proximity effects on wire and coil impedances is thus of critical importance in the design and optimization of electromagnetic devices, and the accurate modelling of the associated inhomogeneous current density may require a fine mesh. Meshsizes in conducting regions, and in their direct vicinity, must indeed be significantly smaller than the skin depth, a characteristic length that decreases as the inverse of the square root of the working frequency, and that is close to 0.1mm in Copper at 1MHz, to fix the idea.

State of the Art

Modeling of thin wires is an active research topic. Some of the most common techniques are homogenization methods [59], analytical methods [1, 2, 62] and hybrid methods including numerical approximations [28]. Edelvik, in particular, proposed in [28] a method for the modeling of thin wires of arbitrary shapes using FETD, which was subsequently documented and popularized by Jin in [49]. This approach uses the telegrapher's equations by means of a hybrid field-wire technique. More specifically, the method relies in the mapping of the electric field along the edges of the finite element mesh (using edge basis functions) to impose global current sources that can be coupled to circuit networks. This allows the introduction of frequency-dependent impedances via circuit relations. The method accounts for skin effect in the wires, however, does not account for proximity effects on the resistance of the wire. Similarly, [86] developed a thin wire method in which a complex resistivity is applied on the conducting domain to account for skin effect and complex permeability to the elements surrounding the thin wire to account for the internal inductance of the wire, but once again impedance variations due to proximity effects are neglected.

Another common approach in the study of multi-turn coils, bundles and litz-type wires is that of homogenization techniques. In this case the modeling of individual strands or turns is avoided, for the benefit of a modeling of the outer shape of the packaging. In [12, 13, 14], Bossavit presented an approach to model composite type materials by using frequency and space dependent material properties to map large and small scale fields. Furthermore, periodic conditions were used by implementing a cell-type approach. This elementary cell approach is vastly used and can be found in [30] and early works by Podoltsev in [74]. Gyselinck introduced a way to account for proximity and skin effect in round and rectangular conductors by using an effective complex reluctivity and internal impedance, respectively [42]. This work includes time-domain extensions [43] and 3D cases in collaboration with Sabariego Vazquez [75].

Dissertation goals

This thesis proposes a technique to model conductors (wires, strands, turns) in a Finite Element (FE) model at a reasonable computational cost, while still accounting accurately for skin and proximity effects. In particular we focus on conductors whose axial geometrical dimensions are vast to the radial dimensions, which we shall refer to throughout as *thin wires*. Since each individual conductor is modeled, extensions to different packaging, conductor shapes, and location asymmetry are possible. The proposed method is in particular useful for the numerical modeling of windings in motors/generators [53, 55, 54], for complex inductor systems, and even for electronic packages in high-speed/high-frequency integrated circuits [86]. It is sufficient in the context of this analysis to assume that the physical behavior is linear (or linearized), allowing the use of a time-harmonic approach.

The idea of the proposed technique, called Semi-Analytical (SA) method, is three-fold. Real conductors, with thus a finite extension, are represented in the FE model by idealized thin wires with vanishing radius. In 2D models, this means that the cross section of each individual real wire is replaced by a node of the finite element mesh located at the center of the real wire. This geometric simplification implies of course a significant mesh-dependent modelling error, which can however be neatly canceled by means of a field truncation based on the solution of a small auxiliary FE problem, which is described in detail below. Finally, analytical results for a single conductor in isolation or plunged in an homogeneous magnetic field are invoked to reconstruct the local field solution and to evaluate the losses and impedances with, in general, an excellent accuracy with respect to the solution of the real problem, but at a much smaller computational cost.

Dissertation outline

This dissertation is divided into 4 chapters.

Chapter 1 presents a general review of electromagnetics, mainly focusing on the conditions and assumptions used to model linear conducting domains. The main goal is to lay out the foundations and physical notations of the magnetodynamics time-harmonic formulation.

Chapter 2 develops the framework to model thin wires using a semi-analytical approximation. First, the geometrical concept of the *sleeve* is introduced as a tool to truncate the field solution and eliminate the singularity arising from the thin-wire approximation. A thorough analytical derivation of the magnetic vector potential in a round conductor in isolation -using current excitation- is provided, which is ultimately used as a skin-effect correction term in the finite-element model. The thin wire semi-analytical (**SA**) model is validated against the solution of fully discretized (**FM**) massive conductors in the case of single and multiple parallel conductors. The validation focuses on the accuracy of local (i.e., magnetic vector potential) and global quantities (i.e., inductance matrix) at a broad range of frequencies and conductor spacing, highlighting the proximity effects.

Chapter 3 presents a thorough analytical derivation of the magnetic vector potential in the case of round conductors in the presence of a time-varying sinusoidal field is presented. The derivation of the magnetic vector potential of a single wire in isolation is applied again - this time using B-field excitation, leading to the correction contribution of the magnetic vector potential due to proximity effects. The analytical expression is compared against the fully discretized value in the case of a single conductor. Then, the focus is turned to the study of the local correction accuracy when both: skin and proximity correction of the magnetic vector potential is included into the $\mathbf{a} - v$ formulation. The comparison between the **FM** and the fully corrected **SA** model is performed in the case of multiple parallel conductors.

Chapter 4 The semi-analytical method is extended to incorporate global sources,

enabling circuit coupling to incorporate Joule losses -through frequency dependent resistance and inductance values, due to skin and proximity effects. Furthermore, electrical network constraints are introduced to enable connection in series. The use of voltage (or current) sources and series connection between each of the turn segments in 2D serves as a simplification in modeling multi-turn coils. The comparison and validation of the semi-analytical method against the fully discretized model is presented in the case of multi-turn coils, focusing on the accuracy of the inductance and resistance due to skin and proximity effects.

Original contributions

Hereafter is a list of contributions that are considered to be original:

- Field-truncation to remove the singularity introduced by the thin-wire approximation in a finite-element framework, using the *sleeve* geometrical concept (Chapter 2).
- Semi-analytical local correction of the magnetic vector potential including skin (Chapter 2) and proximity (Chapter 3) effects. The analytical expression is thoroughly derived by using skin- and proximity excitation in the case of a single conductor in isolation.
- Formulation extension to incorporate global sources and global material parameters (e.g., resistance and inductance) alongside the use of electrical network constraints to define parallel and series connections. The latter serves as the simplification used to model multi-turn coils (Chapter 4).
- Thorough analytical derivation of the impedance terms arising from skin- and proximity effect excitation (Chapter 4)

All models and finite element formulations have been implemented using ONELAB (Gmsh [38] and GetDP [25]) using linear direct solver MUMPS [6] .

Magnetoquasistatics

This chapter presents the laws of electromagnetism used in the modeling of linear conducting materials. Maxwell's field equations are introduced in differential form in the frequency domain, with their respective material laws. Furthermore, general notation, problem statement, simplifications, and mathematical framework are defined.

1.1. Maxwell's Equations in Macroscopic Media

In an Euclidean three-dimensional space (\mathbb{E}^3), Maxwell's equations in time-domain read

$$\mathbf{curl} \mathbf{H} - \partial_t \mathbf{D} = \mathbf{J}, \quad (1.1a)$$

$$\mathbf{curl} \mathbf{E} + \partial_t \mathbf{B} = 0, \quad (1.1b)$$

$$\operatorname{div} \mathbf{B} = 0, \quad (1.1c)$$

$$\operatorname{div} \mathbf{D} = Q, \quad (1.1d)$$

where \mathbf{H} , \mathbf{E} , \mathbf{D} and, \mathbf{B} are the magnetic field strength, the electric field, the electric flux and the magnetic flux density. These four vector field quantities construe the mathematical description of the physical phenomenon known as *electromagnetism*.

By applying, the divergence div on both sides of eq. (1.1a) we obtain the local differential relation describing the conservation of charge, where Q is the electric charge. This differential expression is also known in the literature as *Continuity equation*[10], stating that the divergence of the current density is equal to the negative rate of change of the electric charge

$$\partial_t Q + \operatorname{div} \mathbf{J} = 0. \quad (1.2)$$

1.2. Maxwell's Model in Frequency Domain

1

Under the assumption of sinusoidal excitation, Maxwell equations can be solved in frequency domain. This implies that the field variables are expressed as complex variables with real and imaginary components.

A periodic function can be expressed in terms of frequency by using Fourier integral representation

$$\mathbf{f}(\mathbf{x}, t) = \frac{1}{2\pi} \int_{-\infty}^{\infty} \underline{f}(\mathbf{x}, f) \exp^{i2\pi ft} df \quad (1.3)$$

with a time derivative

$$\partial_t \mathbf{f}(\mathbf{x}, t) = \frac{1}{2\pi} i2\pi f \int_{-\infty}^{\infty} \underline{f}(\mathbf{x}, f) \exp^{i2\pi ft} df \quad (1.4)$$

where the angular frequency can be written in terms of the excitation frequency $\omega = 2\pi f$. Hence, the time derivative operator becomes $\partial_t = i\omega$, where $i = \sqrt{-1}$ denotes the imaginary unit.

Note that the function $\underline{f} = \underline{f}_{re} + i\underline{f}_{im}$ is a phasor field with real and imaginary parts, respectively. This relation also applies to complex vector fields; therefore, we may re-write Maxwell equations in the harmonic regime

$$\mathbf{curl} \mathbf{h} - i\omega \mathbf{d} = \mathbf{j}, \quad (1.5a)$$

$$\mathbf{curl} \mathbf{e} + i\omega \mathbf{b} = 0, \quad (1.5b)$$

$$\text{div} \mathbf{b} = 0, \quad (1.5c)$$

$$\text{div} \mathbf{d} = \mathbf{q}, \quad (1.5d)$$

where \mathbf{h} , \mathbf{b} , \mathbf{e} and \mathbf{d} are all phasor fields.

1.3. Magnetoquasistatic Approximation

The Magnetoquasistatic approximation is commonly used as a simplification of the full Maxwell problem in the case of negligible displacement currents. Equation (1.2) in frequency-domain

$$i\omega \mathbf{q} + \text{div} \mathbf{j} = 0, \quad (1.6)$$

observe that if the charge density does not vary with respect to time ($\dot{\rho} = 0$) the electric current becomes divergenceless or solenoidal:

$$\operatorname{div} \mathbf{j} = 0. \quad (1.7)$$

This implies that the streamlines of steady electric currents close upon themselves.

Hence, the Magnetoquasistatic approximation reads:

$$\operatorname{curl} \mathbf{h} = \mathbf{j}, \quad (1.8a)$$

$$\operatorname{curl} \mathbf{e} + i\omega \mathbf{b} = 0, \quad (1.8b)$$

$$\operatorname{div} \mathbf{b} = 0 \quad (1.8c)$$

1.4. Constitutive Laws for the Magnetoquasistatic Approximation

The relevance of establishing material relations lies in the complex nature of systems made out of a large variety of materials. Hence, the assumption of a homogeneous environment would be a naive simplification and expressions of electric flux density, magnetic field and electric current in terms of the electric and magnetic flux density such that: $\mathbf{d} = \mathbf{d}(\mathbf{e}, \mathbf{b})$, $\mathbf{h} = \mathbf{h}(\mathbf{e}, \mathbf{b})$ and, $\mathbf{j} = \mathbf{j}(\mathbf{e}, \mathbf{b})$, are needed.

These macroscopic relations construe the physical behavior of matter in the presence of a magnetic or electric field:

$$\mathbf{j} = \sigma \mathbf{e} \quad (1.9a)$$

$$\mathbf{b} = \mu_0(\mathbf{h} + \mathbf{m}), \quad (1.9b)$$

$$\mathbf{d} = \epsilon_0 \mathbf{e} + \mathbf{p} \quad (1.9c)$$

where \mathbf{j} , \mathbf{m} , and \mathbf{p} are the the electric current, magnetic polarization, and electric polarization. Each expression handles different types of behavior when exposed to an electric or magnetic field in terms of charge conduction (i.e., the flow of electric current), magnetic, and electric polarization. This allows us to organize materials into three categories: conducting, magnetic, and dielectrics materials. These are rarely treated in isolation as many material alloys and/or composites, combining properties from each individual category, are found in modern applications. However, this doesn't prevent us from studying each material individually.

In Maxwell's magnetoquasistatics case displacement currents are negligible and material relation (1.9c) will be disregarded.

1.4.1. Ohm's Law and Conductors

1

Ohm's law (eq. 1.9a) states that the relationship between the electric current and electric field is directly proportional, by introducing an electrical conductivity σ . Furthermore, (1.9a) is presented in the case of non-moving/stationary circuits. Otherwise, the electric field should be re-written as $\mathbf{e}' = \mathbf{e} + \mathbf{v} \times \mathbf{b}$, to account for the currents due to presence of the *Lorentz Force*.

The term *conductor* describes type of materials which allow flow of electrical charges as they are not bound to atoms. This relationship is achieved by applying an electrical conductivity $\sigma > 0$, where the higher the value, the easier the transport of carrier throughout the material.

For generality, and to account for conductors, insulators and external sources in stationary circuits, we may write the generalized Ohm's law as

$$\mathbf{j} = \sigma \mathbf{e} + \mathbf{j}_e \quad (1.10)$$

Note that the external source \mathbf{j}_e implies that the magnitude and direction of the current is known a priori and is independent of the local electromagnetic field.

1.4.2. Magnetization

In the presence of an external magnetic field, magnetic dipoles are produced or aligned/oriented at the atomic scale within a particular material. These type of materials that exhibit magnetic behavior are known as *magnetic materials*.

This alignment implies that a relationship between the magnetization \mathbf{m} and the magnetic field \mathbf{h} is needed

$$\mathbf{m} = \chi_m \mathbf{h} + \mathbf{h}_m \quad (1.11)$$

which once again provides a proportionality between the fields via the introduction the *magnetic susceptibility* χ_m . Equation (1.11) is presented in its most general form, accounting for a permanent magnetic field independent from the local field.

It is quite common to express magnetic materials in terms of the relative magnetic permeability $\mu_r = 1 + \chi_m$. By substituting the magnetic susceptibility into eq. (1.9b) we obtain

$$\mathbf{b} = \mu \mathbf{h} + \mu_0 \mathbf{h}_m \quad (1.12)$$

where $\mu = \mu_r \mu_0$, and $\mu_0 = 4\pi 10^{-7} \text{H/m}$ is the magnetic permeability in vacuum.

Magnetic materials is a very rich subject for which in-depth description can be found in classical magnetic material books [18, 68, 77, 85].

1.5. General Remarks

Material non-linearity is beyond the scope of this dissertation, the focus being on linear, memory-less, isotropic materials. To ensure the validity of the magnetoquasistatics case we may solve the continuity equation (1.7) in a simple medium which leads to the general solution of the charge density

$$q = q_0 \exp [(-\sigma/\epsilon)t] \quad (1.13a)$$

where the relaxation time

$$\tau = \frac{\epsilon}{\sigma} \quad (1.14a)$$

For good conductors such as copper the relaxation time is in the order of 10^{-19} s. This ensures that the frequencies and materials throughout this work belong to the magnetoquasistatics approximation.

Lastly, all formulations used describe non-moving circuits.

1.6. $\mathbf{a} - v$ formulation with classical massive conductors

1

Electrical systems commonly comprise electrical circuits as driving components. In this section, we derive the general expression of the $\mathbf{a} - v$ weak formulation accounting for voltage and current sources through circuit relations, specifically in the modeling of massive conductors.

Defining the magnetic flux density in terms of the magnetic vector potential \mathbf{a} such that $\mathbf{b} = \mathbf{curl} \mathbf{a}$ in Ω , we obtain the electric field directly from Faraday's law in terms of the magnetic vector potential \mathbf{a} and the electric scalar potential v

$$\mathbf{e} = -i\omega\mathbf{a} - \mathbf{grad} v. \quad (1.15)$$

Substituting the electric field \mathbf{e} in the magnetodynamics case of Ampere's Law, and Ohm's Law we obtain the strong formulation of the eddy current problem.

$$\mathbf{curl} \nu \mathbf{curl} \mathbf{a} + i\omega\sigma\mathbf{a} + \sigma\mathbf{grad} v = \mathbf{j}_e. \quad (1.16)$$

Note that both Faraday's and Ampere's Laws are satisfied. Multiplying each term in the strong formulation (1.16) by an appropriate test function λ' , we can obtain the general weak expression of the magnetodynamics problem. Find \mathbf{a} and v such that

$$\begin{aligned} (\nu \mathbf{curl} \mathbf{a}, \mathbf{curl} \lambda')_{\Omega} + (\hat{\mathbf{n}} \times \mathbf{h}, \lambda')_{\partial\Omega} + i\omega(\sigma\mathbf{a}, \lambda')_{\Omega_c} + (\sigma\mathbf{grad} v, \lambda')_{\Omega_c} \\ - (\mathbf{j}_e, \lambda')_{\Omega_e} = 0 \quad (1.17) \\ \forall \lambda' \in F_{\lambda}(\Omega) \end{aligned}$$

where $F_{\lambda}(\Omega)$ is the appropriate function space where the test function λ' lives defined in Ω . Note that the trace of the magnetic field arises from Stoke's theorem and unless specified, it vanishes. Hence, the term $\hat{\mathbf{n}} \times \mathbf{h} = 0$ is the case for a homogeneous Neumann boundary condition.

Let us define the problem in the case of massive conductors in 2D, which will serve as the fully discretized formulation (FM) used to validate our proposed semi-analytical (SA) method. Let the conducting region

$$\Omega_c = \bigcup_i \Omega_{c_i}$$

be the union of the conductors Ω_{c_i} with cross section area A_i , and Ω_c^C be the complementary non-conduction regions. The computation domain is thus $\Omega =$

$\Omega_c^C \cup \Omega_c$. The conductors Ω_{c_i} are supplied with a sinusoidal current source $I_i = \hat{I}_i \cos(\omega t + \theta_i)$, where \hat{I}_i is the current peak value, ω the angular frequency, and θ_i the phase shift.

In 2D, the magnetic vector potential field is discretized as

$$\mathbf{a} = \sum_n a_n \alpha_n \hat{\mathbf{z}},$$

where α_n are nodal basis functions and $\hat{\mathbf{z}}$ is the unit vector perpendicular to the domain of analysis Ω . The gradient of the scalar electric potential, on the other hand, is discretized as

$$-\mathbf{grad} v = - \sum_i (\Delta v)_i \beta_i \hat{\mathbf{z}},$$

where $(\Delta v)_i$ are the voltage drop per unit length in z direction imposed to the conductors Ω_{c_i} , and β_i are the corresponding regionwise constant basis functions.

Applying Galerkin's method, the $\mathbf{a} - v$ formulation writes in weak form as a set of field equations associated with the free nodes of the mesh. Let us choose the $F_{\mathbf{a}}(\mathcal{T})$ and $F_v(\mathcal{T})$ conforming FE-space in a mesh $\mathcal{T} = \bigcup_h \mathcal{T}_h$, for the fields \mathbf{a} and v respectively. Defining $(\cdot, \cdot)_{\Omega}$ as the volume integral in Ω of the dot product of its vector field arguments, the discrete Galerkin approximation of the $\mathbf{a} - v$ magnetodynamics problem is formulated as follows:

Find \mathbf{a} and v such that:

$$\begin{aligned} \sum_n a_n (\nu \mathbf{curl} \alpha_n \hat{\mathbf{z}}, \mathbf{curl} \alpha_k \hat{\mathbf{z}})_{\Omega} + \omega \sigma \sum_n a_n (\alpha_n \hat{\mathbf{z}}, \alpha_k \hat{\mathbf{z}})_{\Omega_c} + \\ \sigma \sum_i (\Delta v)_i (\beta_i \hat{\mathbf{z}}, \alpha_k \hat{\mathbf{z}})_{\Omega_c} = 0 \end{aligned} \quad (1.18)$$

$$\forall \alpha_k \in F_{\mathbf{a}}^0(\mathcal{T})$$

$$\begin{aligned} -\omega \sigma \sum_n a_n (\alpha_n \hat{\mathbf{z}}, \beta_k \hat{\mathbf{z}})_{\Omega_c} - \sigma \sum_i (\Delta v)_i (\beta_i \hat{\mathbf{z}}, \beta_k \hat{\mathbf{z}})_{\Omega_c} - I_k = 0 \end{aligned} \quad (1.19)$$

$$\forall \beta_k \in F_v(\mathcal{T})$$

where ν is the magnetic reluctivity, σ the electric conductivity and I the global electric current flowing in current carrying conductors, and where $F_{\mathbf{a}}^0(\mathcal{T})$ is the space corresponding to $F_{\mathbf{a}}(\mathcal{T})$ but assuming homogeneous Dirichlet type boundary conditions.

Semi-Analytical Modeling of the Skin Effect in Thin Wires

In this chapter we introduce a semi-analytical method to model thin conducting wires in frequency-domain in a finite element (FE) framework under magnetodynamics conditions. The proposed method enables the use of nodal elements within a finite element mesh (Fig. 2.1), avoiding a dense and costly discretization, but still accounting for skin effect.

The method contains two main steps which can be summarized as:

- Removal of the singularity -introduced by the thin wire approximation- by truncation of the field solution
- Reconstruction of the magnetic vector potential by incorporating the analytical solution of a single wire in isolation into the finite-element model

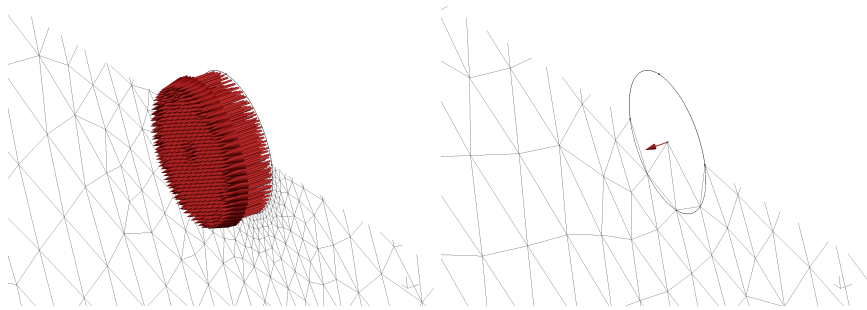


Figure 2.1: *Current density in Full Model (Left) and Thin Wire Approximation (Right)*

2.1. Biot-Savart Law: Modeling of Thin Wires

Before presenting the thin wire approximation in the $\mathbf{a} - v$ formulation it is important to review the Biot-Savart law as it will serve as a building block in modeling of thin conducting wires. In 1820 Biot and Savart presented a relation between the magnetic induction \mathbf{b} to the total current I flowing through a wire. Note that this is a simplified version of the more elaborate relation presented by Ampere’s Law [47].

Under the assumption of a thin conductor with radius tending to zero, the physical domain is seen as a collection of line elements—each acting as a source to flux density volume elements in a three-dimensional space, following the right-hand rule.

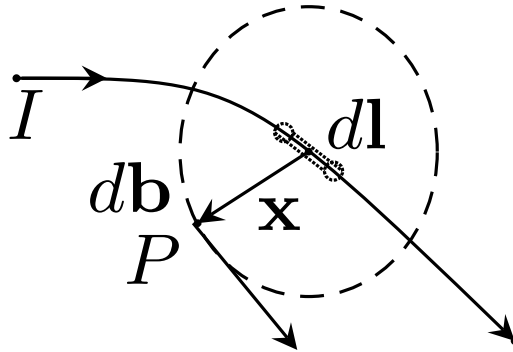


Figure 2.2: Elemental magnetic induction $d\mathbf{b}$ due to current element $I d\mathbf{l}$

As shown in Fig. 2.2, $d\mathbf{l}$ is a line element pointing in the same direction as the global current I flows. Moreover, \mathbf{x} is the coordinate vector pointing in the direction of an observation point P . Hence the elemental flux density at point P can be expressed as

$$d\mathbf{b} = I \frac{\mu_0}{4\pi} \frac{d\mathbf{l} \times \mathbf{x}}{|\mathbf{x}|^3}. \tag{2.1}$$

Hence, we can calculate the magnitude of the magnetic flux by integrating each element as a succession of basic magnetic-flux elements

$$|\mathbf{b}| = IR \frac{\mu_0}{4\pi} \int_{-\infty}^{\infty} \frac{dl}{(R^2 + l^2)^{3/2}} = \frac{\mu_0}{2\pi} \frac{I}{R} \tag{2.2}$$

Under the assumption of radial symmetry the magnitude of the field generated around the conductor can be easily expressed in cylindrical coordinates. Let $\mathbf{b} = \mathbf{b}_r + \mathbf{b}_\phi + \mathbf{b}_z$ where $\mathbf{b}_r = \mathbf{b}_z = 0$

$$\mathbf{b}_\phi = \frac{\mu_0 I}{2\pi r} \hat{\phi} \quad (2.3)$$

where $\hat{\phi}$ is the unit vector in the direction defined by the right-hand rule, and r the radial-distance variable from the line element.

It is appropriate to issue certain caveats arising from this model, the first one being that it is only valid in empty space (or air), i.e., it is assumed that no magnetic material is present. The distribution of magnetic flux density within the wire filament is not included under this assumption. Secondly, time-dependency is disregarded altogether.

2.2. The a-v Thin Wire Idealization

The thin wire approximation -arising from Biot Savart's Law- refers to the relationship between the electric current and induction field found around conductors with vanishing radii. Under such conditions, and exploiting radial symmetry, the magnetic field around the wire can be calculated analytically for a single wire.

The goal is to develop an efficient method for the modeling of thin wires for which the discretization of the conductor itself is avoided, allowing the accurate calculation of the field problem at a broad range of frequencies, without the need of fine meshes. In a FE framework the thin wires can be represented as a sequence of edges in a 3D mesh, or by mesh nodes in 2D. The theoretical background of the method is presented for the 2D frequency-domain case, to focus on the technique and avoid complexity arising from time-stepping, gauging, etc, which do not have direct effect on the proposed method.

The thin wire idealization implies that the flux distribution within the cross section of the wire is not part of the solution, however, the analytical solution of a single wire is known and will be used to reconstruct the field solution.

Similarly to (1.18) the thin wire idealized $\mathbf{a} - v$ formulation can be expressed as:

Find \mathbf{a} such that:

$$(\nu \mathbf{curl} \mathbf{a}, \mathbf{curl}(\alpha_n \hat{\mathbf{z}}))_{\Omega} - A_c(I_i, \alpha_n \hat{\mathbf{z}})_{\Omega_{LR}} = 0, \quad \forall \alpha_n \in F_a(\Omega). \quad (2.4)$$

which is the magnetostatics weak formulation. Note that notation Ω_{LR} refers to the conducting "Line Region" (term coined in [58]) and A_c the cross section of the actual physical wire. The field distribution around thin conductors is still correctly represented in the model, as it only depends on the total current I_i flowing in the wire.

The thin wire approximation enables the use of coarser meshes, which ultimately decreases the computational cost of electromagnetic systems with high aspect ratio components. By removing the cross section of the conductor and replacing it by a mesh-node, we remove the need for discretization of the wire, however, we introduce a singularity as $R \rightarrow 0$ -as seen in Biot-Savart's thin wire expression. In Fig. 2.3 this issue is evident, as the solution of the Full Model (FM) and the Thin Wire model without correction become dissimilar the closer they get to the center of the conductor -depicted by the orange rectangle. However, the solution discrepancy in the wire, and the agreement in the non-conducting domain are expected, and the treatment of the singularity is required to obtain an analogous solution to the classical problem.

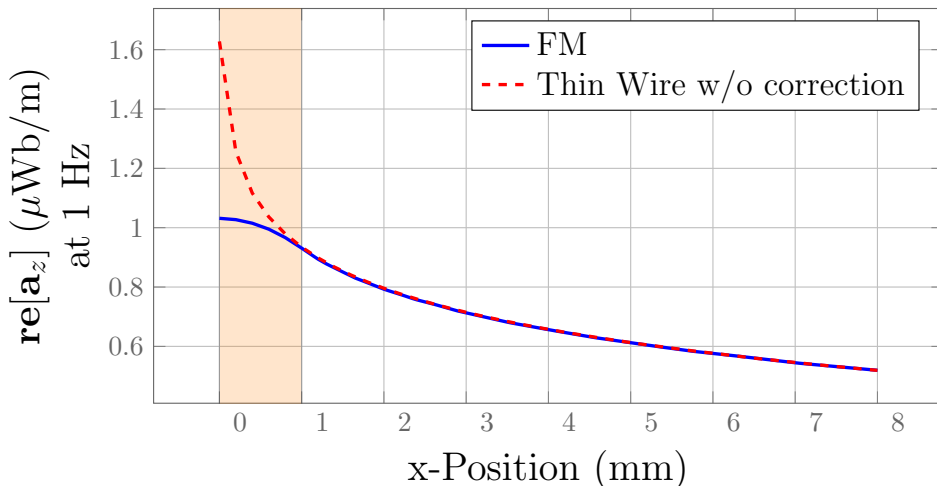


Figure 2.3: Magnetic vector potential along the r-axis at 1Hz, showing the non-physical mesh-related overestimation of the peak \mathbf{a} -field due to the thin wire idealization compared to the physical solution obtained with the Full model.

2.3. Field Truncation

The field truncation refers to our method's step to remove the non-physical mesh-dependent behavior arising from the wire's geometrical idealization. The challenge therein is to remove the singularity without modifying the solution in the non-conducting region, which is already correct.

In order to isolate and treat this singularity we will introduce a geometrical concept known as the *sleeve*. We call *sleeve* the region Ω_{SL} made of the finite elements in the mesh having at least one node on Ω_{LR} , as shown in Fig. 2.4. The color code highlights two regions. In orange we depict the conducting domain in both cases: fully discretized model (Top) and the thin wire approximation (Bottom). In cyan, we depict the so-called sleeve region which may be larger or smaller than the original cross section of the conductor. Furthermore, the sleeve, being a set of element of the air region surrounding the idealized conductor, is a subset of the non-conducting domain ($\Omega_{SL} \subset \Omega_c^C$).

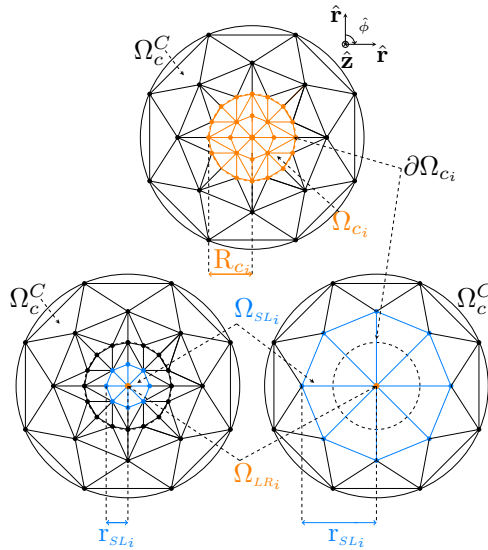


Figure 2.4: Top: Mesh with explicit discretization of the real round conductor Ω_{c_i} highlighted. Bottom: Mesh around the idealized (pointwise) thin conductor Ω_{LR_i} with a fine (Left) or a coarser (Right) discretization, and with highlighted mesh dependent sleeve Ω_{SL_i} .

We call \mathbf{a}^c the solution of the problem (2.4) on Ω , and \mathbf{a}^w the solution of the auxiliary problem on the sleeve region $\Omega_{SL} = \cup_i \Omega_{r_{SL_i}}$. The idea behind solving the problem a second time on the sleeve region, is that the non-physical peaklike overestimation of the vector magnetic potential \mathbf{a} introduced by the idealization of conductors as lines (Fig. 2.3), can be cancelled by subtracting two FE solutions.

The solution \mathbf{a}^c is thus obtained by conventionally solving the Maxwell problem in the full domain of analysis Ω , whereas the solution \mathbf{a}^w is obtained by solv-

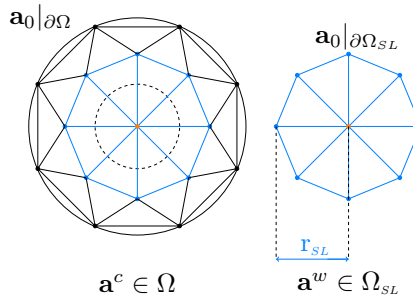


Figure 2.5: Domain of analysis of the initial problem (Left), and of the auxiliary problem (Right).

ing an auxiliary boundary value problem, whose formulation is identical to (2.4), except that it is solved on the restricted region Ω_{SL} , with a homogeneous Dirichlet boundary conditions $\mathbf{a} = 0$ imposed directly on the external boundary of the sleeves $\partial\Omega_{SL}$, as depicted in Fig. 2.5.

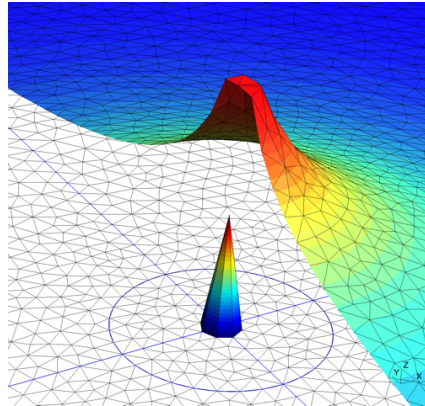


Figure 2.6: Solution \mathbf{a}^w of the auxiliary problem, and cut-view of truncated field $\mathbf{a}^c - \mathbf{a}^w$.

The FE fields \mathbf{a}^w and \mathbf{a}^c , being computed using exactly the same finite elements in the region Ω_{SL} where they are both defined, they contain exactly the same mesh-dependent peak artifact, which can thus be neatly canceled out by subtraction of \mathbf{a}^w from \mathbf{a}^c . The result of the subtraction, the so called truncated field $\mathbf{a}^c - \mathbf{a}^w$, is depicted in Fig. 2.6, together with the auxiliary field \mathbf{a}^w .

The truncated field is already the sought solution of the problem everywhere outside the sleeves Ω_{SL} . Only inside the sleeves must it be modified in order to reintroduce the details of the field distribution inside the real wire, accounting for its actual shape (round, square, rectangle) and structure (massive, coaxial, twisted). The theoretical framework is presented in the case of solid round wires but the extension to more complex cases should follow the same principle.

2.4. Semi-analytical Modeling of Thin Wires

The general principle of the correction is a one-liner: calculate the analytical solution \mathbf{a}_{corr} for the real wire carrying a current I_i with a zero-flux boundary condition imposed on the sleeve boundary. The corrected \mathbf{a} -field writes then simply

$$\mathbf{a} = \mathbf{a}^c - \mathbf{a}^w + \mathbf{a}_{corr}. \quad (2.5)$$

In order to establish the analytical derivation of \mathbf{a}_{corr} , a number of reasonable simplifications are done in practice: the thin wire is assumed straight, the sleeve is assumed cylindrical, the analytical solution is assumed radial. This assumption still takes into account two types of sleeve formations. The sleeve arrangement where the symmetry of the sleeve is ensured is labeled as *structured*, as seen in Fig. 2.7. However, ultimately the size and shape of the sleeve will be defined by the meshing tool used (e.g., Gmsh [38]), and the characteristic length of the element specified on Ω_{LR} . In the latter case the sleeve will be described as *unstructured*, where the effective radius of the sleeve is estimated from the area of the sleeve A_{SL} such that $r_{SL} = \sqrt{A_{SL}/\pi}$.

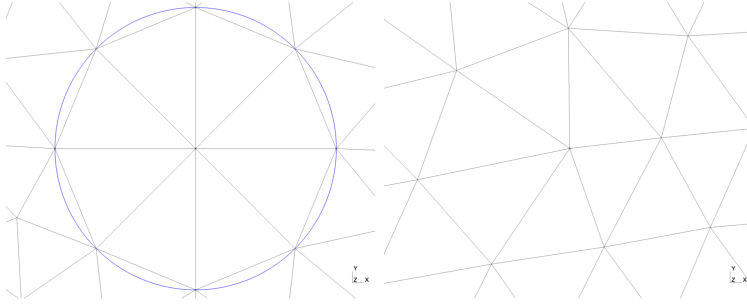


Figure 2.7: Sleeve in a Finite-Element Mesh: Structured (Left) and Unstructured (Right).

In this section only straight massive conductors with round cross sections of radius R are considered. This allows solving the magnetodynamics problem analytically with a 1D differential equation, in a cylindrical coordinate system aligned with the center-line of the wire, to obtain the correction factors due to skin effect [82]

$$a_{corr_s}(r) = \frac{\mu_0 I}{2\pi} \left[\frac{\mu_r J_0(kr) - J_0(kR)}{kR J_1(kR)} + \log\left(\frac{R_\infty}{R}\right) \right], \quad r \leq R \quad (2.6a)$$

$$a_{corr_s}(r) = \frac{\mu_0 I}{2\pi} \log\left(\frac{R_\infty}{r}\right), \quad r > R \quad (2.6b)$$

The numerical validations have been performed with a wire radius $R_i = 1$ mm, a sleeve radius (i.e., a prescribed mesh size on the wire) $r_{SL_i} = 3$ mm, a current $\hat{I} = 1$ A, an electrical conductivity $\sigma = 5.96e7$ S/m, and a relative permeability $\mu_r = 1$.

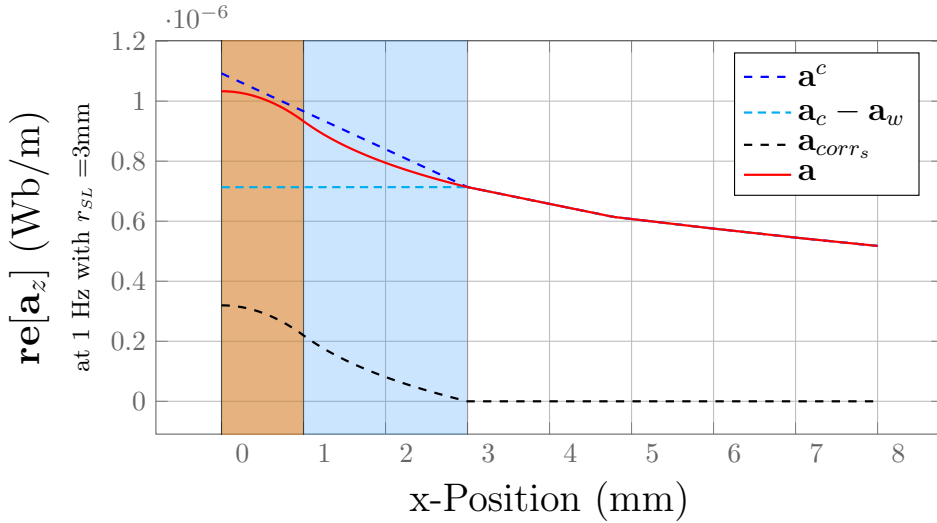


Figure 2.8: Graphical representation of the local correction of the magnetic vector potential \mathbf{a} as of (2.5), for a single round conductor of radius $R = 1\text{mm}$ and a structured sleeve of radius $r_{SL} = 3\text{mm}$. The term \mathbf{a}^c represents the solution in the whole domain, $\mathbf{a}^c - \mathbf{a}^w$ the truncation of the field solution, and \mathbf{a}_{corr_s} the analytical correction as of (2.6)

In Fig. 2.8 we see the progression of the reconstruction of the \mathbf{a} field, plotting the individual terms of (2.5). Fig. 2.9 shows that the corrected field (2.5) matches closely the field obtained by means of the conventional FE formulation with a fine discretization of the wire, both at low and high frequency.

The flux ϕ_i is obtained in the thin wire approach by substituting (2.5) into

$$\phi_i = \frac{1}{A_{c_i}} \int_{\Omega_{c_i}} \mathbf{a} \cdot \hat{\mathbf{z}} \beta_i d\Omega_{c_i} = \sum_j L_{i,j} I_j \quad (2.7)$$

where β_i are the corresponding regionwise constant basis functions.

As the real thin wire region is not available in the geometry in the thin wire approach, the first two terms are approximated by the value of the truncated field $\mathbf{a}^c - \mathbf{a}^w$ on the idealized wire, whereas the third term is evaluated analytically:

$$\phi_i = (\mathbf{a}^c - \mathbf{a}^w)|_{\Omega_{c_i}} + \frac{\mu_0 I_i}{2\pi} \left(\nu \mu_r \left(\frac{\delta}{R} \right)^2 - \frac{\mu_r}{kR} \frac{J_0(kR)}{J_1(kR)} + \log \left(\frac{r_{SL}}{R} \right) \right). \quad (2.8)$$

Fig. 2.10 shows that the proposed technique allows recovering the exact flux, and hence the exact impedance of the thin wire, with an excellent accuracy up to

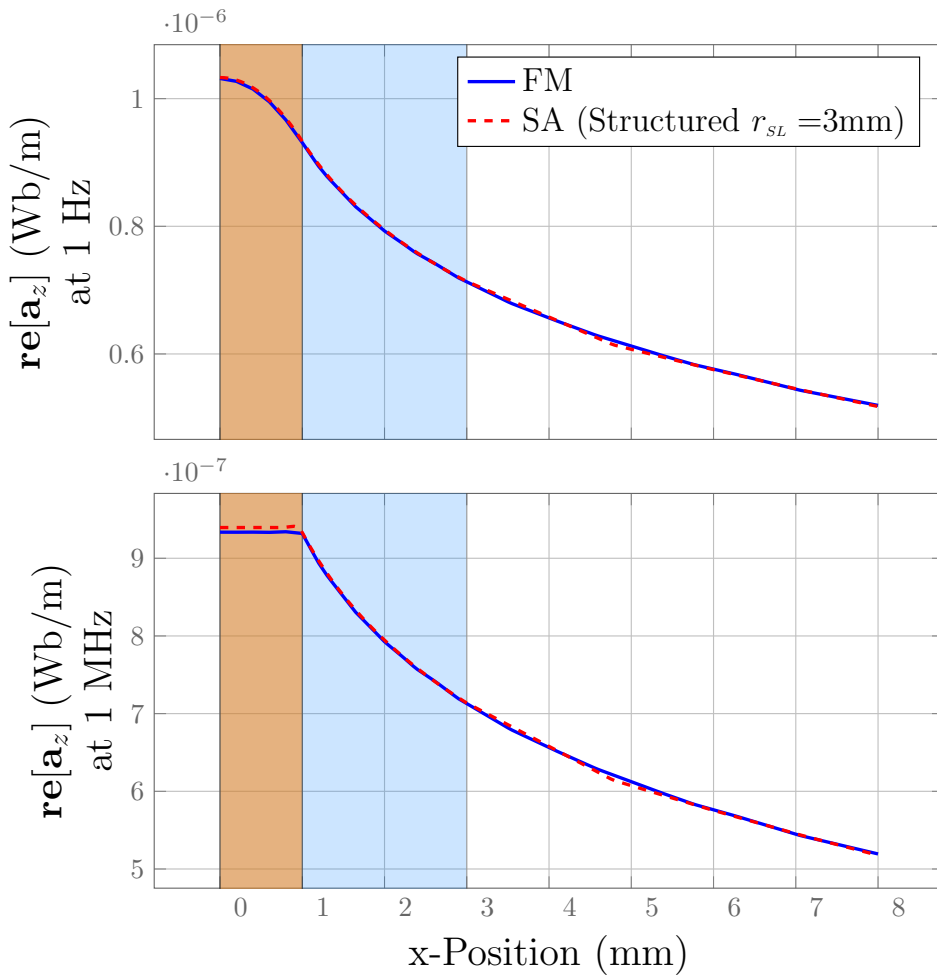


Figure 2.9: Comparative view of the magnetic vector potential \mathbf{a} along the r-axis for a single wire at 1Hz (Top) and 1MHz (Bottom).

1MHz, with however a significantly coarser mesh, since one has 14404 Dofs (mesh size = 0.02mm) for the Full model and only 1555 Dofs (mesh size = 3mm) for the LR model.

2.5. Analytical Solution of a Wire in Isolation - Skin Effect

The development of our semi-analytical method to solve thin conducting structures is based on the solution of Maxwell's equations for a single straight conductor in empty space. Let us consider an infinitely long round wire Ω_c with a radius R , and its material properties: electrical conductivity (σ) and magnetic permeability (μ), excited by a sinusoidal source. For good conductors, it is safe to assume that

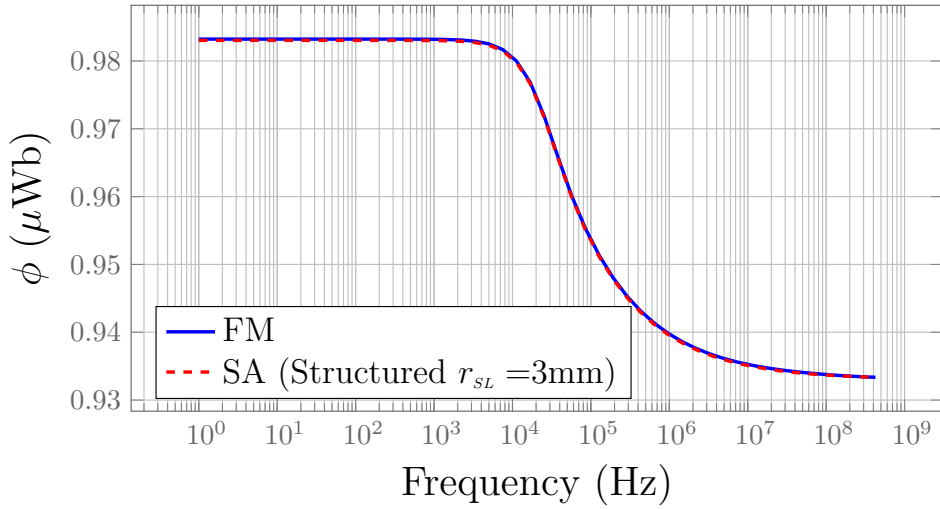


Figure 2.10: Comparative view of the flux (2.7) vs frequency characteristic, computed with the thin wire approach and with the conventional FE method for a single wire.

the relaxation time is short enough to neglect charges inside of the conductor, simplifying our model to the magnetodynamics case.

Defining the magnetic flux density as the curl of the magnetic vector potential \mathbf{a} such that $\mathbf{b} = \mathbf{curl} \mathbf{a}$, enables us to determine the electric field as $\mathbf{e} = -i\omega \mathbf{a} - \mathbf{grad} v$, where v is a scalar potential. In this fashion we equate Ampere's law and Faraday's law to obtain the strong $\mathbf{a} - v$ formulation:

$$\mathbf{curl} v \mathbf{curl} \mathbf{a} + i\omega \sigma \mathbf{a} + \sigma \mathbf{grad} v = \mathbf{j}_e, \quad (2.9)$$

where

$$\begin{aligned} \mathbf{curl} \mathbf{curl} \mathbf{a} = & \\ & \left(\frac{1}{r} \partial_\phi \left[\frac{1}{r} (\partial_r (r a_\phi) - \partial_\phi a_r) \right] - \partial_z \left[\partial_z a_r - \partial_r a_z \right] \right) \hat{\mathbf{r}} \\ & \left(\partial_z \left[\frac{1}{r} \partial_\phi a_z - \partial_z a_\phi \right] - \partial_r \left[\frac{1}{r} (\partial_r (r a_\phi) - \partial_\phi a_r) \right] \right) \hat{\boldsymbol{\phi}} \\ & \frac{1}{r} (\partial_r (r \left[\partial_z a_r - \partial_r a_z \right]) - \partial_\phi \left[\frac{1}{r} \partial_\phi a_z - \partial_z a_\phi \right]) \hat{\mathbf{z}} \end{aligned}$$

Under the assumption of an infinitely long wire, the variation in the $\hat{\mathbf{z}}$ direction is negligible ($\partial_z = 0$), and the 1D approximation is sufficient to solve the field

problem. Setting the magnetic vector potential in the $\hat{\mathbf{z}}$ direction (i.e., $\mathbf{a} = a_z \hat{\mathbf{z}}$), the terms in the $\hat{\mathbf{r}}$ and $\hat{\phi}$ vanish, and the $\mathbf{curl\,curl}$ term simplifies to

$$\mathbf{curl\,curl}\ \mathbf{a} = \left(-\partial_r^2 a_z - \frac{1}{r} \partial_r a_z - \frac{1}{r^2} \partial_\phi a_z\right) \hat{\mathbf{z}}$$

In the absence of external sources, the 1D approximation of (2.10) reads

$$\nu \left(-\partial_r^2 a_z - \frac{1}{r} \partial_r a_z - \frac{1}{r^2} \partial_\phi a_z\right) + i\omega\sigma a_z = 0.$$

Multiplying the whole expression by $-\mu r^2$ and rearranging the terms relative to their derivatives we obtain

$$r^2 \partial_r^2 a_z + r \partial_r a_z + k^2 r^2 a_z = -\partial_\phi^2 a_z, \quad (2.10)$$

where the complex wavenumber $k = \sqrt{-i\omega\mu\sigma}$.

As the frequency increases in a conductor carrying an harmonic current $I = \hat{I} \exp(i\theta)$, the current density becomes more prominent towards the conductor's surface, as shown in Fig. 2.11. This is known as the skin effect phenomenon.

Under these conditions, the \mathbf{b} -field is parallel to the $\hat{\phi}$ direction and the electric current flows in the same direction as the electric field $\mathbf{e}(r) = -i\omega a_z(r) \hat{\mathbf{z}}$ for which (2.10) simplifies to

$$r^2 \partial_r^2 a_z + r \partial_r a_z + k^2 r^2 a_z = 0 \quad (2.11)$$

leading to the general solution of the Bessel differential equation.

$$a_z(r) = C_1 J_0(kr) + C_2 Y_0(kr) \quad (2.12)$$

The Bessel function $Y_0(kr) \rightarrow \infty$ when $r \rightarrow 0$, hence, it does not have any physical meaning in our problem, and C_2 is set to zero. Using Ohm's law ($\mathbf{j}_z = \sigma \mathbf{e}_z$) and integrating the current density over the conductor's cross sectional area, we obtain the net current flowing within the conductor

$$\begin{aligned} I &= -i\omega\sigma A \int_0^{2\pi} \int_0^R J_0(kr) r \, dr \, d\phi \\ &= -i\omega\sigma C_1 2\pi \frac{R J_1(kR)}{k} \end{aligned} \quad (2.13)$$

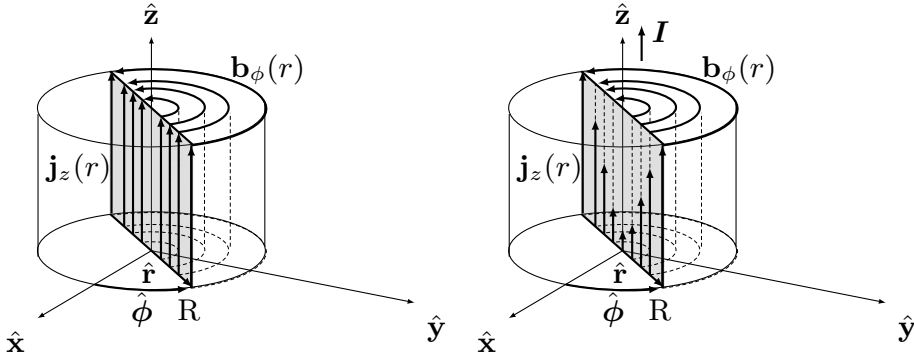


Figure 2.11: Static (DC - Left) and Dynamic (AC - Right) Current Density Distribution.

multiplying and dividing by the magnetic permeability of the material and performing some basic algebra we obtain that $C_1 = \frac{\mu I}{2\pi R k J_1(kR)}$.

The magnetic vector potential can thus be written as

$$\mathbf{a}_z(r) = \frac{\mu I}{2\pi k R} \frac{J_0(kr)}{J_1(kR)}, \quad r \leq R, \quad (2.14)$$

and the analytical expression of the current density distribution as

$$\mathbf{j}_z(r) = \frac{kI}{2\pi R} \frac{J_0(kr)}{J_1(kR)}, \quad r \leq R. \quad (2.15)$$

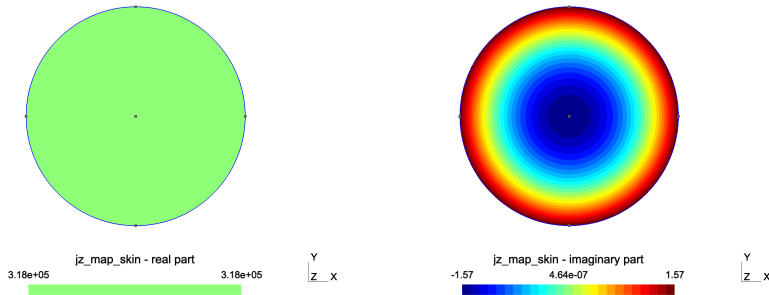


Figure 2.12: Color map of the current density distribution within the cross section of a round wire at 1Hz: Real(Left), Imaginary(Right)

Equation (2.15) serves as the analytical expression of the frequency-dependent current density distribution within a round conductor and can be used to validate

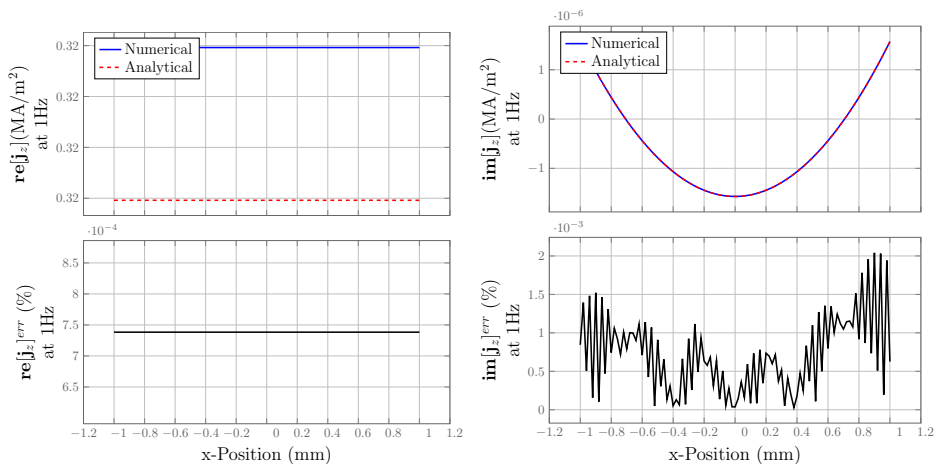


Figure 2.13: Line plot of the current density distribution within the cross section of a round wire due to skin-excitation at 1Hz and relative error: Real(Left), Imaginary(Right)

compare and validate the results against the Finite Element Method. In order to have a grasp of the level of accuracy we will introduce a local comparison term that for readability and simplicity we will call *relative error* and it will be defined as

$$f_{err} = \frac{|f_{ref}(x) - f_{approx}(x)|}{|f_{ref}^{max}(x)|} \quad (2.16)$$

Where $|f^{max}(x)|$, in the local comparison refers to $f^{max} = \sqrt{\mathbf{re}[f]^2 + \mathbf{im}[f]^2}$. In Figures 2.13, and 2.15 the results of such comparison is presented in the case of 1Hz and 1MHz. The comparison is displayed as a line plot across the cross section of the wire ($y = 0$). Furthermore, the color map obtained from the numerical solution is presented in 2.12, and 2.14 for 1Hz and 1MHz respectively. In the case of 1Hz we see that the relative error between the numerical and analytical solutions are negligible, and in the case of 1MHz we still find a high level of agreement between both results, however we see that the relative error is slightly higher but still negligible.

The magnetic vector potential in the non-conducting domain surrounding the conductor can be derived from the solution of the second order ordinary differential equation arising from Eq. (2.11) when $k \rightarrow 0$

$$r^2 \partial_r^2 a_z + r \partial_r a_z = 0, \quad (2.17)$$

with the general solution

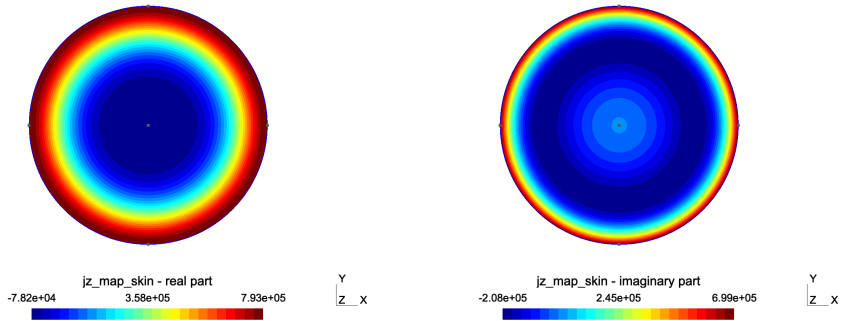


Figure 2.14: Color map of the current density distribution within the cross section of a round wire at 1MHz: Real(Left), Imaginary(Right)

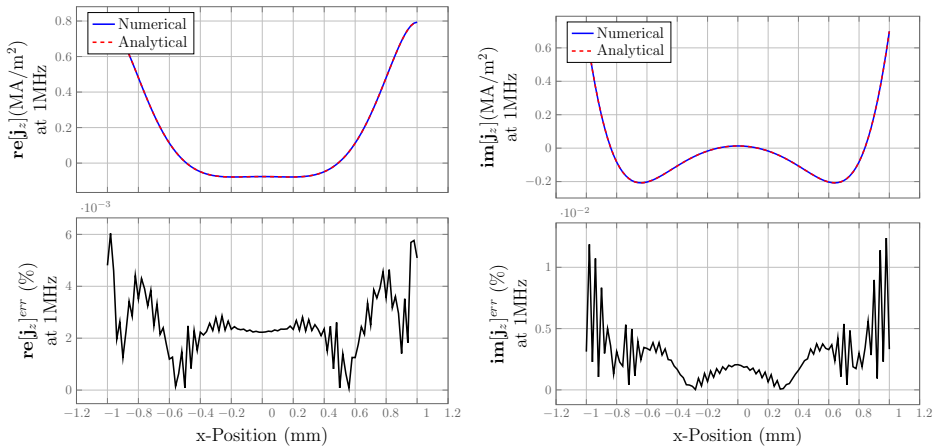


Figure 2.15: Line plot of the current density distribution within the cross section of a round wire due to skin-excitation at 1MHz and relative error : Real(Left), Imaginary(Right)

$$a_z(r) = C \log(r) + D. \quad (2.18)$$

The solution of interest lies within the radial range $R \leq r < R_\infty$. This enables the use of the solution of (2.14) evaluated at the surface to ensure continuity between the interior of the conductor and the non-conducting exterior domain. Setting up (2.14) equal to (2.18) we obtain

$$D = \frac{\mu I}{2\pi k R} \frac{J_0(kR)}{J_1(kR)} - C \log(R),$$

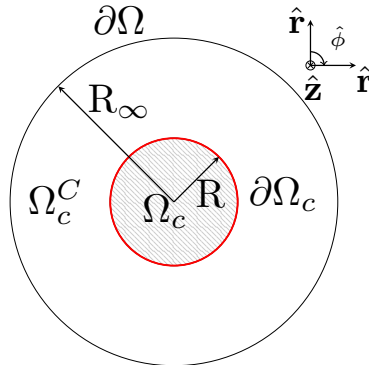


Figure 2.16: Single wire in Isolation

which substituted back into (2.18)

$$a_z(r) = C \log\left(\frac{r}{R}\right) + \frac{\mu I}{2\pi k R} \frac{J_0(kR)}{J_1(kR)}.$$

In the case of round conductors the solution of the magnetic field $\mathbf{b} = \frac{\mu_0 I}{2\pi r} \hat{\phi}$ is known at any point at a distance r from the current carrying conductor. Hence, the continuity of the tangential component of the magnetic field can be ensured through C at the $r = R_\infty$ boundary. Calculating the magnetic flux density such that $\mathbf{b} = \text{curl } \mathbf{a}$

$$\begin{aligned} -\partial_r \left[C \log\left(\frac{r}{R}\right) + \frac{\mu I}{2\pi k R} \frac{J_0(kR)}{J_1(kR)} \right] &= \frac{\mu_0 I}{2\pi r}, \\ -C \frac{1}{r} &= \frac{\mu_0 I}{2\pi r}, \end{aligned}$$

enables the field solution calculation in the non-conducting region.

$$a_z(r) = -\frac{\mu_0 I}{2\pi} \log\left(\frac{r}{R}\right) + \frac{\mu I}{2\pi k R} \frac{J_0(kR)}{J_1(kR)}, \quad r \geq R. \tag{2.19}$$

To calculate the magnetic vector potential in the interior of the wire, we take the expression (2.14) and subtract the magnitude of the vector potential outside of the wire (2.19). Outside of the conductor, the expression coming from the straight thin wire approximation is sufficient.

$$a_z(r) = \frac{\mu_0 I}{2\pi} \left[\frac{\mu_r}{kR} \frac{J_0(kr) - J_0(kR)}{J_1(kR)} + \log \left(\frac{R_\infty}{R} \right) \right], \quad r \leq R, \quad (2.20a)$$

$$a_z(r) = \frac{\mu_0 I}{2\pi} \log \left(\frac{R_\infty}{r} \right), \quad r > R. \quad (2.20b)$$

2

The analytical expression of the single wire in isolation will serve as the correction factor due to skin effect in the finite element model, where the radius at infinity will be the radius of the *sleeve* $R_\infty = r_{SL}$.

2.6. Limitation and Proximity Effect

It has been shown in the previous section that the proposed technique is able to accurately compute the true field distribution over the whole domain of analysis and a large range of working frequencies, in the case of a single wire. One must still verify that, despite the fact that the correction is made with the analytical solution of a single wire in isolation, the effect of distant wires on a given thin wire is properly taken into consideration. A system of three equidistant thin wires is considered for this purpose. Fig. 2.17 (Top) shows the breakdown of the computed \mathbf{a} -field into the different terms of (2.5) at 1MHz. The flux part due to distant wires, i.e., the mutual inductance effect, is taken into account through the $\mathbf{a}^c - \mathbf{a}^w$ part. Skin effect, on the other hand, is taken into account by the correction \mathbf{a}_{corr} . The major limitation of our technique appears in the bottom view in Fig. 2.17. Eddy currents should distribute asymmetrically in a wire in order to shield its interior against other current carrying conductors in the vicinity. This is the proximity effect [42], which is so far disregarded by our approach, as a consequence of the fact that the correction is made with the analytical solution of a single wire in isolation.

This simplification has however little impact on the accuracy of the computed flux and impedance. As one can see in Fig. 2.17 (Bottom), the corrected field (semi-analytical) is not flat in the rightmost thin wire, but the computation (2.8) of ϕ_i involves the value of the truncated field $\mathbf{a}^c - \mathbf{a}^w$ at the center of the wire, which is close to the exact value because the eddy currents responsible for the proximity effect are zero in average. Joule losses could however be slightly underestimated. But one can use the analytical solution of a single wire, no longer in isolation but plunged in a uniform \mathbf{b} field, to account rigorously for the proximity effect (with thus correct Joule losses). This will be addressed in the next chapter.

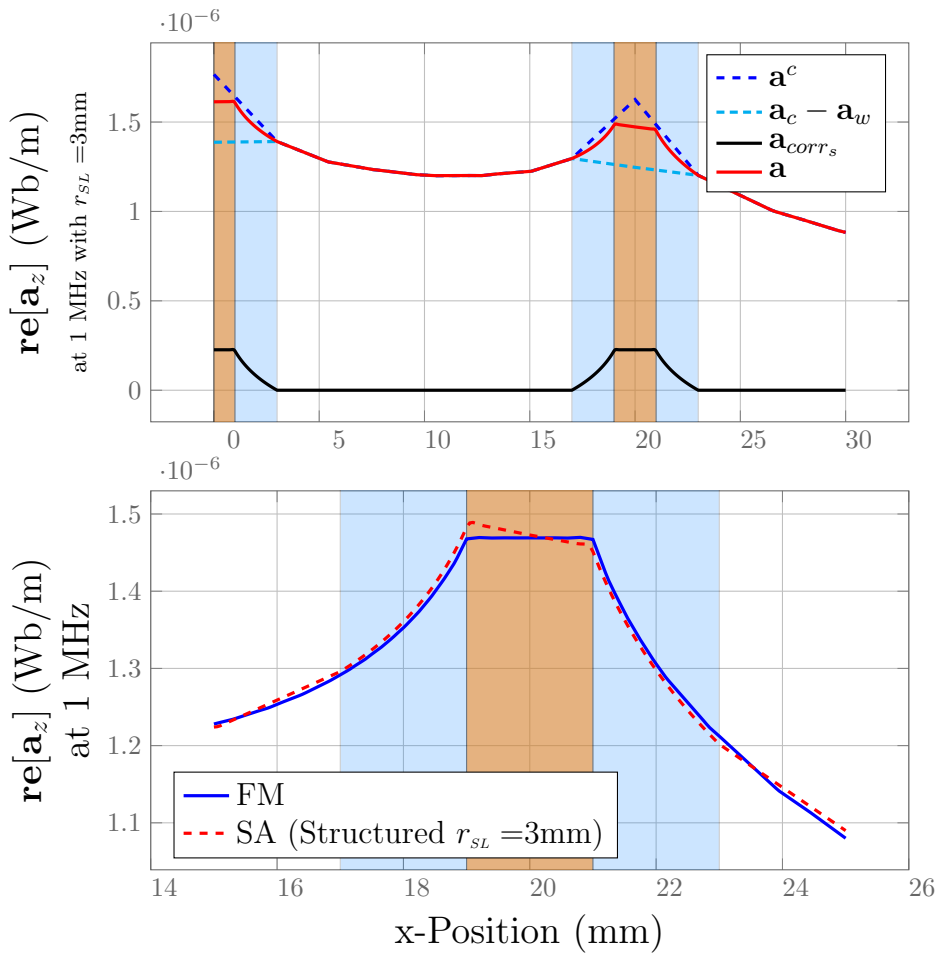


Figure 2.17: Different components of the corrected field \mathbf{a} as of (2.5) with three wires at 1MHz (Top), and comparative view of the computed \mathbf{a} field focused on the rightmost wire (Bottom).

2.7. Semi-Analytical Modeling of the Skin Effect in Thin Wires - A Summary

In this section we have laid out the foundation blocks of the so-called Semi-Analytical (SA) method to model thin wires. For clarity, the method's mathematical framework is summarized in this section as a concise formulation that can be ultimately implemented as a stand-alone model or a feature in any finite-element platform.

The idealized thin wire finite-element weak formulation can be expressed as

$$(\nu \mathbf{curl} \mathbf{a}^c, \mathbf{curl} (\alpha_n^c \hat{\mathbf{z}}))_{\Omega} - A_c(I_i, \alpha_n^c \hat{\mathbf{z}})_{\Omega_{LR}} = 0, \quad \forall \alpha_n^c \in F_a(\Omega). \quad (2.21a)$$

$$(\nu \mathbf{curl} \mathbf{a}^w, \mathbf{curl} (\alpha_n^w \hat{\mathbf{z}}))_{\Omega_{SL}} - A_c(I_i, \alpha_n^w \hat{\mathbf{z}})_{\Omega_{LR}} = 0, \quad \forall \alpha_n^w \in F_a(\Omega_{SL}). \quad (2.21b)$$

The field is solved by the magnetostatics weak formulation (2.21), which is associated to the global current I_i in each conductor of the model.

The nodal basis function α_n^c and α_n^w are defined on the whole domain Ω and on the sleeve domain Ω_{SL} . This implies that in both equations the second term on the left-hand side of the equation is identical and when performing the subtraction of the sleeve domain in the finite-element model we end up with the solution of the background field and the singularity around the sleeve is removed.

The magnetic vector potential can be calculated analytically for each single wire. If the total current is known the analytical expression of the magnetic vector potential can be expressed as a correction term

$$a_{corr_s}(r) = \frac{\mu_0 I}{2\pi} \left[\frac{\mu_r}{kR} \frac{J_0(kr) - J_0(kR)}{J_1(kR)} + \log \left(\frac{r_{SL}}{R} \right) \right], \quad r \leq R \quad (2.22a)$$

$$a_{corr_s}(r) = \frac{\mu_0 I}{2\pi} \log \left(\frac{r_{SL}}{r} \right), \quad r > R \quad (2.22b)$$

Hence, the distribution of the magnetic vector potential can be reconstructed by adding up the analytical solution to the truncated-field solution in the finite-element model, naturally falling onto our one liner description (2.5)

$$\mathbf{a} = \mathbf{a}^c - \mathbf{a}^w + \mathbf{a}_{corr}.$$

where $\mathbf{a}_{corr} = \mathbf{a}_{corr_s} + \mathbf{a}_{corr_p}$ reconstructs the solution in Ω_{SL}

From a global point of view, the reconstruction of the magnetic vector potential enables the calculation of the magnetic flux, as shown in (2.8). Similarly to the

correction of the magnetic vector potential, the magnetic flux is reconstructed by combining the truncated solution with the flux's analytical solution.

$$\phi_i = (\mathbf{a}^c - \mathbf{a}^w)|_{\Omega_{c_i}} + \frac{\mu_0 I_i}{2\pi} \left(\mu_r \left(\frac{\delta}{R} \right)^2 - \frac{\mu_r}{\tau} \frac{J_0(\tau)}{J_1(\tau)} + \log \left(\frac{r_{SL}}{R} \right) \right).$$

Since the current I is known, the calculation of the inductance of the wire becomes straightforward (2.7).

2.8. Numerical Tests: Three Parallel Wires

The tests presented in this section have been performed under the same conditions presented earlier in the development of the theoretical framework, with 3 wires of radius $R_i = 1$ mm, a sleeve radius (i.e., a prescribed mesh size on the wire) in the case of structured sleeves r_{SL_i} and controlled by the characteristic length l_{c_i} in the case of unstructured sleeves, a current $I = 1$ A, an electrical conductivity $\sigma = 5.96 \cdot 10^7$ S/m (i.e. copper), and a relative permeability $\mu_r = 1$. In Fig. 2.18 the depiction of the model is described, where each conductor is numbered from left to right, each with a current source and spaced out at a specific conductor distance d . The top figure depicts the fully discretized model, hence the fully orange color describing the round conductors, whereas the analogous problem is described below, where the conductor is reduced to a line within the mesh, surrounded by the sleeve of the conductor. Note that Fig. 2.18 is presented in 3D however, the model is in fact 2D, where each of these conductors are infinitely long. The 3D description is to ensure understanding of the concept of the sleeve, conductor spacing and numbering of each individual entity. Lastly, the discretization of each conductor in the FM model is created using a characteristic length $l_c = \frac{\delta|_{1MHz}}{3}$, where $\delta|_{1MHz} = 6.52 \cdot 10^{-5}$ m is the skin depth evaluated at 1MHz. This mesh is constant throughout all the tests unless stated otherwise: 66390 DoF for $d = 8$ mm and 46019 DoF for $d = 2.05$ mm.

These numerical tests attempt to target local and global comparisons and study the level of accuracy under the different conditions: high and low frequencies and using large and short conductor spacing. The latter has essential physical relevance in terms of proximity effects.

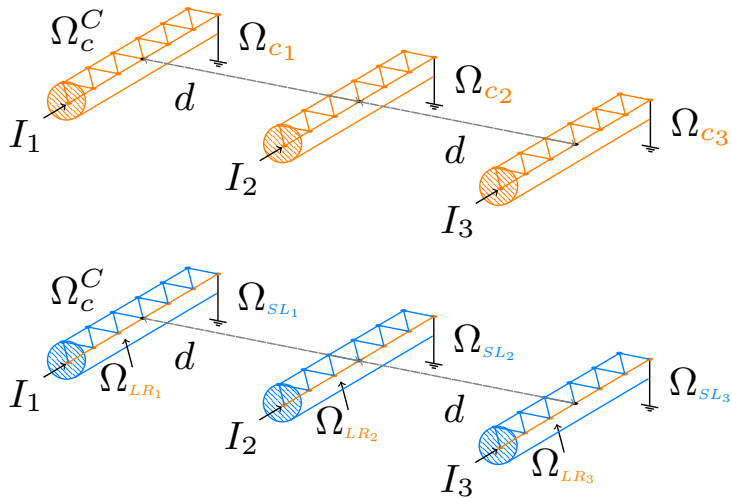


Figure 2.18: Three parallel wires model description with current excitation I and conductor spacing d . Top figure represents the fully discretized model and bottom model represents the analogous semi-analytical model

2.8.1. Local Agreement - Magnetic Vector Potential

The local agreement tests are presented in four cases:

- Frequency 1Hz and conductor spacing of 8mm
- Frequency 1MHz and conductor spacing of 8mm
- Frequency 1Hz and conductor spacing of 2.05mm
- Frequency 1MHz and conductor spacing of 2.05mm

Note that the orange rectangles depict each parallel wire of the Full Model (FM) which is compared against the Semi-analytical model (SA) in the case of both structured and unstructured sleeves. The depiction of the real wires by an orange-colored rectangle in the figures helps to reader to visualize the actual spacing between conductors. when located far from each other (i.e. 8mm) and when located in close proximity (i.e. an inter-axis distance of 2.05mm, which means that the conductors are only separated by 0.05mm). This is relevant when the wires are close to each other. In that case, the radius of the structured sleeve must be equal or smaller to the radius of the real wire. In the unstructured case, such a constraint does not exist, as the radius of the sleeve is determined by the mesh generator. (Fig. 2.19).

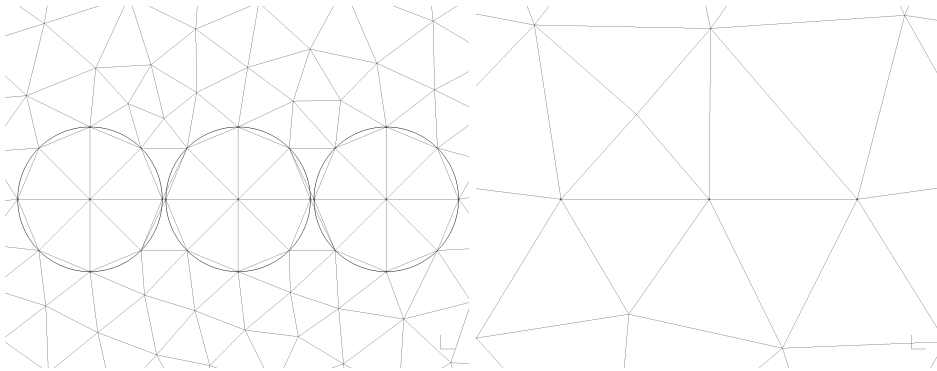


Figure 2.19: Small conductor spacing (2.05mm): Structured Sleeve 1mm (Left), Unstructured Sleeve 3mm (Right)

2.8.1.1. Frequency 1Hz and conductor spacing of 8mm

This test case showcases the behavior of the magnetic vector potential at **low frequencies** when the **conductor spacing is large**.

In Fig 2.20 we observe that the highest local relative error of the **real part** of the magnetic vector potential in the case of structured sleeves remains under 0.1%, 0.6% and 3% for r_{SL} 1mm, 0.5mm and 3mm, respectively. In the case of unstructured sleeves the local error peaks at values of 2.9%, 3.5% and 1.5% for l_c 1mm, 0.5 and 3mm, respectively. Most local values however in the case of structured sleeves remain under a relative error of 0.6% and in the case of unstructured sleeves 1.5%. Note that in the case of unstructured sleeves the behavior is more noisy due to a lack of symmetry and to the fact that the radius used to evaluate the correction field \mathbf{a}_{corr} is an approximation calculated from the area of the sleeve. Furthermore, note that the error peak generated in both cases structured and unstructured at sleeves smaller than the size of the conductor is natural as the correction has only been performed within the sleeve region, hence, part of the singularity remains in the model.

In Fig 2.21, the **imaginary part** of the magnetic vector potential is presented. Under structured sleeves the highest local relative error calculated reports $1.2 \cdot 10^{-4}\%$, $1.8 \cdot 10^{-4}\%$ and $1.2 \cdot 10^{-4}\%$ for r_{SL} 1mm, 0.5mm and 3mm and most local error data points fall under $10^{-4}\%$. In the case of unstructured sleeves the highest local relative error reaches values of $1.4 \cdot 10^{-4}\%$, $1.9 \cdot 10^{-4}\%$ and $1.4 \cdot 10^{-4}\%$ or l_c 1mm, 0.5mm and 3mm, respectively.

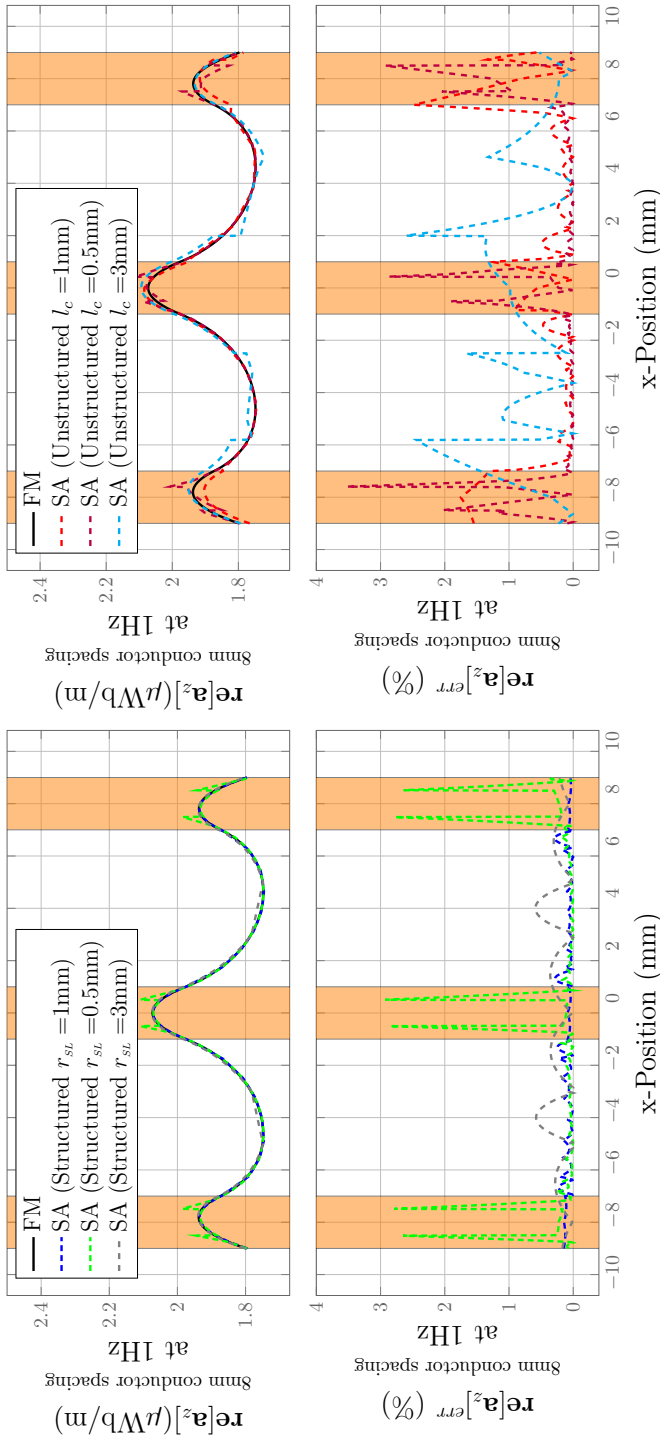


Figure 2.20: Real part of \mathbf{a} in three parallel wires at 1Hz with conductor spacing of 8mm: Structured Sleeves (Left) and Unstructured Sleeves (Right)

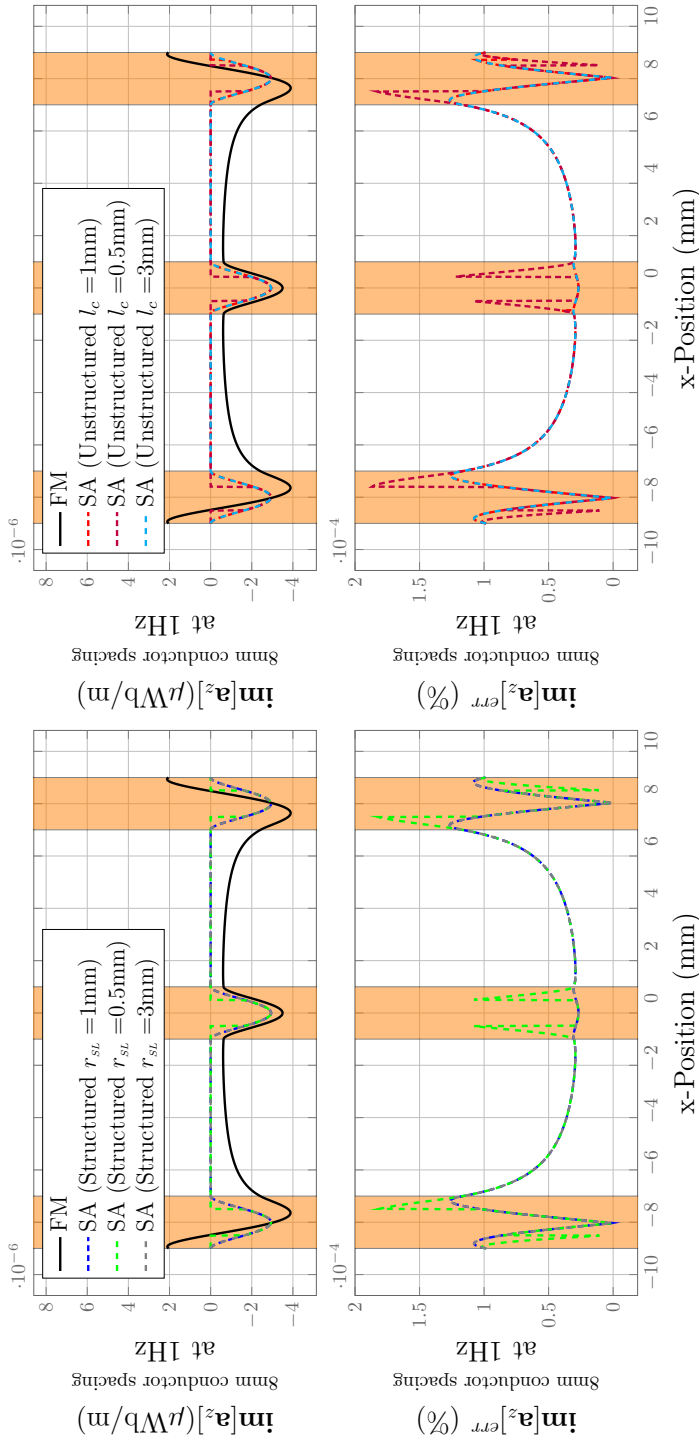


Figure 2.21: Imaginary part of \mathbf{a} in three parallel wires at 1Hz with conductor spacing of 8mm: Structured Sleeves (Left) and Unstructured Sleeves (Right)

2.8.1.2. Frequency 1MHz and conductor spacing of 8mm

This test case showcases the behavior of the magnetic vector potential at **higher frequencies** when the **conductor spacing is large**.

In Fig 2.22 we observe that the highest local relative error of the **real part** of the magnetic vector potential in the case of structured sleeves remains under 2%, 7.9% and 2% for r_{SL} 1mm, 0.5mm and 3mm, respectively. In the case of unstructured sleeves the highest local error peaks at values of 2.9%, 3.5% and 1.5% for l_c 1mm, 0.5 and 3mm, respectively. Note that inside the conductor the error is under 2% for 1mm, 0.5mm structured sleeves and under 3% for 1mm, 0.5mm unstructured sleeves.

In Fig 2.23, the **imaginary part** of the magnetic vector potential is presented. Under structured sleeves the highest local relative error calculated reports 0.15%, 0.39% and 0.15% for r_{SL} 1mm, 0.5mm and 3mm and most local error data points fall under 0.15%. In the case of unstructured sleeves the highest local relative error reaches values of 0.38%, 0.39% and 0.15% for l_c 1mm, 0.5 and 3mm, respectively but most local error data falls under 0.15%.

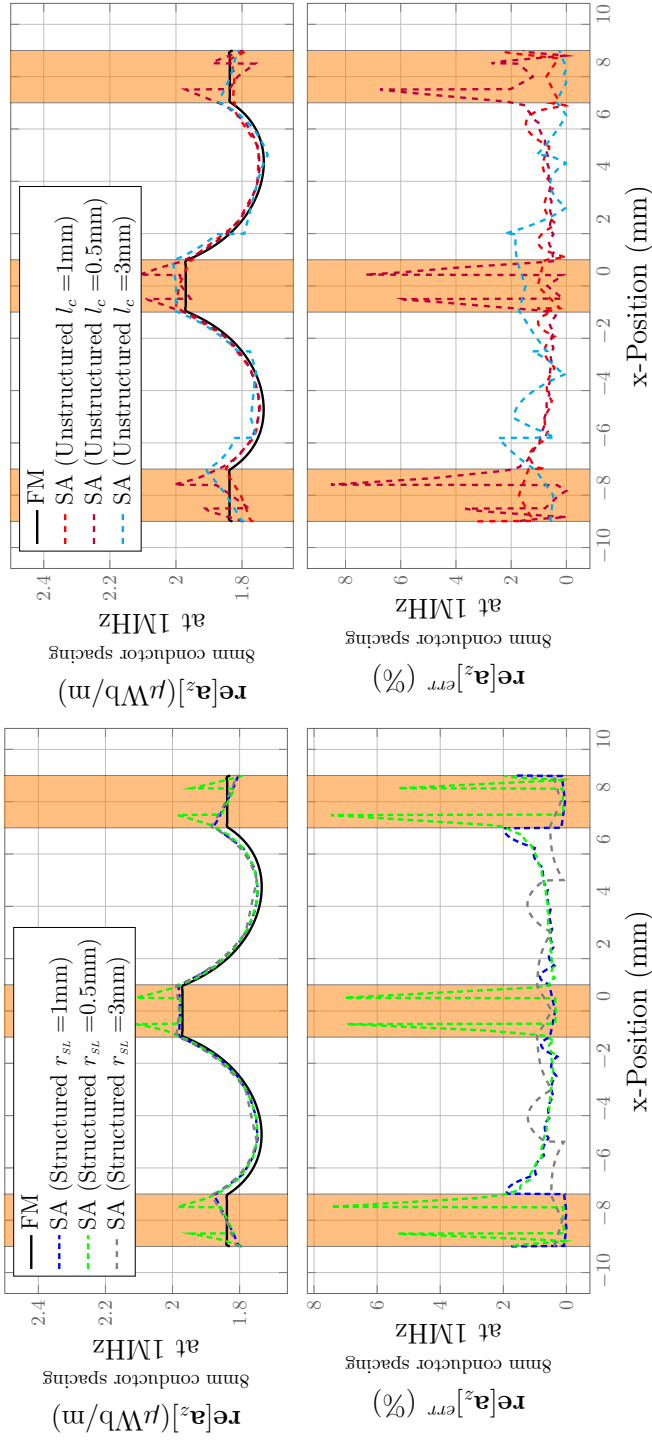


Figure 2.22: Real part of \mathbf{a} in three parallel wires at 1MHz with conductor spacing of 8mm: Structured Sleeves (Left) and Unstructured Sleeves (Right)

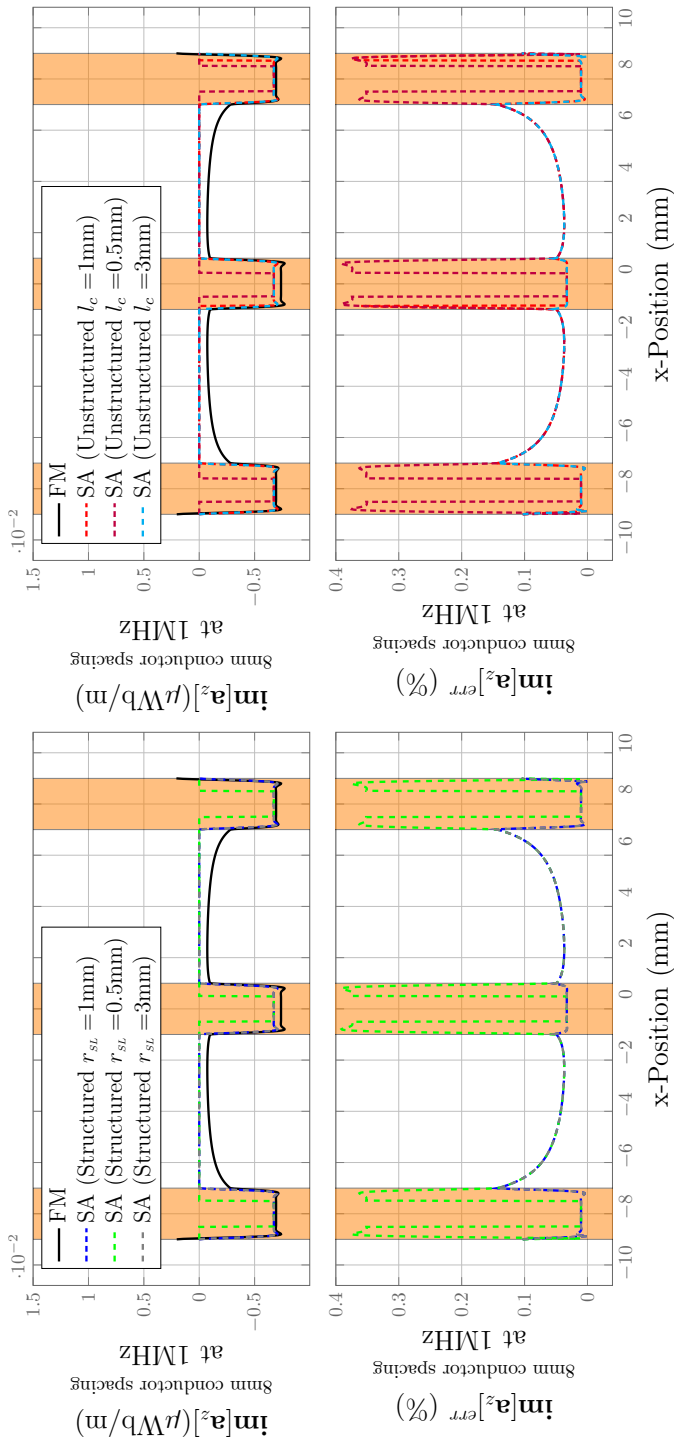


Figure 2.23: Imaginary part of \mathbf{a} in three parallel wires at 1Hz with conductor spacing of 8mm: Structured Sleeves (Left) and Unstructured Sleeves (Right)

2.8.1.3. Frequency 1Hz and conductor spacing of 2.05mm

This test case showcases the behavior of the magnetic vector potential at **lower frequencies** when the **conductor spacing is small**.

In Fig 2.24 we observe that the highest local relative error of the **real part** of the magnetic vector potential in the case of structured sleeves remains under 0.5%, 2.5% for r_{SL} 1mm, 0.5mm, respectively. In the case of unstructured sleeves the highest local error peaks at values of 2%, 6% and 2.25% for l_c 1mm, 0.5 and 3mm, respectively. Note that in this particular test case there is no structured sleeve of 3mm due to geometrical limitations. In the case of unstructured sleeves the limitation does not apply as each conducting node can share common edges.

In Fig 2.25, the **imaginary part** of the magnetic vector potential is presented. Under structured sleeves the highest local relative error calculated reports $5.2 \cdot 10^{-4}\%$, $5.2 \cdot 10^{-4}\%$ for r_{SL} 1mm, 0.5mm, respectively, and most local error data points fall under $3.5 \cdot 10^{-4}\%$. In the case of unstructured sleeves the highest local relative error reaches values of $5.2 \cdot 10^{-4}\%$, $5.2 \cdot 10^{-4}\%$ and $5.2 \cdot 10^{-4}\%$ for l_c 1mm, 0.5 and 3mm, respectively but most local error data falls under $3.5 \cdot 10^{-4}\%$.

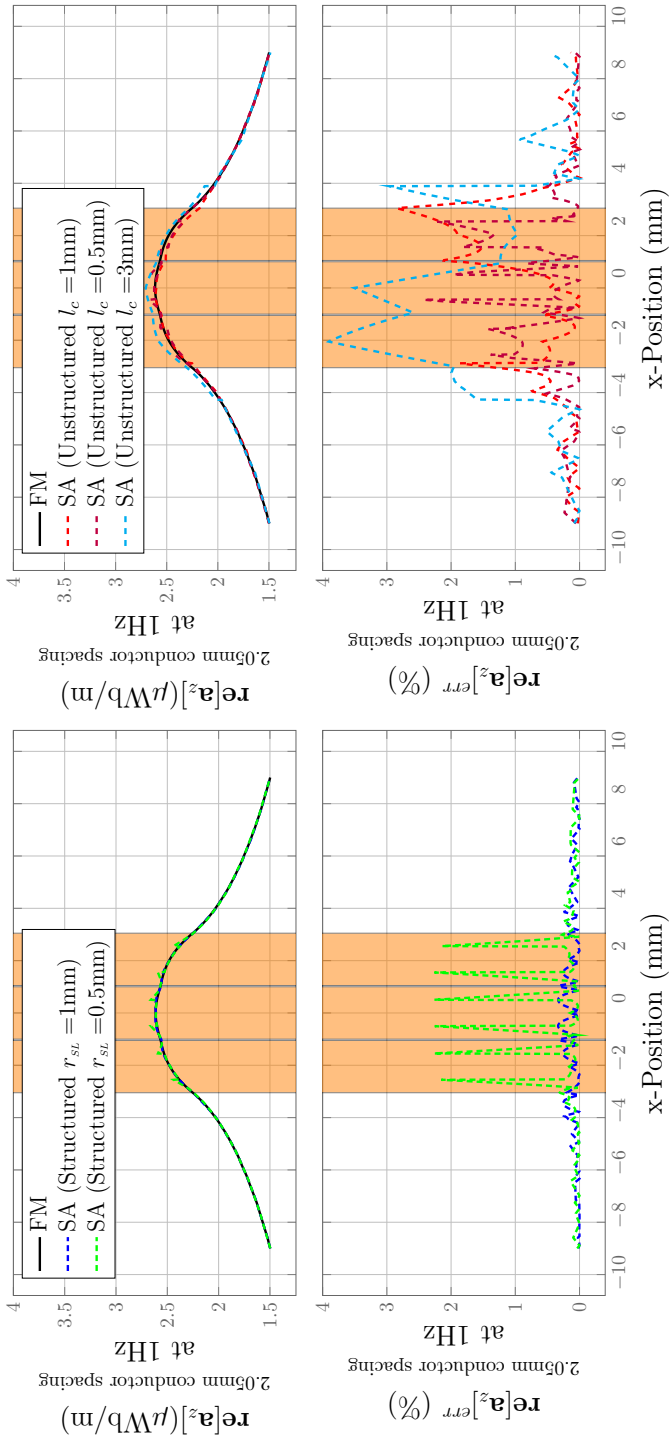


Figure 2.24: Real part of \mathbf{a} in three parallel wires at 1Hz with conductor spacing of 2.05mm: Structured Sleeves (Left) and Unstructured Sleeves (Right)

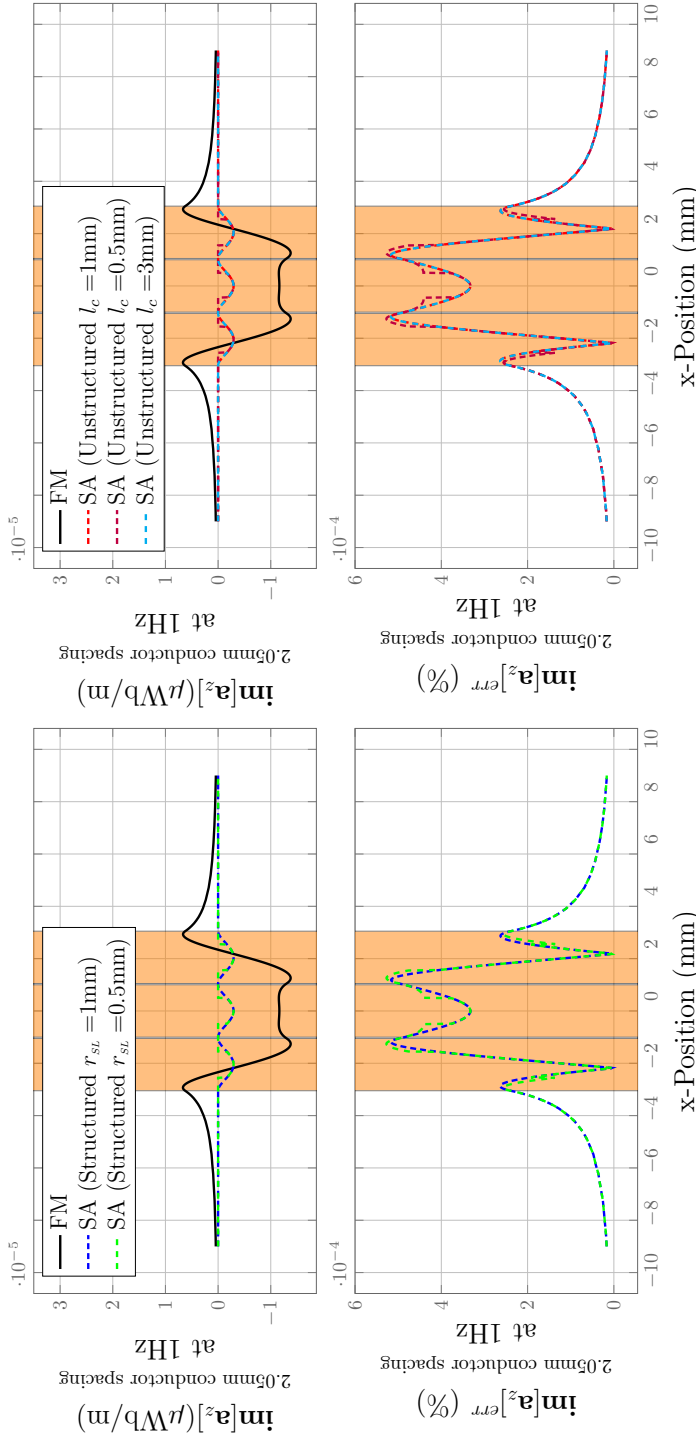


Figure 2.25: Imaginary part of \mathbf{a} in three parallel wires at 1Hz with conductor spacing of 2.05mm: Structured Sleeves (Left) and Unstructured Sleeves (Right)

2.8.1.4. Frequency 1MHz and conductor spacing of 2.05mm

This test case showcases the behavior of the magnetic vector potential at **higher frequencies** when the **conductor spacing is small**.

In Fig 2.26 we observe that the highest local relative error of the **real part** of the magnetic vector potential in the case of structured sleeves remains under 8.2%, 11.9% for r_{SL} 1mm, 0.5mm, respectively. Most error data points fall under 8%. In the case of unstructured sleeves the local error peaks at values of 7%, 11% and 13% for l_c 1mm, 0.5 and 3mm, respectively. Most error data points fall under 8%. Note that in this particular test case there is no structured sleeve of 3mm due to geometrical limitations. In the case of unstructured sleeves the limitation does not apply as each conducting node can share common edges.

In Fig 2.27, the **imaginary part** of the magnetic vector potential is presented. Under structured sleeves the highest local relative error calculated reports 0.63%, 0.79% for r_{SL} 1mm, 0.5mm, respectively, and most local error data points fall under 0.5% . In the case of unstructured sleeves the highest local relative error reaches values of 0.62%, 0.79% and 0.63% or l_c 1mm, 0.5 and 3mm, respectively but most local error data fall under 0.5%.

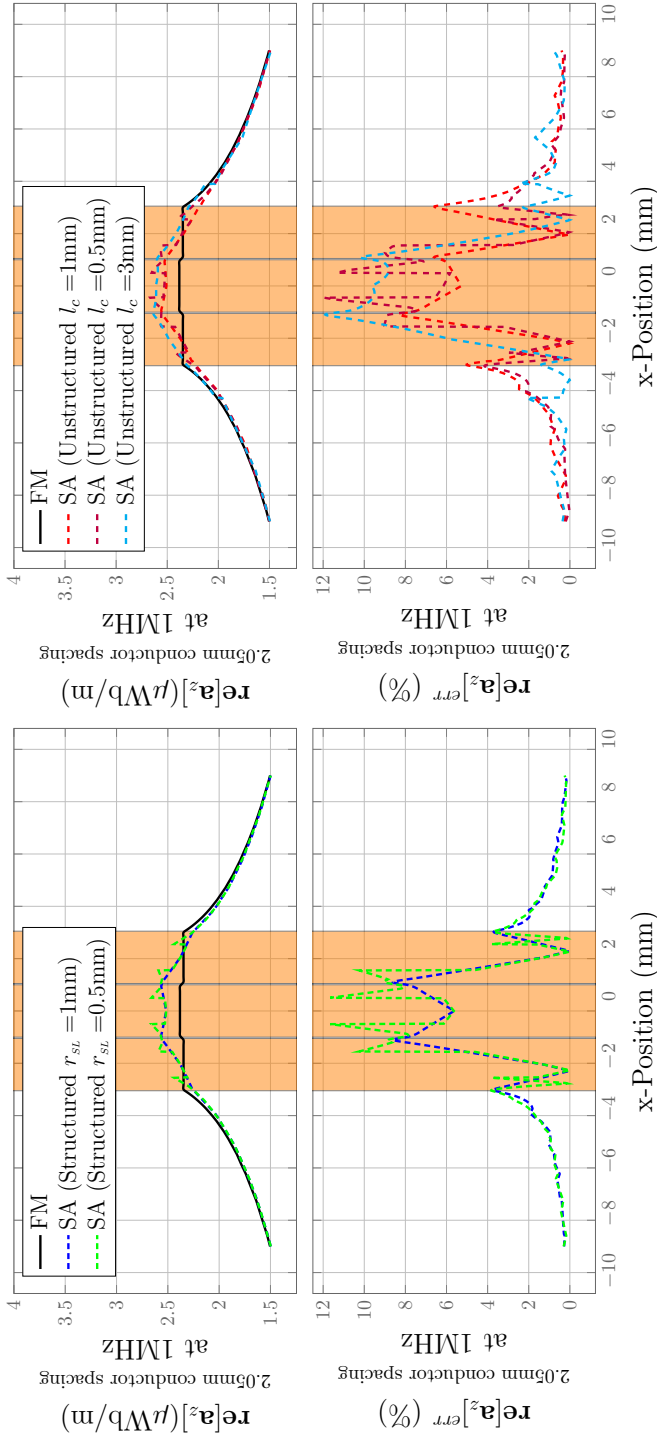


Figure 2.26: Real part of \mathbf{a} in three parallel wires at 1 MHz with conductor spacing of 2.05 mm: Structured Sleeves (Left) and Unstructured Sleeves (Right)

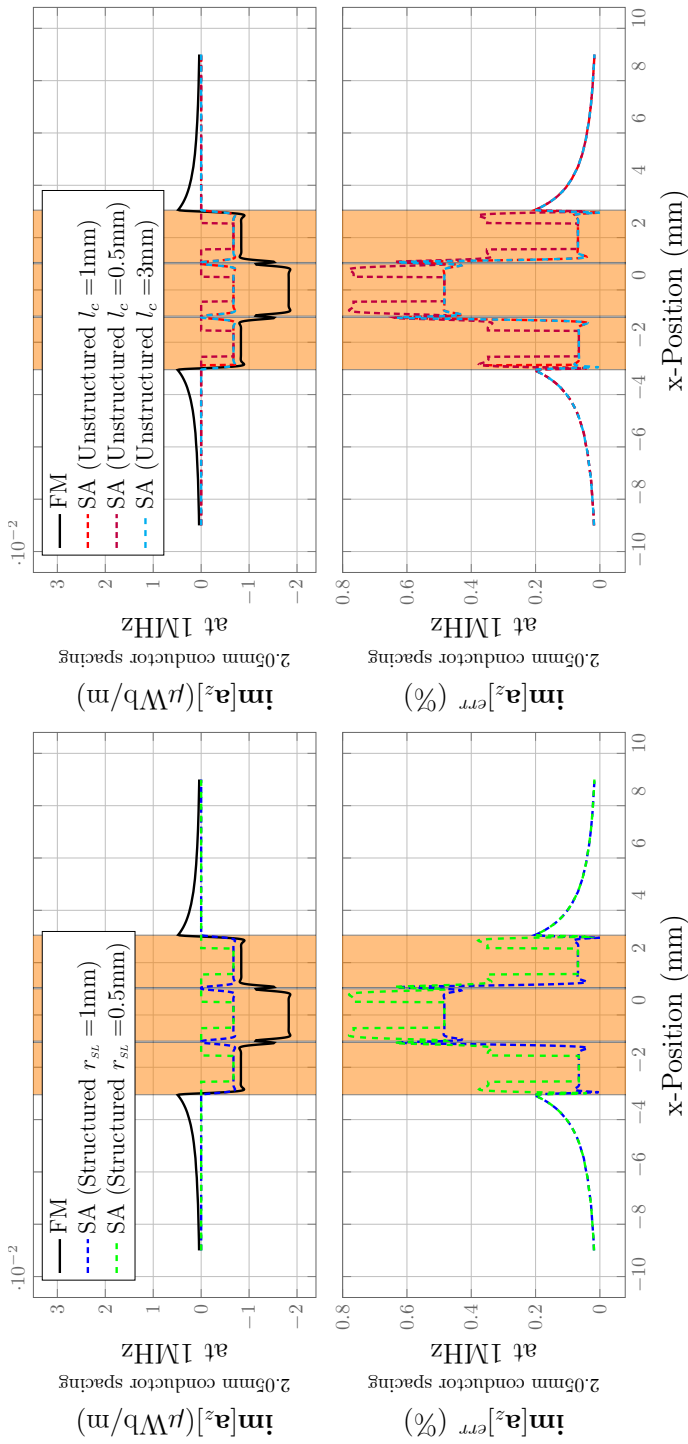


Figure 2.27: Imaginary part of \mathbf{a} in three parallel wires at 1MHz with conductor spacing of 2.05mm: Structured Sleeves (Left) and Unstructured Sleeves (Right)

2.8.1.5. Conclusion - Local Agreement

The local correction of field solution shows a great level of accuracy when compared to the reference solution of a fully discretized model (FM) at low (1Hz) and higher frequencies (1MHz). Furthermore, the validity of the method was also tested in cases where the conductor spacing is extremely small, i.e., when the conductors were nearly touching each other. In the latter case shows that although the accuracy of the method is clear, the method needs further development to account for not only skin but also proximity effects.

These studies were also performed and tested using structured and unstructured sleeves of different sizes. The goal is that of verification that the removal of the singularity also eliminates the mesh dependency of the method. This test was successful in the structured and unstructured sleeve cases. The results of the structured sleeves however are smoother, which is natural as the radius of the sleeve is indeed known and not approximated via the surface of the sleeve.

2.8.2. Global Agreement - Inductance Matrix

In this section we focus on the accuracy of the results at a global level. The numerical tests target the accuracy of the Semi-Analytical method in the calculation of a system of parallel wires. The solutions are compared against the full model for both self L_i and mutual $M_{i,j}$ inductance of 3 parallel wires. Due to symmetry only three components of the mutual inductance matrix are presented (i.e. $M_{2,1}$, $M_{3,1}$ and $M_{3,2}$). Similarly, as in the previous section all cases are displayed and compared against structured and unstructured sleeves of different sizes, and comparing the solution obtained at a broad range of frequencies at close (2.05mm) and distant (8mm) conductor spacing. All testing conditions remain the same. All plots present a vertical line depicting $\delta = R$, this is meant to indicate the frequency at which the skin-depth and the radius of the conductor are equal.

2.8.2.1. Self-Inductance

This test case showcases the behavior of the self inductance at a broad range of frequencies when the conductor spacing is both large (8mm) and small (2.05mm). The comparisons of the fully discretized model (FM) against the semi-analytical model using structured sleeves are presented to the left, and to the right the comparisons against unstructured sleeves. Furthermore, each solution presents their relative error appended at the bottom part of the figure.

Self-Inductance of 3 parallel conductors at a spacing of 8mm

Fig 2.28 reports the results in the case of using sleeve radii of the **same size** as the radius of the actual physical conductor (1mm). A great level of agreement is observed in the inductance values using structured sleeves and confirmed by the relative error. The error remains steady close to zero to frequencies under $\delta = R$ and start slowly rising as frequency increases. The error values of L_1 and L_3 are roughly the same and remain under 0.4% in the MHz range, and L_2 rises up smoothly to an error of 0.61 in the MHz range. In the case of unstructured sleeves, the self inductance of each wire as expected is slightly different. The difference relies in the fact that the background field and the correction rely on the assumption of a symmetric sleeve. However, the error values at low frequencies remains around 4.5%, 0.8% and 2.5% and slowly decrease at frequencies about the $\delta = R$ line to values around 4.2%, $10^{-3}\%$ and 2.2% for L_1 , L_2 , and L_3 , respectively, in the MHz range.

Fig 2.29 reports the results in the case of using sleeve radii **smaller** than the radius of the actual physical conductor (0.5mm). In the structured sleeve case (left), the relative error lies around 14% and slowly increases past the $\delta = R$ limit to values of 15.4% and 15.4% for L_2 , $L_1 = L_3$, respectively. In the unstructured sleeve case (right) once again each inductance value is relatively different, however they still remain around the same order of magnitude. The error values at low frequencies remains around 16.2%, 14.1% and 16.8% and slowly increase at frequencies about

the $\delta = R$ line to values around 17.8%, 15.5% and 17.4% for L_1 , L_2 , and L_3 , respectively, in the MHz range.

Fig 2.30 reports the results in the case of using sleeve radii **larger** than the radius of the actual physical conductor (3mm). In the structured sleeve case (left), the values at low frequency the relative error is steady at 22.23%, 22.1% and 22.05% and slowly increase past the $\delta = R$ limit to values of 23%, 22.88% and 22.7% for L_1 , L_1 , and L_3 , respectively. Note that unlike the previous two cases, there's a dip in error right after the $\delta = R$ limit and picks up again slowly right after. In the unstructured sleeve case (right) once again each inductance value is relatively different, however they still remain around the same order of magnitude. The error values at low frequencies remains around 21.4%, 22.6% and 19.5% and slowly increase at frequencies about the $\delta = R$ line to values around 22%, 23.1% and 20% for L_1 , L_2 , and L_3 , respectively, in the MHz range.

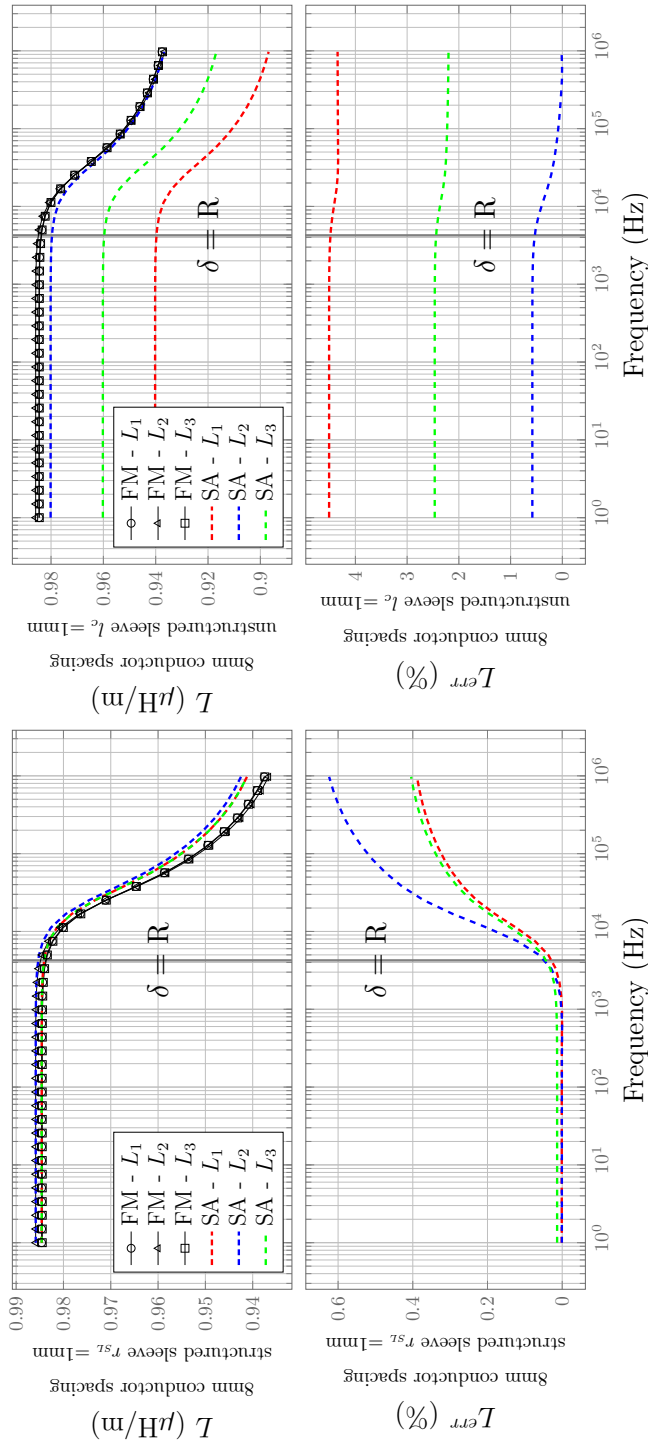


Figure 2.28: Self inductance with conductor spacing of 8mm using sleeve parameter of 1mm: Structured Sleeves (Left) and Unstructured Sleeves (Right)

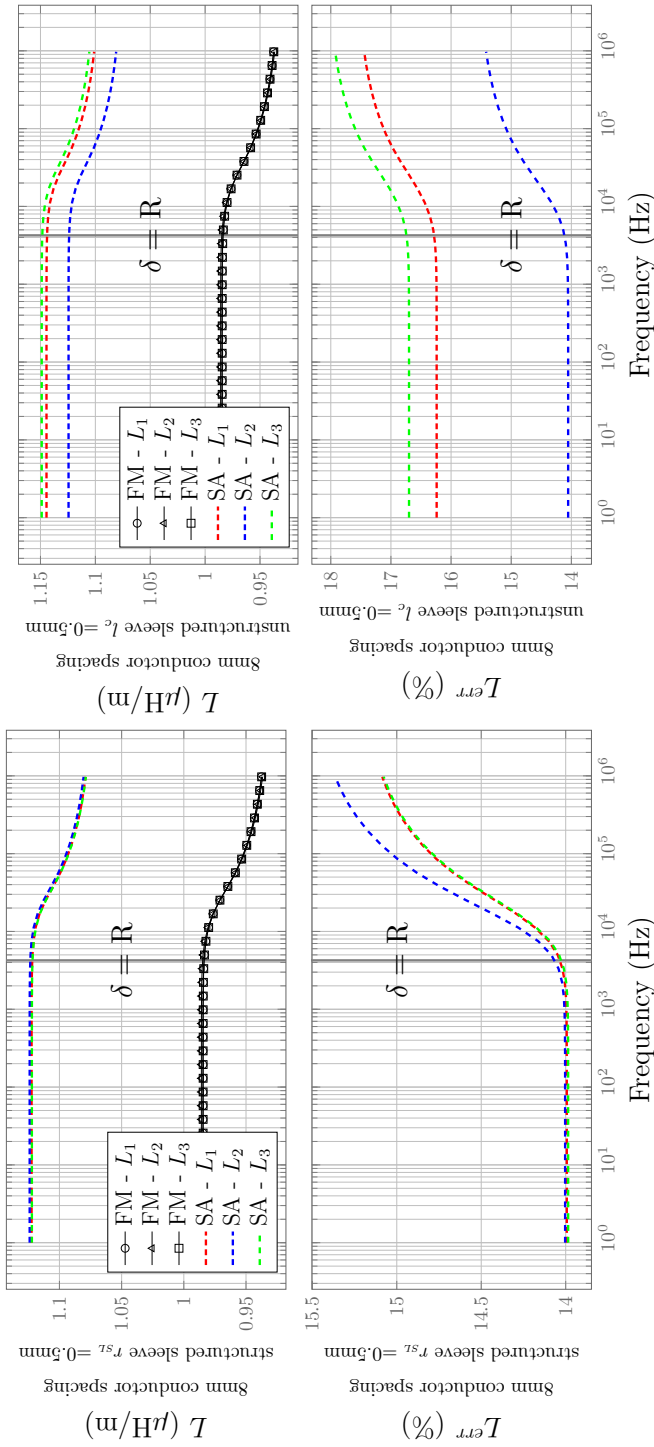


Figure 2.29: Self inductance with conductor spacing of 8mm using sleeve parameter of 0.5mm: Structured Sleeves (Left) and Unstructured Sleeves (Right)

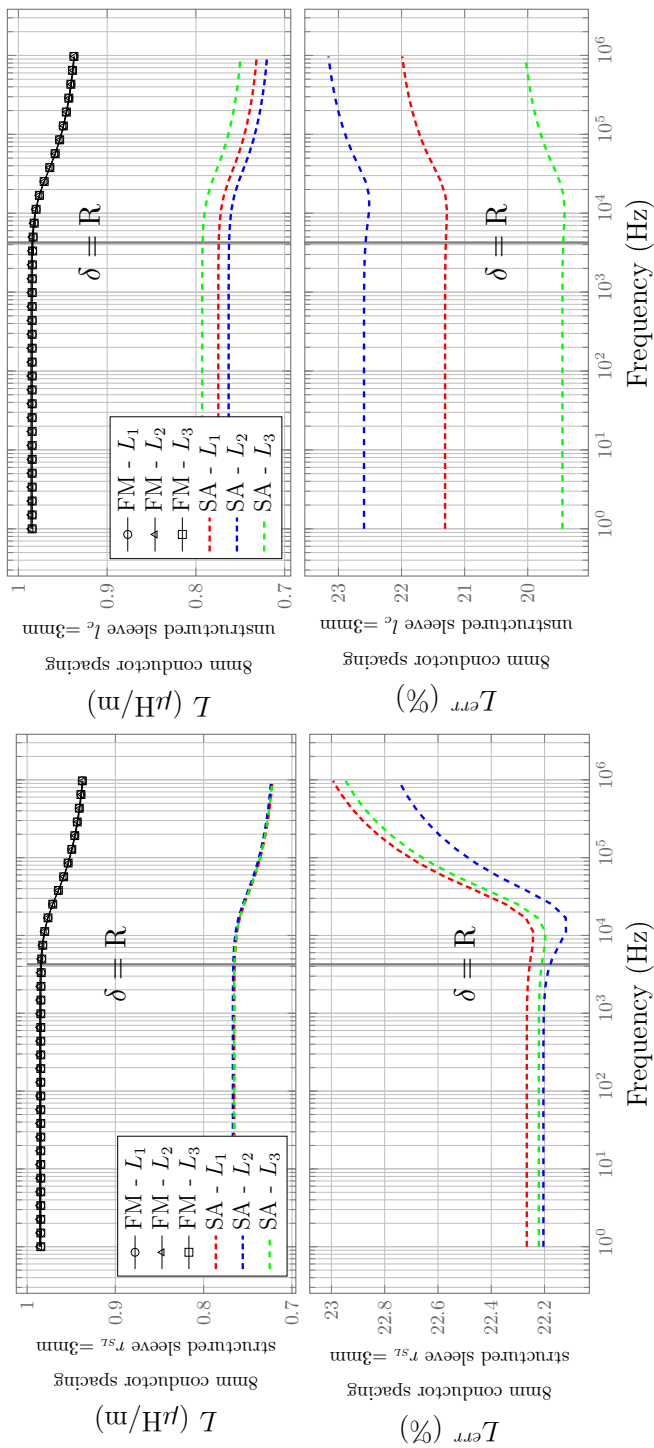


Figure 2-30: Self inductance with conductor spacing of 8mm using sleeve parameter of 3mm: Structured Sleeves (Left) and Unstructured Sleeves (Right)

Self-Inductance of 3 parallel conductors at a spacing of 2.05mm

Fig 2.31 reports the results in the case of using sleeve radii of the **same size** as the radius of the actual physical conductor (1mm). In the case of structured sleeves (left), the error remains steady close to zero at frequencies under $\delta = R$ and start slowly rising as frequency increases. The error values of L_1 and L_3 are roughly the same and reach 10.1% relative error in the MHz range, and L_2 rises up smoothly to an error of 15% in the MHz range. In the case of unstructured sleeves, the self inductance of each wire as expected is slightly different. The difference relies in the fact that the background field and the correction rely on the assumption of a symmetric sleeve. However, the error values at low frequencies remains around 2.5%, 1.9% and $10^{-3}\%$ and slowly increases at frequencies about the $\delta = R$ line to values around 9%, 15.5% and 10.1% for L_1 , L_2 , and L_3 , respectively, in the MHz range.

Fig 2.32 reports the results in the case of using sleeve radii **smaller** than the radius of the actual physical conductor (0.5mm). In the case of structured sleeves (left), the error remains steady close to 14% at frequencies under $\delta = R$ and start slowly rising as frequency increases. The error values of L_1 and L_3 are roughly the same and reach 26% relative error in the MHz range, and L_2 rises up smoothly to an error of 29% in the MHz range. In the case of unstructured sleeves the difference relies in the fact that the background field and the correction rely on the assumption of a symmetric sleeve. However, the error values at low frequencies remains around 14%, 16% and 15% and slowly increases at frequencies about the $\delta = R$ line to values around 26%, 32% and 27% for L_1 , L_2 , and L_3 , respectively, in the MHz range.

To make a fair comparison between structured and unstructured sleeves, note that we are only comparing structured and unstructured sleeves of radii: 1mm and 0.5mm, as the structured sleeve in the case 3mm is limited by the distance between conductors.

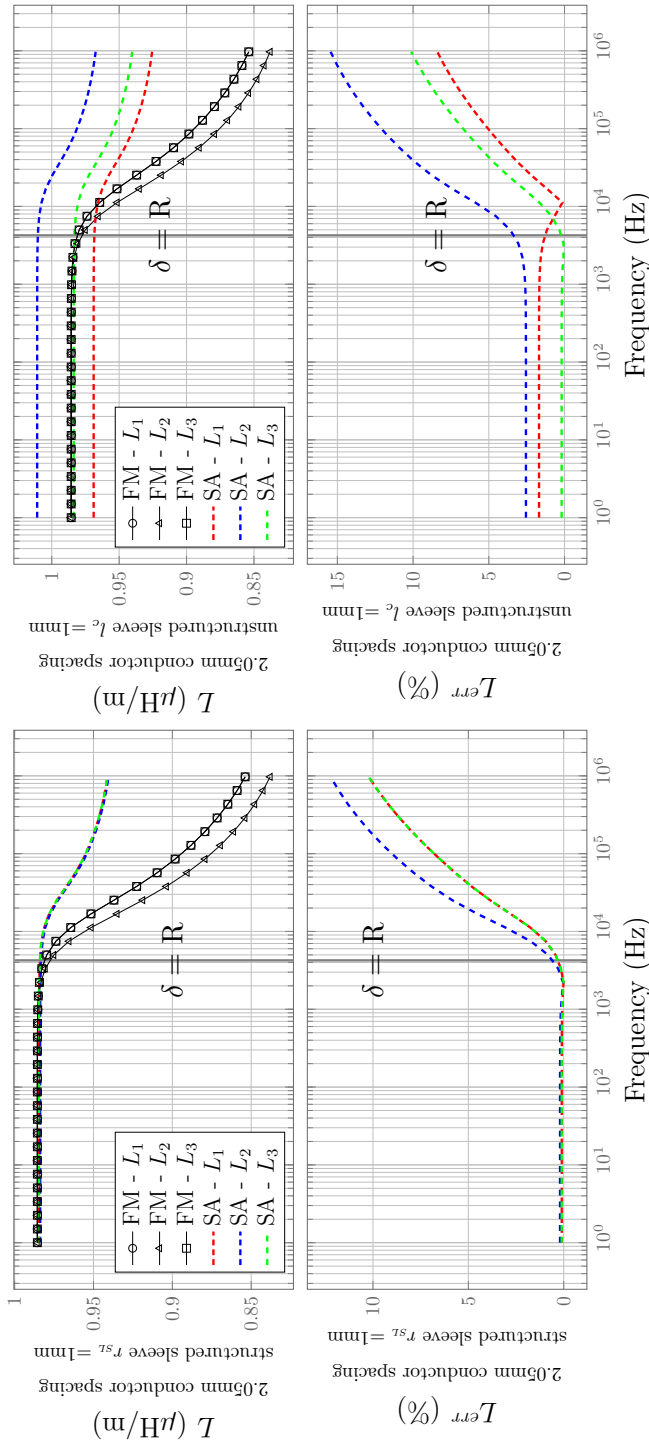


Figure 2.31: Self inductance with conductor spacing of 2.05mm using sleeve parameter of 1mm: Structured Sleeves (Left) and Unstructured Sleeves (Right)

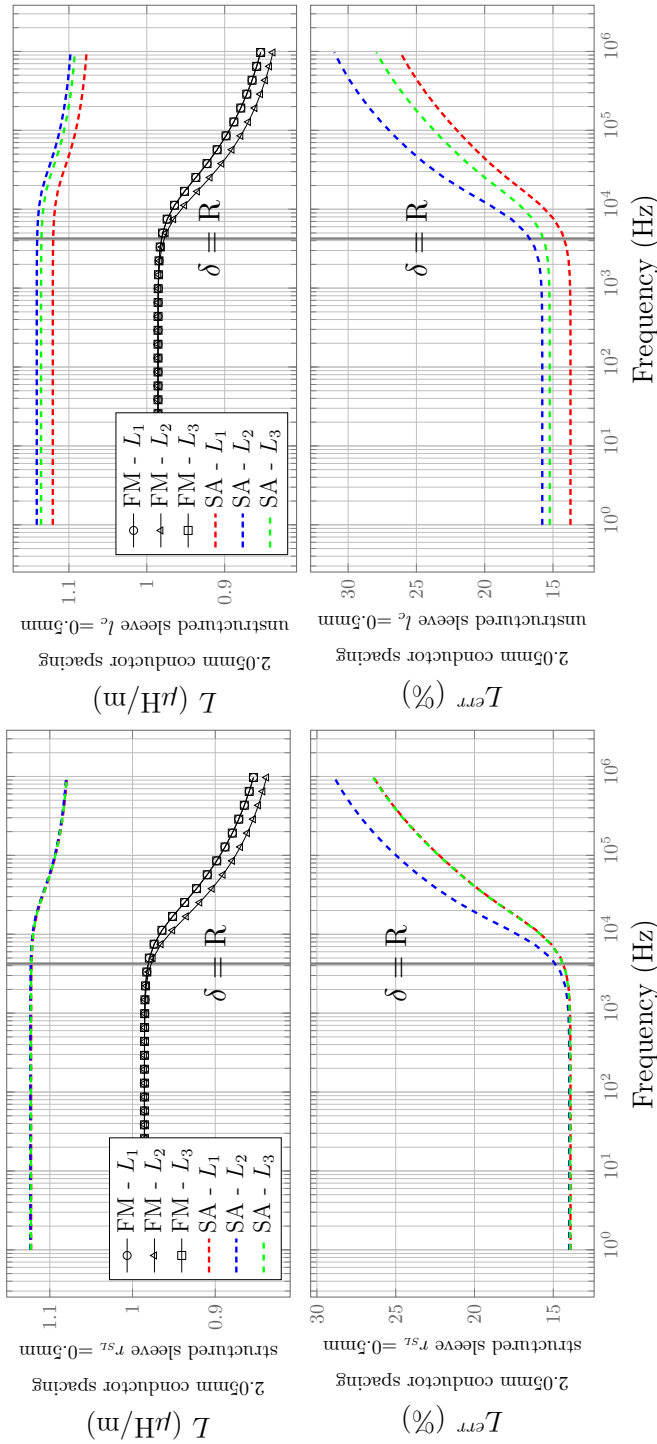


Figure 2.32: Self inductance with conductor spacing of 2.05mm using sleeve parameter of 0.5mm: Structured Sleeves (Left) and Unstructured Sleeves (Right)

2.8.2.2. Mutual-Inductance

This test case showcases the behavior of the mutual inductance at a broad range of frequencies when the conductor spacing is both large (8mm) and small (2.05mm). The comparisons of the fully discretized model (FM) against the semi-analytical model using structured sleeves are presented to the left, and to the right the comparisons against unstructured sleeves. Furthermore, each solution presents their relative error appended at the bottom part of the figure.

Mutual Inductance of 3 parallel conductors at a spacing of 8mm

Fig 2.33 reports the results in the case of using sleeve radii of the **same size** as the radius of the actual physical conductor (1mm). In the case of structured sleeves (left) the relative error in the low frequency range stays at a negligible value. At higher frequencies it raises to 0.25%, 0.75% and 0.25% for M_{21} , M_{21} and M_{21} at the MHz range. In the unstructured sleeve case (right), the relative error at lower frequencies remain at negligible values for M_{31} and M_{32} and around 0.16% for M_{21} . At frequencies past the $\delta = R$ line the error increases slowly to values of 0.39%, 0.77% and 0.24% for M_{21} , M_{31} and M_{32} at the MHz range.

Fig 2.34 reports the results in the case of using sleeve radii of **smaller** size than the radius of the actual physical conductor (0.5mm). In the case of structured sleeves (left) the relative error in the low frequency range stays at a negligible value. At higher frequencies it raises to 0.29%, 0.77% and 0.29% for M_{21} , M_{31} and M_{32} at the MHz range. In the unstructured sleeve case (right), the relative error at lower frequencies remain about 0.05% for M_{21} and M_{31} and M_{32} . At frequencies past the $\delta = R$ line the error increases slowly to values of 0.25%, 0.75% and 0.3% for M_{21} , M_{31} and M_{32} at the MHz range. An observation to be noted is that the relative error values dip past the $\delta = R$ line before having an error increase.

Fig 2.35 reports the results in the case of using sleeve radii **larger** than the radius of the actual physical conductor (3mm). In the case of structured sleeves (left) the relative error in the low frequency range stays at a negligible value. At higher frequencies it raises to 0.3%, 0.79% and 0.3% for M_{21} , M_{31} and M_{32} at the MHz range. In the unstructured sleeve case (right), the relative error at lower frequencies remain at a negligible error value for M_{21} , and around 1.6% and 2.5% for M_{31} for M_{32} . At frequencies past the $\delta = R$ line the error increases slowly to values of 0.2%, 0.9% and 2.8% for M_{21} , M_{31} and M_{32} at the MHz range.

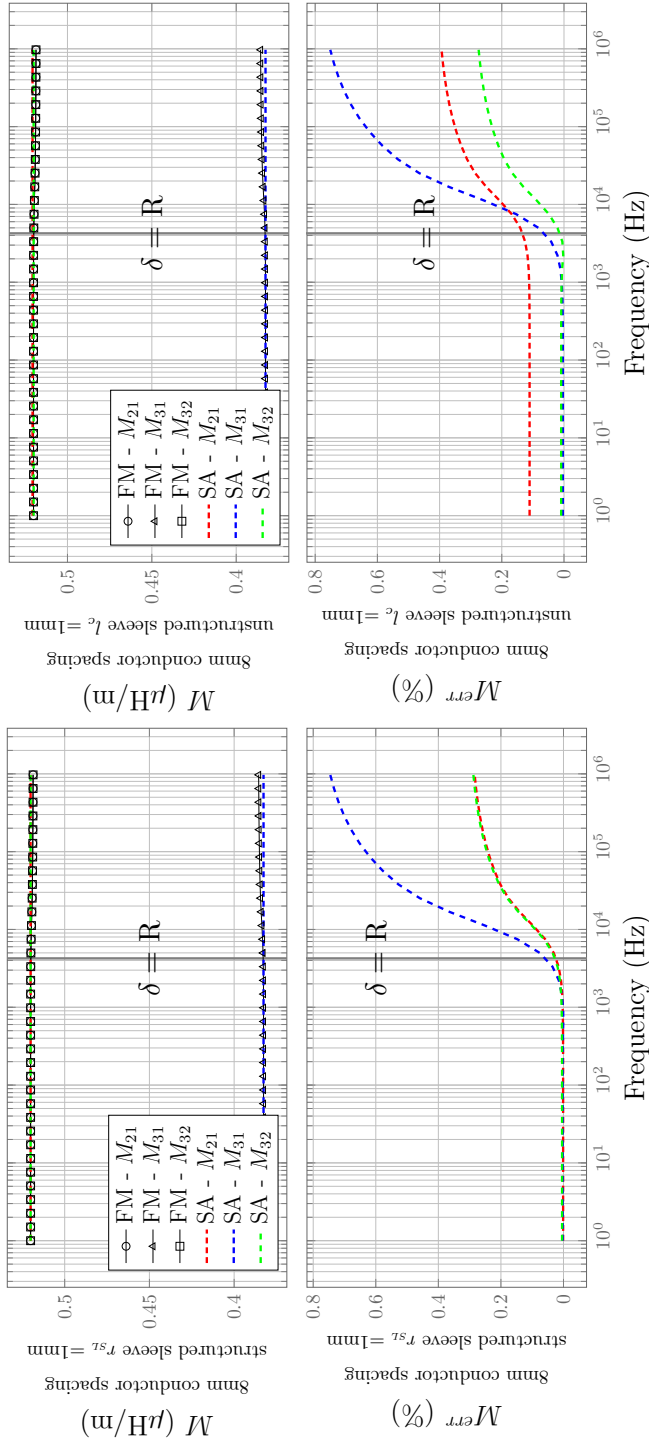


Figure 2.33: Self inductance with conductor spacing of 8mm using sleeve parameter of 1mm: Structured Sleeves (Left) and Unstructured Sleeves (Right)

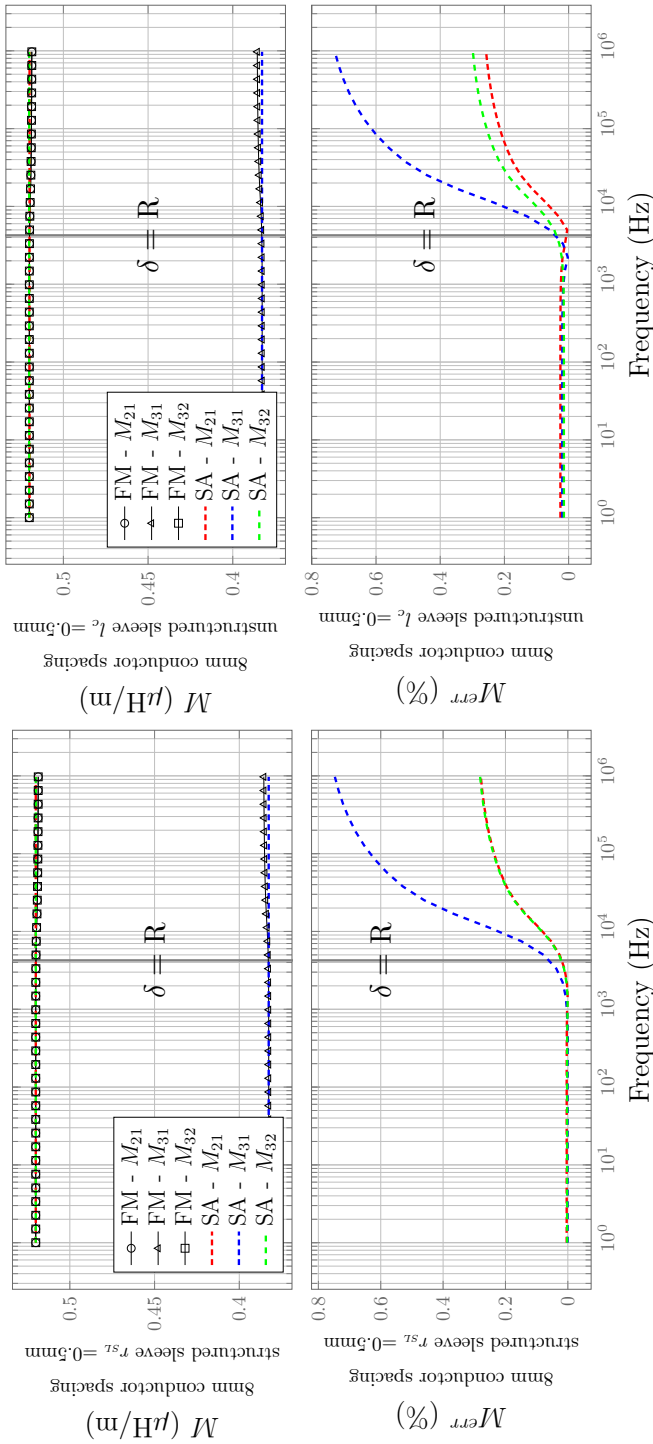


Figure 2.34: Self inductance with conductor spacing of 8mm using sleeve parameter of 0.5mm: Structured Sleeves (Left) and Unstructured Sleeves (Right)

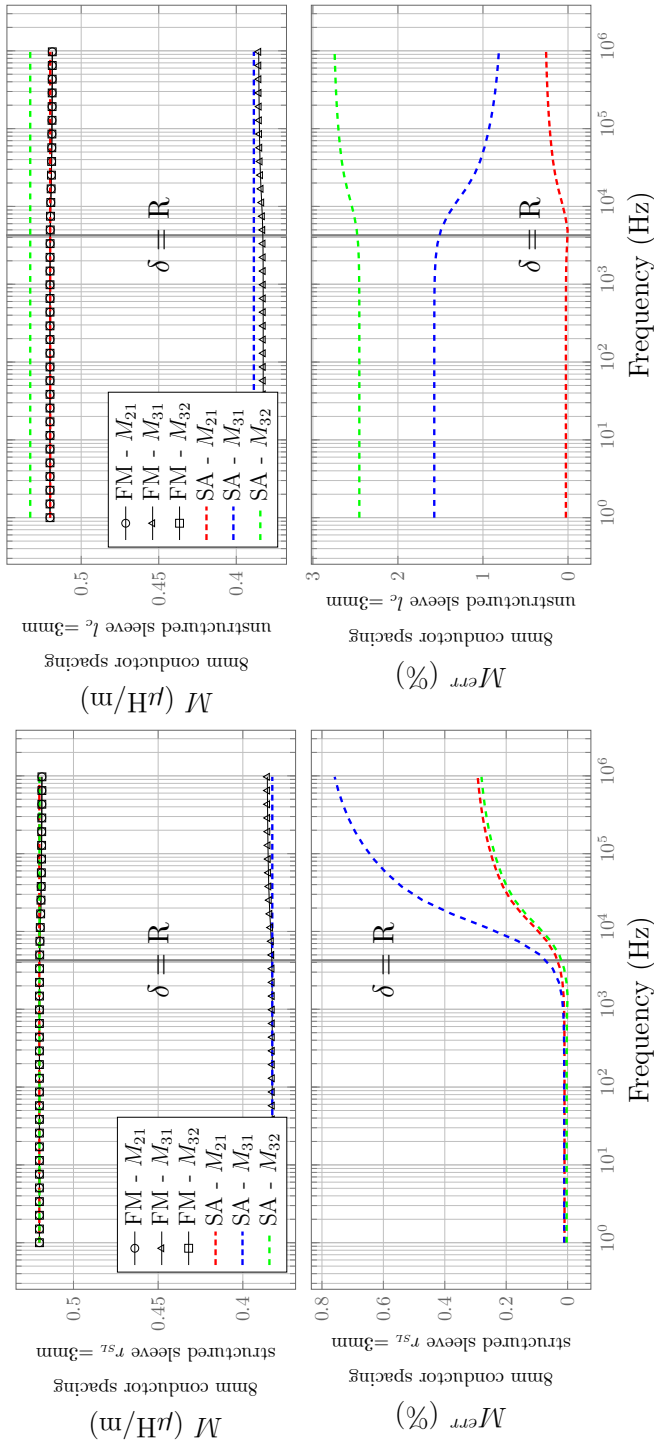


Figure 2.35: Self inductance with conductor spacing of 8mm using sleeve parameter of 3mm: Structured Sleeves (Left) and Unstructured Sleeves (Right)

Mutual Inductance of 3 parallel conductors at a spacing of 2.05mm

Fig 2.36 reports the results in the case of using sleeve radii of the **same size** as the radius of the actual physical conductor (1mm). In the case of structured sleeves (left) the relative error in the low frequency range stays at negligible levels. At higher frequencies it raises to 2.1%, 9.9% and 2.1% for M_{21} , M_{21} and M_{21} at the MHz range. In the unstructured sleeve case (right), the relative error at lower frequencies remain about 3%, 1.4% and 1.6% for M_{21} , M_{31} and M_{32} respectively. At frequencies past the $\delta = R$ line the error increases slowly to values of 5%, 9% and 3.5% for M_{21} , M_{31} and M_{32} at the MHz range.

Fig 2.37 reports the results in the case of using sleeve radii of **smaller size** than the radius of the actual physical conductor (0.5mm). In the case of structured sleeves (left) the relative error in the low frequency range stays at a negligible value. At higher frequencies it raises to 2.1%, 9.9% and 2.1% for M_{21} , M_{31} and M_{32} at the MHz range. In the unstructured sleeve case (right), the relative error at lower frequencies remain about 0.2%, 0.1% and 0.1% for M_{21} , M_{31} and M_{32} . At frequencies past the $\delta = R$ line the error increases slowly to values of 2.2%, 9.9% and 2% for M_{21} , M_{31} and M_{32} at the MHz range.

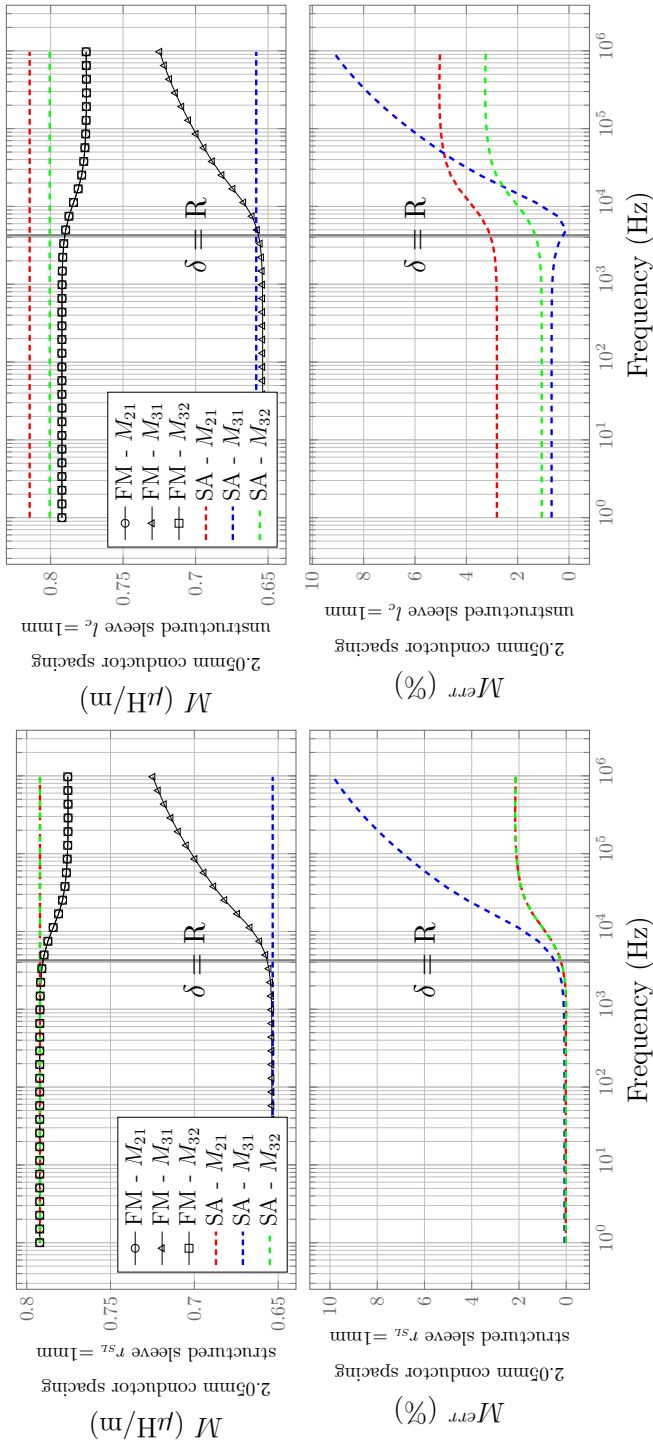


Figure 2.36: Self inductance with conductor spacing of 2.05mm using sleeve parameter of 1mm: Structured Sleeves (Left) and Unstructured Sleeves (Right)

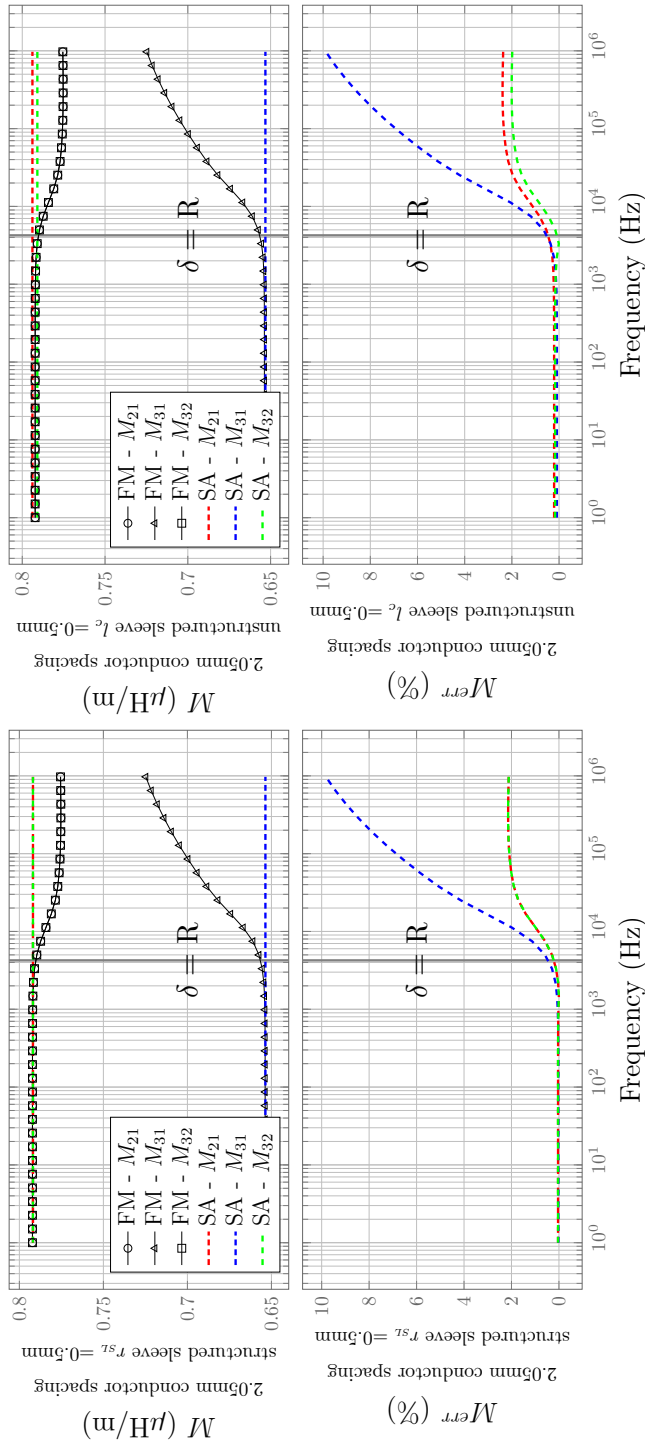


Figure 2.37: Self inductance with conductor spacing of 2.05mm using sleeve parameter of 0.5mm: Structured Sleeves (Left) and Unstructured Sleeves (Right)

2.8.3. Conclusions

This section builds the theoretical framework used in the modeling of thin wires. The chapter first introduces a truncation technique to remove the singularity obtained from the thin wire approximation. The technique relies on the integration of a subproblem (i.e. sleeve), which removes the singularity while keeping the right solution of the background field. The analytical solution of a conductor in isolation under net current $I \neq 0$ is then used as a correction factor to reconstruct the frequency dependent distribution of the magnetic vector potential in the sleeve domain.

The model case describes 3 wires. This model is tested for local and global accuracy. Every test is presented to account for small (2.05mm) and large (8mm) conductor spacing. Furthermore, three different sleeve radii are compared to test accuracy under radii: smaller, equals and larger than the size of the physical conductor. The inductance matrix is also presented to study at frequencies where the skin depth becomes smaller than the size of the conductor $\delta \leq R$.

The frequency values become an important indicative in the accuracy of the method. Note that at lower frequencies below the $\delta = R$ line the values are roughly the same as in the case of fully discretized conductors. This can be observed locally and globally through the magnetic vector potential plots and the inductance matrix respectively. At frequencies past the $\delta = R$ the relative error increases slowly but steadily. This can be observed locally in the case of 1MHz and globally in the inductance matrix for all values past $\delta = R$. This becomes evident as the proximity effects are not properly accounted for and this can be corroborated by the short conductor spacing case where the error becomes more pronounced. Further treatment to account for proximity effects in the modeling of thin conductors is needed.

This method is intended to be mesh-independent. The studies for different sleeve sizes make it clear that for structured sleeves, the results are smoother and more agreeable. On the other hand, in the case of unstructured sleeves, the solution is not as smooth as in the case of structured sleeves, yet there is also an excellent level of agreement compared to the fully discretized method. The solution of unstructured sleeves is expected to be less accurate as the symmetry of the sleeve is lost, and the radius of the sleeve included in the correction term is calculated from the sleeve area, which does not necessarily have radial symmetry.

In this chapter we have provided an efficient method to model thin wires accounting for skin effect in a FE framework without much loss of accuracy. However, in the case-study of short conductor spacing, it is clear that proximity effects need to be accounted for to increase the accuracy in the field solution.

Semi-Analytical Modeling of the Proximity Effect in Thin Wires

In the previous chapter the solution in the sleeve was reconstructed to account for skin effect only, but an additional treatment is needed to account for proximity effects. For this purpose, a second analytical solution is needed to correct the computed field, that of a single cylindrical conductor immersed in a uniform harmonic B -field. Under such conditions, the conductor behaves as a massive conductor and develops internal currents by proximity effect with a zero net current $I = 0$. The analytical solution is developed in this chapter and validated against a fully discretized model and then the correction factor is tested on our 3 parallel wire model.

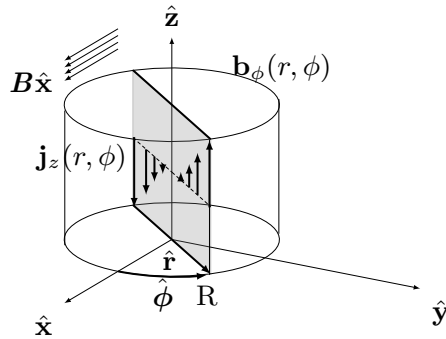


Figure 3.1: Proximity excitation.

3.1. Analytical Modelling of a Wire Subjected to an External Magnetic Field

In this case, the current density flows in the $\hat{\mathbf{z}}$ -direction (Fig. 3.1), except that the magnetic vector potential will vary along both axes: $\hat{\mathbf{r}}$ and $\hat{\phi}$. For readability let us rewrite (2.10)

$$r^2 \partial_r^2 \mathbf{a}_z + r \partial_r \mathbf{a}_z + k^2 r^2 \mathbf{a}_z = -\partial_\phi^2 \mathbf{a}_z \quad (3.1)$$

Using separation of variables we substitute $\mathbf{a}_z(r, \phi) = R(r)\Phi(\phi)$ into our partial differential equation and we obtain

$$r^2 R(r)'' \Phi(\phi) + r R(r)' \Phi(\phi) + k^2 r^2 R(r) \Phi(\phi) = -R(r) \Phi(\phi)''$$

Multiply both sides by $\frac{1}{R(r)\Phi(\phi)}$ in order to split our functions

$$r^2 \frac{R(r)''}{R(r)} + r \frac{R(r)'}{R(r)} + k^2 r^2 = -\frac{\Phi(\phi)''}{\Phi(\phi)} = \lambda^2$$

where the complex wavenumber $k = \sqrt{-i\omega\mu\sigma}$.

We can now solve each partial differential equation separately by using the separation constant $\pm\lambda^2$. Hence

$$\Phi(\phi)'' \pm \lambda^2 \Phi(\phi) = 0 \quad (3.2)$$

$$r^2 R(r)'' + r R(r)' + (k^2 r^2 \pm \lambda^2) R(r) = 0 \quad (3.3)$$

The general solution of (3.3)

$$R(r)'' + \frac{1}{r} R(r)' + \left(n^2 + k^2 - \frac{\lambda^2}{r^2} \right) R(r) = 0$$

Under the assumption of a positive separation constant $\lambda^2 > 0$ we obtain the general solution for both differential equations

$$R(r) = \sum_{\lambda=0}^{\infty} A_{\lambda} J_{\lambda}(kr) + B_{\lambda} Y_{\lambda}(kr), \quad r \leq R \quad (3.4a)$$

$$R(r) = C|r|^{\lambda} + D|r|^{-\lambda}, \quad r > R \quad (3.4b)$$

The radial is solution is composed of two different solutions, the first one being inside the conductor, described by the Bessel equation, and the latter outside of the conductor described by the second order Euler equation.

The angular solution is, on the other hand, described by the simple harmonic motion equation

$$\Phi(\phi) = E \sin(\lambda\phi) + F \cos(\lambda\phi) \quad (3.5)$$

The round conductor is immersed in a homogeneous magnetic field in the $\mathbf{B} = \hat{B}\hat{\mathbf{x}}$ direction. In cylindrical coordinates it is expressed as $\mathbf{B} = \hat{B} \cos \phi \hat{\mathbf{r}}$. Hence, at infinity the magnetic vector potential may be written as $\mathbf{a}_z = \hat{B}r \sin \phi \hat{\mathbf{z}}$. This enables us to set $\lambda = 1$ and obtaining constants $F = 0$ and $C = \hat{B}$ and $E = 1$

We can re-write the magnetic vector potential as

$$\mathbf{a}_z = \sin \phi A J_1(kr) \hat{\mathbf{z}}, \quad r \leq R \quad (3.6a)$$

$$\mathbf{a}_z = \sin \phi \left(\hat{B}r + D \frac{1}{r} \right) \hat{\mathbf{z}}, \quad r > R \quad (3.6b)$$

In order to ensure continuity, the two expressions of \mathbf{a}_z must be equal on the surface of the conductor ($a_z|_{r=R}$).

$$A J_1(kR) = \left(\hat{B}R + D \frac{1}{R} \right)$$

The tangential component of the \mathbf{b} -field $\mathbf{b}_t = \hat{\mathbf{r}} \times (\mathbf{b} \times \hat{\mathbf{r}})$ should also be continuous at the boundary.

Calculating the curl of the magnetic vector potential

$$\mathbf{b} = \mathbf{curl} \mathbf{a} = \left(\frac{1}{r} \partial_{\phi} a_z - \partial_z a_{\phi} \right) \hat{\mathbf{r}} + (\partial_z a_r - \partial_r a_z) \hat{\phi} + \frac{1}{r} (\partial_r (r a_{\phi}) - \partial_{\phi} a_r) \hat{\mathbf{z}}$$

Note that the magnetic vector potential is a vector in the $\hat{\mathbf{z}}$ direction and varies in both $\hat{\mathbf{r}}$ and $\hat{\phi}$. In other words $\mathbf{a}_\phi = \mathbf{a}_r = 0$ and $\partial_z = 0$. The tangential component of the \mathbf{b} -field reads

$$\mathbf{b}_t = \hat{\mathbf{r}} \times ((-\partial_z \mathbf{a}_\phi \hat{\mathbf{r}} - \partial_r \mathbf{a}_z \hat{\phi}) \times \hat{\mathbf{r}}) = -\partial_r \mathbf{a}_z \hat{\phi}$$

We can calculate the **curl** of the magnetic vector potential to obtain the actual expression of the \mathbf{b} -field

$$A \partial_r J_1(kr) \hat{\phi} = \left(\partial_r \hat{B} r + D_4 \partial_r \frac{1}{r} \right) \hat{\phi}$$

This leads to

$$A J'_1(kr) \hat{\phi} = \left(\hat{B} - D \frac{1}{r^2} \right) \hat{\phi}$$

Where the $J'_1(kr) = \frac{1}{2}k(J_0(kr) - J_2(kr))$. This expression is only valid at the surface of the conductor. Let us evaluate the expression at $r = R$

$$A J'_1(kR) = \left(\hat{B} - D \frac{1}{R^2} \right)$$

Let's multiply both sides by R^2

$$AR^2 J'_1(kR) = \left(\hat{B}R^2 - D \right) \tag{3.7}$$

The coefficients can be calculated and we obtain,

$$A = \frac{4\hat{B}R}{Rk(J_0(kR) - J_2(kR)) + 2J_1(kR)} \tag{3.8}$$

$$D = \frac{4\hat{B}R^2 J_1(kR)}{Rk(J_0(kR) - J_2(kR)) + 2J_1(kR)} - \hat{B}R^2 \tag{3.9}$$

The current density inside of the conductor in terms of the vector potential $\mathbf{j}_z(r, \phi) = -i\omega\sigma\mathbf{a}_z(r, \phi)$ reads

$$\mathbf{j}_z(r, \phi) = -i\omega\sigma \left[\left(\frac{4\hat{B}R}{Rk(J_0(kR) - J_2(kR)) + 2J_1(kR)} \right) J_1(kr) \sin \phi \right] \hat{\mathbf{z}} \quad (3.10)$$

Equation (3.10) serves as the analytical expression of the frequency-dependent current density distribution within a round conductor due to the presence of a time-varying field, and can be used to validate compare and validate the results obtained for a single wire against the Finite Element Method.

In Figures 3.3, and 3.5 the results of such comparison is presented in the case of 1Hz and 1MHz. The comparison is displayed as a line plot across the cross section of the wire ($x = 0$). Furthermore, the color map obtained from the numerical solution is presented in 3.2, and 3.4 for 1Hz and 1MHz respectively. In the case of the presence of a time-variant field of a frequency of 1Hz we see that the relative error between the numerical and analytical solutions rise slowly up the closer it gets to the surface of the conductor on the real component of the current density, whereas the relative error on the imaginary component is negligible. In the case of a time-varying field of 1MHz we still find a high level of agreement between both results, however we see that peaks appear on the relative error plots which rise to values close to 8%.

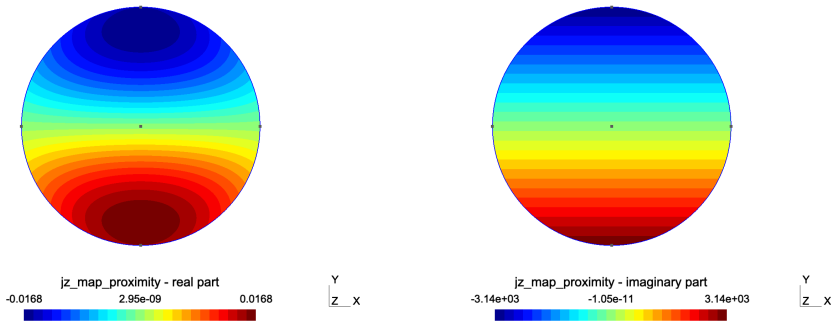


Figure 3.2: Current density distribution due to proximity-effect excitation: Real(Left), Imaginary(Right) at 1Hz

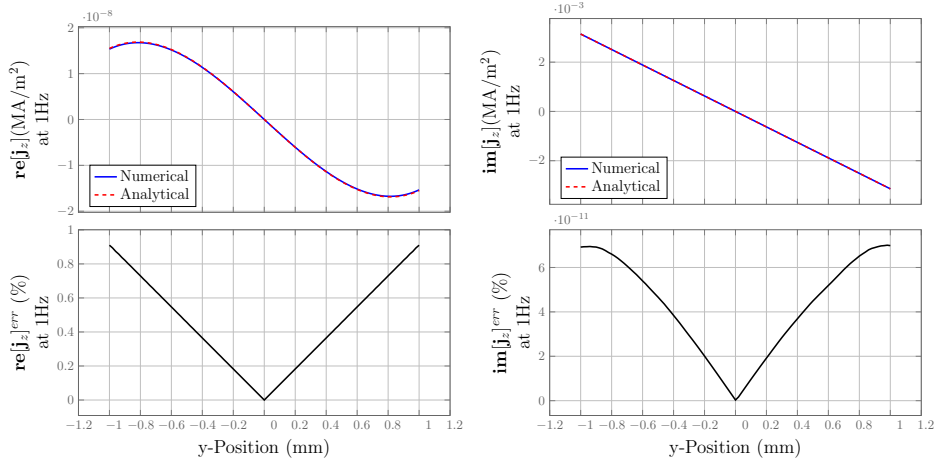


Figure 3.3: Current Density Distribution within the Cross Section of a Round Wire due to proximity-excitation at 1Hz

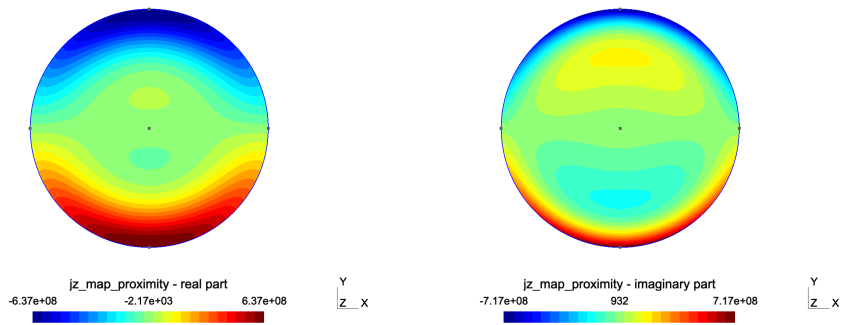


Figure 3.4: Current density distribution due to proximity-effect excitation: Real(Left), Imaginary(Right) at 1MHz

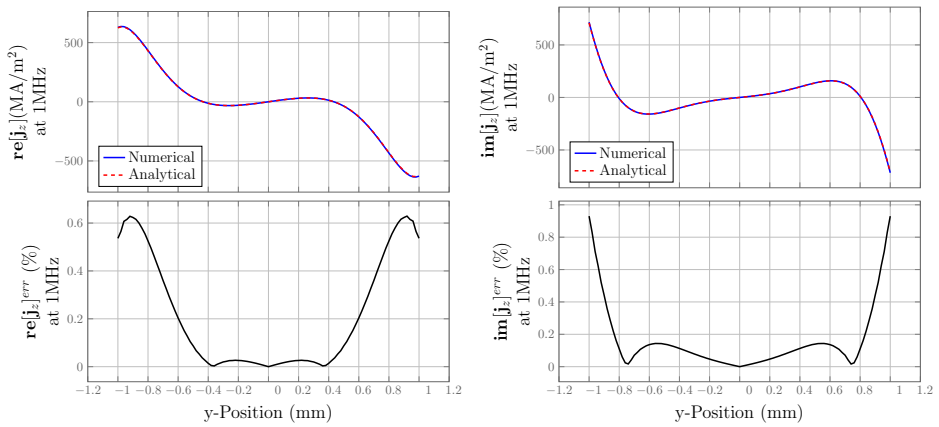


Figure 3.5: Current Density Distribution within the Cross Section of a Round Wire due to proximity-excitation at 1MHz

3.2. Semi-Analytical Modeling of Thin Wires Accounting for Proximity Effects

In the previous sections, we have laid out the foundation blocks of the so-called Semi-Analytical (SA) method to model thin wires. For clarity, the method's mathematical framework is summarized in this section as a concise formulation that can be ultimately implemented as a stand-alone model or a feature on any finite-element platform.

The finite-element weak formulation can be expressed as

$$(\nu \mathbf{curl} \mathbf{a}^c, \mathbf{curl} (\alpha_n^c \hat{\mathbf{z}}))_{\Omega} - A_c(I_i, \alpha_n^c \hat{\mathbf{z}})_{\Omega_{LR}} = 0, \quad \forall \alpha_n^c \in F_a(\Omega). \quad (3.11a)$$

$$(\nu \mathbf{curl} \mathbf{a}^w, \mathbf{curl} (\alpha_n^w \hat{\mathbf{z}}))_{\Omega_{SL}} - A_c(I_i, \alpha_n^w \hat{\mathbf{z}})_{\Omega_{LR}} = 0, \quad \forall \alpha_n^w \in F_a(\Omega_{SL}). \quad (3.11b)$$

Note that the nodal basis function α_n^c and α_n^w are supported on the whole domain Ω and on the sleeve domain Ω_{SL} respectively. This implies that in both equations the second term on the left-hand side of the equation is identical and when performing the subtraction of the sleeve domain in the finite-element model we end up with the solution of the background field. Hence, the singularity around the sleeve is removed.

The background field is solved by the weak formulation (3.11), which is associated to the global current I_i in each conductor of the model. However, as mentioned earlier the source I_i is removed by subtracting the solution of the sleeve from the solution obtained in the whole domain Ω .

The analytical correction of the magnetic vector potential due to **skin effect** can be expressed as

$$a_{corr_s}(r) = \frac{\mu_0 I}{2\pi} \left[\frac{\mu_r}{kR} \frac{J_0(kr) - J_0(kR)}{J_1(kR)} + \log \left(\frac{r_{SL}}{R} \right) \right], \quad r \leq R$$

$$a_{corr_s}(r) = \frac{\mu_0 I}{2\pi} \log \left(\frac{r_{SL}}{r} \right), \quad r > R$$

whereas the additional correction term to account for the **proximity effect** can be expressed as

$$a_{corr_p} = -B \left(\frac{2J_1(kr)}{kJ_0(kR)} - r \right) \cos \phi, \quad r \leq R \quad (3.13a)$$

$$a_{corr_p} = -B \frac{R}{r} \left(\frac{2J_1(kR)}{kR J_0(kR)} - 1 \right) \cos \phi, \quad r > R \quad (3.13b)$$

Hence, the frequency-dependent distribution of the magnetic vector potential can be reconstructed by adding up the analytical solution to the truncated-field solution in the finite-element model, naturally falling onto our one liner description (2.5)

$$\mathbf{a} = \mathbf{a}^c - \mathbf{a}^w + \mathbf{a}_{corr}.$$

where $\mathbf{a}_{corr} = \mathbf{a}_{corr_s} + \mathbf{a}_{corr_p}$ reconstructs the solution in Ω_{SL}

In Fig 3.6 we observe the increase in agreement when both correction contributions (skin and proximity) are taken into account.

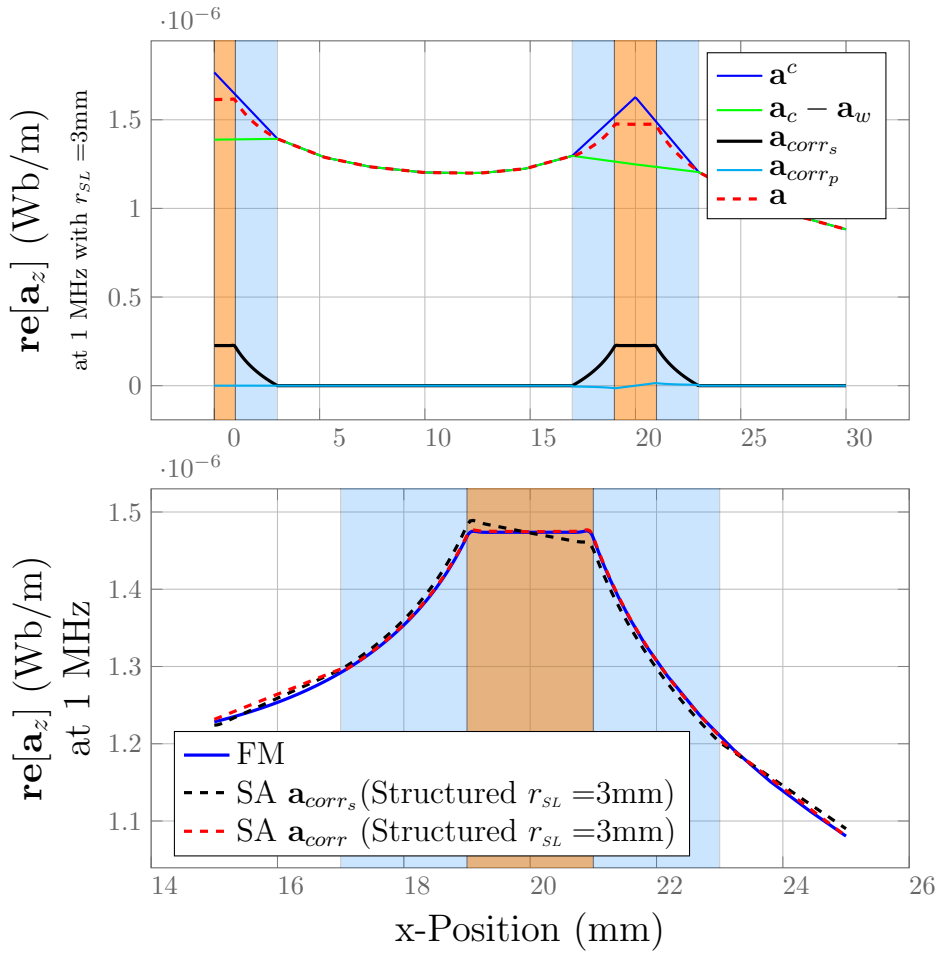


Figure 3.6: Different components of the corrected field \mathbf{a} as of (2.5) with three wires at 1MHz (Top), and comparative view of the computed \mathbf{a} field focused on the rightmost wire (Bottom).

3.3. Numerical Results

The numerical tests presented in this section have been performed under the same conditions presented earlier in 2.8.1 *Local Agreement - Magnetic Vector Potential*. All tests are performed with 3 parallel connected wires of radius $R_i = 1$ mm, a sleeve radius (i.e., a prescribed mesh size on the wire) in the case of structured sleeves r_{SL_i} and controlled by the characteristic length l_{c_i} in the case of unstructured sleeves, a current $I = 1$ A, an electrical conductivity $\sigma = 5.96 \cdot 10^7$ S/m (i.e. copper), and a relative permeability $\mu_r = 1$. Lastly, the discretization of each conductor in the **FM** model is created using a characteristic length $l_c = \frac{\delta|_{1MHz}}{3}$, where $\delta|_{1MHz}$ is the skin depth evaluated at 1MHz. This mesh is constant throughout all the tests unless stated otherwise, and fine enough to solve accurately the complex current density distribution induced by skin- and proximity-effect in the wire over the considered frequency range.

The focus of these results is on the introduction and study of the proximity correction factor into our suggested semi-analytical (SA) method.

For simplicity the tests performed in this section will be the same as in the previous section:

- Frequency 1Hz and conductor spacing of 8mm
- Frequency 1MHz and conductor spacing of 8mm
- Frequency 1Hz and conductor spacing of 2.05mm
- Frequency 1MHz and conductor spacing of 2.05mm

This enables the effortless comparison against the results under purely skin effect analytical correction.

The proximity effect does have an effect on the current distribution within the wire and this ultimately has an effect on the resistance of the given system. For this chapter to be self contained, the focus is merely on the local proximity effects. Losses and introduction of global sources will be presented in the next chapter.

All calculations have been performed using ONELAB software (Gmsh [38] and GetDP [25]) using linear direct solver MUMPS [6] .

3.3.1. Frequency 1Hz and conductor spacing of 8mm

This test case showcases the behavior of the magnetic vector potential at **low frequencies** when the **conductor spacing is large**. Fig. 3.7 and Fig. 3.8 are analogous to the skin-effect-only correction counterpart Fig. 2.20 and Fig. 2.21.

In Fig. 3.7 we observe that the highest local relative error of the **real part** of the magnetic vector potential in the case of structured sleeves remains under 0.4%, 3% and 0.6% for r_{SL} 1mm, 0.5mm and 3mm, respectively. In the case of unstructured sleeves the highest local error peaks at values of 2.5%, 3.6% and 2.6% for l_c 1mm, 0.5 and 3mm, respectively. Most local values however in the case of structured sleeves remain under a relative error of 0.6% and in the case of unstructured sleeves 1.5%.

In Fig. 3.8 we observe that the highest local relative error of the **imaginary part** of the magnetic vector potential in the case of structured sleeves remains under $1.2 \cdot 10^{-4}\%$, $1.8 \cdot 10^{-4}\%$ and $1.2 \cdot 10^{-4}\%$ for r_{SL} 1mm, 0.5mm and 3mm, respectively. In the case of unstructured sleeves the highest local error peaks at values of $1.4 \cdot 10^{-4}\%$, $1.9 \cdot 10^{-4}\%$ and $1.4 \cdot 10^{-4}\%$ for l_c 1mm, 0.5 and 3mm, respectively. Most local values however in the case of structured sleeves remain under a relative error of $10^{-4}\%$ and in the case of unstructured sleeves $10^{-4}\%$ as well.

Note that in the case of unstructured sleeves the behavior is more noisy due to asymmetry, note that the radius used to correct the unstructured sleeve is calculated from the area of the sleeve. Furthermore, note that the error peak generated in both cases structured and unstructured at sleeves smaller than the size of the conductor (see *Semi-analytical Modeling of Thin Wires*). Another important observation is that the proximity correction factor has a direct impact on the reconstruction of the imaginary part of the magnetic vector potential, which is clearly seen in the case of larger sleeves (grey curve).

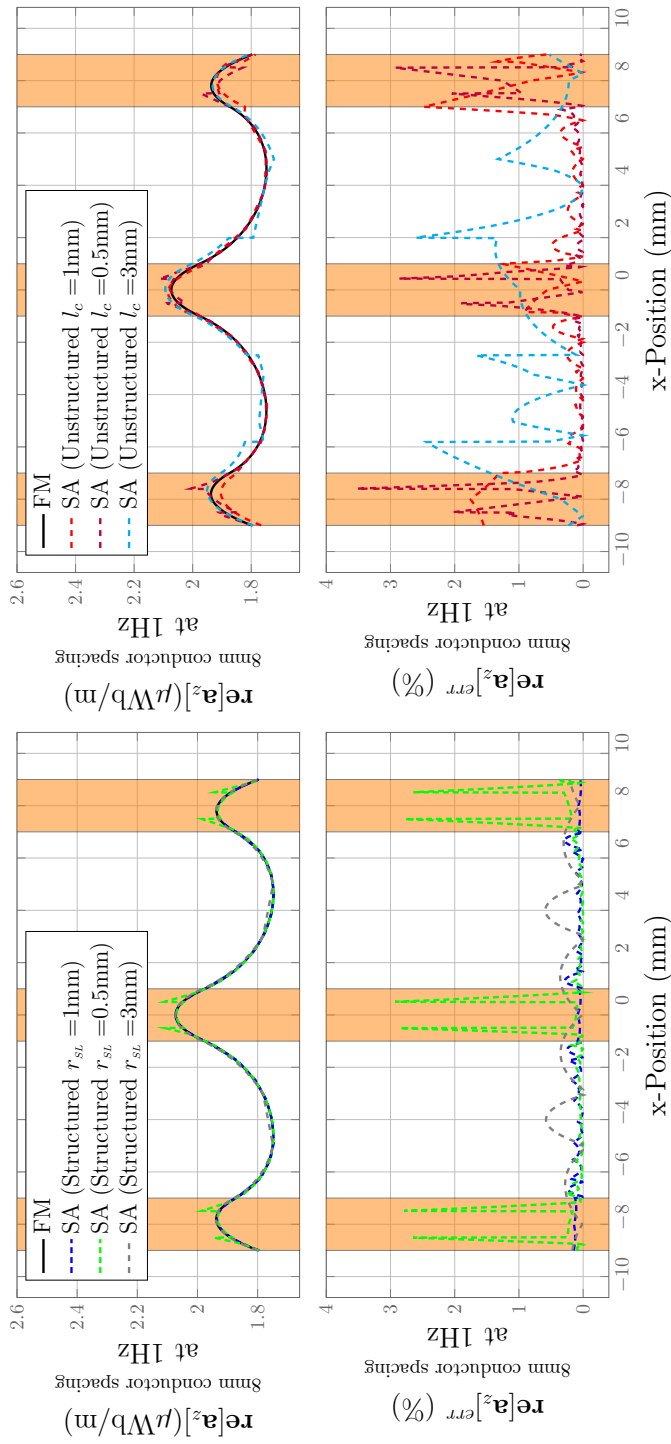


Figure 3.7: Real part of \mathbf{a} in three parallel wires at 1Hz with conductor spacing of 8mm: Structured Sleeves (Left) and Unstructured Sleeves (Right)

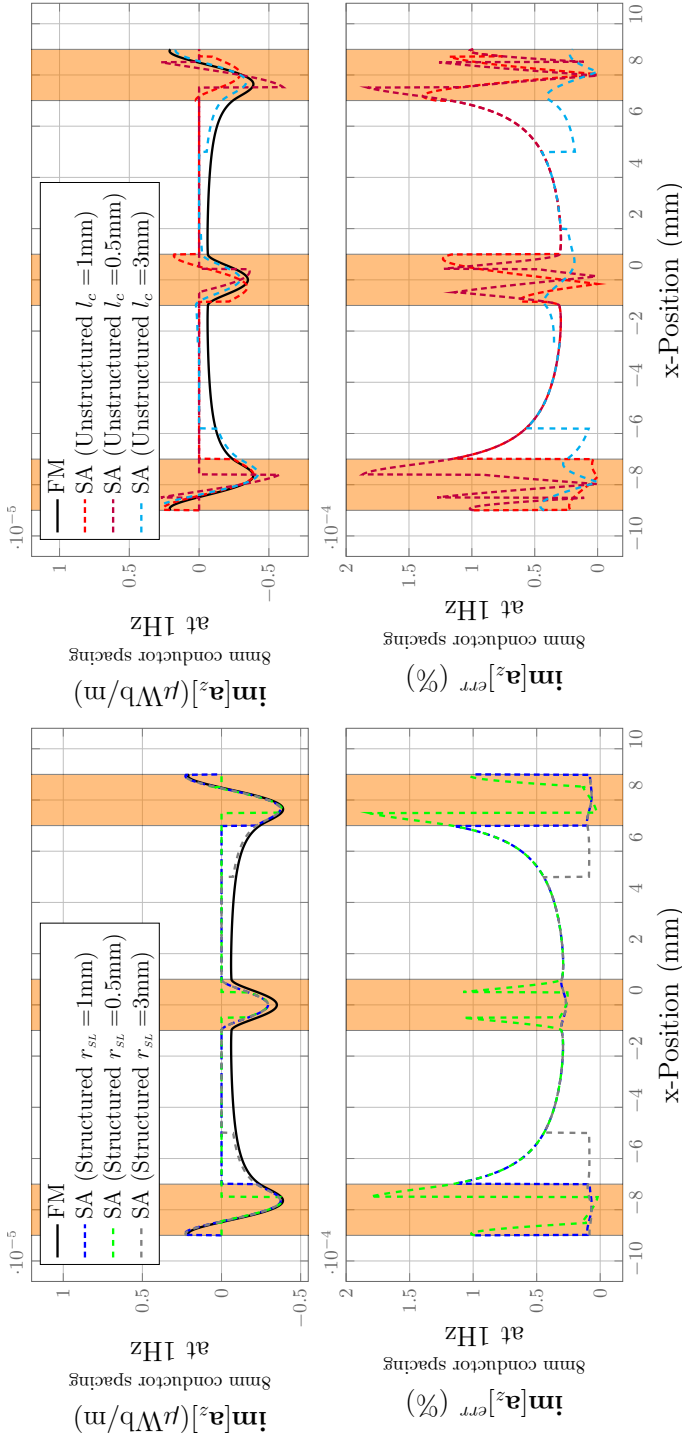


Figure 3.8: Imaginary part of \mathbf{a} in three parallel wires at 1Hz with conductor spacing of 8mm: Structured Sleeves (Left) and Unstructured Sleeves (Right)

3.3.2. Frequency 1MHz and conductor spacing of 8mm

This test case showcases the behavior of the magnetic vector potential at **high frequencies** when the **conductor spacing is large**. Fig. 3.9 and Fig. 3.10 are analogous to the skin-effect-only correction counterpart Fig. 2.22 and Fig. 2.23.

In Fig. 3.9 we observe that the highest local relative error of the **real part** of the magnetic vector potential in the case of structured sleeves remains under 1.99%, 7.2% and 1.8% for r_{SL} 1mm, 0.5mm and 3mm, respectively. In the case of unstructured sleeves the highest local error peaks at values of 3.2%, 6.9% and 2.2% for l_c 1mm, 0.5 and 3mm, respectively. Most local values however in the case of structured sleeves remain under a relative error of 2% and in the case of unstructured sleeves 3.9%.

In Fig. 3.10 we observe that the highest local relative error of the **imaginary part** of the magnetic vector potential in the case of structured sleeves remains under 0.14%, 0.38% and 0.14% for r_{SL} 1mm, 0.5mm and 3mm, respectively. In the case of unstructured sleeves the highest local error peaks at values of 0.37%, 0.39% and 0.08% for l_c 1mm, 0.5 and 3mm, respectively. Most local values however in the case of structured sleeves remain under a relative error of 0.15% and in the case of unstructured sleeves 0.15%.

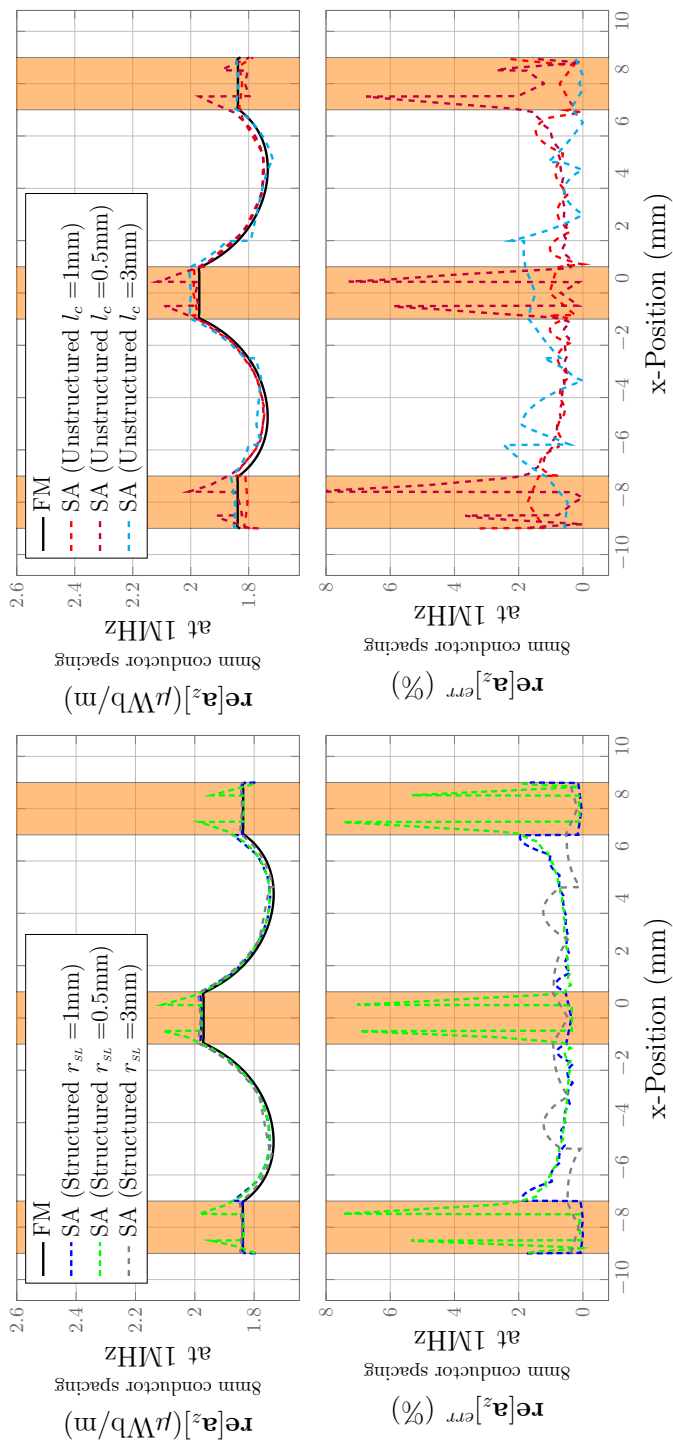


Figure 3.9: Real part of \mathbf{a} in three parallel wires at 1MHz with conductor spacing of 8mm: Structured Sleeves (Left) and Unstructured Sleeves (Right)

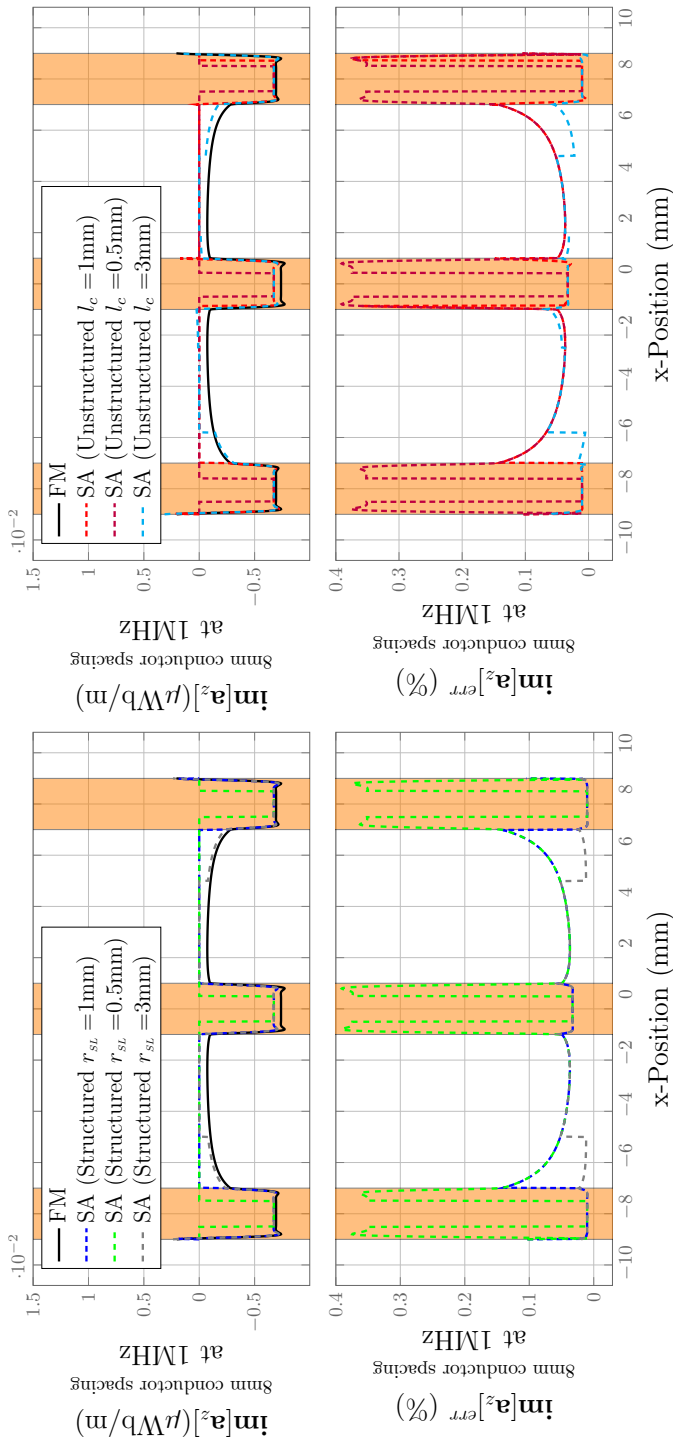


Figure 3.10: Imaginary part of \mathbf{a} in three parallel wires at 1MHz with conductor spacing of 8mm: Structured Sleeves (Left) and Unstructured Sleeves (Right)

3.3.3. Frequency 1Hz and conductor spacing of 2.05mm

This test case showcases the behavior of the magnetic vector potential at **low frequencies** when the **conductor spacing is small**. Fig. 3.11 and Fig. 3.12 are analogous to the skin-effect-only correction counterpart Fig. 2.24 and Fig. 2.25. Note that in the case of small conductor spacing, the structured sleeve is constraint by the geometrical dimensions. For this reason, the values at greater size structured sleeves are not presented.

In Fig. 3.11 we observe that the highest local relative error of the **real part** of the magnetic vector potential in the case of structured sleeves remains under 0.5% and 2.4% for r_{SL} 1mm, and 0.5mm, respectively. In the case of unstructured sleeves the highest local error peaks at values of 2.9%, 2.5% and 4% for l_c 1mm, 0.5 and 3mm, respectively. Most local values however in the case of structured sleeves remain under a relative error of 0.5% and in the case of unstructured sleeves 2.5%.

In Fig. 3.12, the **imaginary part** of the magnetic vector potential is presented. Under structured sleeves the highest local relative error calculated reports $5.2 \cdot 10^{-4}\%$, $5.2 \cdot 10^{-4}\%$ for r_{SL} 1mm, 0.5mm, respectively, and most local error data points fall under $3.5 \cdot 10^{-4}\%$. In the case of unstructured sleeves the highest local relative error reaches values of $5.2 \cdot 10^{-4}\%$, $5.2 \cdot 10^{-4}\%$ and $5.2 \cdot 10^{-4}\%$ or l_c 1mm, 0.5 and 3mm, respectively but most local error data falls under $3.5 \cdot 10^{-4}\%$.

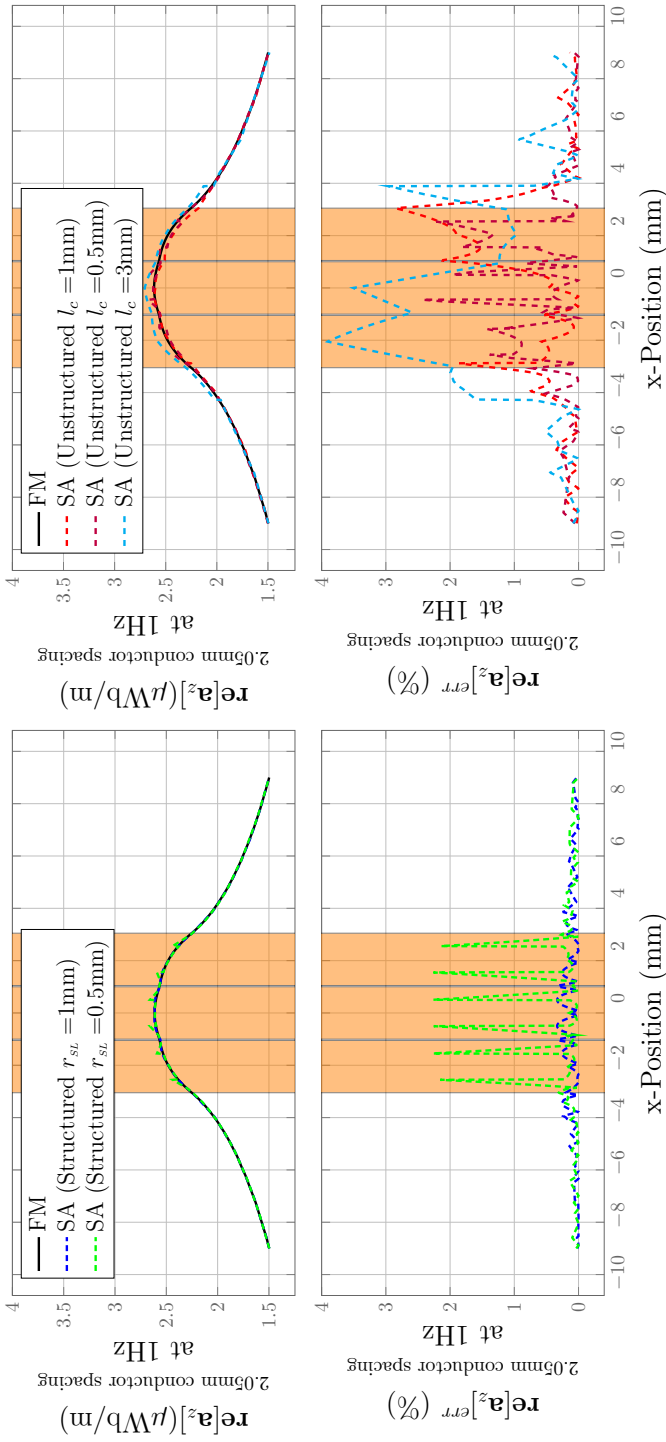


Figure 3.11: Real part of \mathbf{a} in three parallel wires at 1Hz with conductor spacing of 2.05mm: Structured Sleeves (Left) and Unstructured Sleeves (Right)

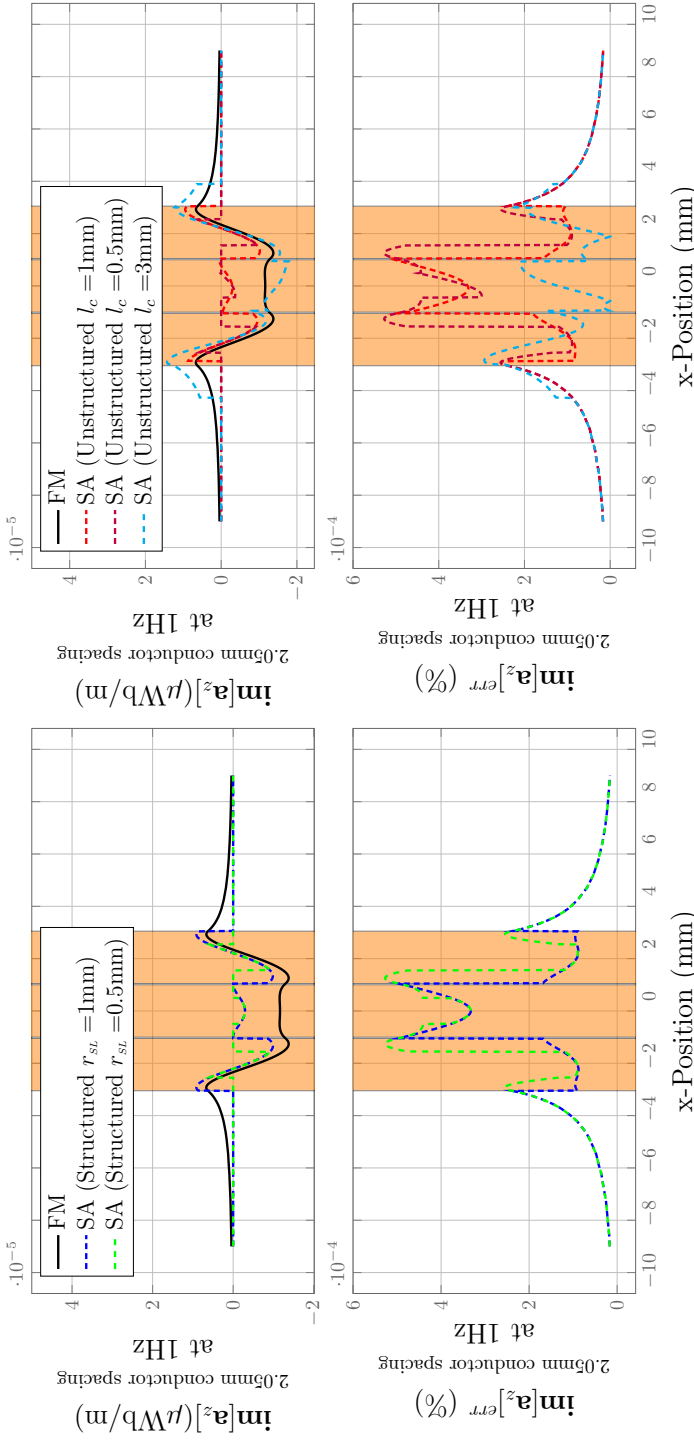


Figure 3.12: Imaginary part of \mathbf{a} in three parallel wires at 1Hz with conductor spacing of 2.05mm: Structured Sleeves (Left) and Unstructured Sleeves (Right)

3.3.4. Frequency 1MHz and conductor spacing of 2.05mm

This test case showcases the behavior of the magnetic vector potential at **high frequencies** when the conductor spacing is small. Fig. 3.13 and Fig. 3.14 are analogous to the skin-effect-only correction counterpart Fig. 2.26 and Fig. 2.27. Note that in the case of small conductor spacing, the structured sleeve is constrained by the geometrical dimensions. For this reason, the values at greater size structured sleeves are not presented.

In Fig. 3.13 we observe that the highest local relative error of the **real part** of the magnetic vector potential in the case of structured sleeves remains under 8.1% and 11.8% for r_{SL} 1mm, and 0.5mm, respectively. In the case of unstructured sleeves the highest local error peaks at values of 8%, 11% and 7% for l_c 1mm, 0.5 and 3mm, respectively. Most local values however in the case of structured sleeves remain under a relative error of 9% and in the case of unstructured sleeves 9%.

In Fig. 3.14, the **imaginary part** of the magnetic vector potential is presented. Under structured sleeves the highest local relative error calculated reports 0.63%, 0.79% for r_{SL} 1mm, 0.5mm, respectively, and most local error data points fall under 0.5% . In the case of unstructured sleeves the highest local relative error reaches values of 0.62%, 0.79% and 0.63% or l_c 1mm, 0.5 and 3mm, respectively but most local error data fall under 0.5%.

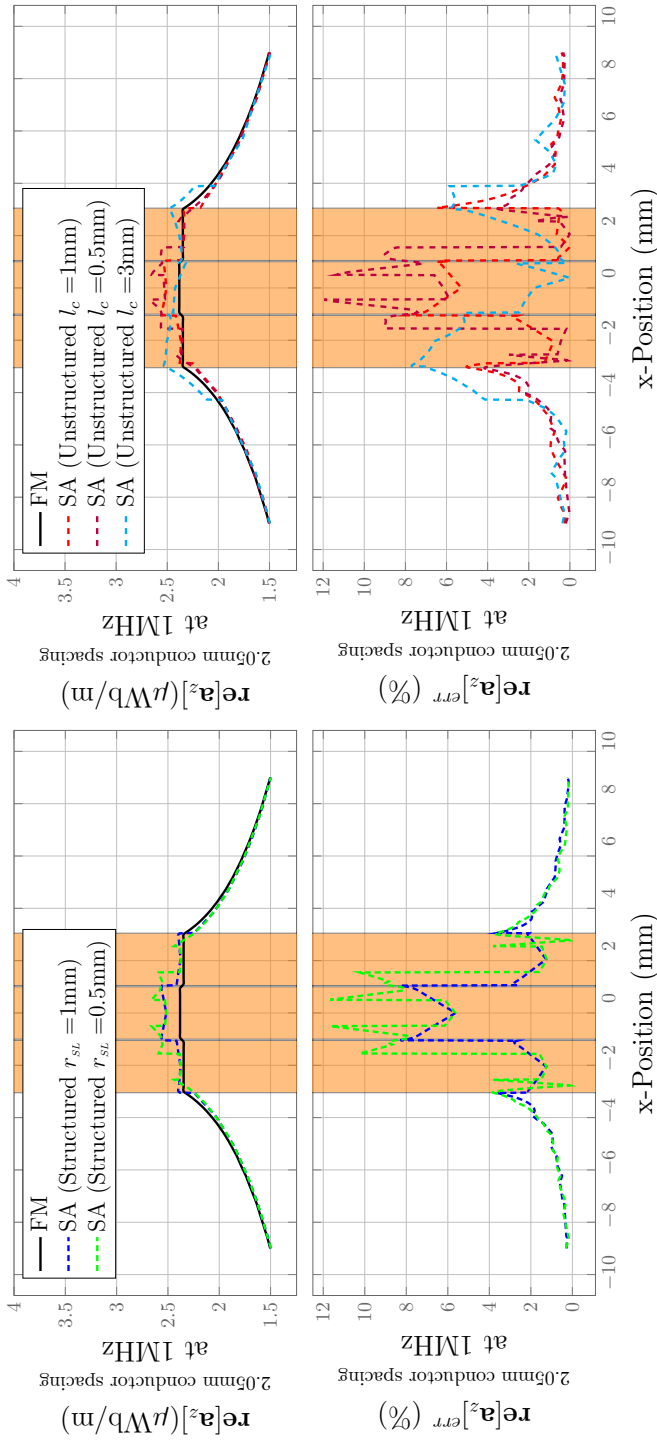


Figure 3.13: Real part of \mathbf{a} in three parallel wires at 1MHz with conductor spacing of 2.05mm: Structured Sleeves (Left) and Unstructured Sleeves (Right)

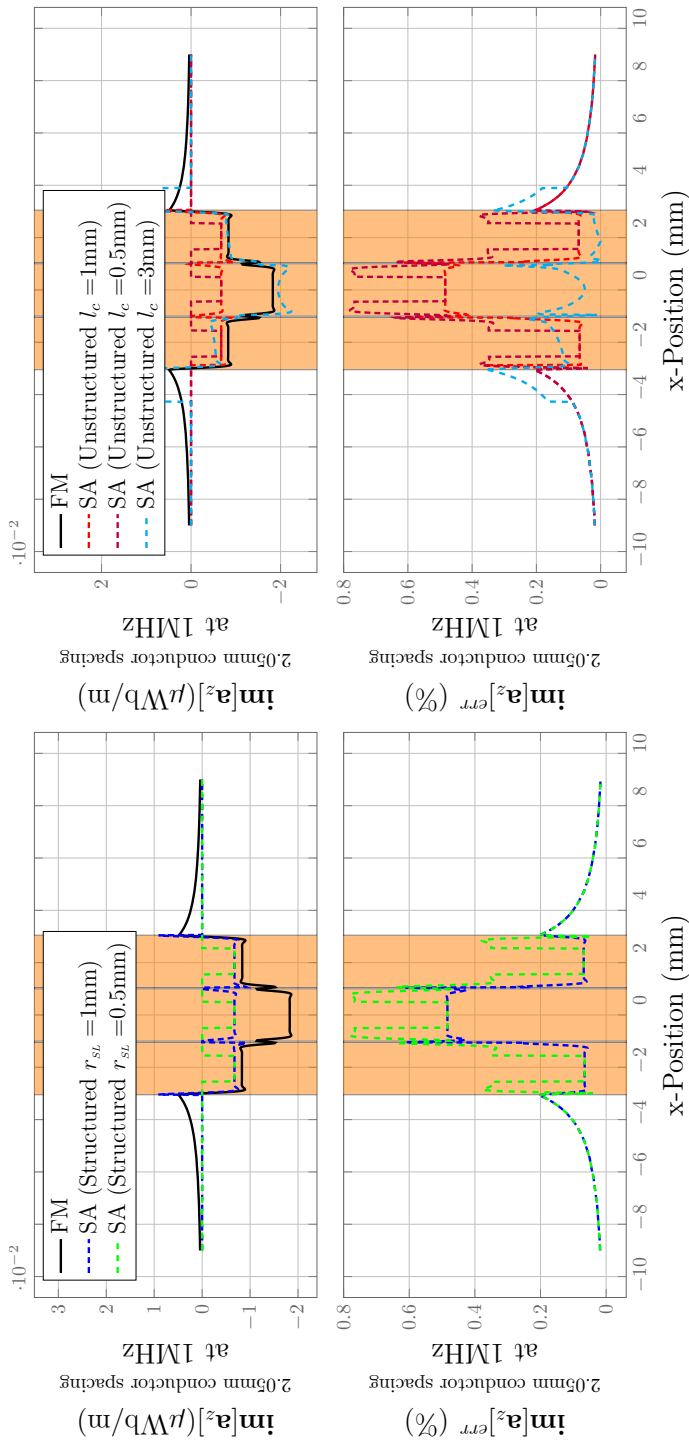


Figure 3.14: Imaginary part of \mathbf{a} in three parallel wires at 1Hz with conductor spacing of 2.05mm: Structured Sleeves (Left) and Unstructured Sleeves (Right)

3.4. Highlights and Remarks

In this chapter we presented the derivation of the analytical solution of a conductor in isolation in the case where $B \neq 0$ and $I = 0$. The solution is then included in our semi-analytical method where $\mathbf{a} = \mathbf{a}^c - \mathbf{a}^w + \mathbf{a}_{corr}$, where $\mathbf{a}_{corr} = \mathbf{a}_{corr_s} + \mathbf{a}_{corr_p}$ is the analytical correction factor accounting for skin and proximity effects. The analytical solution is validated for high (1MHz) and low (1Hz) frequencies. Lastly, the method is introduced into the 3 parallel wire study case.

In Fig. 3.6 it is shown that even though the contribution of the proximity effect is small at large distances, the proximity effects still has an strong impact on the solution of the magnetic vector potential. This becomes even more evident when the distance between conductor becomes small.

3

The inclusion of the proximity effect in our calculations proves to have a positive impact by improving the agreement between the fully discretized model and the semi analytical model. This is most notorious in the relative error values inside of each conductor where it decreases in comparison to the only-skin-effect correction test cases. Furthermore, the imaginary part of the vector potential can be retrieved through the proximity correction factor. This is quite visible in test cases where the sleeve is larger than the size of the conductor.

Efficient Modeling of Multi-turn Coils

This chapter presents the application of the semi-analytical (SA) technique to the modeling of multi-turn coils. The SA method described in the previous chapters has been shown to be able to reconstruct accurately the complex electromagnetic field inside and around any thin conductor subjected to skin effect and proximity effect, without the need to discretize explicitly its cross-section. The steps of the method are a FE field truncation followed by an analytic correction. These steps also provide the necessary information to evaluate the impedance of the thin conductor, i.e., resistance, self inductance and possibly also mutual inductance with neighbouring current carrying wires. In this chapter, the constructive elements of the SA method are exploited to evaluate the natural **global quantities** (i.e., currents and voltage drops) associated with each FE conductor. These global quantities then serve as variables to represent the thin wires in **external electric networks**, making it possible to connect them arbitrarily in parallel or in series, or with external voltage and/or current sources and external RLC lumped parameters.

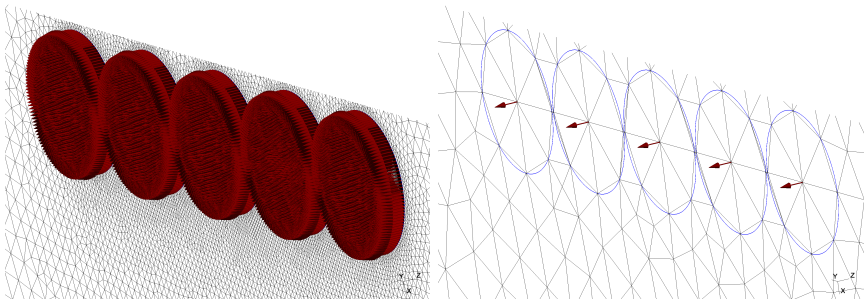


Figure 4.1: Current density in Full Model FM (Left) and Semi-Analytical SA (Right) in a 5 Turn Coil.

Multi-turn coils are commonly represented as stranded conductors in different

types of packaging shapes. In Fig. 4.2, a multi-turn coil Ω_s is presented as a stranded coil connected to a generator Ω_g , enabling the use of global sources such as Voltages and Currents.

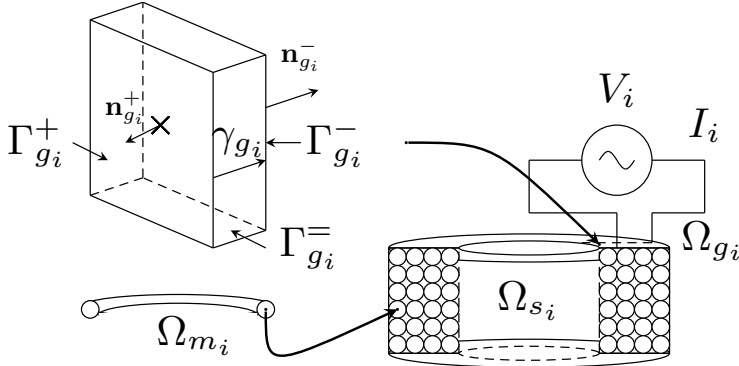


Figure 4.2: Voltage Driven Multi-turn coil

Thin wire were always treated independently in the previous chapters. In order to model a multi-turn coil, thin wires must now be connected in series (Fig. 4.3). This can be done by using network constraints and accounting for the impedances of each individual thin wire identified with the SA method. The main challenge is here to account for the proximity effect in tightly wound coils when the spacing between turns becomes very small.

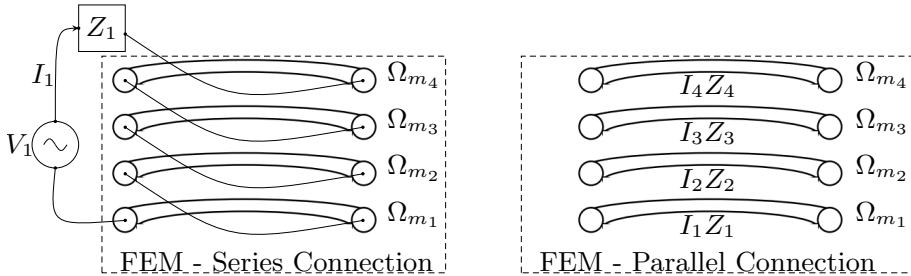


Figure 4.3: Comparison between multi-turn inductors and massive inductors

4.1. Global Quantities for thin wires

In the thin wire formulation, the electric current I_i is imposed in each thin wire, and an additional equation is thus needed to evaluate the associated voltage V_i , which is implicit in this formulation [27].

One starts for that with the electric field in the region occupied by the i^{th} thin wire

$$\mathbf{e} = -\mathbf{grad} v - i\omega(\mathbf{a}^c - \mathbf{a}^w + \mathbf{a}_{corr_s} + \mathbf{a}_{corr_p}), \quad (4.1)$$

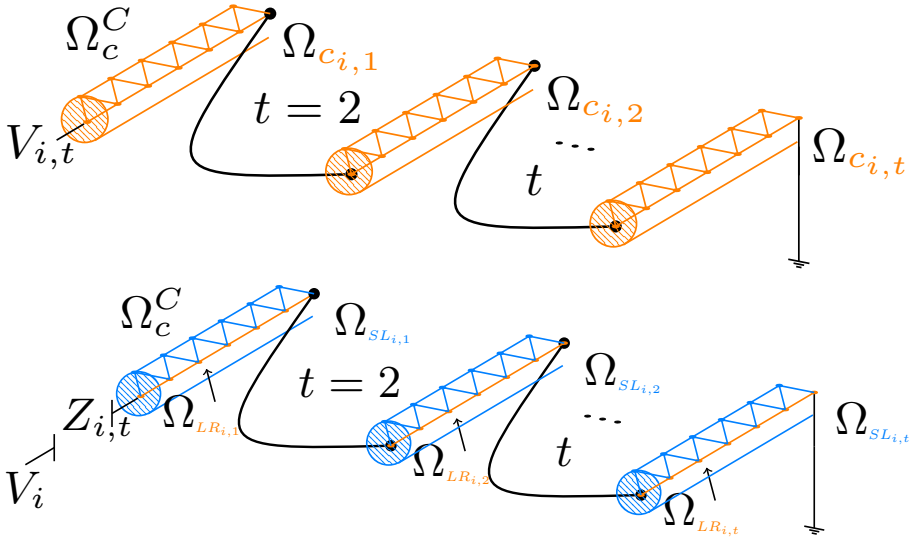


Figure 4.4: Multi-turn coil in FE model

which can be rewritten grouping terms appropriately

$$\mathbf{grad} v = - \left(\frac{\mathbf{j}}{\sigma} - \omega \mathbf{a}_{corr_s} \right) + \omega \mathbf{a}_{corr_p} - \omega (\mathbf{a}^c - \mathbf{a}^w). \quad (4.2)$$

The first term between parenthesis is the $\mathbf{grad} v$ term obtained from the analytical solution introduced in Chapter 2 Eq. (2.22). Due to the 2D symmetry, this term is a vector uniform over the cross section of the thin wire. One has found from Eq. (2.19) that

$$- \left(\frac{\mathbf{j}}{\sigma} + \omega \mathbf{a}_{corr_s} \right) = \left(\frac{k}{2\pi R \sigma} \frac{J_0(kR)}{J_1(kR)} - \frac{\mu_0}{2\pi} \omega \log\left(\frac{R_\infty}{R}\right) \right) I_i \hat{\mathbf{z}} \quad (4.3)$$

The second term is obtained from the analytical solution introduced in Chapter 3 Eq. (3.13). Because of the $\cos(\phi)$ term, this flux term is zero in average over the cross section of the wire, and plays therefore no role in the lumped inductance of the thin wire. The proximity effect is decoupled from the global quantities I_i and V_i of the thin wire. The third term, finally, is the voltage induced by the time variation of truncated field (background field), which is caused not only by the current I_i flowing in the considered thin wire, but also by the currents flowing in the other conductors of the system, $I_j, j \neq i$.

The global voltage V_i across the i^{th} thin wire region is now obtained by integration of (4.2) along the corresponding line region LR_i . One obtains

$$V_i = \left(\frac{k}{2\pi R \sigma} \frac{J_0(kR)}{J_1(kR)} + \frac{\mu_0}{2\pi} \omega \log\left(\frac{R_\infty}{R}\right) \right)_{\Omega_{LR_i}} I_i - \omega (\mathbf{a}^c - \mathbf{a}^w)_{\Omega_{LR_i}}, \quad (4.4)$$

which can be written

$$V_i = R_i I_i + \omega \phi_i \quad (4.5)$$

with the definitions

$$R_i = \Re \left\{ \frac{k}{2\pi R \sigma} \frac{J_0(kR)}{J_1(kR)} \right\} l \quad (4.6)$$

$$\phi_i = \Im \left\{ \frac{k}{2\pi R \sigma \omega} \frac{J_0(kR)}{J_1(kR)} \right\} I_i l - \left(\frac{\mu_0}{2\pi} \log\left(\frac{R_\infty}{R}\right) \right) I_i l - (\mathbf{a}^c - \mathbf{a}^w) l \quad (4.7)$$

where $\Re\{\cdot\}$ and $\Im\{\cdot\}$ denote the real part and the imaginary part of their complex argument, respectively.

4.2. Joule losses

We now turn to the computation of Joule losses in the thin wire system. The total Joule losses are given by

$$\begin{aligned} P &= \int_{\Omega_c} \sigma^{-1} |\mathbf{j}_{skin}(r) + \mathbf{j}_{prox}(r)|^2 dV \\ &= \int_{\Omega_c} \sigma^{-1} \left(|\mathbf{j}_{skin}(r)|^2 + 2\Re \{ \mathbf{j}_{skin}(r) \cdot \mathbf{j}_{prox}^*(r) \} + |\mathbf{j}_{prox}(r)|^2 \right) dV. \end{aligned}$$

By inspection of the spatial distribution of $\mathbf{j}_{skin}(r)$ and $\mathbf{j}_{prox}(r)$ and their symmetries as computed in the previous chapters Eq. (2.15) and Eq. (3.10), one however observes that their cross product should be close to zero in average over the thin wire's cross section, and hence negligible with respect to the quadratic terms in most cases. One thus makes the following approximation

$$P \approx \int_{\Omega_c} \sigma^{-1} \left(|\mathbf{j}_{skin}(r)|^2 + |\mathbf{j}_{prox}(r)|^2 \right) dV = P_{skin} + P_{prox}$$

that the true Joule losses can be estimated by simply adding the Joule losses P_{skin} and P_{prox} evaluated, as detailed in the next two subsections, from the corresponding analytical solutions.

4.2.1. Joule losses P_{skin} in the Skin effect analytical solution

Joule losses in the analytical solution for skin effect in the i^{th} thin wire can be evaluated by integration of the Poynting vector in cylindrical coordinates

$$\mathbf{s} = \mathbf{e} \times \mathbf{h}^* = (e_\phi h_r^* - e_z h_\phi^*) \hat{\mathbf{r}} + (e_z h_r^* - e_r h_z^*) \hat{\boldsymbol{\phi}} + (e_r h_\phi^* - e_\phi h_r^*) \hat{\mathbf{z}},$$

which involves the electric field \mathbf{e} , and the magnetic field \mathbf{h} . The magnetic field is calculated from the \mathbf{b} -field, $\mathbf{b} = \mathbf{curl} \mathbf{a}$. One has the the magnetic vector potential from Eq. (2.14)

$$\mathbf{curl} \mathbf{a}_z(r) = \frac{\mu I_i}{2\pi R} \frac{J_1(kr)}{J_1(kR)} \hat{\boldsymbol{\phi}}, \quad r \leq R$$

Hence,

$$\mathbf{h}^*(r) = \frac{I_i^*}{2\pi R} \frac{J_1(k^*r)}{J_1(k^*R)} \hat{\phi}, \quad r \leq R \quad (4.8)$$

The electric field, on the other hand, is derived directly from Ohm's law using Eq. (2.15) as

$$\mathbf{e}(r) = \frac{kI_i}{2\pi R\sigma} \frac{J_0(kr)}{J_1(kR)} \hat{\mathbf{z}}, \quad r \leq R \quad (4.9)$$

so that the Poynting vector reads

$$\begin{aligned} \mathbf{s} &= \mathbf{e} \times \mathbf{h}^* = -e_z h_\phi^* \hat{\mathbf{r}} \\ &= -I_i I_i^* \left(\frac{k}{(2\pi R)^2 \sigma J_1(kR) J_1(k^*R)} J_0(kr) J_1(k^*r) \right) \hat{\mathbf{r}}. \end{aligned} \quad (4.10)$$

The flux of the Poynting vector across the surface of the conductor ($r = R$) is the complex power received by the thin wire. One has

$$\begin{aligned} S_{skin} &= - \oint_{\partial\Omega_c} \mathbf{s} = I_i I_i^* \frac{k}{(2\pi R)^2 \sigma J_1(kR) J_1(k^*R)} J_0(kR) J_1(k^*R) \int_0^l \int_0^{2\pi} R d\phi dz \\ &= I_i I_i^* \frac{k}{(2\pi R)^2 \sigma J_1(kR)} J_0(kR) 2\pi R l \\ &= I_i I_i^* \frac{k}{2\pi R \sigma} \frac{J_0(kR)}{J_1(kR)} l \end{aligned} \quad (4.11)$$

which finally gives

$$S_{skin} = R_{dc} \frac{kR}{2} \frac{J_0(kR)}{J_1(kR)} |I_i|^2 = P_{skin} + iQ_{skin}. \quad (4.12)$$

where

$$R_{dc} = \frac{l}{\sigma \pi R^2} \quad (4.13)$$

is the DC resistance of the thin wire.

The real part of S_{skin} , i.e., P_{skin} , represents the Joule losses in the thin wire, which confirms the result (4.6) obtained above. The imaginary part, on the other hand, is the reactive power associated to the part of the flux that flows inside the conductor and that is also due to the current I_i . This is only a part of the self inductance of the thin wire, as can be checked by comparison with (4.7).

4.2.2. Joule losses P_{prox} in the proximity effect analytical solution

The current carrying thin wire is also immersed in the induction \mathbf{b} -field caused by currents in neighboring thin wires. This time-varying \mathbf{b} -field induces eddy currents $\mathbf{j}_{prox}(r)$ in the considered wire. The corresponding Joule losses are calculated by integration of $\mathbf{j}^* \cdot \mathbf{e}$ over the desired volume, with \mathbf{j} and \mathbf{e} the analytic solution of the proximity effect only problem. One has

$$\begin{aligned}
 P_{prox} &= \int_V \mathbf{j}^* \cdot \mathbf{e} dV \\
 &= BB^* \left[\left(\frac{16\omega^2 \sigma R^2}{D} \right) \int_0^l \int_0^{2\pi} \int_0^R J_1(k^* r) J_1(kr) \sin^2 \phi r dr d\phi dz \right] \\
 P_{prox} &= |B|^2 \left(\frac{16\omega^2 \sigma R^2}{D} \right) \frac{\pi R l (k^* J_1(kR) J_0(k^* R) - k J_0(kR) J_1(k^* R))}{k^2 - (k^*)^2}
 \end{aligned} \tag{4.14}$$

4

where the denominator reads

$$D = [Rk^*(J_0(k^*R) - J_2(k^*R)) + 2J_1(k^*R)][Rk(J_0(kR) - J_2(kR)) + 2J_1(kR)],$$

and involves the wave number $k = \frac{1-i}{\delta}$ and its complex conjugate $k^* = \frac{1+i}{\delta}$.

As explained above, the \mathbf{a}_{corr_p} field is decoupled from the global quantities I_i and V_i of the thin wires. The term P_{prox} can therefore be evaluated in post-processing, and simply added to P_{skin} to obtain a good approximation of the total Joule losses, accounting for both skin- and proximity effect. This approximation is validated numerically in the following of this chapter.

4.3. Numerical Tests

To illustrate the proposed method, three cases are set-up for comparison between the Full Model **FM** and the Semi-Analytical **SA** model. The first model is a single layer 5-turn winding, the second model is a double layer 10-turn winding and the last test case is a three-layer 15-turn winding. In Fig. 4.5 we present the geometrical description of the 5-turn and 15-turn case, where only half of the winding is presented due to symmetry which in the FE model it is enforced by a no-flux boundary condition.

For simplicity, wire radius $R = 1\text{mm}$ and peak voltage $\hat{V}_i = 1\text{V}$, an electrical conductivity $\sigma = 5.96 \cdot 10^7\text{S/m}$, and a relative permeability $\mu_r = 1$ are used in all test cases. The conductor spacing is treated such that $d_x = d_y = d$. The subscript on the radius $R_{1,t}$ in Fig. 4.5, this indicates that in all test examples the winding arrangement consists of a single coil with t turns.

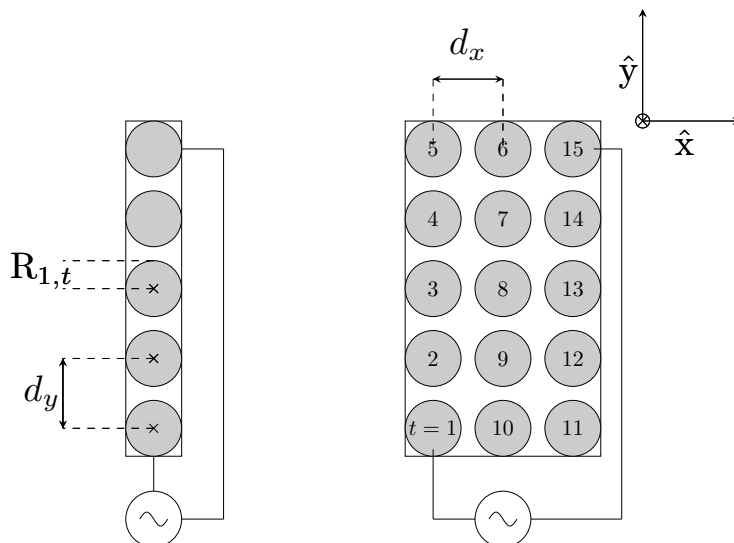


Figure 4.5: Application cases with geometrical description and connection order: Symmetrical-half in the case of 5-turn winding (Left), 15-turn winding (Right).

The tests in this chapter are targeted mainly to the application to the case of multi-turn windings, the calculation of the impedance and accuracy at a broad range of frequencies including skin and proximity effects.

The first numerical test is based on the distance between coil turns at high (1MHz) and low (1Hz) frequencies. This study focuses on the limitations of the method, as we can visually see the rise in the relative error as the turns become closer to each other, which is expected due to proximity effects.

The second numerical test is a frequency-sweeps with close and large inter-turn

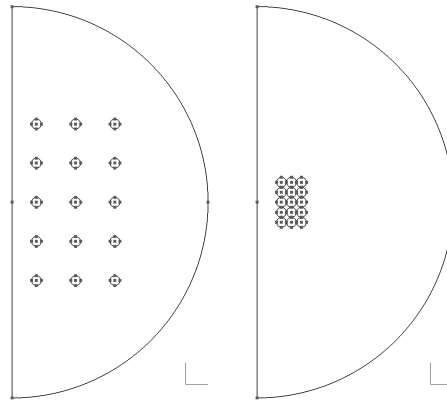


Figure 4.6: Geometrical representation of a 15-turn coil with an inter-turn distance of: 8mm (left) and 2.05mm (right)

4

spacing: 2.05mm and 8mm respectively. Recall that an inter-turn distance of 2.05mm means that neighboring turns of radius 1mm are only separated by 0.05mm, i.e., nearly touching each other. This case is that of a tightly wound coil. This study focuses on the accuracy of the impedance calculation for a broad range of frequencies. Furthermore, the frequency-sweep is linked to a table to study the decrease of the computational size of the problem (number of unknown in the FE system). Each numerical experiment is discussed in terms of the relative difference in degrees-of-freedom (DoF) and the relative error obtained in the comparison of the impedance between the Full (FM) and Semi-analytical (SA) models. The goal is to present the compromise between the size of the problem and the accuracy of the method.

4.3.1. 5-Turn Coil

4.3.1.1. Impedance vs. inter-turn spacing at 1Hz and 1MHz

In Fig. 4.7 we observe the effect of inter-turn spacing **at 1Hz**. The relative error of the resistance R^{err} is constant about a value of 1.64% throughout all inter-turn spacing values, which is expected as at lower frequencies proximity effects are negligible. It is also important to acknowledge that the relative error is relatively high, which is mainly due to the coarser mesh used at lower frequencies. The relative error of the inductance L^{err} is relatively constant with overall values under 5% except in the case of unstructured sleeve larger than the size of the conductor (3mm) where the error value rises up to values close to 15% after an inter-turn spacing of 4mm.

In Fig. 4.8 we observe the effect of inter-turn spacing **at 1MHz**. The relative error of the resistance R^{err} increases as the inter-turn spacing decreases, due to the presence of proximity effects. In the case of structured sleeves, the R^{err} values increase slowly from values close to zero up to 18% at small inter-turn spacing. In the case of unstructured sleeves, the behavior is more erratic. The $l_c = 0.5\text{mm}$ case holds the highest error from values oscillating between 20% and 60% past the 6mm mark. The rest of the unstructured sleeve cases 1mm and 3mm, the values oscillate between 19% and 30%. The L^{err} values remain under 2% for all sleeve cases except for the 0.5mm case (smaller than the size of the conductor), which sits at around 4%. at distances greater than 4mm. From the distance range between 4mm to 2.05mm, the error for the unstructured sleeve of 3mm oscillates up to values close to 10% whereas the rest of the values have a smoother increase to values close to 8%.

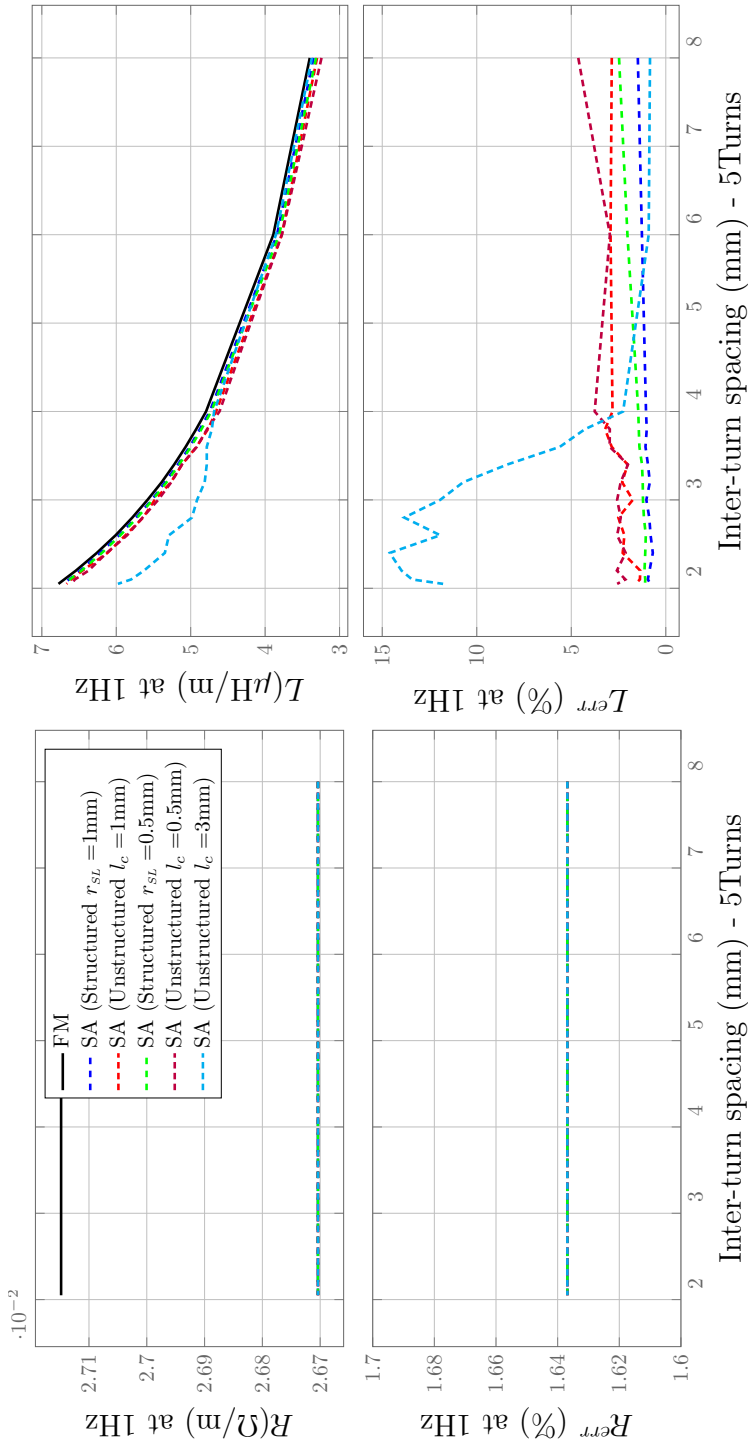


Figure 4.7: Impact of Inter-turn spacing on Impedance of a 5-turn multi-turn coil at 1Hz: Resistance (Left), Inductance (Right)

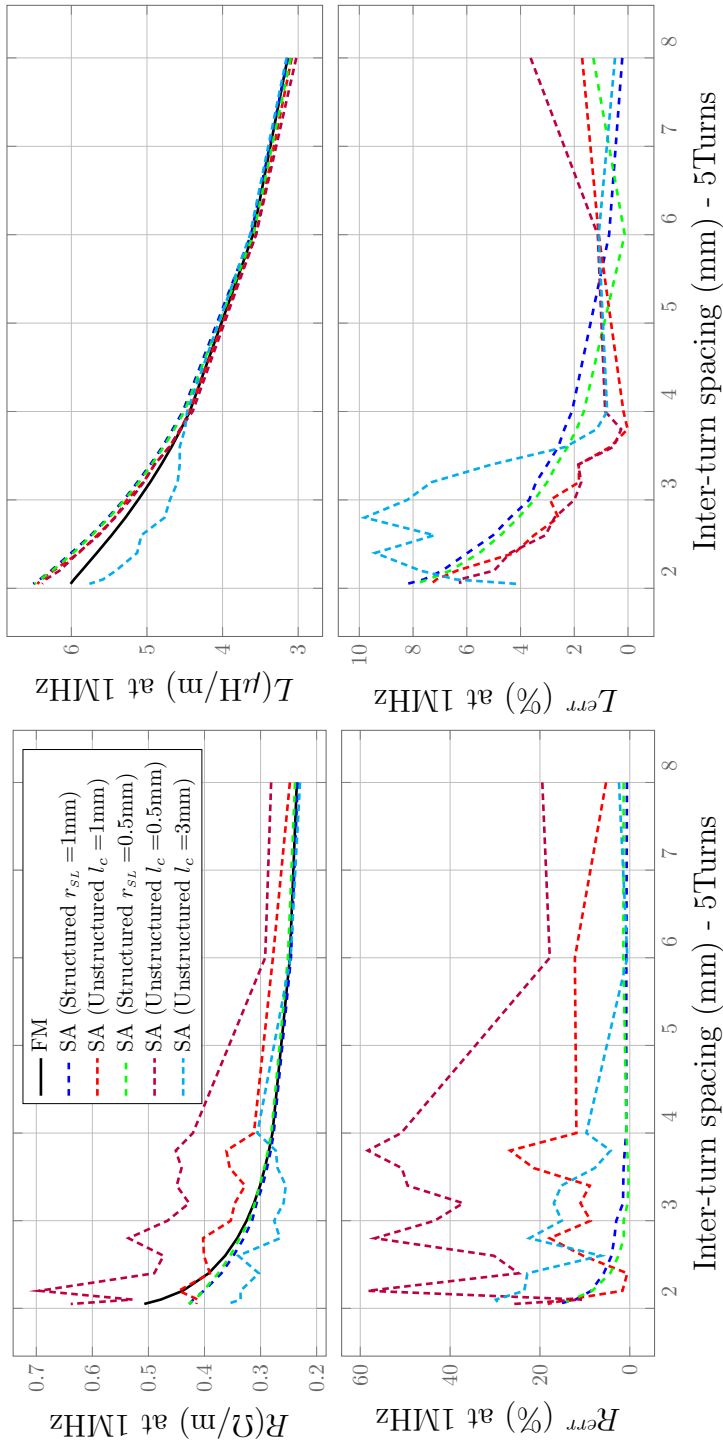


Figure 4.8: Impact of Inter-turn spacing on Impedance of a 5-turn multi-turn coil at 1MHz: Resistance (Left), Inductance (Right)

4.3.1.2. Impedance at a broad range of frequencies at a inter-turn spacing of 8mm

Fig 4.9 reports the resistance and the inductance values at an inter-turn spacing of 8mm at a broad range of frequencies.

The relative error in the resistance values **resistance** in the case of **structured sleeves** remains in a range between 1.64%–0.64% for $r_{SL} = 1\text{mm}$, 1.64%–1.35% for $r_{SL} = 0.5\text{mm}$, and 1.64%–1.34% for $r_{SL} = 3\text{mm}$. In the case of **unstructured sleeves** the relative error remains in a range between 1.64%–5.26% for $l_c = 1\text{mm}$, 1.64%–19.44% for $l_c = 0.5\text{mm}$, and 1.64%–2.42% for $l_c = 3\text{mm}$.

The relative error in the **inductance** values in the case of **structured sleeves** remains in a range between 1.48%–0.20% for $r_{SL} = 1\text{mm}$, 2.47%–1.28% for $r_{SL} = 0.5\text{mm}$, and 0.78%–0.56% for $r_{SL} = 3\text{mm}$. In the case of **unstructured sleeves** the relative error remains in a range between 2.86%–1.69% for $l_c = 1\text{mm}$, 4.63%–3.61% for $l_c = 0.5\text{mm}$, and 0.83%–0.5% for $l_c = 3\text{mm}$.

The compromise between error and computational cost is studied throughout tables 4.1 -4.3. The tables showcase the variation and relationship between the degrees-of-freedom (Dof) and the relative error in the resistance and inductance for each sleeve case (structured and unstructured). Note that the semi-analytical method allows a fixed cost whereas the mesh built for the fully discretized model is based on the skin-depth at each individual frequency. For sleeves of radii 1mm (tab. 4.1) the size can decrease at higher frequencies by 98.66% and 99.13% at the higher frequency range in the case of structured and unstructured sleeves. In table 4.2 the behavior is similar with a DoF relative difference between 48.71% and 64.34% at lower frequencies and decreasing the size problem by 98.21% and 98.75% at the higher frequencies for structured and unstructured sleeves respectively. Lastly, for sleeves larger than the conductor's radius (3mm) at lower frequencies the structured case ranges between decreasing values 83.20%–99.41% and unstructured sleeves between 87.88%–99.58%.

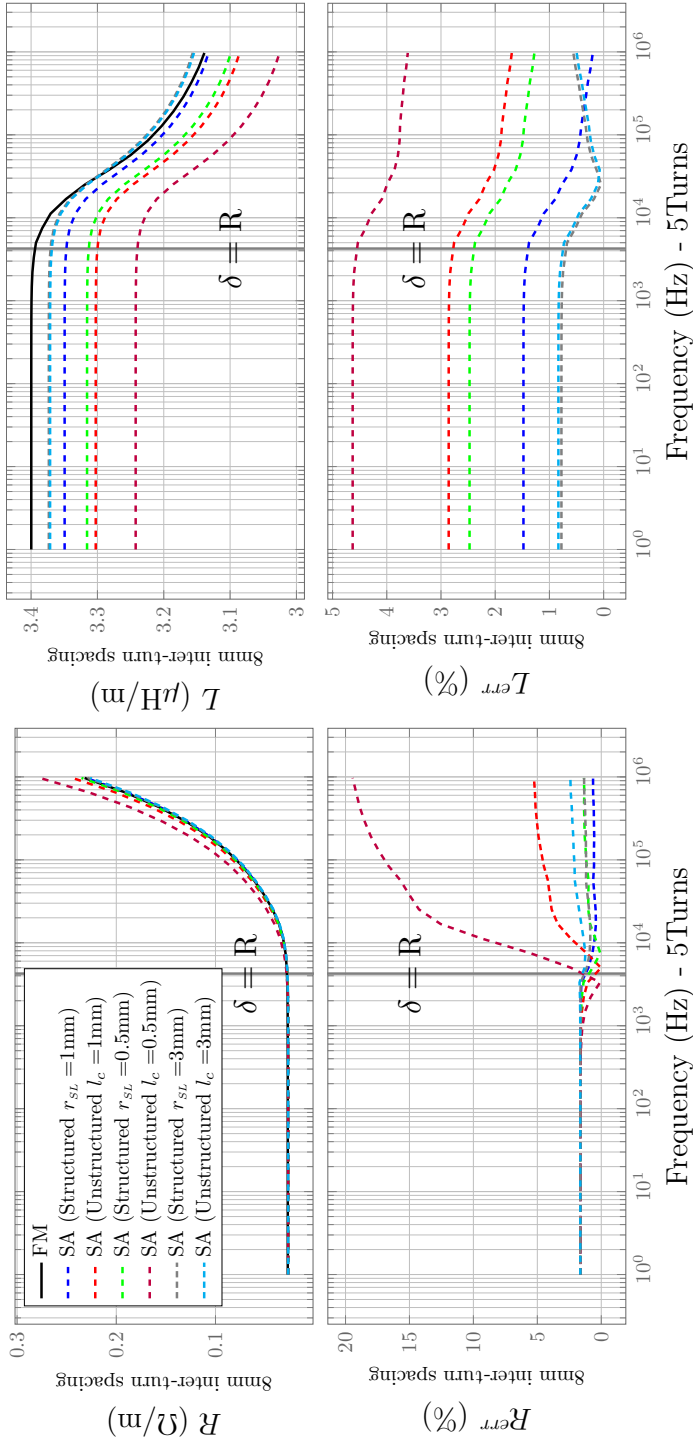


Figure 4.9: Impedance at a broad range of frequencies with large inter-turn spacing on a 5-Turn coil: Resistance (Left), Inductance (Right)

| 5 Turns Inter-turn distance 8mm | FM | | SA (Structured) $r_{SL} = 1mm$ | | | | | | SA (Unstructured) $l_c = 1mm$ | | | | | |
|---------------------------------------|-------|-----|-----------------------------------|----------------|-----------------------------|-----------------------------|--------|----------------|----------------------------------|-----------------------------|-----|----------------|-----------------------------|-----------------------------|
| | DoF | DoF | DoF | Rel. Diff. (%) | Resistance Rel. Err. (%) | Inductance Rel. Err. (%) | DoF | Rel. Diff. (%) | Resistance Rel. Err. (%) | Inductance Rel. Err. (%) | DoF | Rel. Diff. (%) | Resistance Rel. Err. (%) | Inductance Rel. Err. (%) |
| | | | | | | | | | | | | | | |
| 1.00 | 1708 | 665 | -61.07 | 1.64 | 1.48 | 425 | -75.12 | 1.64 | 2.86 | | | | | |
| 1.50 | 1708 | 665 | -61.07 | 1.64 | 1.48 | 425 | -75.12 | 1.64 | 2.86 | | | | | |
| 2.25 | 1708 | 665 | -61.07 | 1.64 | 1.48 | 425 | -75.12 | 1.64 | 2.86 | | | | | |
| 3.38 | 1708 | 665 | -61.07 | 1.64 | 1.48 | 425 | -75.12 | 1.64 | 2.86 | | | | | |
| 5.06 | 1708 | 665 | -61.07 | 1.64 | 1.48 | 425 | -75.12 | 1.64 | 2.86 | | | | | |
| 7.59 | 1708 | 665 | -61.07 | 1.64 | 1.48 | 425 | -75.12 | 1.64 | 2.86 | | | | | |
| 11.39 | 1708 | 665 | -61.07 | 1.64 | 1.48 | 425 | -75.12 | 1.64 | 2.86 | | | | | |
| 17.09 | 1708 | 665 | -61.07 | 1.64 | 1.48 | 425 | -75.12 | 1.64 | 2.86 | | | | | |
| 25.63 | 1708 | 665 | -61.07 | 1.64 | 1.48 | 425 | -75.12 | 1.64 | 2.86 | | | | | |
| 38.44 | 1708 | 665 | -61.07 | 1.64 | 1.48 | 425 | -75.12 | 1.64 | 2.86 | | | | | |
| 57.67 | 1708 | 665 | -61.07 | 1.64 | 1.48 | 425 | -75.12 | 1.64 | 2.86 | | | | | |
| 86.50 | 1708 | 665 | -61.07 | 1.64 | 1.48 | 425 | -75.12 | 1.64 | 2.86 | | | | | |
| 129.75 | 1708 | 665 | -61.07 | 1.64 | 1.48 | 425 | -75.12 | 1.64 | 2.86 | | | | | |
| 194.62 | 1708 | 665 | -61.07 | 1.64 | 1.48 | 425 | -75.12 | 1.63 | 2.86 | | | | | |
| 291.93 | 1708 | 665 | -61.07 | 1.64 | 1.48 | 425 | -75.12 | 1.63 | 2.86 | | | | | |
| 437.89 | 1708 | 665 | -61.07 | 1.64 | 1.48 | 425 | -75.12 | 1.63 | 2.86 | | | | | |
| 656.84 | 1708 | 665 | -61.07 | 1.63 | 1.48 | 425 | -75.12 | 1.61 | 2.86 | | | | | |
| 985.26 | 1708 | 665 | -61.07 | 1.63 | 1.47 | 425 | -75.12 | 1.58 | 2.85 | | | | | |
| 1477.89 | 1708 | 665 | -61.07 | 1.62 | 1.47 | 425 | -75.12 | 1.52 | 2.84 | | | | | |
| 2216.84 | 1708 | 665 | -61.07 | 1.60 | 1.45 | 425 | -75.12 | 1.37 | 2.83 | | | | | |
| 3325.26 | 1708 | 665 | -61.07 | 1.55 | 1.41 | 425 | -75.12 | 1.07 | 2.79 | | | | | |
| 4987.89 | 1755 | 665 | -62.11 | 1.01 | 1.38 | 425 | -75.78 | 0.02 | 2.76 | | | | | |
| 7481.83 | 2041 | 665 | -67.42 | 0.69 | 1.22 | 425 | -79.18 | 1.14 | 2.61 | | | | | |
| 11222.74 | 2617 | 665 | -74.59 | 0.52 | 1.10 | 425 | -83.76 | 2.38 | 2.50 | | | | | |
| 16834.11 | 3329 | 665 | -80.02 | 0.42 | 0.89 | 425 | -87.23 | 3.40 | 2.29 | | | | | |
| 25251.17 | 3518 | 665 | -81.10 | 0.44 | 0.77 | 425 | -87.92 | 3.88 | 2.18 | | | | | |
| 37876.75 | 4510 | 665 | -85.25 | 0.54 | 0.59 | 425 | -90.58 | 4.04 | 2.02 | | | | | |
| 56815.13 | 6423 | 665 | -89.65 | 0.63 | 0.50 | 425 | -93.38 | 4.18 | 1.94 | | | | | |
| 85222.69 | 7337 | 665 | -90.94 | 0.57 | 0.44 | 425 | -94.21 | 4.50 | 1.90 | | | | | |
| 127834.04 | 9423 | 665 | -92.94 | 0.57 | 0.41 | 425 | -95.49 | 4.71 | 1.88 | | | | | |
| 191751.06 | 12788 | 665 | -94.80 | 0.55 | 0.37 | 425 | -96.68 | 4.91 | 1.84 | | | | | |
| 287626.59 | 17157 | 665 | -96.12 | 0.57 | 0.33 | 425 | -97.52 | 5.03 | 1.81 | | | | | |
| 431439.88 | 24043 | 665 | -97.23 | 0.59 | 0.29 | 425 | -98.23 | 5.14 | 1.77 | | | | | |
| 647159.82 | 33929 | 665 | -98.04 | 0.64 | 0.24 | 425 | -98.75 | 5.19 | 1.73 | | | | | |
| 970739.74 | 48907 | 665 | -98.64 | 0.64 | 0.20 | 425 | -99.13 | 5.26 | 1.69 | | | | | |

Table 4.1: Relative difference between Degrees-of-Freedom used in Full-Model and Semi-analytical Model versus the relative error in the solution of the impedance at a broad range of frequencies for a 5-turn winding with 8mm of inter-turn distance and a sleeve size of 1mm

| 5 Turns Inter-turn distance 8mm Frequency (Hz) | FM | | SA (Structured) $r_{SL} = 0.5\text{mm}$ | | | | SA (Unstructured) $l_c = 0.5\text{mm}$ | | | |
|---------------------------------------------------------|-------|-----|--------------------------------------------|----------------|-----------------------------|-----------------------------|-------------------------------------------|----------------|-----------------------------|-----------------------------|
| | DoF | DoF | DoF | Rel. Diff. (%) | Resistance Rel. Err. (%) | Inductance Rel. Err. (%) | DoF | Rel. Diff. (%) | Resistance Rel. Err. (%) | Inductance Rel. Err. (%) |
| 1.00 | 1708 | 876 | 876 | -48.71 | 1.64 | 2.47 | 609 | -64.34 | 1.64 | 4.63 |
| 1.50 | 1708 | 876 | 876 | -48.71 | 1.64 | 2.47 | 609 | -64.34 | 1.64 | 4.63 |
| 2.25 | 1708 | 876 | 876 | -48.71 | 1.64 | 2.47 | 609 | -64.34 | 1.64 | 4.63 |
| 3.38 | 1708 | 876 | 876 | -48.71 | 1.64 | 2.47 | 609 | -64.34 | 1.64 | 4.63 |
| 5.06 | 1708 | 876 | 876 | -48.71 | 1.64 | 2.47 | 609 | -64.34 | 1.64 | 4.63 |
| 7.59 | 1708 | 876 | 876 | -48.71 | 1.64 | 2.47 | 609 | -64.34 | 1.64 | 4.63 |
| 11.39 | 1708 | 876 | 876 | -48.71 | 1.64 | 2.47 | 609 | -64.34 | 1.64 | 4.63 |
| 17.09 | 1708 | 876 | 876 | -48.71 | 1.64 | 2.47 | 609 | -64.34 | 1.64 | 4.63 |
| 25.63 | 1708 | 876 | 876 | -48.71 | 1.64 | 2.47 | 609 | -64.34 | 1.64 | 4.63 |
| 38.44 | 1708 | 876 | 876 | -48.71 | 1.64 | 2.47 | 609 | -64.34 | 1.64 | 4.63 |
| 57.67 | 1708 | 876 | 876 | -48.71 | 1.64 | 2.47 | 609 | -64.34 | 1.64 | 4.63 |
| 86.50 | 1708 | 876 | 876 | -48.71 | 1.64 | 2.47 | 609 | -64.34 | 1.64 | 4.63 |
| 129.75 | 1708 | 876 | 876 | -48.71 | 1.64 | 2.47 | 609 | -64.34 | 1.63 | 4.63 |
| 194.62 | 1708 | 876 | 876 | -48.71 | 1.64 | 2.47 | 609 | -64.34 | 1.63 | 4.63 |
| 291.93 | 1708 | 876 | 876 | -48.71 | 1.63 | 2.47 | 609 | -64.34 | 1.62 | 4.63 |
| 437.89 | 1708 | 876 | 876 | -48.71 | 1.63 | 2.47 | 609 | -64.34 | 1.60 | 4.63 |
| 656.84 | 1708 | 876 | 876 | -48.71 | 1.63 | 2.47 | 609 | -64.34 | 1.56 | 4.63 |
| 985.26 | 1708 | 876 | 876 | -48.71 | 1.61 | 2.47 | 609 | -64.34 | 1.47 | 4.62 |
| 1477.89 | 1708 | 876 | 876 | -48.71 | 1.58 | 2.46 | 609 | -64.34 | 1.27 | 4.62 |
| 2216.84 | 1708 | 876 | 876 | -48.71 | 1.52 | 2.44 | 609 | -64.34 | 0.83 | 4.60 |
| 3325.26 | 1708 | 876 | 876 | -48.71 | 1.39 | 2.41 | 609 | -64.34 | 0.09 | 4.57 |
| 4987.89 | 1755 | 876 | 876 | -50.09 | 0.68 | 2.37 | 609 | -65.30 | 2.36 | 4.53 |
| 7481.83 | 2041 | 876 | 876 | -57.08 | 0.07 | 2.22 | 609 | -70.16 | 5.53 | 4.39 |
| 11222.74 | 2617 | 876 | 876 | -66.53 | 0.46 | 2.11 | 609 | -76.73 | 9.34 | 4.28 |
| 16834.11 | 3329 | 876 | 876 | -73.69 | 0.87 | 1.90 | 609 | -81.71 | 12.56 | 4.09 |
| 25251.17 | 3518 | 876 | 876 | -75.10 | 1.02 | 1.78 | 609 | -82.69 | 14.26 | 3.99 |
| 37876.75 | 4510 | 876 | 876 | -80.58 | 1.01 | 1.62 | 609 | -86.50 | 15.01 | 3.86 |
| 56815.13 | 6423 | 876 | 876 | -86.36 | 1.00 | 1.54 | 609 | -90.52 | 15.72 | 3.79 |
| 85222.69 | 7337 | 876 | 876 | -88.06 | 1.15 | 1.49 | 609 | -91.70 | 16.66 | 3.76 |
| 127834.04 | 9423 | 876 | 876 | -90.70 | 1.21 | 1.47 | 609 | -93.54 | 17.39 | 3.76 |
| 191751.06 | 12788 | 876 | 876 | -93.15 | 1.29 | 1.43 | 609 | -95.24 | 18.02 | 3.73 |
| 287626.59 | 17157 | 876 | 876 | -94.89 | 1.32 | 1.39 | 609 | -96.45 | 18.49 | 3.70 |
| 431439.88 | 24043 | 876 | 876 | -96.36 | 1.35 | 1.36 | 609 | -97.47 | 18.89 | 3.68 |
| 647159.82 | 33929 | 876 | 876 | -97.42 | 1.33 | 1.31 | 609 | -98.21 | 19.17 | 3.64 |
| 970739.74 | 48907 | 876 | 876 | -98.21 | 1.35 | 1.28 | 609 | -98.75 | 19.44 | 3.61 |

Table 4.2: Relative difference between Degrees-of-Freedom used in Full-Model and Semi-analytical Model versus the relative error in the solution of the impedance at a broad range of frequencies for a 5-turn winding with 8mm of inter-turn distance and a sleeve size of 0.5mm

| 5 Turns Inter-turn distance 8mm Frequency (Hz) | FM | | SA (Structured) $r_{SL} = 3\text{mm}$ | | | | | | SA (Unstructured) $l_c = 3\text{mm}$ | | | | | |
|---------------------------------------------------------|-------|-----|------------------------------------------|----------------|-----------------------------|-----------------------------|--------|----------------|-----------------------------------------|-----------------------------|--------|----------------|-----------------------------|-----------------------------|
| | DoF | DoF | DoF | Rel. Diff. (%) | Resistance Rel. Err. (%) | Inductance Rel. Err. (%) | DoF | Rel. Diff. (%) | Resistance Rel. Err. (%) | Inductance Rel. Err. (%) | DoF | Rel. Diff. (%) | Resistance Rel. Err. (%) | Inductance Rel. Err. (%) |
| | | | | | | | | | | | | | | |
| 1.00 | 1708 | 287 | 83.20 | 1.64 | 0.78 | 207 | -87.88 | 1.64 | 0.83 | 207 | -87.88 | 1.64 | 0.83 | |
| 1.50 | 1708 | 287 | -83.20 | 1.64 | 0.78 | 207 | -87.88 | 1.64 | 0.83 | 207 | -87.88 | 1.64 | 0.83 | |
| 2.25 | 1708 | 287 | -83.20 | 1.64 | 0.78 | 207 | -87.88 | 1.64 | 0.83 | 207 | -87.88 | 1.64 | 0.83 | |
| 3.38 | 1708 | 287 | -83.20 | 1.64 | 0.78 | 207 | -87.88 | 1.64 | 0.83 | 207 | -87.88 | 1.64 | 0.83 | |
| 5.06 | 1708 | 287 | -83.20 | 1.64 | 0.78 | 207 | -87.88 | 1.64 | 0.83 | 207 | -87.88 | 1.64 | 0.83 | |
| 7.59 | 1708 | 287 | -83.20 | 1.64 | 0.78 | 207 | -87.88 | 1.64 | 0.83 | 207 | -87.88 | 1.64 | 0.83 | |
| 11.39 | 1708 | 287 | -83.20 | 1.64 | 0.78 | 207 | -87.88 | 1.64 | 0.83 | 207 | -87.88 | 1.64 | 0.83 | |
| 17.09 | 1708 | 287 | -83.20 | 1.64 | 0.78 | 207 | -87.88 | 1.64 | 0.83 | 207 | -87.88 | 1.64 | 0.83 | |
| 25.63 | 1708 | 287 | -83.20 | 1.64 | 0.78 | 207 | -87.88 | 1.64 | 0.83 | 207 | -87.88 | 1.64 | 0.83 | |
| 38.44 | 1708 | 287 | -83.20 | 1.64 | 0.78 | 207 | -87.88 | 1.64 | 0.83 | 207 | -87.88 | 1.64 | 0.83 | |
| 57.67 | 1708 | 287 | -83.20 | 1.64 | 0.78 | 207 | -87.88 | 1.64 | 0.83 | 207 | -87.88 | 1.64 | 0.83 | |
| 86.50 | 1708 | 287 | -83.20 | 1.64 | 0.78 | 207 | -87.88 | 1.64 | 0.83 | 207 | -87.88 | 1.64 | 0.83 | |
| 129.75 | 1708 | 287 | -83.20 | 1.64 | 0.78 | 207 | -87.88 | 1.64 | 0.83 | 207 | -87.88 | 1.64 | 0.83 | |
| 194.62 | 1708 | 287 | -83.20 | 1.64 | 0.78 | 207 | -87.88 | 1.64 | 0.83 | 207 | -87.88 | 1.64 | 0.83 | |
| 291.93 | 1708 | 287 | -83.20 | 1.64 | 0.78 | 207 | -87.88 | 1.64 | 0.83 | 207 | -87.88 | 1.64 | 0.83 | |
| 437.89 | 1708 | 287 | -83.20 | 1.64 | 0.78 | 207 | -87.88 | 1.64 | 0.83 | 207 | -87.88 | 1.64 | 0.83 | |
| 656.84 | 1708 | 287 | -83.20 | 1.64 | 0.78 | 207 | -87.88 | 1.64 | 0.83 | 207 | -87.88 | 1.64 | 0.83 | |
| 985.26 | 1708 | 287 | -83.20 | 1.63 | 0.77 | 207 | -87.88 | 1.64 | 0.83 | 207 | -87.88 | 1.64 | 0.83 | |
| 1477.89 | 1708 | 287 | -83.20 | 1.63 | 0.76 | 207 | -87.88 | 1.65 | 0.82 | 207 | -87.88 | 1.65 | 0.82 | |
| 2216.84 | 1708 | 287 | -83.20 | 1.62 | 0.75 | 207 | -87.88 | 1.66 | 0.80 | 207 | -87.88 | 1.66 | 0.80 | |
| 3325.26 | 1708 | 287 | -83.20 | 1.61 | 0.71 | 207 | -87.88 | 1.70 | 0.77 | 207 | -87.88 | 1.70 | 0.77 | |
| 4987.89 | 1755 | 287 | -83.65 | 1.13 | 0.67 | 207 | -88.21 | 1.31 | 0.73 | 207 | -88.21 | 1.31 | 0.73 | |
| 7481.83 | 2041 | 287 | -85.94 | 0.91 | 0.52 | 207 | -89.86 | 1.24 | 0.58 | 207 | -89.86 | 1.24 | 0.58 | |
| 11222.74 | 2617 | 287 | -89.03 | 0.86 | 0.40 | 207 | -92.09 | 1.39 | 0.45 | 207 | -92.09 | 1.39 | 0.45 | |
| 16834.11 | 3329 | 287 | -91.38 | 0.87 | 0.18 | 207 | -93.78 | 1.56 | 0.24 | 207 | -93.78 | 1.56 | 0.24 | |
| 25251.17 | 3518 | 287 | -91.84 | 0.96 | 0.05 | 207 | -94.12 | 1.74 | 0.11 | 207 | -94.12 | 1.74 | 0.11 | |
| 37876.75 | 4510 | 287 | -93.64 | 1.08 | 0.13 | 207 | -95.41 | 1.91 | 0.07 | 207 | -95.41 | 1.91 | 0.07 | |
| 56815.13 | 6423 | 287 | -95.53 | 1.20 | 0.23 | 207 | -96.78 | 2.07 | 0.18 | 207 | -96.78 | 2.07 | 0.18 | |
| 85222.69 | 7337 | 287 | -96.09 | 1.17 | 0.30 | 207 | -97.18 | 2.09 | 0.24 | 207 | -97.18 | 2.09 | 0.24 | |
| 127834.04 | 9423 | 287 | -96.95 | 1.20 | 0.33 | 207 | -97.80 | 2.16 | 0.27 | 207 | -97.80 | 2.16 | 0.27 | |
| 191751.06 | 12788 | 287 | -97.76 | 1.20 | 0.38 | 207 | -98.38 | 2.19 | 0.32 | 207 | -98.38 | 2.19 | 0.32 | |
| 287626.59 | 17157 | 287 | -98.33 | 1.24 | 0.42 | 207 | -98.79 | 2.26 | 0.36 | 207 | -98.79 | 2.26 | 0.36 | |
| 431439.88 | 24043 | 287 | -98.81 | 1.27 | 0.46 | 207 | -99.14 | 2.31 | 0.40 | 207 | -99.14 | 2.31 | 0.40 | |
| 647159.82 | 33929 | 287 | -99.15 | 1.33 | 0.52 | 207 | -99.39 | 2.39 | 0.46 | 207 | -99.39 | 2.39 | 0.46 | |
| 970739.74 | 48907 | 287 | -99.41 | 1.34 | 0.56 | 207 | -99.58 | 2.42 | 0.50 | 207 | -99.58 | 2.42 | 0.50 | |

Table 4.3: Relative difference between Degrees-of-Freedom used in Full-Model and Semi-analytical Model versus the relative error in the solution of the impedance at a broad range of frequencies for a 5-turn winding with 8mm of inter-turn distance and a sleeve size of 0.5mm

4.3.1.3. Impedance at a broad range of frequencies at an inter-turn spacing of 2.05mm

Fig 4.10 reports the resistance and the inductance values at an inter-turn spacing of 2.05mm at a broad range of frequencies.

The relative error in the **resistance** values in the case of **structured sleeves** remains in a range between 1.64% – 15.83% for $r_{SL} = 1\text{mm}$, 1.64% – 15.55% for $r_{SL} = 0.5\text{mm}$. In the case of **unstructured sleeves** the relative error remains in a range between 1.64% – 18.22% for $l_c = 1\text{mm}$, 1.64% – 25.92% for $l_c = 0.5\text{mm}$, and 1.64% – 29.18% for $l_c = 3\text{mm}$.

The relative error in the **inductance** values in the case of **structured sleeves** remains in a range between 0.81% – 8.14% for $r_{SL} = 1\text{mm}$, 1.10% – 7.82% for $r_{SL} = 0.5\text{mm}$. In the case of **structured sleeves** the relative error remains in a range between 1.61% – 7.25% for $l_c = 1\text{mm}$, 2.57% – 6.16% for $l_c = 0.5\text{mm}$, and 11.78% – 4.21% for $l_c = 3\text{mm}$.

The compromise between error and computational cost is studied throughout tables 4.4 -4.6. The tables showcase the variation and relationship between the degrees-of-freedom (Dof) and the relative error in the resistance and inductance for each sleeve case (structured and unstructured). Note that the semi-analytical method allows a fixed cost whereas the mesh built for the fully discretized model is based on the skin-depth at each individual frequency. For sleeves of radii 1mm (tab. 4.4) the size can decrease at higher frequencies by 99.12% and 99.34% at the higher frequency range in the case of structured and unstructured sleeves. In table 4.5 the behavior is similar with a DoF relative difference between 40.80% and 54.33% at lower frequencies and decreasing the size problem by 98.83% and 99.09% at the higher frequencies for structured and unstructured sleeves respectively. Lastly, for unstructured sleeves larger than the conductor's radius (tab. 4.6) the problem size decrease ranges between 75.32% – 99.51%.

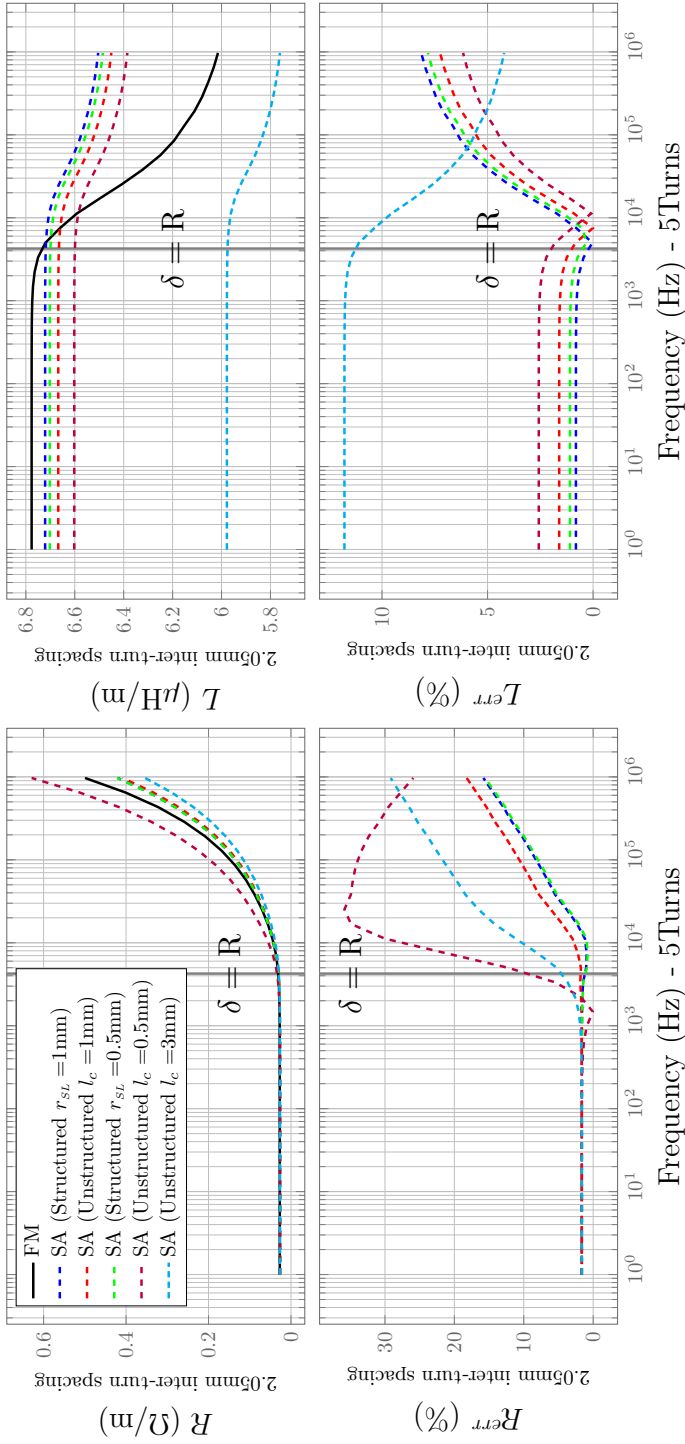


Figure 4.10: Impedance at a broad range of frequencies with small inter-turn spacing on a 5-Turn coil: Resistance (Left), Inductance (Right)

| 5 Turns Inter-turn distance 2.05mm Frequency (Hz) | FM | | SA (Structured) $r_{SL} = 1\text{mm}$ | | | | SA (Unstructured) $l_c = 1\text{mm}$ | | | |
|------------------------------------------------------|-------|-----|------------------------------------------|----------------|--------------------------|--------------------------|-----------------------------------------|----------------|--------------------------|--------------------------|
| | DoF | DoF | DoF | Rel. Diff. (%) | Resistance Rel. Err. (%) | Inductance Rel. Err. (%) | DoF | Rel. Diff. (%) | Resistance Rel. Err. (%) | Inductance Rel. Err. (%) |
| 1.00 | 924 | 411 | | -55.52 | 1.64 | 0.81 | 308 | -66.67 | 1.64 | 1.61 |
| 1.50 | 924 | 411 | | -55.52 | 1.64 | 0.81 | 308 | -66.67 | 1.64 | 1.61 |
| 2.25 | 924 | 411 | | -55.52 | 1.64 | 0.81 | 308 | -66.67 | 1.64 | 1.61 |
| 3.38 | 924 | 411 | | -55.52 | 1.64 | 0.81 | 308 | -66.67 | 1.64 | 1.61 |
| 5.06 | 924 | 411 | | -55.52 | 1.64 | 0.81 | 308 | -66.67 | 1.64 | 1.61 |
| 7.59 | 924 | 411 | | -55.52 | 1.64 | 0.81 | 308 | -66.67 | 1.64 | 1.61 |
| 11.39 | 924 | 411 | | -55.52 | 1.64 | 0.81 | 308 | -66.67 | 1.64 | 1.61 |
| 17.09 | 924 | 411 | | -55.52 | 1.64 | 0.81 | 308 | -66.67 | 1.64 | 1.61 |
| 25.63 | 924 | 411 | | -55.52 | 1.64 | 0.81 | 308 | -66.67 | 1.64 | 1.61 |
| 38.44 | 924 | 411 | | -55.52 | 1.64 | 0.81 | 308 | -66.67 | 1.64 | 1.61 |
| 57.67 | 924 | 411 | | -55.52 | 1.64 | 0.81 | 308 | -66.67 | 1.64 | 1.61 |
| 86.50 | 924 | 411 | | -55.52 | 1.64 | 0.81 | 308 | -66.67 | 1.64 | 1.61 |
| 129.75 | 924 | 411 | | -55.52 | 1.64 | 0.81 | 308 | -66.67 | 1.64 | 1.61 |
| 194.62 | 924 | 411 | | -55.52 | 1.64 | 0.81 | 308 | -66.67 | 1.64 | 1.60 |
| 291.93 | 924 | 411 | | -55.52 | 1.64 | 0.81 | 308 | -66.67 | 1.64 | 1.59 |
| 437.89 | 924 | 411 | | -55.52 | 1.63 | 0.81 | 308 | -66.67 | 1.64 | 1.60 |
| 656.84 | 924 | 411 | | -55.52 | 1.63 | 0.80 | 308 | -66.67 | 1.65 | 1.59 |
| 985.26 | 924 | 411 | | -55.52 | 1.62 | 0.78 | 308 | -66.67 | 1.66 | 1.57 |
| 1477.89 | 924 | 411 | | -55.52 | 1.60 | 0.74 | 308 | -66.67 | 1.69 | 1.53 |
| 2216.84 | 924 | 411 | | -55.52 | 1.55 | 0.65 | 308 | -66.67 | 1.74 | 1.44 |
| 3325.26 | 924 | 411 | | -55.52 | 1.46 | 0.45 | 308 | -66.67 | 1.86 | 1.25 |
| 4987.89 | 1105 | 411 | | -62.81 | 1.01 | 0.03 | 308 | -72.13 | 1.77 | 0.83 |
| 7481.83 | 1224 | 411 | | -66.42 | 0.93 | 0.79 | 308 | -74.84 | 2.20 | 0.02 |
| 11222.74 | 1526 | 411 | | -73.07 | 1.19 | 1.72 | 308 | -79.82 | 2.98 | 0.90 |
| 16834.11 | 1878 | 411 | | -78.12 | 2.32 | 2.89 | 308 | -83.60 | 4.45 | 2.07 |
| 25251.17 | 2436 | 411 | | -83.13 | 3.83 | 4.00 | 308 | -87.36 | 6.11 | 3.16 |
| 37876.75 | 3203 | 411 | | -87.17 | 5.47 | 4.93 | 308 | -90.38 | 7.79 | 4.08 |
| 56815.13 | 4232 | 411 | | -90.29 | 6.55 | 5.70 | 308 | -92.72 | 8.92 | 4.84 |
| 85222.69 | 5768 | 411 | | -92.87 | 7.74 | 6.26 | 308 | -94.66 | 10.14 | 5.39 |
| 127834.04 | 7695 | 411 | | -94.66 | 8.98 | 6.64 | 308 | -96.00 | 11.42 | 5.77 |
| 191751.06 | 10963 | 411 | | -96.25 | 10.25 | 7.11 | 308 | -97.19 | 12.70 | 6.23 |
| 287626.59 | 15445 | 411 | | -97.34 | 11.72 | 7.44 | 308 | -98.01 | 14.16 | 6.56 |
| 431439.88 | 22240 | 411 | | -98.15 | 12.93 | 7.70 | 308 | -98.62 | 15.36 | 6.82 |
| 647159.82 | 32347 | 411 | | -98.73 | 14.40 | 7.95 | 308 | -99.05 | 16.82 | 7.06 |
| 970739.74 | 46614 | 411 | | -99.12 | 15.83 | 8.14 | 308 | -99.34 | 18.22 | 7.25 |

Table 4.4: Relative difference between Degrees-of-Freedom used in Full-Model and Semi-analytical Model versus the relative error in the solution of the impedance at a broad range of frequencies for a 5-turn winding with 2.05mm of inter-turn distance and a sleeve size of 1mm

| 5 Turns Inter-turn distance 2.05mm Frequency (Hz) | FM | SA (Structured) $r_{SL} = 0.5\text{mm}$ | | | | SA (Unstructured) $l_c = 0.5\text{mm}$ | | | |
|------------------------------------------------------------|-------|--------------------------------------------|-----------------------|-----------------------------|-----------------------------|-------------------------------------------|-----------------------|-----------------------------|-----------------------------|
| | | DoF | DoF Rel. Diff. (%) | Resistance Rel. Err. (%) | Inductance Rel. Err. (%) | DoF | DoF Rel. Diff. (%) | Resistance Rel. Err. (%) | Inductance Rel. Err. (%) |
| 1.00 | 924 | 547 | -40.80 | 1.64 | 1.10 | 422 | -54.33 | 1.64 | 2.57 |
| 1.50 | 924 | 547 | -40.80 | 1.64 | 1.10 | 422 | -54.33 | 1.64 | 2.57 |
| 2.25 | 924 | 547 | -40.80 | 1.64 | 1.10 | 422 | -54.33 | 1.64 | 2.57 |
| 3.38 | 924 | 547 | -40.80 | 1.64 | 1.10 | 422 | -54.33 | 1.64 | 2.57 |
| 5.06 | 924 | 547 | -40.80 | 1.64 | 1.10 | 422 | -54.33 | 1.64 | 2.57 |
| 7.59 | 924 | 547 | -40.80 | 1.64 | 1.10 | 422 | -54.33 | 1.64 | 2.57 |
| 11.39 | 924 | 547 | -40.80 | 1.64 | 1.10 | 422 | -54.33 | 1.64 | 2.57 |
| 17.09 | 924 | 547 | -40.80 | 1.64 | 1.10 | 422 | -54.33 | 1.64 | 2.57 |
| 25.63 | 924 | 547 | -40.80 | 1.64 | 1.10 | 422 | -54.33 | 1.64 | 2.57 |
| 38.44 | 924 | 547 | -40.80 | 1.64 | 1.10 | 422 | -54.33 | 1.64 | 2.57 |
| 57.67 | 924 | 547 | -40.80 | 1.64 | 1.10 | 422 | -54.33 | 1.63 | 2.57 |
| 86.50 | 924 | 547 | -40.80 | 1.64 | 1.10 | 422 | -54.33 | 1.63 | 2.57 |
| 129.75 | 924 | 547 | -40.80 | 1.64 | 1.10 | 422 | -54.33 | 1.62 | 2.57 |
| 194.62 | 924 | 547 | -40.80 | 1.64 | 1.10 | 422 | -54.33 | 1.61 | 2.57 |
| 291.93 | 924 | 547 | -40.80 | 1.63 | 1.09 | 422 | -54.33 | 1.57 | 2.57 |
| 437.89 | 924 | 547 | -40.80 | 1.63 | 1.09 | 422 | -54.33 | 1.49 | 2.57 |
| 656.84 | 924 | 547 | -40.80 | 1.63 | 1.08 | 422 | -54.33 | 1.32 | 2.56 |
| 985.26 | 924 | 547 | -40.80 | 1.61 | 1.06 | 422 | -54.33 | 0.92 | 2.54 |
| 1477.89 | 924 | 547 | -40.80 | 1.59 | 1.02 | 422 | -54.33 | 0.06 | 2.50 |
| 2216.84 | 924 | 547 | -40.80 | 1.53 | 0.93 | 422 | -54.33 | 1.78 | 2.41 |
| 3325.26 | 924 | 547 | -40.80 | 1.42 | 0.73 | 422 | -54.33 | 5.45 | 2.22 |
| 4987.89 | 1105 | 547 | -50.50 | 0.92 | 0.32 | 422 | -61.81 | 12.23 | 1.81 |
| 7481.83 | 1224 | 547 | -55.31 | 0.79 | 0.50 | 422 | -65.52 | 21.20 | 1.00 |
| 11222.74 | 1526 | 547 | -64.15 | 0.98 | 1.43 | 422 | -72.35 | 30.01 | 0.09 |
| 16834.11 | 1878 | 547 | -70.87 | 2.07 | 2.60 | 422 | -77.53 | 34.89 | 1.06 |
| 25251.17 | 2436 | 547 | -77.55 | 3.57 | 3.70 | 422 | -82.68 | 35.84 | 2.14 |
| 37876.75 | 3203 | 547 | -82.92 | 5.21 | 4.62 | 422 | -86.82 | 34.92 | 3.04 |
| 56815.13 | 4232 | 547 | -87.07 | 6.28 | 5.39 | 422 | -90.03 | 34.63 | 3.79 |
| 85222.69 | 5768 | 547 | -90.52 | 7.46 | 5.95 | 422 | -92.68 | 34.19 | 4.34 |
| 127834.04 | 7695 | 547 | -92.89 | 8.71 | 6.33 | 422 | -94.52 | 33.40 | 4.71 |
| 191751.06 | 10963 | 547 | -95.01 | 9.97 | 6.79 | 422 | -96.15 | 32.34 | 5.16 |
| 287626.59 | 15445 | 547 | -96.46 | 11.44 | 7.13 | 422 | -97.27 | 30.81 | 5.48 |
| 431439.88 | 22240 | 547 | -97.54 | 12.65 | 7.39 | 422 | -98.10 | 29.52 | 5.74 |
| 647159.82 | 32347 | 547 | -98.31 | 14.12 | 7.63 | 422 | -98.70 | 27.73 | 5.97 |
| 970739.74 | 46614 | 547 | -98.83 | 15.55 | 7.82 | 422 | -99.09 | 25.92 | 6.16 |

Table 4-5: Relative difference between Degrees-of-Freedom used in Full-Model and Semi-analytical Model versus the relative error in the solution of the impedance at a broad range of frequencies for a 5-turn winding with 2.05mm of inter-turn distance and a sleeve size of 0.5mm

| 5 Turns Inter-turn distance 2.05mm Frequency (Hz) | FM | | SA (Structured) $r_{SL} = 3\text{mm}$ | | | | SA (Unstructured) $l_c = 3\text{mm}$ | | | |
|------------------------------------------------------------|-------|-----|------------------------------------------|-----------------------------|-----------------------------|-----|-----------------------------------------|-----------------------------|-----------------------------|--|
| | DoF | DoF | DoF Rel. Diff. (%) | Resistance Rel. Err. (%) | Inductance Rel. Err. (%) | DoF | DoF Rel. Diff. (%) | Resistance Rel. Err. (%) | Inductance Rel. Err. (%) | |
| 1.00 | 924 | N/A | N/A | N/A | N/A | 228 | -75.32 | 1.64 | 11.78 | |
| 1.50 | 924 | N/A | N/A | N/A | N/A | 228 | -75.32 | 1.64 | 11.78 | |
| 2.25 | 924 | N/A | N/A | N/A | N/A | 228 | -75.32 | 1.64 | 11.78 | |
| 3.38 | 924 | N/A | N/A | N/A | N/A | 228 | -75.32 | 1.64 | 11.78 | |
| 5.06 | 924 | N/A | N/A | N/A | N/A | 228 | -75.32 | 1.64 | 11.78 | |
| 7.59 | 924 | N/A | N/A | N/A | N/A | 228 | -75.32 | 1.64 | 11.78 | |
| 11.39 | 924 | N/A | N/A | N/A | N/A | 228 | -75.32 | 1.64 | 11.78 | |
| 17.09 | 924 | N/A | N/A | N/A | N/A | 228 | -75.32 | 1.64 | 11.78 | |
| 25.63 | 924 | N/A | N/A | N/A | N/A | 228 | -75.32 | 1.64 | 11.78 | |
| 38.44 | 924 | N/A | N/A | N/A | N/A | 228 | -75.32 | 1.64 | 11.78 | |
| 57.67 | 924 | N/A | N/A | N/A | N/A | 228 | -75.32 | 1.64 | 11.78 | |
| 86.50 | 924 | N/A | N/A | N/A | N/A | 228 | -75.32 | 1.64 | 11.78 | |
| 129.75 | 924 | N/A | N/A | N/A | N/A | 228 | -75.32 | 1.64 | 11.78 | |
| 194.62 | 924 | N/A | N/A | N/A | N/A | 228 | -75.32 | 1.66 | 11.78 | |
| 291.93 | 924 | N/A | N/A | N/A | N/A | 228 | -75.32 | 1.68 | 11.77 | |
| 437.89 | 924 | N/A | N/A | N/A | N/A | 228 | -75.32 | 1.73 | 11.77 | |
| 656.84 | 924 | N/A | N/A | N/A | N/A | 228 | -75.32 | 1.84 | 11.75 | |
| 985.26 | 924 | N/A | N/A | N/A | N/A | 228 | -75.32 | 2.09 | 11.71 | |
| 1477.89 | 924 | N/A | N/A | N/A | N/A | 228 | -75.32 | 2.62 | 11.63 | |
| 2216.84 | 924 | N/A | N/A | N/A | N/A | 228 | -75.32 | 3.67 | 11.46 | |
| 3325.26 | 924 | N/A | N/A | N/A | N/A | 228 | -79.37 | 5.24 | 11.09 | |
| 4987.89 | 1105 | N/A | N/A | N/A | N/A | 228 | -81.37 | 8.01 | 10.37 | |
| 7481.83 | 1224 | N/A | N/A | N/A | N/A | 228 | -85.06 | 11.17 | 9.56 | |
| 11222.74 | 1526 | N/A | N/A | N/A | N/A | 228 | -87.86 | 14.22 | 8.54 | |
| 16834.11 | 1878 | N/A | N/A | N/A | N/A | 228 | -90.64 | 16.53 | 7.59 | |
| 25251.17 | 2436 | N/A | N/A | N/A | N/A | 228 | -92.88 | 18.39 | 6.83 | |
| 37876.75 | 3203 | N/A | N/A | N/A | N/A | 228 | -94.61 | 19.73 | 6.19 | |
| 56815.13 | 4232 | N/A | N/A | N/A | N/A | 228 | -96.05 | 21.15 | 5.74 | |
| 85222.69 | 5768 | N/A | N/A | N/A | N/A | 228 | -97.04 | 22.54 | 5.43 | |
| 127834.04 | 7695 | N/A | N/A | N/A | N/A | 228 | -97.92 | 23.87 | 5.05 | |
| 191751.06 | 10963 | N/A | N/A | N/A | N/A | 228 | -98.52 | 25.32 | 4.78 | |
| 287626.59 | 15445 | N/A | N/A | N/A | N/A | 228 | -98.97 | 26.51 | 4.57 | |
| 431439.88 | 22240 | N/A | N/A | N/A | N/A | 228 | -99.30 | 27.87 | 4.37 | |
| 647159.82 | 32347 | N/A | N/A | N/A | N/A | 228 | -99.51 | 29.18 | 4.21 | |
| 970739.74 | 46614 | N/A | N/A | N/A | N/A | 228 | | | | |

Table 4.6: Relative difference between Degrees-of-Freedom used in Full-Model and Semi-analytical Model versus the relative error in the solution of the impedance at a broad range of frequencies for a 5-turn winding with 2.05mm of inter-turn distance and a sleeve size of 3mm

4.3.2. 10-Turn Coil

4.3.2.1. Impedance vs. inter-turn spacing at 1Hz and 1MHz

In Fig. 4.11 we observe the effect of inter-turn spacing **at 1Hz**. The relative error of the resistance R^{err} is constant about a value of 1.64% throughout all inter-turn spacing values, which is expected as at lower frequencies proximity effects are negligible. It is also important to acknowledge that the relative error is relatively high, which is mainly due to the coarser mesh used at lower frequencies. The relative error of the inductance L^{err} is relatively constant with overall values under 4% except in the case of unstructured sleeve larger than the size of the conductor (3mm) where the error value rises up to values close to 8% after an inter-turn spacing of 6mm.

In Fig. 4.12 we observe the effect of inter-turn spacing **at 1MHz**. The relative error of the resistance R^{err} increases as the inter-turn spacing decreases, due to the presence of proximity effects. In the case of structured sleeves, the R^{err} values increase slowly from values close to 1.6% up to 42% at small inter-turn spacing. In the case of structured sleeve with radius $r_{SL} = 0.5$ rises up to a relative error of 95% In the case of unstructured sleeves, the behavior is roughly the same as the structured sleeve case except for the case with $l_c = 1\text{mm}$ which has a larger error value, however the behavior of the curve is similar to the rest. The L^{err} values remain between 4% – 8% for the sleeve cases $r_{SL} = 3\text{mm}$. All other cases for both structured and unstructured the relative error ranges from 0.5% – 16%.

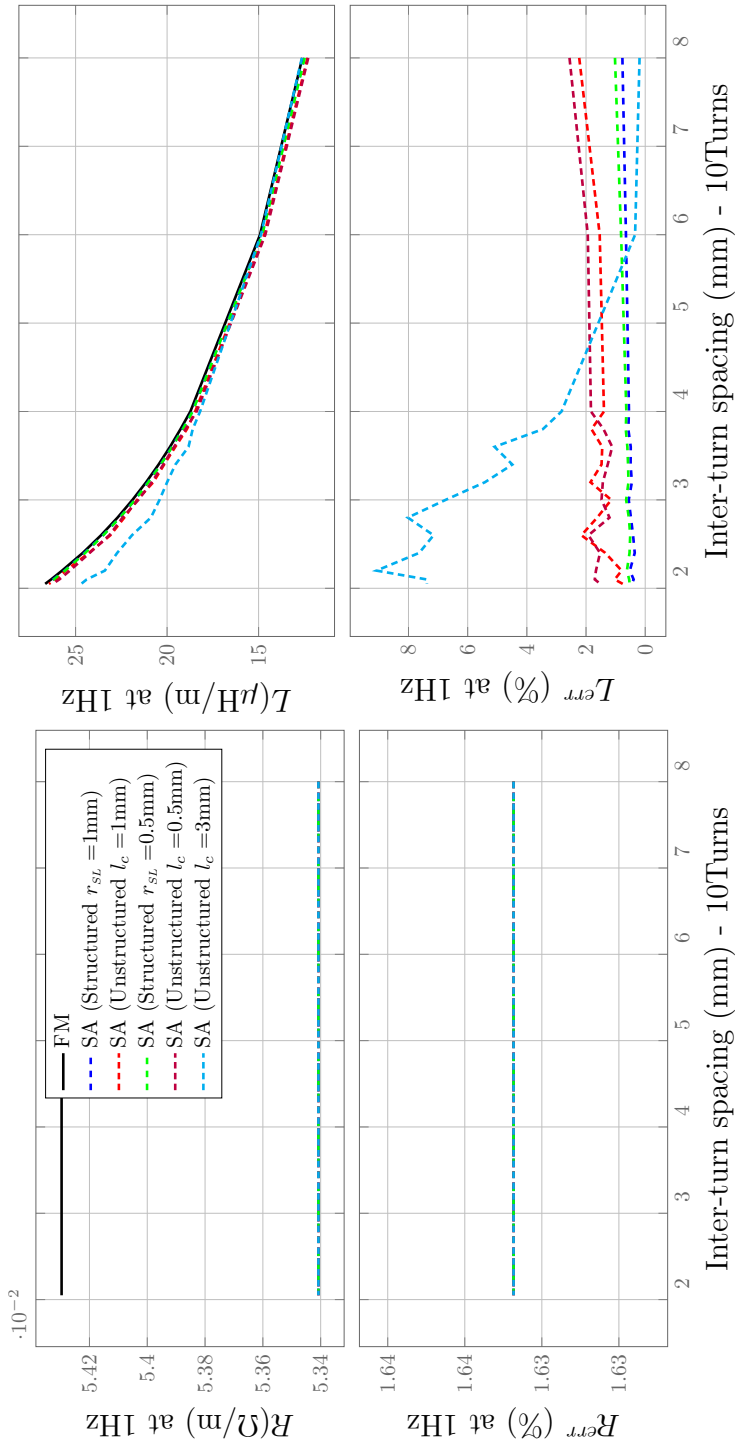


Figure 4.11: Impact of Inter-turn spacing on Impedance of a 10-turn multi-turn coil at 1Hz: Resistance (Left), Inductance (Right)

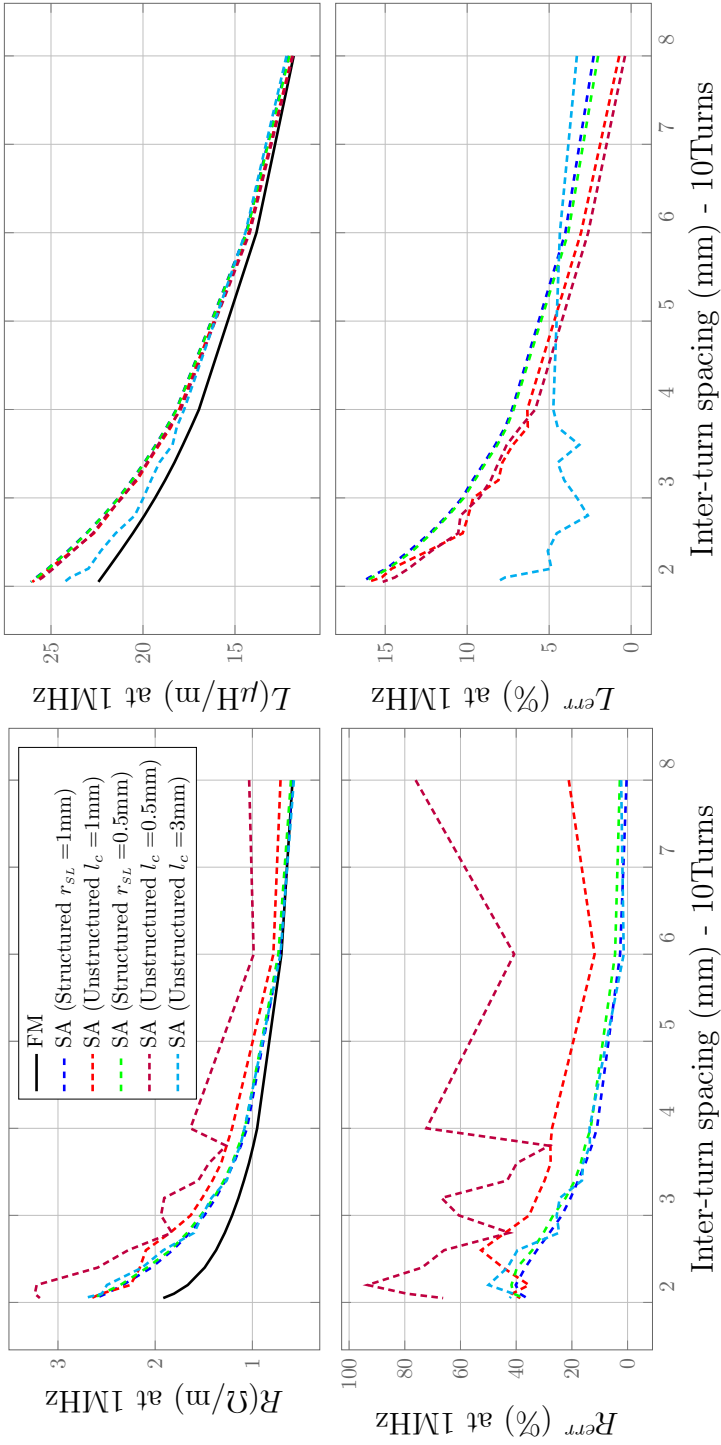


Figure 4.12: Impact of Inter-turn spacing on Impedance of a 10-turn multi-turn coil at 1MHz: Resistance (Left), Inductance (Right)

4.3.2.2. Impedance at a broad range of frequencies at an inter-turn spacing of 8mm

Fig 4.13 reports the resistance and the inductance values at an inter-turn spacing of 8mm at a broad range of frequencies.

The relative error in **resistance** values in the case of **structured sleeves** remains in a range between 1.64% – 0.24% for $r_{SL} = 1\text{mm}$, 1.64% – 2.55% for $r_{SL} = 0.5\text{mm}$, and 1.64% – 0.49% for $r_{SL} = 3\text{mm}$. In the case of **unstructured sleeves** the relative error remains in a range between 1.64% – 20.96% for $l_c = 1\text{mm}$, 1.64% – 75.85% for $l_c = 0.5\text{mm}$, and 1.64% – 2.41% for $l_c = 3\text{mm}$.

The relative error in **inductance** values in the case of **structured sleeves** remains in a range between 0.77% – 2.28% for $r_{SL} = 1\text{mm}$, 1.02% – 2.02% for $r_{SL} = 0.5\text{mm}$, and 0.48% – 2.59% for $r_{SL} = 3\text{mm}$. In the case of **unstructured sleeves** the relative error remains in a range between 2.23% – 0.73% for $l_c = 1\text{mm}$, 2.56% – 0.32% for $l_c = 0.5\text{mm}$, and 0.19% – 3.31% for $l_c = 3\text{mm}$.

The compromise between error and computational cost is studied throughout tables 4.10 -4.11. For sleeve radius 1mm in the structured case the problem size decreases from low frequencies to higher frequencies in a range between 75% – 99.71% and similarly in the case of unstructured sleeves 85.23% – 99.82%. In the 0.5mm case, the decrease in problem size in the structured case, ranges in percentage between 1.63% – 98.83% and the unstructured sleeves 65.39% – 99.59%. Lastly, in the 3mm case the structured case problem size percentage decrease ranges between 92.88% – 99.92% and in the unstructured case 95% – 99.94%.

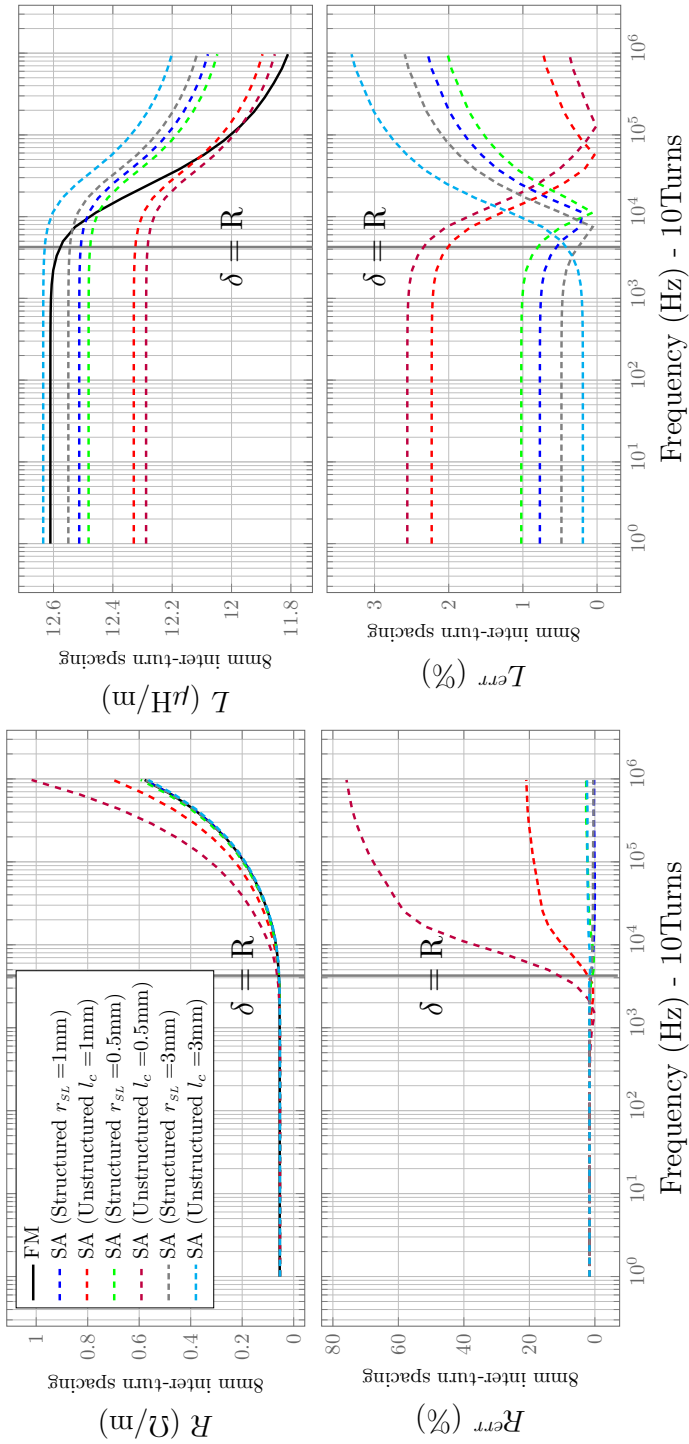


Figure 4.13: Impedance at a broad range of frequencies with large inter-turn spacing on a 10-Turn coil: Resistance (Left), Inductance (Right)

| 10 Turns Inter-turn distance 8mm Frequency (Hz) | FM | | SA (Structured) $r_{SL} = 1\text{mm}$ | | | | SA (Unstructured) $l_c = 1\text{mm}$ | | | |
|----------------------------------------------------------|--------|------|------------------------------------------|-----------------------------|-----------------------------|-----|-----------------------------------------|-----------------------------|-----------------------------|--|
| | DoF | DoF | DoF Rel. Diff. (%) | Resistance Rel. Err. (%) | Inductance Rel. Err. (%) | DoF | DoF Rel. Diff. (%) | Resistance Rel. Err. (%) | Inductance Rel. Err. (%) | |
| 1.00 | 4903 | 1201 | -75.50 | 1.64 | 0.77 | 724 | -85.23 | 1.64 | 2.23 | |
| 1.50 | 4903 | 1201 | -75.50 | 1.64 | 0.77 | 724 | -85.23 | 1.64 | 2.23 | |
| 2.25 | 4903 | 1201 | -75.50 | 1.64 | 0.77 | 724 | -85.23 | 1.64 | 2.23 | |
| 3.38 | 4903 | 1201 | -75.50 | 1.64 | 0.77 | 724 | -85.23 | 1.64 | 2.23 | |
| 5.06 | 4903 | 1201 | -75.50 | 1.64 | 0.77 | 724 | -85.23 | 1.64 | 2.23 | |
| 7.59 | 4903 | 1201 | -75.50 | 1.64 | 0.77 | 724 | -85.23 | 1.64 | 2.23 | |
| 11.39 | 4903 | 1201 | -75.50 | 1.64 | 0.77 | 724 | -85.23 | 1.64 | 2.23 | |
| 17.09 | 4903 | 1201 | -75.50 | 1.64 | 0.77 | 724 | -85.23 | 1.64 | 2.23 | |
| 25.63 | 4903 | 1201 | -75.50 | 1.64 | 0.77 | 724 | -85.23 | 1.64 | 2.23 | |
| 38.44 | 4903 | 1201 | -75.50 | 1.64 | 0.77 | 724 | -85.23 | 1.64 | 2.23 | |
| 57.67 | 4903 | 1201 | -75.50 | 1.64 | 0.77 | 724 | -85.23 | 1.64 | 2.23 | |
| 86.50 | 4903 | 1201 | -75.50 | 1.64 | 0.77 | 724 | -85.23 | 1.64 | 2.23 | |
| 129.75 | 4903 | 1201 | -75.50 | 1.64 | 0.77 | 724 | -85.23 | 1.63 | 2.23 | |
| 194.62 | 4903 | 1201 | -75.50 | 1.64 | 0.77 | 724 | -85.23 | 1.63 | 2.23 | |
| 291.93 | 4903 | 1201 | -75.50 | 1.64 | 0.77 | 724 | -85.23 | 1.62 | 2.23 | |
| 437.89 | 4903 | 1201 | -75.50 | 1.63 | 0.77 | 724 | -85.23 | 1.59 | 2.23 | |
| 656.84 | 4903 | 1201 | -75.50 | 1.63 | 0.77 | 724 | -85.23 | 1.54 | 2.22 | |
| 985.26 | 4903 | 1201 | -75.50 | 1.62 | 0.76 | 724 | -85.23 | 1.42 | 2.22 | |
| 1477.89 | 4903 | 1201 | -75.50 | 1.60 | 0.74 | 724 | -85.23 | 1.15 | 2.20 | |
| 2216.84 | 4903 | 1201 | -75.50 | 1.56 | 0.70 | 724 | -85.23 | 0.58 | 2.16 | |
| 3325.26 | 4903 | 1201 | -75.50 | 1.48 | 0.63 | 724 | -85.23 | 0.60 | 2.09 | |
| 4987.89 | 6362 | 1201 | -81.12 | 0.91 | 0.49 | 724 | -88.62 | 3.25 | 1.95 | |
| 7481.83 | 7910 | 1201 | -84.82 | 0.55 | 0.23 | 724 | -90.85 | 6.88 | 1.70 | |
| 11222.74 | 10498 | 1201 | -88.56 | 0.36 | 0.20 | 724 | -93.10 | 10.91 | 1.28 | |
| 16834.11 | 15043 | 1201 | -92.02 | 0.19 | 0.66 | 724 | -95.19 | 14.16 | 0.83 | |
| 25251.17 | 19440 | 1201 | -93.82 | 0.04 | 1.04 | 724 | -96.28 | 15.94 | 0.46 | |
| 37876.75 | 28525 | 1201 | -95.79 | 0.02 | 1.34 | 724 | -97.46 | 16.79 | 0.17 | |
| 56815.13 | 38799 | 1201 | -96.90 | 0.03 | 1.56 | 724 | -98.13 | 17.53 | 0.04 | |
| 85222.69 | 55386 | 1201 | -97.83 | 0.06 | 1.73 | 724 | -98.69 | 18.32 | 0.20 | |
| 127834.04 | 72198 | 1201 | -98.34 | 0.14 | 1.87 | 724 | -99.00 | 19.06 | 0.34 | |
| 191751.06 | 104691 | 1201 | -98.85 | 0.16 | 1.99 | 724 | -99.31 | 19.59 | 0.45 | |
| 287626.59 | 148497 | 1201 | -99.19 | 0.28 | 2.07 | 724 | -99.51 | 20.16 | 0.53 | |
| 431439.88 | 206630 | 1201 | -99.42 | 0.33 | 2.15 | 724 | -99.65 | 20.56 | 0.60 | |
| 647159.82 | 298878 | 1201 | -99.60 | 0.25 | 2.23 | 724 | -99.76 | 20.74 | 0.68 | |
| 970739.74 | 410779 | 1201 | -99.71 | 0.24 | 2.28 | 724 | -99.82 | 20.96 | 0.73 | |

Table 4.7: Relative difference between Degrees-of-Freedom used in Full-Model and Semi-analytical Model versus the relative error in the solution of the impedance at a broad range of frequencies for a 10-turn winding with 8mm of inter-turn distance and a sleeve size of 1mm

| 10 Turns Inter-turn distance 8mm Frequency (Hz) | FM | | SA (Structured) $r_{SL} = 0.5\text{mm}$ | | | | SA (Unstructured) $l_c = 0.5\text{mm}$ | | | |
|----------------------------------------------------------|--------|------|--------------------------------------------|-----------------------------|-----------------------------|------|-------------------------------------------|-----------------------------|-----------------------------|--|
| | DoF | DoF | DoF Rel. Diff. (%) | Resistance Rel. Err. (%) | Inductance Rel. Err. (%) | DoF | DoF Rel. Diff. (%) | Resistance Rel. Err. (%) | Inductance Rel. Err. (%) | |
| 1.00 | 4903 | 4823 | -1.63 | 1.64 | 1.02 | 1697 | -65.39 | 1.64 | 2.56 | |
| 1.50 | 4903 | 4823 | -1.63 | 1.64 | 1.02 | 1697 | -65.39 | 1.64 | 2.56 | |
| 2.25 | 4903 | 4823 | -1.63 | 1.64 | 1.02 | 1697 | -65.39 | 1.64 | 2.56 | |
| 3.38 | 4903 | 4823 | -1.63 | 1.64 | 1.02 | 1697 | -65.39 | 1.64 | 2.56 | |
| 5.06 | 4903 | 4823 | -1.63 | 1.64 | 1.02 | 1697 | -65.39 | 1.64 | 2.56 | |
| 7.59 | 4903 | 4823 | -1.63 | 1.64 | 1.02 | 1697 | -65.39 | 1.64 | 2.56 | |
| 11.39 | 4903 | 4823 | -1.63 | 1.64 | 1.02 | 1697 | -65.39 | 1.64 | 2.56 | |
| 17.09 | 4903 | 4823 | -1.63 | 1.64 | 1.02 | 1697 | -65.39 | 1.64 | 2.56 | |
| 25.63 | 4903 | 4823 | -1.63 | 1.64 | 1.02 | 1697 | -65.39 | 1.64 | 2.56 | |
| 38.44 | 4903 | 4823 | -1.63 | 1.64 | 1.02 | 1697 | -65.39 | 1.64 | 2.56 | |
| 57.67 | 4903 | 4823 | -1.63 | 1.64 | 1.02 | 1697 | -65.39 | 1.63 | 2.56 | |
| 86.50 | 4903 | 4823 | -1.63 | 1.64 | 1.02 | 1697 | -65.39 | 1.62 | 2.56 | |
| 129.75 | 4903 | 4823 | -1.63 | 1.64 | 1.02 | 1697 | -65.39 | 1.61 | 2.56 | |
| 194.62 | 4903 | 4823 | -1.63 | 1.64 | 1.02 | 1697 | -65.39 | 1.57 | 2.56 | |
| 291.93 | 4903 | 4823 | -1.63 | 1.63 | 1.02 | 1697 | -65.39 | 1.49 | 2.56 | |
| 437.89 | 4903 | 4823 | -1.63 | 1.63 | 1.02 | 1697 | -65.39 | 1.30 | 2.55 | |
| 656.84 | 4903 | 4823 | -1.63 | 1.62 | 1.02 | 1697 | -65.39 | 0.89 | 2.55 | |
| 985.26 | 4903 | 4823 | -1.63 | 1.60 | 1.01 | 1697 | -65.39 | 0.03 | 2.53 | |
| 1477.89 | 4903 | 4823 | -1.63 | 1.55 | 0.99 | 1697 | -65.39 | 2.01 | 2.49 | |
| 2216.84 | 4903 | 4823 | -1.63 | 1.44 | 0.96 | 1697 | -65.39 | 6.10 | 2.42 | |
| 3325.26 | 4903 | 4823 | -1.63 | 1.24 | 0.88 | 1697 | -73.33 | 14.27 | 2.28 | |
| 4987.89 | 6362 | 4823 | -24.19 | 0.43 | 0.74 | 1697 | -78.55 | 26.56 | 2.03 | |
| 7481.83 | 7910 | 4823 | -39.03 | 0.32 | 0.49 | 1697 | -83.84 | 40.77 | 1.61 | |
| 11222.74 | 10498 | 4823 | -54.06 | 0.95 | 0.06 | 1697 | -88.72 | 52.18 | 1.17 | |
| 16834.11 | 15043 | 4823 | -67.94 | 1.48 | 0.40 | 1697 | -91.27 | 58.27 | 0.80 | |
| 25251.17 | 19440 | 4823 | -75.19 | 1.82 | 0.78 | 1697 | -94.05 | 61.21 | 0.51 | |
| 37876.75 | 28525 | 4823 | -83.09 | 1.98 | 1.08 | 1697 | -95.63 | 63.88 | 0.31 | |
| 56815.13 | 38799 | 4823 | -87.57 | 2.07 | 1.30 | 1697 | -96.94 | 66.70 | 0.14 | |
| 85222.69 | 55386 | 4823 | -91.29 | 2.18 | 1.47 | 1697 | -97.65 | 69.16 | 0.01 | |
| 127834.04 | 72198 | 4823 | -93.32 | 2.34 | 1.61 | 1697 | -98.38 | 71.06 | 0.10 | |
| 191751.06 | 104691 | 4823 | -95.39 | 2.42 | 1.72 | 1697 | -98.86 | 72.81 | 0.18 | |
| 287626.59 | 148497 | 4823 | -96.75 | 2.60 | 1.81 | 1697 | -99.18 | 74.14 | 0.25 | |
| 431439.88 | 206630 | 4823 | -97.67 | 2.68 | 1.88 | 1697 | -99.43 | 75.02 | 0.33 | |
| 647159.82 | 298878 | 4823 | -98.39 | 2.63 | 1.96 | 1697 | -99.59 | 75.85 | 0.37 | |
| 970739.74 | 410779 | 4823 | -98.83 | 2.65 | 2.02 | 1697 | | | | |

Table 4.8: Relative difference between Degrees-of-Freedom used in Full-Model and Semi-analytical Model versus the relative error in the solution of the impedance at a broad range of frequencies for a 10-turn winding with 8mm of inter-turn distance and a sleeve size of 0.5mm

| 10 Turns Inter-turn distance 8mm Frequency (Hz) | FM | | SA (Structured) $r_{SL} = 3\text{mm}$ | | | | SA (Unstructured) $l_c = 3\text{mm}$ | | | |
|----------------------------------------------------------|--------|-----|------------------------------------------|-----------------------------|-----------------------------|-----|-----------------------------------------|-----------------------------|-----------------------------|--|
| | DoF | DoF | DoF Rel. Diff. (%) | Resistance Rel. Err. (%) | Inductance Rel. Err. (%) | DoF | DoF Rel. Diff. (%) | Resistance Rel. Err. (%) | Inductance Rel. Err. (%) | |
| 1.00 | 4903 | 349 | -92.88 | 1.64 | 0.48 | 245 | -95.00 | 1.64 | 0.19 | |
| 1.50 | 4903 | 349 | -92.88 | 1.64 | 0.48 | 245 | -95.00 | 1.64 | 0.19 | |
| 2.25 | 4903 | 349 | -92.88 | 1.64 | 0.48 | 245 | -95.00 | 1.64 | 0.19 | |
| 3.38 | 4903 | 349 | -92.88 | 1.64 | 0.48 | 245 | -95.00 | 1.64 | 0.19 | |
| 5.06 | 4903 | 349 | -92.88 | 1.64 | 0.48 | 245 | -95.00 | 1.64 | 0.19 | |
| 7.59 | 4903 | 349 | -92.88 | 1.64 | 0.48 | 245 | -95.00 | 1.64 | 0.19 | |
| 11.39 | 4903 | 349 | -92.88 | 1.64 | 0.48 | 245 | -95.00 | 1.64 | 0.19 | |
| 17.09 | 4903 | 349 | -92.88 | 1.64 | 0.48 | 245 | -95.00 | 1.64 | 0.19 | |
| 25.63 | 4903 | 349 | -92.88 | 1.64 | 0.48 | 245 | -95.00 | 1.64 | 0.19 | |
| 38.44 | 4903 | 349 | -92.88 | 1.64 | 0.48 | 245 | -95.00 | 1.64 | 0.19 | |
| 57.67 | 4903 | 349 | -92.88 | 1.64 | 0.48 | 245 | -95.00 | 1.64 | 0.19 | |
| 86.50 | 4903 | 349 | -92.88 | 1.64 | 0.48 | 245 | -95.00 | 1.64 | 0.19 | |
| 129.75 | 4903 | 349 | -92.88 | 1.64 | 0.48 | 245 | -95.00 | 1.64 | 0.19 | |
| 194.62 | 4903 | 349 | -92.88 | 1.64 | 0.48 | 245 | -95.00 | 1.64 | 0.19 | |
| 291.93 | 4903 | 349 | -92.88 | 1.64 | 0.48 | 245 | -95.00 | 1.64 | 0.19 | |
| 437.89 | 4903 | 349 | -92.88 | 1.63 | 0.48 | 245 | -95.00 | 1.64 | 0.19 | |
| 656.84 | 4903 | 349 | -92.88 | 1.63 | 0.47 | 245 | -95.00 | 1.64 | 0.20 | |
| 985.26 | 4903 | 349 | -92.88 | 1.63 | 0.47 | 245 | -95.00 | 1.65 | 0.20 | |
| 1477.89 | 4903 | 349 | -92.88 | 1.62 | 0.45 | 245 | -95.00 | 1.66 | 0.22 | |
| 2216.84 | 4903 | 349 | -92.88 | 1.59 | 0.41 | 245 | -95.00 | 1.68 | 0.26 | |
| 3325.26 | 4903 | 349 | -92.88 | 1.55 | 0.34 | 245 | -95.00 | 1.74 | 0.34 | |
| 4987.89 | 6362 | 349 | -94.51 | 1.06 | 0.20 | 245 | -96.15 | 1.44 | 0.48 | |
| 7481.83 | 7910 | 349 | -95.59 | 0.81 | 0.06 | 245 | -96.90 | 1.50 | 0.74 | |
| 11222.74 | 10498 | 349 | -96.68 | 0.76 | 0.49 | 245 | -97.67 | 1.80 | 1.17 | |
| 16834.11 | 15043 | 349 | -97.68 | 0.70 | 0.95 | 245 | -98.37 | 2.03 | 1.64 | |
| 25251.17 | 19440 | 349 | -98.20 | 0.61 | 1.34 | 245 | -98.74 | 2.09 | 2.03 | |
| 37876.75 | 28525 | 349 | -98.78 | 0.57 | 1.64 | 245 | -99.14 | 2.13 | 2.34 | |
| 56815.13 | 38799 | 349 | -99.10 | 0.59 | 1.86 | 245 | -99.37 | 2.21 | 2.56 | |
| 85222.69 | 55386 | 349 | -99.37 | 0.58 | 2.04 | 245 | -99.56 | 2.28 | 2.74 | |
| 127834.04 | 72198 | 349 | -99.52 | 0.52 | 2.18 | 245 | -99.66 | 2.28 | 2.89 | |
| 191751.06 | 104691 | 349 | -99.67 | 0.53 | 2.30 | 245 | -99.77 | 2.33 | 3.01 | |
| 287626.59 | 148497 | 349 | -99.76 | 0.42 | 2.38 | 245 | -99.84 | 2.26 | 3.09 | |
| 431439.88 | 206630 | 349 | -99.83 | 0.38 | 2.46 | 245 | -99.88 | 2.26 | 3.17 | |
| 647159.82 | 298878 | 349 | -99.88 | 0.47 | 2.54 | 245 | -99.92 | 2.38 | 3.26 | |
| 970739.74 | 410779 | 349 | -99.92 | 0.49 | 2.59 | 245 | -99.94 | 2.41 | 3.31 | |

Table 4-9: Relative difference between Degrees-of-Freedom used in Full-Model and Semi-analytical Model versus the relative error in the solution of the impedance at a broad range of frequencies for a 10-turn winding with 8mm of inter-turn distance and a sleeve size of 3mm

4.3.2.3. Impedance at a broad range of frequencies at a inter-turn spacing of 2.05mm

Fig 4.14 reports the resistance and the inductance values at an inter-turn spacing of 2.05mm at a broad range of frequencies.

The relative error in **resistance** values in the case of **structured sleeves** remains in a range between 1.64% – 36.16% for $r_{SL} = 1\text{mm}$, and 1.64% – 37.35% for $r_{SL} = 0.5\text{mm}$. In the case of **unstructured sleeves** the relative error remains in a range between 1.64% – 38.59% for $l_c = 1\text{mm}$, 1.64% – 66.29% for $l_c = 0.5\text{mm}$, and 1.64% – 42.37% for $l_c = 3\text{mm}$.

The relative error in **inductance** values in the case of **structured sleeves** remains in a range between 0.45% – 16.43% for $r_{SL} = 1\text{mm}$, and 0.53% – 16.34% for $r_{SL} = 0.5\text{mm}$. In the case of **unstructured sleeves** the relative error remains in a range between 0.76% – 16.06% for $l_c = 1\text{mm}$, 1.52% – 15.16% for $l_c = 0.5\text{mm}$, and 7.38% – 8.19% for $l_c = 3\text{mm}$.

The compromise between error and computational cost is studied throughout tables 4.10 -4.11. For sleeve radius 1mm in the structured case the problem size decreases from low frequencies to higher frequencies in a range between 63.01% – 99.50% and similarly in the case of unstructured sleeves it ranges between 72.62% – 99.63%. In the 0.5mm case, the decrease in problem size in the structured case, ranges in percentage between 41.68% – 99.21% and the unstructured sleeves 60.36% – 99.46%. Lastly, in the 3mm in the unstructured case 80.64% – 99.74%.

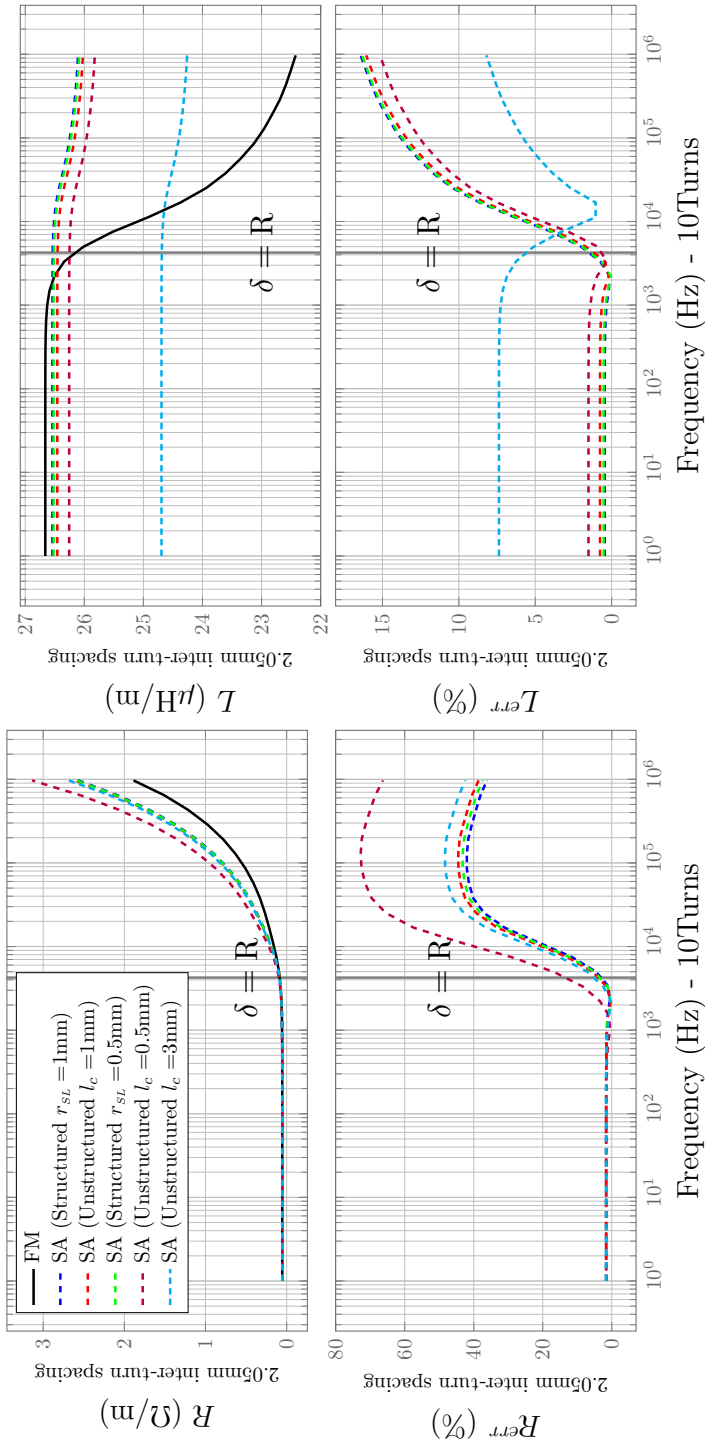


Figure 4.14: Impedance at a broad range of frequencies with small inter-turn spacing on a 10-Turn coil: Resistance (Left), Inductance (Right)

| 10 Turns Inter-turn distance 2.05mm Frequency (Hz) | FM | SA (Structured) $r_{SL} = 1mm$ | | | | SA (Unstructured) $l_c = 1mm$ | | | |
|-------------------------------------------------------------|-------|-----------------------------------|-----------------------|-----------------------------|-----------------------------|----------------------------------|-----------------------|-----------------------------|-----------------------------|
| | | DoF | DoF Rel. Diff. (%) | Resistance Rel. Err. (%) | Inductance Rel. Err. (%) | DoF | DoF Rel. Diff. (%) | Resistance Rel. Err. (%) | Inductance Rel. Err. (%) |
| 1.00 | 1322 | 489 | -63.01 | 1.64 | 0.45 | 362 | -72.62 | 1.64 | 0.76 |
| 1.50 | 1322 | 489 | -63.01 | 1.64 | 0.45 | 362 | -72.62 | 1.64 | 0.76 |
| 2.25 | 1322 | 489 | -63.01 | 1.64 | 0.45 | 362 | -72.62 | 1.64 | 0.76 |
| 3.38 | 1322 | 489 | -63.01 | 1.64 | 0.45 | 362 | -72.62 | 1.64 | 0.76 |
| 5.06 | 1322 | 489 | -63.01 | 1.64 | 0.45 | 362 | -72.62 | 1.64 | 0.76 |
| 7.59 | 1322 | 489 | -63.01 | 1.64 | 0.45 | 362 | -72.62 | 1.64 | 0.76 |
| 11.39 | 1322 | 489 | -63.01 | 1.64 | 0.45 | 362 | -72.62 | 1.64 | 0.76 |
| 17.09 | 1322 | 489 | -63.01 | 1.64 | 0.45 | 362 | -72.62 | 1.64 | 0.76 |
| 25.63 | 1322 | 489 | -63.01 | 1.64 | 0.45 | 362 | -72.62 | 1.64 | 0.76 |
| 38.44 | 1322 | 489 | -63.01 | 1.64 | 0.45 | 362 | -72.62 | 1.64 | 0.76 |
| 57.67 | 1322 | 489 | -63.01 | 1.64 | 0.45 | 362 | -72.62 | 1.64 | 0.76 |
| 86.50 | 1322 | 489 | -63.01 | 1.64 | 0.45 | 362 | -72.62 | 1.63 | 0.76 |
| 129.75 | 1322 | 489 | -63.01 | 1.63 | 0.45 | 362 | -72.62 | 1.63 | 0.76 |
| 194.62 | 1322 | 489 | -63.01 | 1.63 | 0.45 | 362 | -72.62 | 1.63 | 0.76 |
| 291.93 | 1322 | 489 | -63.01 | 1.62 | 0.44 | 362 | -72.62 | 1.62 | 0.75 |
| 437.89 | 1322 | 489 | -63.01 | 1.60 | 0.43 | 362 | -72.62 | 1.59 | 0.74 |
| 656.84 | 1322 | 489 | -63.01 | 1.56 | 0.40 | 362 | -72.62 | 1.53 | 0.71 |
| 985.26 | 1322 | 489 | -63.01 | 1.46 | 0.34 | 362 | -72.62 | 1.39 | 0.64 |
| 1477.89 | 1322 | 489 | -63.01 | 1.22 | 0.19 | 362 | -72.62 | 1.06 | 0.50 |
| 2216.84 | 1322 | 489 | -63.01 | 0.61 | 0.11 | 362 | -72.62 | 0.28 | 0.19 |
| 3325.26 | 1322 | 489 | -63.01 | 0.94 | 0.75 | 362 | -72.62 | 1.54 | 0.44 |
| 4987.89 | 1582 | 489 | -69.09 | 4.58 | 1.99 | 362 | -77.12 | 5.57 | 1.68 |
| 7481.83 | 1835 | 489 | -73.35 | 11.52 | 3.90 | 362 | -80.27 | 12.94 | 3.58 |
| 11222.74 | 2273 | 489 | -78.49 | 21.34 | 6.36 | 362 | -84.07 | 23.16 | 6.03 |
| 16834.11 | 3043 | 489 | -83.93 | 31.06 | 8.62 | 362 | -88.10 | 33.18 | 8.29 |
| 25251.17 | 4069 | 489 | -87.98 | 37.03 | 10.42 | 362 | -91.10 | 39.33 | 10.08 |
| 37876.75 | 5624 | 489 | -91.31 | 40.14 | 11.69 | 362 | -93.56 | 42.51 | 11.34 |
| 56815.13 | 7719 | 489 | -93.66 | 41.38 | 12.67 | 362 | -95.31 | 43.80 | 12.32 |
| 85222.69 | 10797 | 489 | -95.47 | 41.99 | 13.53 | 362 | -96.65 | 44.45 | 13.18 |
| 127834.04 | 14616 | 489 | -96.65 | 42.00 | 14.21 | 362 | -97.52 | 44.48 | 13.85 |
| 191751.06 | 21220 | 489 | -97.70 | 41.59 | 14.77 | 362 | -98.29 | 44.08 | 14.41 |
| 287626.59 | 30609 | 489 | -98.40 | 40.55 | 15.30 | 362 | -98.82 | 43.03 | 14.94 |
| 431439.88 | 45025 | 489 | -98.91 | 39.32 | 15.72 | 362 | -99.20 | 41.79 | 15.36 |
| 647159.82 | 66256 | 489 | -99.26 | 38.04 | 16.08 | 362 | -99.45 | 40.49 | 15.71 |
| 970739.74 | 97180 | 489 | -99.50 | 36.16 | 16.43 | 362 | -99.63 | 38.59 | 16.06 |

Table 4.10: Relative difference between Degrees-of-Freedom used in Full-Model and Semi-analytical Model versus the relative error in the solution of the impedance at a broad range of frequencies for a 10-turn winding with 2.05mm of inter-turn distance and a sleeve size of 1mm

| 10 Turns Inter-turn distance 2.05mm Frequency (Hz) | FM | | SA (Structured) $r_{SL} = 0.5\text{mm}$ | | | | SA (Unstructured) $l_c = 0.5\text{mm}$ | | | |
|-------------------------------------------------------------|-------|-----|--------------------------------------------|-----------------------------|-----------------------------|-----|-------------------------------------------|-----------------------------|-----------------------------|--|
| | DoF | DoF | DoF Rel. Diff. (%) | Resistance Rel. Err. (%) | Inductance Rel. Err. (%) | DoF | DoF Rel. Diff. (%) | Resistance Rel. Err. (%) | Inductance Rel. Err. (%) | |
| 1.00 | 1322 | 771 | -41.68 | 1.64 | 0.53 | 524 | -60.36 | 1.64 | 1.52 | |
| 1.50 | 1322 | 771 | -41.68 | 1.64 | 0.53 | 524 | -60.36 | 1.64 | 1.52 | |
| 2.25 | 1322 | 771 | -41.68 | 1.64 | 0.53 | 524 | -60.36 | 1.64 | 1.52 | |
| 3.38 | 1322 | 771 | -41.68 | 1.64 | 0.53 | 524 | -60.36 | 1.64 | 1.52 | |
| 5.06 | 1322 | 771 | -41.68 | 1.64 | 0.53 | 524 | -60.36 | 1.64 | 1.52 | |
| 7.59 | 1322 | 771 | -41.68 | 1.64 | 0.53 | 524 | -60.36 | 1.64 | 1.52 | |
| 11.39 | 1322 | 771 | -41.68 | 1.64 | 0.53 | 524 | -60.36 | 1.64 | 1.52 | |
| 17.09 | 1322 | 771 | -41.68 | 1.64 | 0.53 | 524 | -60.36 | 1.64 | 1.52 | |
| 25.63 | 1322 | 771 | -41.68 | 1.64 | 0.53 | 524 | -60.36 | 1.64 | 1.52 | |
| 38.44 | 1322 | 771 | -41.68 | 1.64 | 0.53 | 524 | -60.36 | 1.64 | 1.52 | |
| 57.67 | 1322 | 771 | -41.68 | 1.64 | 0.53 | 524 | -60.36 | 1.63 | 1.52 | |
| 86.50 | 1322 | 771 | -41.68 | 1.64 | 0.53 | 524 | -60.36 | 1.63 | 1.51 | |
| 129.75 | 1322 | 771 | -41.68 | 1.63 | 0.52 | 524 | -60.36 | 1.62 | 1.51 | |
| 194.62 | 1322 | 771 | -41.68 | 1.62 | 0.52 | 524 | -60.36 | 1.54 | 1.51 | |
| 291.93 | 1322 | 771 | -41.68 | 1.60 | 0.50 | 524 | -60.36 | 1.41 | 1.49 | |
| 437.89 | 1322 | 771 | -41.68 | 1.54 | 0.47 | 524 | -60.36 | 1.14 | 1.46 | |
| 656.84 | 1322 | 771 | -41.68 | 1.42 | 0.41 | 524 | -60.36 | 0.54 | 1.40 | |
| 985.26 | 1322 | 771 | -41.68 | 1.14 | 0.27 | 524 | -60.36 | 0.76 | 1.26 | |
| 1477.89 | 1322 | 771 | -41.68 | 0.45 | 0.04 | 524 | -60.36 | 3.42 | 0.95 | |
| 2216.84 | 1322 | 771 | -41.68 | 1.24 | 0.67 | 524 | -60.36 | 8.42 | 0.33 | |
| 3325.26 | 1322 | 771 | -51.26 | 5.06 | 1.91 | 524 | -66.88 | 16.85 | 0.90 | |
| 4987.89 | 1582 | 771 | -57.98 | 12.22 | 3.82 | 524 | -71.44 | 29.16 | 2.79 | |
| 7481.83 | 1835 | 771 | -66.08 | 22.24 | 6.28 | 524 | -76.95 | 43.97 | 5.22 | |
| 11222.74 | 2273 | 771 | -66.08 | 32.10 | 8.54 | 524 | -82.78 | 57.45 | 7.46 | |
| 16834.11 | 3043 | 771 | -74.66 | 38.16 | 10.34 | 524 | -87.12 | 65.48 | 9.24 | |
| 25251.17 | 4069 | 771 | -81.05 | 41.31 | 11.61 | 524 | -90.68 | 69.60 | 10.49 | |
| 37876.75 | 5624 | 771 | -86.29 | 42.57 | 12.58 | 524 | -93.21 | 71.43 | 11.46 | |
| 56815.13 | 7719 | 771 | -90.01 | 43.20 | 13.45 | 524 | -95.15 | 72.50 | 12.31 | |
| 85222.69 | 10797 | 771 | -92.86 | 43.22 | 14.12 | 524 | -96.41 | 72.76 | 12.97 | |
| 127834.04 | 14616 | 771 | -94.72 | 42.82 | 14.68 | 524 | -97.53 | 72.47 | 13.52 | |
| 191751.06 | 21220 | 771 | -96.37 | 41.77 | 15.22 | 524 | -98.29 | 71.36 | 14.06 | |
| 287626.59 | 30609 | 771 | -97.48 | 40.54 | 15.64 | 524 | -98.84 | 69.98 | 14.47 | |
| 431439.88 | 45025 | 771 | -98.29 | 39.25 | 15.99 | 524 | -99.21 | 68.51 | 14.82 | |
| 647159.82 | 66256 | 771 | -98.84 | 37.35 | 16.34 | 524 | -99.46 | 66.29 | 15.16 | |
| 970739.74 | 97180 | 771 | -99.21 | | | 524 | | | | |

Table 4.11: Relative difference between Degrees-of-Freedom used in Full-Model and Semi-analytical Model versus the relative error in the solution of the impedance at a broad range of frequencies for a 10-turn winding with 2.05mm of inter-turn distance and a sleeve size of 0.5mm

| 10 Turns Inter-turn distance 2.05mm | FM | SA (Structured) $r_{SL} = 3\text{mm}$ | | | | SA (Unstructured) $l_c = 3\text{mm}$ | | | |
|-------------------------------------------|-------|------------------------------------------|-----------------------|-----------------------------|-----------------------------|-----------------------------------------|-----------------------|-----------------------------|-----------------------------|
| | | DoF | DoF Rel. Diff. (%) | Resistance Rel. Err. (%) | Inductance Rel. Err. (%) | DoF | DoF Rel. Diff. (%) | Resistance Rel. Err. (%) | Inductance Rel. Err. (%) |
| 1.00 | 1322 | N/A | N/A | N/A | N/A | 256 | -80.64 | 1.64 | 7.38 |
| 1.50 | 1322 | N/A | N/A | N/A | N/A | 256 | -80.64 | 1.64 | 7.38 |
| 2.25 | 1322 | N/A | N/A | N/A | N/A | 256 | -80.64 | 1.64 | 7.38 |
| 3.38 | 1322 | N/A | N/A | N/A | N/A | 256 | -80.64 | 1.64 | 7.38 |
| 5.06 | 1322 | N/A | N/A | N/A | N/A | 256 | -80.64 | 1.64 | 7.38 |
| 7.59 | 1322 | N/A | N/A | N/A | N/A | 256 | -80.64 | 1.64 | 7.38 |
| 11.39 | 1322 | N/A | N/A | N/A | N/A | 256 | -80.64 | 1.64 | 7.38 |
| 17.09 | 1322 | N/A | N/A | N/A | N/A | 256 | -80.64 | 1.64 | 7.38 |
| 25.63 | 1322 | N/A | N/A | N/A | N/A | 256 | -80.64 | 1.64 | 7.38 |
| 38.44 | 1322 | N/A | N/A | N/A | N/A | 256 | -80.64 | 1.64 | 7.38 |
| 57.67 | 1322 | N/A | N/A | N/A | N/A | 256 | -80.64 | 1.64 | 7.38 |
| 86.50 | 1322 | N/A | N/A | N/A | N/A | 256 | -80.64 | 1.63 | 7.38 |
| 129.75 | 1322 | N/A | N/A | N/A | N/A | 256 | -80.64 | 1.63 | 7.38 |
| 194.62 | 1322 | N/A | N/A | N/A | N/A | 256 | -80.64 | 1.62 | 7.37 |
| 291.93 | 1322 | N/A | N/A | N/A | N/A | 256 | -80.64 | 1.60 | 7.37 |
| 437.89 | 1322 | N/A | N/A | N/A | N/A | 256 | -80.64 | 1.56 | 7.36 |
| 656.84 | 1322 | N/A | N/A | N/A | N/A | 256 | -80.64 | 1.47 | 7.33 |
| 985.26 | 1322 | N/A | N/A | N/A | N/A | 256 | -80.64 | 1.27 | 7.27 |
| 1477.89 | 1322 | N/A | N/A | N/A | N/A | 256 | -80.64 | 0.81 | 7.14 |
| 2216.84 | 1322 | N/A | N/A | N/A | N/A | 256 | -80.64 | 0.22 | 6.85 |
| 3325.26 | 1322 | N/A | N/A | N/A | N/A | 256 | -80.64 | 2.48 | 6.26 |
| 4987.89 | 1582 | N/A | N/A | N/A | N/A | 256 | -83.82 | 7.11 | 5.11 |
| 7481.83 | 1835 | N/A | N/A | N/A | N/A | 256 | -86.05 | 15.15 | 3.33 |
| 11222.74 | 2273 | N/A | N/A | N/A | N/A | 256 | -88.74 | 26.00 | 1.05 |
| 16834.11 | 3043 | N/A | N/A | N/A | N/A | 256 | -91.59 | 36.50 | 1.05 |
| 25251.17 | 4069 | N/A | N/A | N/A | N/A | 256 | -93.71 | 42.89 | 2.71 |
| 37876.75 | 5624 | N/A | N/A | N/A | N/A | 256 | -95.45 | 46.21 | 3.87 |
| 56815.13 | 7719 | N/A | N/A | N/A | N/A | 256 | -96.68 | 47.57 | 4.76 |
| 85222.69 | 10797 | N/A | N/A | N/A | N/A | 256 | -97.63 | 48.28 | 5.55 |
| 127834.04 | 14616 | N/A | N/A | N/A | N/A | 256 | -98.25 | 48.34 | 6.17 |
| 191751.06 | 21220 | N/A | N/A | N/A | N/A | 256 | -98.79 | 47.95 | 6.67 |
| 287626.59 | 30609 | N/A | N/A | N/A | N/A | 256 | -99.16 | 46.90 | 7.17 |
| 431439.88 | 45025 | N/A | N/A | N/A | N/A | 256 | -99.43 | 45.64 | 7.55 |
| 647159.82 | 66256 | N/A | N/A | N/A | N/A | 256 | -99.61 | 44.31 | 7.87 |
| 970739.74 | 97180 | N/A | N/A | N/A | N/A | 256 | -99.74 | 42.37 | 8.19 |

Table 4.12: Relative difference between Degrees-of-Freedom used in Full-Model and Semi-analytical Model versus the relative error in the solution of the impedance at a broad range of frequencies for a 10-turn winding with 2.05mm of inter-turn distance and a sleeve size of 3mm

4.3.3. 15-Turn Coil

4.3.3.1. Impedance vs. inter-turn spacing at 1Hz and 1MHz

In Fig. 4.15 we observe the effect of inter-turn spacing **at 1Hz**. The relative error of the resistance R^{err} is constant about a value of 1.64% throughout all inter-turn spacing values, which is expected as at lower frequencies proximity effects are negligible. It is also important to acknowledge that the relative error is relatively high, which is mainly due to the coarser mesh used at lower frequencies. The relative error of the inductance L^{err} is relatively constant with overall values under 2% except in the case of unstructured sleeve larger than the size of the conductor (3mm) where the error value rises up to values close to 6% past an inter-turn spacing of 6mm.

In Fig. 4.16 we observe the effect of inter-turn spacing **at 1MHz**. The relative error of the resistance R^{err} increases as the inter-turn spacing decreases, due to the presence of proximity effects. In the case of structured sleeves, the R^{err} values increase slowly from values close to 1.6% up to 50% at small inter-turn spacing. In the $r_{SL} = 0.5$ case the relative error rises up to 83% relative error. In the case of unstructured sleeves, the behavior is nearly the same as the structured sleeve case except for the case with $l_c = 1\text{mm}$ which has a larger error value, however the behavior of the curve is similar to the rest. The L^{err} values remain under 4% – 15% for the sleeve cases $r_{SL} = 3\text{mm}$. In the rest of cases the relative error ranges from 4% – 20%.

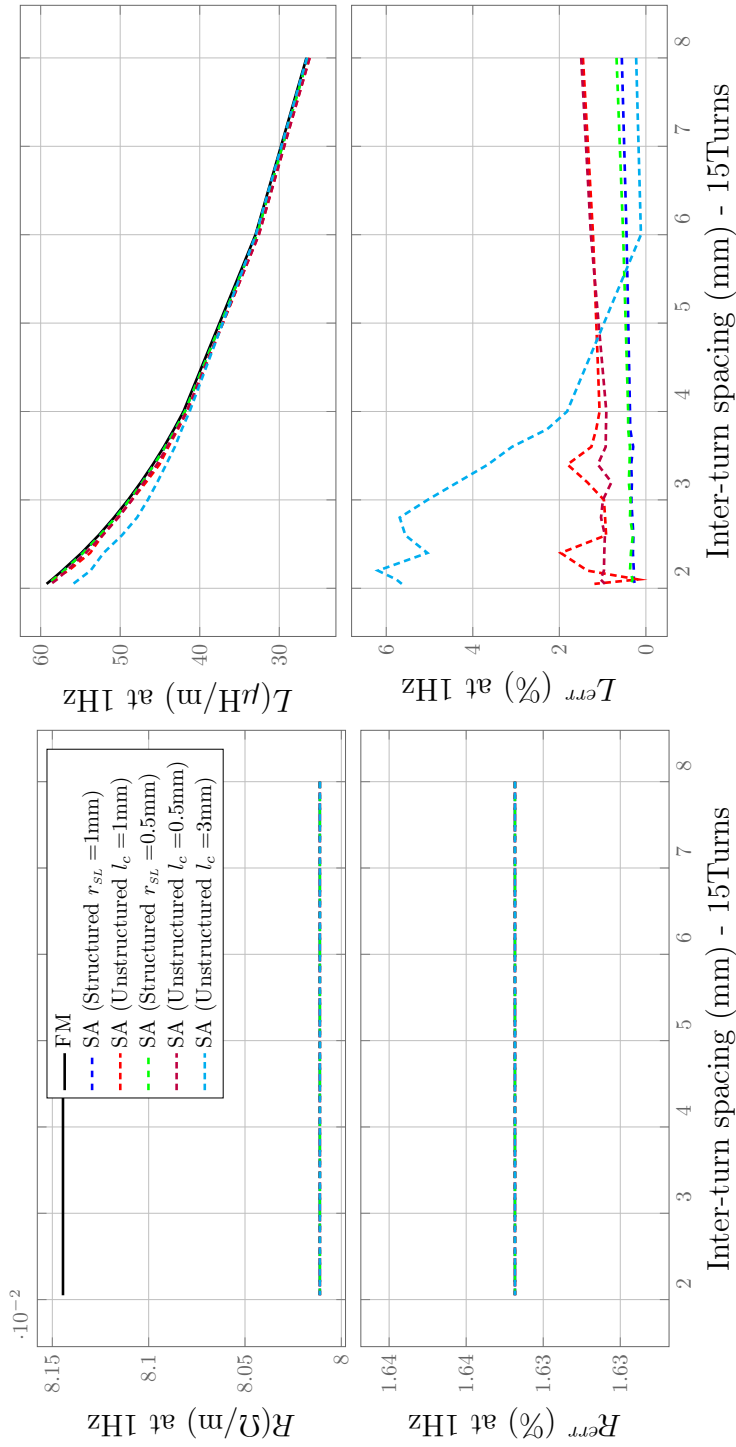


Figure 4.15: Impact of Inter-turn spacing on Impedance of a 15-turn multi-turn coil at 1Hz: Resistance (Left), Inductance (Right)

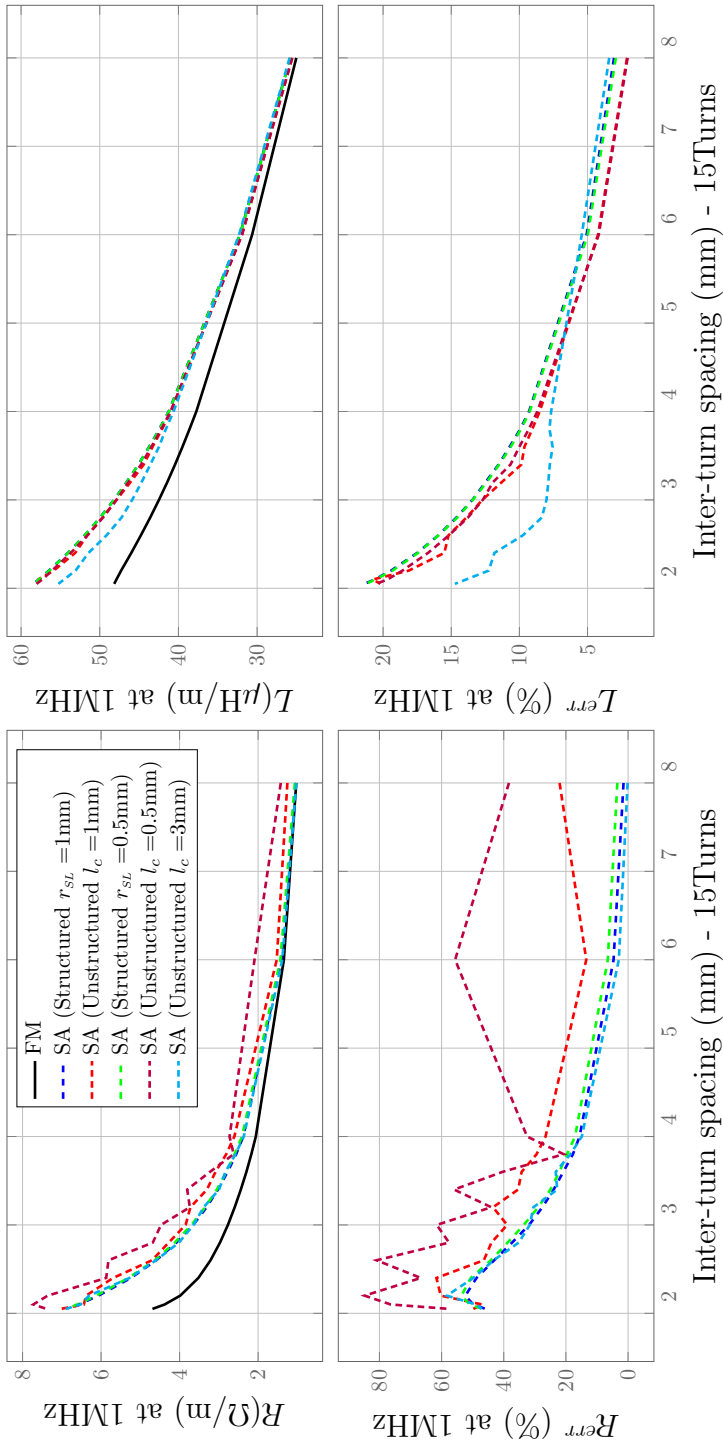


Figure 4.16: Impact of Inter-turn spacing on Impedance of a 15-turn multi-turn coil at 1MHz: Resistance (Left), Inductance (Right)

4.3.3.2. Impedance at a broad range of frequencies at a inter-turn spacing of 8mm

Fig 4.17 reports the resistance and the inductance values at an inter-turn spacing of 8mm at a broad range of frequencies.

The relative error in **resistance** values in the case of **structured sleeves** remains in a range between 1.64% – 1.36% for $r_{SL} = 1\text{mm}$, 1.64% – 3.34% for $r_{SL} = 0.5\text{mm}$, and 1.64% – 0.49% for $r_{SL} = 3\text{mm}$. In the case of **unstructured sleeves** the relative error remains in a range between 1.64% – 21.90% for $l_c = 1\text{mm}$, 1.64% – 38.16% for $l_c = 0.5\text{mm}$, and 1.64% – 0.24% for $l_c = 3\text{mm}$.

The relative error in inductance values in the case of **structured sleeves** remains in a range between 0.56% – 3.06% for $r_{SL} = 1\text{mm}$, 0.68% – 2.93% for $r_{SL} = 0.5\text{mm}$, and 0.33% – 2.29% for $r_{SL} = 3\text{mm}$. In the case of **unstructured sleeves** the relative error remains in a range between 1.45% – 2.10% for $l_c = 1\text{mm}$, 1.49% – 2.06% for $l_c = 0.5\text{mm}$, and 0.22% – 3.41% for $l_c = 3\text{mm}$.

The compromise between error and computational cost is studied throughout tables 4.13 -4.14. For sleeve radius 1mm in the structured case the problem size decreases from low frequencies to higher frequencies in a range between 78.52% – 99.83% and similarly in the case of unstructured sleeves 87.50% – 99.90%. In the 0.5mm case, the decrease in problem size in the structured case, ranges in percentage between 65.82% – 99.73% and the unstructured sleeves 64.90% – 99.72%. Lastly, in the 3mm case the structured case problem size percentage decrease ranges between 95% – 99.96% and in the unstructured case 96.64% – 99.97%.

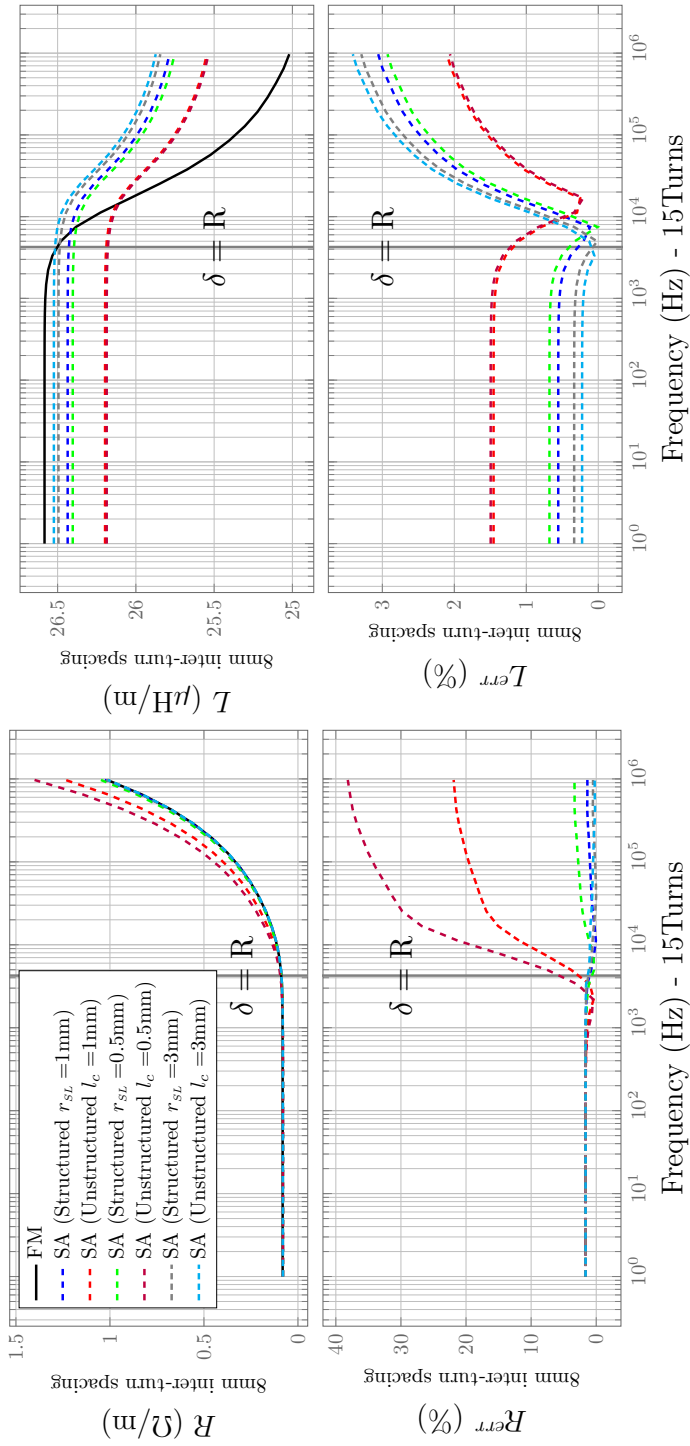


Figure 4.17: Impedance at a broad range of frequencies with large inter-turn spacing on a 15-Turn coil: Resistance (Left), Inductance (Right)

| 15 Turns Inter-turn distance 8mm Frequency (Hz) | FM | | SA (Structured) $r_{SL} = 1\text{mm}$ | | | | SA (Unstructured) $l_c = 1\text{mm}$ | | | |
|----------------------------------------------------------|-------------|------|------------------------------------------|----------------|-----------------------------|-----------------------------|-----------------------------------------|----------------|-----------------------------|-----------------------------|
| | DoF | DoF | DoF | Rel. Diff. (%) | Resistance Rel. Err. (%) | Inductance Rel. Err. (%) | DoF | Rel. Diff. (%) | Resistance Rel. Err. (%) | Inductance Rel. Err. (%) |
| 1.00 | 8147 | 1750 | 1750 | -78.52 | 1.64 | 0.56 | 1018 | -87.50 | 1.64 | 1.45 |
| 1.50 | 8147 | 1750 | 1750 | -78.52 | 1.64 | 0.56 | 1018 | -87.50 | 1.64 | 1.45 |
| 2.25 | 8147 | 1750 | 1750 | -78.52 | 1.64 | 0.56 | 1018 | -87.50 | 1.64 | 1.45 |
| 3.38 | 8147 | 1750 | 1750 | -78.52 | 1.64 | 0.56 | 1018 | -87.50 | 1.64 | 1.45 |
| 5.06 | 8147 | 1750 | 1750 | -78.52 | 1.64 | 0.56 | 1018 | -87.50 | 1.64 | 1.45 |
| 7.59 | 8147 | 1750 | 1750 | -78.52 | 1.64 | 0.56 | 1018 | -87.50 | 1.64 | 1.45 |
| 11.39 | 8147 | 1750 | 1750 | -78.52 | 1.64 | 0.56 | 1018 | -87.50 | 1.64 | 1.45 |
| 17.09 | 8147 | 1750 | 1750 | -78.52 | 1.64 | 0.56 | 1018 | -87.50 | 1.64 | 1.45 |
| 25.63 | 8147 | 1750 | 1750 | -78.52 | 1.64 | 0.56 | 1018 | -87.50 | 1.64 | 1.45 |
| 38.44 | 8147 | 1750 | 1750 | -78.52 | 1.64 | 0.56 | 1018 | -87.50 | 1.64 | 1.45 |
| 57.67 | 8147 | 1750 | 1750 | -78.52 | 1.64 | 0.56 | 1018 | -87.50 | 1.64 | 1.45 |
| 86.50 | 8147 | 1750 | 1750 | -78.52 | 1.64 | 0.56 | 1018 | -87.50 | 1.63 | 1.45 |
| 129.75 | 8147 | 1750 | 1750 | -78.52 | 1.64 | 0.56 | 1018 | -87.50 | 1.63 | 1.45 |
| 194.62 | 8147 | 1750 | 1750 | -78.52 | 1.64 | 0.56 | 1018 | -87.50 | 1.63 | 1.45 |
| 291.93 | 8147 | 1750 | 1750 | -78.52 | 1.63 | 0.55 | 1018 | -87.50 | 1.61 | 1.45 |
| 437.89 | 8147 | 1750 | 1750 | -78.52 | 1.63 | 0.55 | 1018 | -87.50 | 1.58 | 1.45 |
| 656.84 | 8147 | 1750 | 1750 | -78.52 | 1.62 | 0.55 | 1018 | -87.50 | 1.52 | 1.45 |
| 985.26 | 8147 | 1750 | 1750 | -78.52 | 1.61 | 0.54 | 1018 | -87.50 | 1.38 | 1.44 |
| 1477.89 | 8147 | 1750 | 1750 | -78.52 | 1.58 | 0.52 | 1018 | -87.50 | 1.06 | 1.42 |
| 2216.84 | 8147 | 1750 | 1750 | -78.52 | 1.51 | 0.48 | 1018 | -87.50 | 0.38 | 1.38 |
| 3325.26 | 8147 | 1750 | 1750 | -78.52 | 1.37 | 0.39 | 1018 | -87.50 | 0.99 | 1.29 |
| 4987.89 | 10878 | 1750 | 1750 | -83.91 | 0.78 | 0.21 | 1018 | -90.64 | 3.87 | 1.11 |
| 7481.83 | 14062 | 1750 | 1750 | -87.56 | 0.35 | 0.11 | 1018 | -92.76 | 7.74 | 0.79 |
| 11222.74 | 18571 | 1750 | 1750 | -90.58 | 0.05 | 0.62 | 1018 | -94.52 | 11.86 | 0.30 |
| 16834.11 | 26966 | 1750 | 1750 | -93.51 | 0.26 | 1.17 | 1018 | -96.22 | 15.08 | 0.25 |
| 25251.17 | 37108 | 1750 | 1750 | -95.28 | 0.54 | 1.62 | 1018 | -97.26 | 16.86 | 0.69 |
| 37876.75 | 55872 | 1750 | 1750 | -96.87 | 0.71 | 1.97 | 1018 | -98.18 | 17.76 | 1.04 |
| 56815.13 | 78058 | 1750 | 1750 | -97.76 | 0.81 | 2.22 | 1018 | -98.70 | 18.52 | 1.28 |
| 85222.69 | 113323 | 1750 | 1750 | -98.46 | 0.92 | 2.41 | 1018 | -99.10 | 19.31 | 1.47 |
| 127834.04 | 153346 | 1750 | 1750 | -98.86 | 1.04 | 2.58 | 1018 | -99.34 | 20.00 | 1.64 |
| 191751.06 | 227825 | 1750 | 1750 | -99.23 | 1.13 | 2.72 | 1018 | -99.55 | 20.55 | 1.77 |
| 287626.59 | 328712 | 1750 | 1750 | -99.47 | 1.29 | 2.82 | 1018 | -99.69 | 21.09 | 1.87 |
| 431439.88 | 477213 | 1750 | 1750 | -99.63 | 1.38 | 2.91 | 1018 | -99.79 | 21.50 | 1.96 |
| 647159.82 | 703887 | 1750 | 1750 | -99.75 | 1.36 | 3.00 | 1018 | -99.86 | 21.71 | 2.04 |
| 970739.74 | 1.01668E+06 | 1750 | 1750 | -99.83 | 1.36 | 3.06 | 1018 | -99.90 | 21.90 | 2.10 |

Table 4.13: Relative difference between Degrees-of-Freedom used in Full-Model and Semi-analytical Model versus the relative error in the solution of the impedance at a broad range of frequencies for a 15-turn winding with 8mm of inter-turn distance and a sleeve size of 1mm

| 15 Turns Inter-turn distance 8mm Frequency (Hz) | FM | | SA (Structured) $r_{SL} = 0.5\text{mm}$ | | | | SA (Unstructured) $l_c = 0.5\text{mm}$ | | | |
|----------------------------------------------------------|-------------|------|--------------------------------------------|-----------------------------|-----------------------------|------|-------------------------------------------|-----------------------------|-----------------------------|--|
| | DoF | DoF | DoF Rel. Diff. (%) | Resistance Rel. Err. (%) | Inductance Rel. Err. (%) | DoF | DoF Rel. Diff. (%) | Resistance Rel. Err. (%) | Inductance Rel. Err. (%) | |
| 1.00 | 8147 | 2785 | -65.82 | 1.64 | 0.68 | 2860 | -64.90 | 1.64 | 1.49 | |
| 1.50 | 8147 | 2785 | -65.82 | 1.64 | 0.68 | 2860 | -64.90 | 1.64 | 1.49 | |
| 2.25 | 8147 | 2785 | -65.82 | 1.64 | 0.68 | 2860 | -64.90 | 1.64 | 1.49 | |
| 3.38 | 8147 | 2785 | -65.82 | 1.64 | 0.68 | 2860 | -64.90 | 1.64 | 1.49 | |
| 5.06 | 8147 | 2785 | -65.82 | 1.64 | 0.68 | 2860 | -64.90 | 1.64 | 1.49 | |
| 7.59 | 8147 | 2785 | -65.82 | 1.64 | 0.68 | 2860 | -64.90 | 1.64 | 1.49 | |
| 11.39 | 8147 | 2785 | -65.82 | 1.64 | 0.68 | 2860 | -64.90 | 1.64 | 1.49 | |
| 17.09 | 8147 | 2785 | -65.82 | 1.64 | 0.68 | 2860 | -64.90 | 1.64 | 1.49 | |
| 25.63 | 8147 | 2785 | -65.82 | 1.64 | 0.68 | 2860 | -64.90 | 1.64 | 1.49 | |
| 38.44 | 8147 | 2785 | -65.82 | 1.64 | 0.68 | 2860 | -64.90 | 1.64 | 1.49 | |
| 57.67 | 8147 | 2785 | -65.82 | 1.64 | 0.68 | 2860 | -64.90 | 1.64 | 1.49 | |
| 86.50 | 8147 | 2785 | -65.82 | 1.64 | 0.68 | 2860 | -64.90 | 1.63 | 1.49 | |
| 129.75 | 8147 | 2785 | -65.82 | 1.64 | 0.68 | 2860 | -64.90 | 1.63 | 1.49 | |
| 194.62 | 8147 | 2785 | -65.82 | 1.63 | 0.68 | 2860 | -64.90 | 1.62 | 1.49 | |
| 291.93 | 8147 | 2785 | -65.82 | 1.63 | 0.68 | 2860 | -64.90 | 1.60 | 1.49 | |
| 437.89 | 8147 | 2785 | -65.82 | 1.63 | 0.68 | 2860 | -64.90 | 1.55 | 1.49 | |
| 656.84 | 8147 | 2785 | -65.82 | 1.61 | 0.67 | 2860 | -64.90 | 1.44 | 1.49 | |
| 985.26 | 8147 | 2785 | -65.82 | 1.59 | 0.66 | 2860 | -64.90 | 1.19 | 1.48 | |
| 1477.89 | 8147 | 2785 | -65.82 | 1.53 | 0.64 | 2860 | -64.90 | 0.65 | 1.46 | |
| 2216.84 | 8147 | 2785 | -65.82 | 1.40 | 0.60 | 2860 | -64.90 | 0.51 | 1.42 | |
| 3325.26 | 8147 | 2785 | -65.82 | 1.14 | 0.51 | 2860 | -64.90 | 2.86 | 1.33 | |
| 4987.89 | 10878 | 2785 | -74.40 | 0.33 | 0.33 | 2860 | -73.71 | 7.55 | 1.15 | |
| 7481.83 | 14062 | 2785 | -80.19 | 0.43 | 0.01 | 2860 | -79.66 | 14.14 | 0.83 | |
| 11222.74 | 18571 | 2785 | -85.00 | 1.10 | 0.49 | 2860 | -84.60 | 21.29 | 0.34 | |
| 16834.11 | 26966 | 2785 | -89.67 | 1.69 | 1.04 | 2860 | -89.39 | 26.82 | 0.21 | |
| 25251.17 | 37108 | 2785 | -92.49 | 2.11 | 1.49 | 2860 | -92.29 | 29.79 | 0.65 | |
| 37876.75 | 55872 | 2785 | -95.02 | 2.36 | 1.84 | 2860 | -94.88 | 31.25 | 0.99 | |
| 56815.13 | 78058 | 2785 | -96.43 | 2.52 | 2.09 | 2860 | -96.34 | 32.53 | 1.24 | |
| 85222.69 | 113323 | 2785 | -97.54 | 2.70 | 2.28 | 2860 | -97.48 | 33.87 | 1.43 | |
| 127834.04 | 153346 | 2785 | -98.18 | 2.87 | 2.45 | 2860 | -98.13 | 35.02 | 1.60 | |
| 191751.06 | 227825 | 2785 | -98.78 | 3.00 | 2.59 | 2860 | -98.74 | 35.92 | 1.73 | |
| 287626.59 | 328712 | 2785 | -99.15 | 3.20 | 2.69 | 2860 | -99.13 | 36.77 | 1.83 | |
| 431439.88 | 477213 | 2785 | -99.42 | 3.32 | 2.78 | 2860 | -99.40 | 37.42 | 1.91 | |
| 647159.82 | 703887 | 2785 | -99.60 | 3.32 | 2.87 | 2860 | -99.59 | 37.82 | 2.00 | |
| 970739.74 | 1.01668E+06 | 2785 | -99.73 | 3.34 | 2.93 | 2860 | -99.72 | 38.16 | 2.06 | |

Table 4.14: Relative difference between Degrees-of-Freedom used in Full-Model and Semi-analytical Model versus the relative error in the solution of the impedance at a broad range of frequencies for a 15-turn winding with 8mm of inter-turn distance and a sleeve size of 0.5mm

| 15 Turns Inter-turn distance 8mm Frequency (Hz) | FM | | SA (Structured) $r_{SL} = 3\text{mm}$ | | | | SA (Unstructured) $l_c = 3\text{mm}$ | | | |
|----------------------------------------------------------|-------------|-----|------------------------------------------|----------------|-----------------------------|-----------------------------|-----------------------------------------|----------------|-----------------------------|-----------------------------|
| | DoF | DoF | DoF | Rel. Diff. (%) | Resistance Rel. Err. (%) | Inductance Rel. Err. (%) | DoF | Rel. Diff. (%) | Resistance Rel. Err. (%) | Inductance Rel. Err. (%) |
| 1.00 | 8147 | 407 | 407 | -95.00 | 1.64 | 0.33 | 274 | -96.64 | 1.64 | 0.22 |
| 1.50 | 8147 | 407 | 407 | -95.00 | 1.64 | 0.33 | 274 | -96.64 | 1.64 | 0.22 |
| 2.25 | 8147 | 407 | 407 | -95.00 | 1.64 | 0.33 | 274 | -96.64 | 1.64 | 0.22 |
| 3.38 | 8147 | 407 | 407 | -95.00 | 1.64 | 0.33 | 274 | -96.64 | 1.64 | 0.22 |
| 5.06 | 8147 | 407 | 407 | -95.00 | 1.64 | 0.33 | 274 | -96.64 | 1.64 | 0.22 |
| 7.59 | 8147 | 407 | 407 | -95.00 | 1.64 | 0.33 | 274 | -96.64 | 1.64 | 0.22 |
| 11.39 | 8147 | 407 | 407 | -95.00 | 1.64 | 0.33 | 274 | -96.64 | 1.64 | 0.22 |
| 17.09 | 8147 | 407 | 407 | -95.00 | 1.64 | 0.33 | 274 | -96.64 | 1.64 | 0.22 |
| 25.63 | 8147 | 407 | 407 | -95.00 | 1.64 | 0.33 | 274 | -96.64 | 1.64 | 0.22 |
| 38.44 | 8147 | 407 | 407 | -95.00 | 1.64 | 0.33 | 274 | -96.64 | 1.64 | 0.22 |
| 57.67 | 8147 | 407 | 407 | -95.00 | 1.64 | 0.33 | 274 | -96.64 | 1.64 | 0.22 |
| 86.50 | 8147 | 407 | 407 | -95.00 | 1.64 | 0.33 | 274 | -96.64 | 1.64 | 0.22 |
| 129.75 | 8147 | 407 | 407 | -95.00 | 1.64 | 0.33 | 274 | -96.64 | 1.64 | 0.22 |
| 194.62 | 8147 | 407 | 407 | -95.00 | 1.64 | 0.33 | 274 | -96.64 | 1.64 | 0.22 |
| 291.93 | 8147 | 407 | 407 | -95.00 | 1.64 | 0.33 | 274 | -96.64 | 1.64 | 0.22 |
| 437.89 | 8147 | 407 | 407 | -95.00 | 1.63 | 0.33 | 274 | -96.64 | 1.63 | 0.22 |
| 656.84 | 8147 | 407 | 407 | -95.00 | 1.63 | 0.33 | 274 | -96.64 | 1.63 | 0.22 |
| 985.26 | 8147 | 407 | 407 | -95.00 | 1.62 | 0.32 | 274 | -96.64 | 1.63 | 0.21 |
| 1477.89 | 8147 | 407 | 407 | -95.00 | 1.60 | 0.30 | 274 | -96.64 | 1.62 | 0.19 |
| 2216.84 | 8147 | 407 | 407 | -95.00 | 1.55 | 0.26 | 274 | -96.64 | 1.59 | 0.15 |
| 3325.26 | 8147 | 407 | 407 | -95.00 | 1.47 | 0.16 | 274 | -96.64 | 1.56 | 0.05 |
| 4987.89 | 10878 | 407 | 407 | -96.26 | 0.98 | 0.01 | 274 | -97.48 | 1.14 | 0.13 |
| 7481.83 | 14062 | 407 | 407 | -97.11 | 0.70 | 0.34 | 274 | -98.05 | 0.98 | 0.45 |
| 11222.74 | 18571 | 407 | 407 | -97.81 | 0.56 | 0.84 | 274 | -98.52 | 0.90 | 0.95 |
| 16834.11 | 26966 | 407 | 407 | -98.49 | 0.37 | 1.39 | 274 | -98.98 | 0.90 | 1.51 |
| 25251.17 | 37108 | 407 | 407 | -98.90 | 0.16 | 1.85 | 274 | -99.26 | 0.73 | 1.96 |
| 37876.75 | 55872 | 407 | 407 | -99.27 | 0.01 | 2.20 | 274 | -99.51 | 0.62 | 2.31 |
| 56815.13 | 78058 | 407 | 407 | -99.48 | 0.06 | 2.45 | 274 | -99.65 | 0.57 | 2.56 |
| 85222.69 | 113323 | 407 | 407 | -99.64 | 0.14 | 2.64 | 274 | -99.76 | 0.51 | 2.76 |
| 127834.04 | 153346 | 407 | 407 | -99.73 | 0.24 | 2.81 | 274 | -99.82 | 0.43 | 2.93 |
| 191751.06 | 227825 | 407 | 407 | -99.82 | 0.30 | 2.95 | 274 | -99.88 | 0.38 | 3.07 |
| 287626.59 | 328712 | 407 | 407 | -99.88 | 0.45 | 3.05 | 274 | -99.92 | 0.25 | 3.17 |
| 431439.88 | 477213 | 407 | 407 | -99.91 | 0.53 | 3.14 | 274 | -99.94 | 0.18 | 3.26 |
| 647159.82 | 703887 | 407 | 407 | -99.94 | 0.49 | 3.23 | 274 | -99.96 | 0.23 | 3.35 |
| 970739.74 | 1.01668E+06 | 407 | 407 | -99.96 | 0.49 | 3.29 | 274 | -99.97 | 0.24 | 3.41 |

Table 4.15: Relative difference between Degrees-of-Freedom used in Full-Model and Semi-analytical Model versus the relative error in the solution of the impedance at a broad range of frequencies for a 15-turn winding with 8mm of inter-turn distance and a sleeve size of 3mm

4.3.3.3. Impedance at a broad range of frequencies at an inter-turn spacing of 2.05mm

Fig 4.18 reports the resistance and the inductance values at an inter-turn spacing of 8mm at a broad range of frequencies.

The relative error in **resistance** values in the case of **structured sleeves** remains in a range between 1.64% – 46.17% for $r_{SL} = 1\text{mm}$, and 1.64% – 47.09% for $r_{SL} = 0.5\text{mm}$. In the case of **unstructured sleeves** the relative error remains in a range between 1.64% – 50.11% for $l_c = 1\text{mm}$, 1.64% – 57.83% for $l_c = 0.5\text{mm}$, and 1.64% – 47.41% for $l_c = 3\text{mm}$.

The relative error in **inductance** values in the case of **structured sleeves** remains in a range between 0.26% – 21.28% for $r_{SL} = 1\text{mm}$, and 0.35% – 21.16% for $r_{SL} = 0.5\text{mm}$. In the case of **unstructured sleeves** the relative error remains in a range between 1.19% – 20.13% for $l_c = 1\text{mm}$, 0.95% – 20.42% for $l_c = 0.5\text{mm}$, and 5.64% – 14.65% for $l_c = 3\text{mm}$.

The compromise between error and computational cost is studied throughout tables 4.16 -4.17. For sleeve radius 1mm in the structured case the problem size decreases from low frequencies to higher frequencies in a range between 65.76% – 99.61% and similarly in the case of unstructured sleeves 75.87% – 99.72%. In the 0.5mm case, the decrease in problem size in the structured case, ranges in percentage between 40.69% – 99.32% and the unstructured sleeves 60.50% – 99.55%. Lastly, in the 3mm in the unstructured case 82.91% – 99.80%.

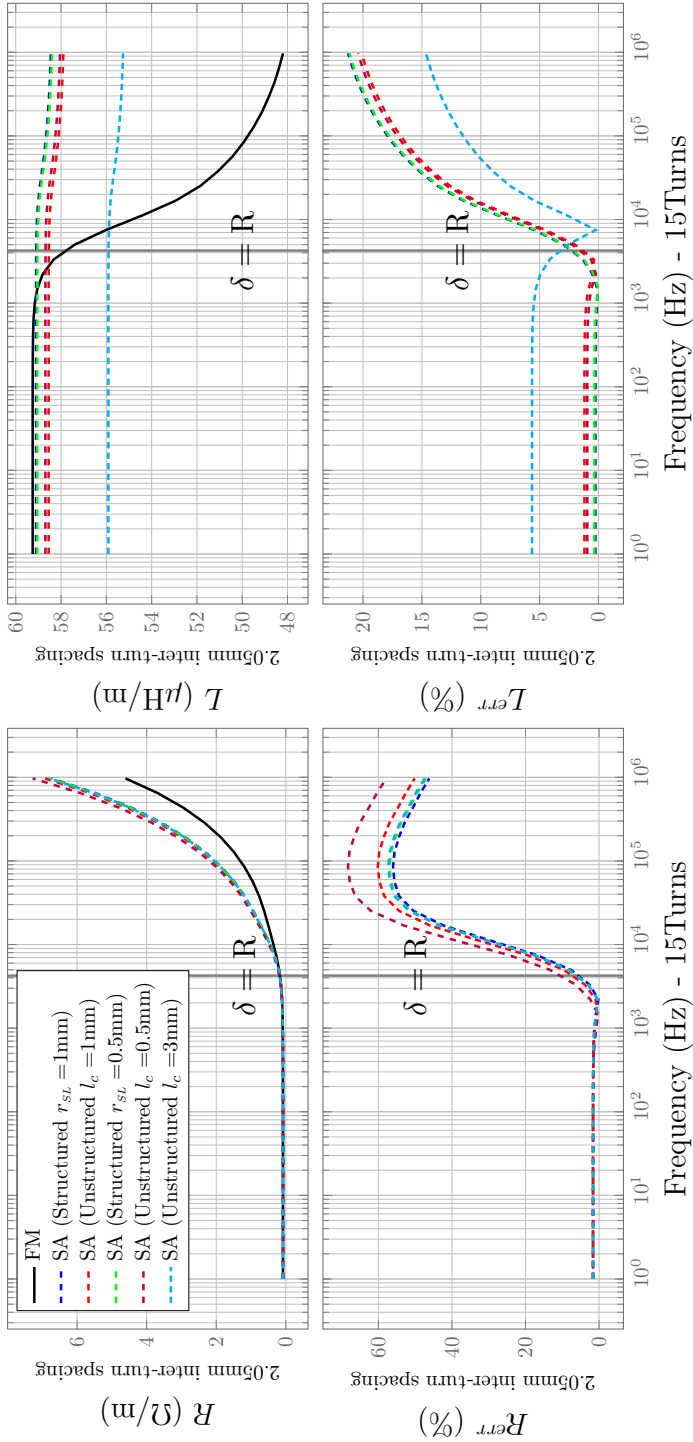


Figure 4.18: Impedance at a broad range of frequencies with large inter-turn spacing on a 15-Turn coil: Resistance (Left), Inductance (Right)

| 15 Turns Inter-turn distance 2.05mm Frequency (Hz) | FM | | SA (Structured) $\tau_{SL} = 1mm$ | | | | SA (Unstructured) $l_c = 1mm$ | | | |
|-------------------------------------------------------------|--------|-----|--------------------------------------|-----------------------------|-----------------------------|-----|----------------------------------|-----------------------------|-----------------------------|--|
| | DoF | DoF | DoF Rel. Diff. (%) | Resistance Rel. Err. (%) | Inductance Rel. Err. (%) | DoF | DoF Rel. Diff. (%) | Resistance Rel. Err. (%) | Inductance Rel. Err. (%) | |
| 1.00 | 1691 | 579 | -65.76 | 1.64 | 0.26 | 408 | -75.87 | 1.64 | 1.19 | |
| 1.50 | 1691 | 579 | -65.76 | 1.64 | 0.26 | 408 | -75.87 | 1.64 | 1.19 | |
| 2.25 | 1691 | 579 | -65.76 | 1.64 | 0.26 | 408 | -75.87 | 1.64 | 1.19 | |
| 3.38 | 1691 | 579 | -65.76 | 1.64 | 0.26 | 408 | -75.87 | 1.64 | 1.19 | |
| 5.06 | 1691 | 579 | -65.76 | 1.64 | 0.26 | 408 | -75.87 | 1.64 | 1.19 | |
| 7.59 | 1691 | 579 | -65.76 | 1.64 | 0.26 | 408 | -75.87 | 1.64 | 1.19 | |
| 11.39 | 1691 | 579 | -65.76 | 1.64 | 0.26 | 408 | -75.87 | 1.64 | 1.19 | |
| 17.09 | 1691 | 579 | -65.76 | 1.64 | 0.26 | 408 | -75.87 | 1.64 | 1.19 | |
| 25.63 | 1691 | 579 | -65.76 | 1.64 | 0.26 | 408 | -75.87 | 1.64 | 1.19 | |
| 38.44 | 1691 | 579 | -65.76 | 1.64 | 0.25 | 408 | -75.87 | 1.64 | 1.19 | |
| 57.67 | 1691 | 579 | -65.76 | 1.64 | 0.25 | 408 | -75.87 | 1.64 | 1.19 | |
| 86.50 | 1691 | 579 | -65.76 | 1.63 | 0.25 | 408 | -75.87 | 1.63 | 1.19 | |
| 129.75 | 1691 | 579 | -65.76 | 1.62 | 0.25 | 408 | -75.87 | 1.63 | 1.19 | |
| 194.62 | 1691 | 579 | -65.76 | 1.63 | 0.25 | 408 | -75.87 | 1.62 | 1.18 | |
| 291.93 | 1691 | 579 | -65.76 | 1.61 | 0.24 | 408 | -75.87 | 1.59 | 1.18 | |
| 437.89 | 1691 | 579 | -65.76 | 1.57 | 0.22 | 408 | -75.87 | 1.53 | 1.16 | |
| 656.84 | 1691 | 579 | -65.76 | 1.49 | 0.19 | 408 | -75.87 | 1.40 | 1.12 | |
| 985.26 | 1691 | 579 | -65.76 | 1.30 | 0.10 | 408 | -75.87 | 1.11 | 1.04 | |
| 1477.89 | 1691 | 579 | -65.76 | 0.86 | 0.09 | 408 | -75.87 | 0.47 | 0.85 | |
| 2216.84 | 1691 | 579 | -65.76 | 0.18 | 0.49 | 408 | -75.87 | 0.94 | 0.45 | |
| 3325.26 | 1691 | 579 | -65.76 | 2.61 | 1.33 | 408 | -75.87 | 3.90 | 0.38 | |
| 4987.89 | 2082 | 579 | -72.19 | 7.69 | 2.94 | 408 | -80.40 | 9.61 | 1.97 | |
| 7481.83 | 2445 | 579 | -76.32 | 16.95 | 5.46 | 408 | -83.31 | 19.52 | 4.47 | |
| 11222.74 | 3059 | 579 | -81.07 | 29.75 | 8.56 | 408 | -86.66 | 32.92 | 7.54 | |
| 16834.11 | 4243 | 579 | -86.35 | 42.23 | 11.48 | 408 | -90.38 | 45.86 | 10.43 | |
| 25251.17 | 5777 | 579 | -89.98 | 50.45 | 13.67 | 408 | -92.94 | 54.36 | 12.60 | |
| 37876.75 | 8124 | 579 | -92.87 | 54.34 | 15.23 | 408 | -94.98 | 58.39 | 14.15 | |
| 56815.13 | 11209 | 579 | -94.83 | 55.63 | 16.52 | 408 | -96.36 | 59.73 | 15.43 | |
| 85222.69 | 15885 | 579 | -96.36 | 56.02 | 17.56 | 408 | -97.43 | 60.16 | 16.45 | |
| 127834.04 | 21654 | 579 | -97.33 | 55.60 | 18.45 | 408 | -98.12 | 59.75 | 17.33 | |
| 191751.06 | 31713 | 579 | -98.17 | 54.41 | 19.21 | 408 | -98.71 | 58.54 | 18.09 | |
| 287626.59 | 46065 | 579 | -98.74 | 52.84 | 19.85 | 408 | -99.11 | 56.94 | 18.72 | |
| 431439.88 | 67908 | 579 | -99.15 | 50.63 | 20.42 | 408 | -99.40 | 54.68 | 19.28 | |
| 647159.82 | 100307 | 579 | -99.42 | 48.56 | 20.88 | 408 | -99.59 | 52.56 | 19.73 | |
| 970739.74 | 147897 | 579 | -99.61 | 46.17 | 21.28 | 408 | -99.72 | 50.11 | 20.13 | |

Table 4.16: Relative difference between Degrees-of-Freedom used in Full-Model and Semi-analytical Model versus the relative error in the solution of the impedance at a broad range of frequencies for a 15-turn winding with 2.05mm of inter-turn distance and a sleeve size of 1mm

| 15 Turns Inter-turn distance 2.05mm Frequency (Hz) | FM | | SA (Structured) $r_{SL} = 0.5\text{mm}$ | | | | SA (Unstructured) $l_c = 0.5\text{mm}$ | | | |
|-------------------------------------------------------------|--------|------|--------------------------------------------|-----------------------------|-----------------------------|-----|-------------------------------------------|-----------------------------|-----------------------------|--|
| | DoF | DoF | DoF Rel. Diff. (%) | Resistance Rel. Err. (%) | Inductance Rel. Err. (%) | DoF | DoF Rel. Diff. (%) | Resistance Rel. Err. (%) | Inductance Rel. Err. (%) | |
| 1.00 | 1691 | 1003 | -40.69 | 1.64 | 0.35 | 668 | -60.50 | 1.64 | 0.95 | |
| 1.50 | 1691 | 1003 | -40.69 | 1.64 | 0.35 | 668 | -60.50 | 1.64 | 0.95 | |
| 2.25 | 1691 | 1003 | -40.69 | 1.64 | 0.35 | 668 | -60.50 | 1.64 | 0.95 | |
| 3.38 | 1691 | 1003 | -40.69 | 1.64 | 0.35 | 668 | -60.50 | 1.64 | 0.95 | |
| 5.06 | 1691 | 1003 | -40.69 | 1.64 | 0.35 | 668 | -60.50 | 1.64 | 0.95 | |
| 7.59 | 1691 | 1003 | -40.69 | 1.64 | 0.35 | 668 | -60.50 | 1.64 | 0.95 | |
| 11.39 | 1691 | 1003 | -40.69 | 1.64 | 0.35 | 668 | -60.50 | 1.64 | 0.95 | |
| 17.09 | 1691 | 1003 | -40.69 | 1.64 | 0.35 | 668 | -60.50 | 1.64 | 0.95 | |
| 25.63 | 1691 | 1003 | -40.69 | 1.64 | 0.35 | 668 | -60.50 | 1.64 | 0.95 | |
| 38.44 | 1691 | 1003 | -40.69 | 1.64 | 0.35 | 668 | -60.50 | 1.64 | 0.95 | |
| 57.67 | 1691 | 1003 | -40.69 | 1.64 | 0.34 | 668 | -60.50 | 1.63 | 0.95 | |
| 86.50 | 1691 | 1003 | -40.69 | 1.63 | 0.34 | 668 | -60.50 | 1.63 | 0.95 | |
| 129.75 | 1691 | 1003 | -40.69 | 1.63 | 0.34 | 668 | -60.50 | 1.62 | 0.94 | |
| 194.62 | 1691 | 1003 | -40.69 | 1.62 | 0.34 | 668 | -60.50 | 1.60 | 0.94 | |
| 291.93 | 1691 | 1003 | -40.69 | 1.60 | 0.33 | 668 | -60.50 | 1.56 | 0.93 | |
| 437.89 | 1691 | 1003 | -40.69 | 1.56 | 0.31 | 668 | -60.50 | 1.45 | 0.92 | |
| 656.84 | 1691 | 1003 | -40.69 | 1.47 | 0.28 | 668 | -60.50 | 1.23 | 0.88 | |
| 985.26 | 1691 | 1003 | -40.69 | 1.26 | 0.19 | 668 | -60.50 | 0.74 | 0.79 | |
| 1477.89 | 1691 | 1003 | -40.69 | 0.77 | 0.00 | 668 | -60.50 | 0.31 | 0.61 | |
| 2216.84 | 1691 | 1003 | -40.69 | 0.36 | 0.40 | 668 | -60.50 | 2.43 | 0.20 | |
| 3325.26 | 1691 | 1003 | -40.69 | 2.91 | 1.24 | 668 | -60.50 | 6.44 | 0.62 | |
| 4987.89 | 2082 | 1003 | -51.83 | 8.13 | 2.84 | 668 | -67.92 | 13.39 | 2.22 | |
| 7481.83 | 2445 | 1003 | -58.98 | 17.55 | 5.37 | 668 | -72.68 | 24.54 | 4.73 | |
| 11222.74 | 3059 | 1003 | -67.21 | 30.49 | 8.46 | 668 | -78.16 | 39.10 | 7.80 | |
| 16834.11 | 4243 | 1003 | -76.36 | 43.07 | 11.38 | 668 | -84.26 | 52.97 | 10.70 | |
| 25251.17 | 5777 | 1003 | -82.64 | 51.36 | 13.57 | 668 | -88.44 | 62.01 | 12.88 | |
| 37876.75 | 8124 | 1003 | -87.65 | 55.28 | 15.13 | 668 | -91.78 | 66.30 | 14.43 | |
| 56815.13 | 11209 | 1003 | -91.05 | 56.59 | 16.42 | 668 | -94.04 | 67.76 | 15.71 | |
| 85222.69 | 15885 | 1003 | -93.69 | 56.98 | 17.45 | 668 | -95.79 | 68.25 | 16.74 | |
| 127834.04 | 21654 | 1003 | -95.37 | 56.57 | 18.34 | 668 | -96.92 | 67.87 | 17.62 | |
| 191751.06 | 31713 | 1003 | -96.84 | 55.37 | 19.11 | 668 | -97.89 | 66.63 | 18.38 | |
| 287626.59 | 46065 | 1003 | -97.82 | 53.80 | 19.74 | 668 | -98.55 | 64.97 | 19.01 | |
| 431439.88 | 67908 | 1003 | -98.52 | 51.57 | 20.31 | 668 | -99.02 | 62.61 | 19.58 | |
| 647159.82 | 100307 | 1003 | -99.00 | 49.49 | 20.77 | 668 | -99.33 | 60.39 | 20.03 | |
| 970739.74 | 147897 | 1003 | -99.32 | 47.09 | 21.16 | 668 | -99.55 | 57.83 | 20.42 | |

Table 4.17: Relative difference between Degrees-of-Freedom used in Full-Model and Semi-analytical Model versus the relative error in the solution of the impedance at a broad range of frequencies for a 15-turn winding with 2.05mm of inter-turn distance and a sleeve size of 0.5mm

| 15 Turns Inter-turn distance 2.05mm Frequency (Hz) | FM | | SA (Structured) $\tau_{SL} = 3\text{mm}$ | | | | SA (Unstructured) $l_c = 3\text{mm}$ | | | |
|-------------------------------------------------------------|--------|-----|---------------------------------------------|-----------------------------|-----------------------------|-----|-----------------------------------------|-----------------------------|-----------------------------|--|
| | DoF | DoF | DoF Rel. Diff. (%) | Resistance Rel. Err. (%) | Inductance Rel. Err. (%) | DoF | DoF Rel. Diff. (%) | Resistance Rel. Err. (%) | Inductance Rel. Err. (%) | |
| 1.00 | 1691 | N/A | N/A | N/A | N/A | 289 | -82.91 | 1.64 | 5.64 | |
| 1.50 | 1691 | N/A | N/A | N/A | N/A | 289 | -82.91 | 1.64 | 5.64 | |
| 2.25 | 1691 | N/A | N/A | N/A | N/A | 289 | -82.91 | 1.64 | 5.64 | |
| 3.38 | 1691 | N/A | N/A | N/A | N/A | 289 | -82.91 | 1.64 | 5.64 | |
| 5.06 | 1691 | N/A | N/A | N/A | N/A | 289 | -82.91 | 1.64 | 5.64 | |
| 7.59 | 1691 | N/A | N/A | N/A | N/A | 289 | -82.91 | 1.64 | 5.64 | |
| 11.39 | 1691 | N/A | N/A | N/A | N/A | 289 | -82.91 | 1.64 | 5.64 | |
| 17.09 | 1691 | N/A | N/A | N/A | N/A | 289 | -82.91 | 1.64 | 5.64 | |
| 25.63 | 1691 | N/A | N/A | N/A | N/A | 289 | -82.91 | 1.64 | 5.64 | |
| 38.44 | 1691 | N/A | N/A | N/A | N/A | 289 | -82.91 | 1.64 | 5.64 | |
| 57.67 | 1691 | N/A | N/A | N/A | N/A | 289 | -82.91 | 1.64 | 5.64 | |
| 86.50 | 1691 | N/A | N/A | N/A | N/A | 289 | -82.91 | 1.63 | 5.64 | |
| 129.75 | 1691 | N/A | N/A | N/A | N/A | 289 | -82.91 | 1.63 | 5.64 | |
| 194.62 | 1691 | N/A | N/A | N/A | N/A | 289 | -82.91 | 1.62 | 5.63 | |
| 291.93 | 1691 | N/A | N/A | N/A | N/A | 289 | -82.91 | 1.60 | 5.63 | |
| 437.89 | 1691 | N/A | N/A | N/A | N/A | 289 | -82.91 | 1.56 | 5.61 | |
| 656.84 | 1691 | N/A | N/A | N/A | N/A | 289 | -82.91 | 1.46 | 5.58 | |
| 985.26 | 1691 | N/A | N/A | N/A | N/A | 289 | -82.91 | 1.24 | 5.49 | |
| 1477.89 | 1691 | N/A | N/A | N/A | N/A | 289 | -82.91 | 0.74 | 5.32 | |
| 2216.84 | 1691 | N/A | N/A | N/A | N/A | 289 | -82.91 | 0.42 | 4.93 | |
| 3325.26 | 1691 | N/A | N/A | N/A | N/A | 289 | -82.91 | 3.02 | 4.14 | |
| 4987.89 | 2082 | N/A | N/A | N/A | N/A | 289 | -86.12 | 8.29 | 2.62 | |
| 7481.83 | 2445 | N/A | N/A | N/A | N/A | 289 | -88.18 | 17.76 | 0.23 | |
| 11222.74 | 3059 | N/A | N/A | N/A | N/A | 289 | -90.55 | 30.75 | 2.69 | |
| 16834.11 | 4243 | N/A | N/A | N/A | N/A | 289 | -93.19 | 43.37 | 5.45 | |
| 25251.17 | 5777 | N/A | N/A | N/A | N/A | 289 | -95.00 | 51.68 | 7.52 | |
| 37876.75 | 8124 | N/A | N/A | N/A | N/A | 289 | -96.44 | 55.62 | 8.98 | |
| 56815.13 | 11209 | N/A | N/A | N/A | N/A | 289 | -97.42 | 56.93 | 10.20 | |
| 85222.69 | 15885 | N/A | N/A | N/A | N/A | 289 | -98.18 | 57.32 | 11.17 | |
| 127834.04 | 21654 | N/A | N/A | N/A | N/A | 289 | -98.67 | 56.91 | 12.00 | |
| 191751.06 | 31713 | N/A | N/A | N/A | N/A | 289 | -99.09 | 55.71 | 12.72 | |
| 287626.59 | 46065 | N/A | N/A | N/A | N/A | 289 | -99.37 | 54.14 | 13.32 | |
| 431439.88 | 67908 | N/A | N/A | N/A | N/A | 289 | -99.57 | 51.91 | 13.85 | |
| 647159.82 | 100307 | N/A | N/A | N/A | N/A | 289 | -99.71 | 49.82 | 14.28 | |
| 970739.74 | 147897 | N/A | N/A | N/A | N/A | 289 | -99.80 | 47.41 | 14.65 | |

Table 4.18: Relative difference between Degrees-of-Freedom used in Full-Model and Semi-analytical Model versus the relative error in the solution of the impedance at a broad range of frequencies for a 15-turn winding with 2.05mm of inter-turn distance and a sleeve size of 3mm

4.3.4. Highlights and Remarks

This chapter has analyzed in detail the modelling of multi-turn coils with the semi-analytical approach, accounting for both skin- and proximity effect over a broad range of frequencies. It has been demonstrated that the **SA** technique is able to considerably reduce the problem size (number of unknowns of the FE problem to solve) without a significant loss of accuracy in most situations.

Coils with 5, 10 and 15 turns with varying inter-turn spaces were considered to compare the **SA** approach against a conventional finely discretized FE model, called **FM** model. The comparison is conducted in terms of the accuracy of the calculated impedances and losses on the one hand, and of the problem size on the other hand. In order to ensure an as fair as possible comparison between the two studied approaches, the **FM** model has been remeshed systematically to ensure at least 3 elements per skin depth at every frequency. However, as observed in the previous chapter, this mesh refinement calibrated for a sufficient resolution of the skin effect, might fall short in some cases to fully resolve the abrupt field gradient caused by the proximity effect near the conductor surface. In such situations, the **FM** model should no longer be regarded as a reference solution, but as an alternative modelling approach with respect to which the **SA** technique, being potentially more accurate with less unknowns, may even prove to be superior.

It has been observed that the level of agreement is high at large inter-turn spacing, whatever the frequency. The SA approach is thus in all cases advantageous when the turns are not too close to each other. Quantitatively, the accuracy using structured sleeves can be kept under 5% as long as the inter-turn distance between conductors is of at least 3 radii all over the considered frequency range (1Hz to 1MHz).

The relative error increases however as the conductors come closer to each other. This is expected because the approximation of the SA method approximates the proximity effect with the analytic solution of a single wire in a uniform field, which is less accurate an approximation when the turns are tightly packed together. This is a limitation inherent to the SA approach.

In conclusion, it is seen that up to 25 KHz, the structured sleeve case remains under 5% relative error in almost every case, which is a strong indicative that the method works well. If one is to obtain a higher accuracy, a computationally prohibitive finer mesh is then needed. Quantitatively, the proposed method also enables the a decrease of the problem size by between 40% and 99% in all cases, which means that large multi-turn coils may be computed efficiently and with a decent level of accuracy at low cost.



Main Achievements and Conclusions

The presented semi-analytical technique allows a considerable reduction of the problem size with a moderate loss of accuracy in many cases. The correct impedance of the thin wire can be restored from an FE solution obtained with idealized thin conductors of vanishing radii, using a correction based on analytical solutions. The technique also works with bundles of thin wires and coils, the effect on each other of neighbouring thin wires being properly taken into account with another analytical solution.

The semi-analytical approach relies the resolution of an local auxiliary FE problem on a region called sleeve around the thin wire. Two types of sleeves have been studied: structured and unstructured. Structured sleeves are defined in the CAD of the problem as symmetrical circular regions around the thin wires, whereas unstructured sleeves are sets of finite elements adjacent to the thin wire. Unstructured sleeves are less symmetrical and their approximated radius is assumed to be the prescribed characteristic length of the elements adjacent to the wire.

Overall, we observe that the size of the problem using the semi-analytical method (SA) presents a significant decrease of around 99% in comparison to the size of the fully discretized model (FM). In terms of accuracy, the method works best using structured sleeves. The accuracy using structured sleeves can be kept under 5% as long as the inter-turn or distance between conductors is of at least 3 radii for a broad range of frequencies (1Hz to 1MHz). In both cases, with structured and unstructured sleeves, the error increases rapidly when the conductors are in close proximity. However, it is important to note that the values still remain of the same order of magnitude as the one given by the expensive fully discretized model, which makes the SA method a powerful tool for quick prototyping and testing.

Future Work

The semi-analytical technique is a rather general technique. Besides the development presented in this dissertation, several very useful extensions can be considered in the future.

1. *Extension to account for capacitive effects*

The SA technique can be expanded to the full-wave Maxwell case in order to also account for capacitive effects in thin wires. In practice, it is enough for that to use for the correction step of the SA approach the solution of the full wave problem with a single wire, instead of the analytical solution of the magnetodynamics problem. The solution of the full wave problem could be analytic in simple cases, or obtained with a 1D discretization, based on the line regions LR_i of the model, of the telegraphers equation.

2. *Non circular wire cross sections*

This technique works has proven accurate for straight conductors and multi-turn wires with circular cross sections. The method can be applied to other cross-sectional shapes (e.g., rectangular, coaxial, twisted cables . . .) on condition that the required analytical solutions can be developed for such cross sections.

3. *Extension to 3D*

The semi-analytical (SA) technique has been demonstrated here in the 2D case only. However, the road to an extension to 3D is already partially paved, since many formulations and theoretical developments presented in this dissertation are also valid in 3D.

4. *Development of excitation ports*

The development of a port-type or source condition for the excitation of thin wires is advantageous, as the inductance values would not be affected by the size of the non-conducting domain surrounding it.



Bibliography

- [1] Beat Aebischer Hubert A. and Aebischer. “The GMD Method for Inductance Calculation Applied to Conductors with Skin Effect”. In: *Advanced Electromagnetics* 6.2 (2017), pp. 77–92.
- [2] Hubert A Aebischer and H Friedli. “Analytical approximation for the inductance of circularly cylindrical two-wire transmission lines with proximity effect”. In: *Advanced Electromagnetics* 7.1 (2018), pp. 25–34.
- [3] Raffaele Albanese and Guglielmo Rubinacci. “Integral formulation for 3D eddy-current computation using edge elements”. In: *IEE Proceedings A (Physical Science, Measurement and Instrumentation, Management and Education, Reviews)* 135.7 (1988), pp. 457–462.
- [4] Ferdinando Alessandri et al. “Conductor loss computation in multiconductor MIC’s by transverse resonance technique and modified perturbational method”. In: *IEEE microwave and guided wave letters* 2.6 (1992), pp. 250–252.
- [5] Yazid Alkraimeen and Pablo Gomez. “On the Computation of Frequency-Dependent Core and Proximity Effects for Transient Analysis of Transformer Windings”. In: *IEEE Transactions on Power Delivery* 34.3 (2019), pp. 891–898.
- [6] P.R. Amestoy et al. “A Fully Asynchronous Multifrontal Solver Using Distributed Dynamic Scheduling”. In: *SIAM Journal on Matrix Analysis and Applications* 23.1 (2001), pp. 15–41.
- [7] Steve Van den Berghe, Frank Olyslager, and Daniel De Zutter. “Accurate modeling of thin conducting layers in FDTD”. In: *IEEE Microwave and Guided Wave Letters* 8.2 (1998), pp. 75–77.
- [8] Oszkár Biro and Kurt Preis. “Finite element analysis of 3-D eddy currents”. In: *IEEE Transactions on Magnetics* 26.2 (1990), pp. 418–423.

- [9] Oszkár Biro, Kurt Preis, and Kurt R. Richter. “On the use of the magnetic vector potential in the nodal and edge finite element analysis of 3D magnetostatic problems”. In: *IEEE Transactions on Magnetics* 32.3 (1996), pp. 651–654.
- [10] Alain Bossavit. *Computational electromagnetism: variational formulations, complementarity, edge elements*. Academic Press, 1998.
- [11] Alain Bossavit. “Effective, frequency-dependent, permeability of “split-ring” metamaterials via homogenization”. In: *IEEE transactions on magnetics* 45.3 (2009), pp. 1276–1279.
- [12] Alain Bossavit. “Effective penetration depth in spatially periodic grids: a novel approach to homogenization”. In: *International Symposium on Electromagnetic Compatibility*. 1994, pp. 13–16.
- [13] Alain Bossavit. “Homogenizing spatially periodic materials with respect to Maxwell equations: Chiral materials by mixing simple ones”. In: *Non Linear Electromagnetic Systems*. IOS Press, 1996, pp. 564–567.
- [14] Alain Bossavit, Georges Griso, and Bernadette Miara. “Modelling of periodic electromagnetic structures bianisotropic materials with memory effects”. In: *Journal de mathématiques pures et appliquées* 84.7 (2005), pp. 819–850.
- [15] David Keun Cheng et al. *Field and wave electromagnetics*. Pearson Education India, 1989.
- [16] John Douglas Cockcroft. “Skin effect in rectangular conductors at high frequencies”. In: *Proceedings of the Royal Society of London. Series A, Containing Papers of a Mathematical and Physical Character* 122.790 (1929), pp. 533–542.
- [17] Didier Cottet et al. “EM simulation of planar bus bars in multi-level power converters”. In: *International Symposium on Electromagnetic Compatibility-EMC EUROPE*. IEEE. 2012, pp. 1–6.
- [18] Bernard Dennis Cullity and Chad D Graham. *Introduction to magnetic materials*. John Wiley & Sons, 2011.
- [19] RB Dingle. “The electrical conductivity of thin wires”. In: *Proceedings of the Royal Society of London. Series A. Mathematical and Physical Sciences* 201.1067 (1950), pp. 545–560.
- [20] PL Dowell. “Effects of eddy currents in transformer windings”. In: *Proceedings of the Institution of Electrical Engineers*. Vol. 113. 8. IET. 1966, pp. 1387–1394.
- [21] Patrick Dular and Christophe Geuzaine. “Modeling of thin insulating layers with dual 3-D magnetodynamic formulations”. In: *IEEE Transactions on magnetics* 39.3 (2003), pp. 1139–1142.
- [22] Patrick Dular, Christophe Geuzaine, and Willy Legros. “A natural method for coupling magnetodynamic h-formulations and circuit equations”. In: *IEEE transactions on magnetics* 35.3 (1999), pp. 1626–1629.

- [23] Patrick Dular, François Henrotte, and Willy Legros. “A general and natural method to define circuit relations associated with magnetic vector potential formulations”. In: *IEEE transactions on magnetics* 35.3 (1999), pp. 1630–1633.
- [24] Patrick Dular et al. “A discrete sequence associated with mixed finite elements and its gauge condition for vector potentials”. In: *IEEE Transactions on Magnetics* 31.3 (1995), pp. 1356–1359.
- [25] Patrick Dular et al. “A general environment for the treatment of discrete problems and its application to the finite element method”. In: *IEEE Transactions on Magnetics* 34.5 (Sept. 1998), pp. 3395–3398.
- [26] Patrick Dular et al. “Correction of thin shell finite element magnetic models via a subproblem method”. In: *IEEE transactions on magnetics* 47.5 (2011), pp. 1158–1161.
- [27] Patrick Dular et al. “Dual magnetodynamic formulations and their source fields associated with massive and stranded inductors”. In: *IEEE Transactions on Magnetics* 36.4 (2000), pp. 1293–1299.
- [28] Fredrik Edelvik. “A new technique for accurate and stable modeling of arbitrarily oriented thin wires in the FDTD method”. In: *IEEE transactions on electromagnetic compatibility* 45.2 (2003), pp. 416–423.
- [29] Fredrik Edelvik et al. “An unconditionally stable subcell model for arbitrarily oriented thin wires in the FETD method”. In: *IEEE Transactions on Antennas and Propagation* 51.8 (2003), pp. 1797–1805.
- [30] M El Feddi et al. “Homogenization technique for Maxwell equations in periodic structures”. In: *IEEE Transactions on magnetics* 33.2 (1997), pp. 1382–1385.
- [31] C Emson and J Simkin. “An optimal method for 3-D eddy currents”. In: *IEEE Transactions on Magnetics* 19.6 (1983), pp. 2450–2452.
- [32] Goran Eriksson. “Efficient 3D simulation of thin conducting layers of arbitrary thickness”. In: *2007 IEEE International Symposium on Electromagnetic Compatibility*. IEEE. 2007, pp. 1–6.
- [33] T. Fawzi, M. Ahmed, and P. Burke. “On the use of the impedance boundary conditions in eddy current problems”. In: *IEEE Transactions on Magnetics* 21.5 (1985), pp. 1835–1840.
- [34] Dieter Gerling. “Approximate analytical calculation of the skin effect in rectangular wires”. In: *2009 International Conference on Electrical Machines and Systems*. IEEE. 2009, pp. 1–6.
- [35] Christophe Geuzaine. “High order hybrid finite element schemes for Maxwell’s equations taking thin structures and global quantities into account”. PhD thesis. 2001.

- [36] Christophe Geuzaine, Patrick Dular, and Willy Legros. “Dual formulations for the modeling of thin conducting magnetic shells”. In: *COMPEL-The international journal for computation and mathematics in electrical and electronic engineering* (1999).
- [37] Christophe Geuzaine, Patrick Dular, and Willy Legros. “Dual formulations for the modeling of thin electromagnetic shells using edge elements”. In: *IEEE transactions on Magnetics* 36.4 (2000), pp. 799–803.
- [38] Christophe Geuzaine and Jean-François Remacle. “Gmsh: A 3-D finite element mesh generator with built-in pre-and post-processing facilities”. In: *International journal for numerical methods in engineering* 79.11 (2009), pp. 1309–1331.
- [39] Gene H Golub and Charles F Van Loan. “Matrix Computations Johns Hopkins University Press”. In: *Baltimore and London* (1996).
- [40] Frederick W Grover. *Inductance calculations: working formulas and tables*. Courier Corporation, 2004.
- [41] Christophe Guérin et al. “A shell element for computing 3D eddy currents-application to transformers”. In: *IEEE Transactions on Magnetics* 31.3 (1995), pp. 1360–1363.
- [42] Johan Gyselinck and Patrick Dular. “Frequency-domain homogenization of bundles of wires in 2-D magnetodynamic FE calculations”. In: *IEEE transactions on magnetics* 41.5 (2005), pp. 1416–1419.
- [43] Johan Gyselinck, RV Sabariego, and Patrick Dular. “Time-domain homogenization of windings in 2-D finite element models”. In: *IEEE transactions on magnetics* 43.4 (2007), pp. 1297–1300.
- [44] Johan Gyselinck et al. “Time-domain finite-element modeling of thin electromagnetic shells”. In: *IEEE transactions on magnetics* 44.6 (2008), pp. 742–745.
- [45] R Horton, B Easter, and A Gopinath. “Variation of microstrip losses with thickness of strip”. In: *Electronics Letters* 7.17 (1971), pp. 490–491.
- [46] Hajime Igarashi. “Semi-analytical approach for finite-element analysis of multi-turn coil considering skin and proximity effects”. In: *IEEE Transactions on Magnetics* 53.1 (2016), pp. 1–7.
- [47] John David Jackson. *Classical electrodynamics*. 1999.
- [48] RH Jansen. “An efficient bessel function approximation for cylindrical skin effect and lossy wave problems”. In: *Archiv für Elektrotechnik* 64.1-2 (1981), pp. 97–100.
- [49] Jian-Ming Jin and Douglas J Riley. *Finite element analysis of antennas and arrays*. John Wiley & Sons, 2008.
- [50] Edward C Jordan and Keith G Balmain. “Electromagnetic waves and radiating systems”. In: (1968).

- [51] Laurent Krahenbuhl and Daniel Muller. “Thin layers in electrical engineering-example of shell models in analysing eddy-currents by boundary and finite element methods”. In: *IEEE Transactions on Magnetics* 29.2 (1993), pp. 1450–1455.
- [52] Tung Le-Duc et al. “A new integral formulation for eddy current computation in thin conductive shells”. In: *IEEE transactions on magnetics* 48.2 (2012), pp. 427–430.
- [53] Antti Lehtikoinen and Antero Arkkio. “Efficient finite-element computation of circulating currents in thin parallel strands”. In: *IEEE Transactions on Magnetics* 52.3 (2015), pp. 1–4.
- [54] Antti Lehtikoinen et al. “Domain decomposition approach for efficient time-domain finite-element computation of winding losses in electrical machines”. In: *IEEE Transactions on Magnetics* 53.5 (2017), pp. 1–9.
- [55] Antti Lehtikoinen et al. “Monte Carlo analysis of circulating currents in random-wound electrical machines”. In: *IEEE Transactions on Magnetics* 52.8 (2016), pp. 1–12.
- [56] Philip C Magnusson et al. *Transmission lines and wave propagation*. CRC press, 2000.
- [57] Isaak D Mayergoyz and Gary Bedrosian. “On calculation of 3-D eddy currents in conducting and magnetic shells”. In: *IEEE transactions on magnetics* 31.3 (1995), pp. 1319–1324.
- [58] Gérard Meunier. *The finite element method for electromagnetic modeling*. Vol. 33. John Wiley & Sons, 2010.
- [59] Gérard Meunier et al. “Homogenization for periodical electromagnetic structure: Which formulation?” In: *IEEE transactions on magnetics* 46.8 (2010), pp. 3409–3412.
- [60] Peter Monk et al. *Finite element methods for Maxwell’s equations*. Oxford University Press, 2003.
- [61] Olivier Moreau, L Popiel, and J L Pages. “Proximity losses computation with a 2D complex permeability modelling”. In: *IEEE Transactions on Magnetics* 34.5 (1998), pp. 3616–3619.
- [62] James R Nagel. “Induced Eddy Currents in Simple Conductive Geometries: Mathematical Formalism Describes the Excitation of Electrical Eddy Currents in a Time-Varying Magnetic Field”. In: *IEEE Antennas and Propagation Magazine* 60.1 (2018), pp. 81–88.
- [63] Takayoshi Nakata et al. “3D magnetic field analysis using special elements”. In: *IEEE Transactions on Magnetics* 26.5 (1990), pp. 2379–2381.
- [64] Xi Nan and Charles R Sullivan. “An improved calculation of proximity-effect loss in high-frequency windings of round conductors”. In: *IEEE 34th Annual Conference on Power Electronics Specialist, 2003. PESC’03*. Vol. 2. IEEE, 2003, pp. 853–860.

- [65] Taku Noda and Shigeru Yokoyama. “Thin wire representation in finite difference time domain surge simulation”. In: *IEEE Transactions on Power Delivery* 17.3 (2002), pp. 840–847.
- [66] Carlo Alberto Nucci and Farhad Rachidi. “On the contribution of the electromagnetic field components in field-to-transmission line interaction”. In: *IEEE Transactions on Electromagnetic Compatibility* 37.4 (1995), pp. 505–508.
- [67] Carlo Alberto Nucci, Farhad Rachidi, and Marcos Rubinstein. “Derivation of telegrapher’s equations and field-to-transmission line interaction”. In: *Electromagnetic Field Interaction with Transmission Lines: From Classical Theory to HF Radiation Effects* 5 (2008), p. 3.
- [68] Robert C O’handley. *Modern magnetic materials: principles and applications*. Wiley, 2000.
- [69] Vlado Ostović. “The Art and Science of Rotating Field Machines Design”. In: (2017).
- [70] O Ouchetto et al. “Homogenization of structured electromagnetic materials and metamaterials”. In: *Journal of materials processing technology* 181.1-3 (2007), pp. 225–229.
- [71] Ouail Ouchetto et al. “Modeling of 3-D periodic multiphase composites by homogenization”. In: *IEEE transactions on microwave theory and techniques* 54.6 (2006), pp. 2615–2619.
- [72] Alan Payne. *Skin effect, proximity effect and the resistance of circular and rectangular conductors*.
- [73] J Pleite et al. “Obtaining a frequency-dependent and distributed-effects model of magnetic components from actual measurements”. In: *IEEE transactions on magnetics* 35.6 (1999), pp. 4490–4502.
- [74] Alexander D Podoltsev, Irina N Kucheryavaya, and Boris B Lebedev. “Analysis of effective resistance and eddy-current losses in multiturn winding of high-frequency magnetic components”. In: *IEEE Transactions on Magnetics* 39.1 (2003), pp. 539–548.
- [75] Ruth V Sabariego, Patrick Dular, and Johan Gyselinck. “Time-domain homogenization of windings in 3-D finite element models”. In: *IEEE transactions on magnetics* 44.6 (2008), pp. 1302–1305.
- [76] Harold Lockwood Seneff. “Study of the method of geometric mean distances used in inductance calculations”. In: (1947).
- [77] Nicola A Spaldin. *Magnetic materials: fundamentals and applications*. Cambridge university press, 2010.
- [78] Dmitro Trushakov, Serhiy Rendzinyak, and Ivanna Vasylchyshyn. “Determining of complex magnetic permeability of the ferromagnetic material by complex impedance of inductance coil with ferromagnetic core”. In: (2013).

- [79] Koradar Umashankar, Allen Taflove, and Benjamin Beker. “Calculation and experimental validation of induced currents on coupled wires in an arbitrary shaped cavity”. In: *IEEE Transactions on Antennas and Propagation* 35.11 (1987), pp. 1248–1257.
- [80] Janne Väänänen. “Combination of power electronic models with the two-dimensional finite element analysis of electrical machines”. In: *NASA STI/Recon Technical Report N 95* (1994).
- [81] Jonathan Velasco, François Henrotte, and Christophe Geuzaine. “Finite-Element Modeling of Multi-turn Coils Using a Thin Wire Approximation”. In: *In Progress* (2021).
- [82] Jonathan Velasco, François Henrotte, and Christophe Geuzaine. “Finite-Element Modeling of Thin Conductors in Frequency Domain”. In: *IEEE Transactions on Magnetics* 56.4 (2020), pp. 1–4.
- [83] Jiri Vlach and Kishore Singhal. *Computer methods for circuit analysis and design*. Springer Science & Business Media, 1983.
- [84] Hao Wang et al. “Impedance boundary conditions in a hybrid FEM/MOM formulation”. In: *IEEE transactions on electromagnetic compatibility* 45.2 (2003), pp. 198–206.
- [85] Erich Peter Wohlfarth. *Handbook of magnetic materials*. Vol. 2. Elsevier, 1986.
- [86] Hong Wu and Andreas C Cangellaris. “Efficient finite element electromagnetic modeling of thin wires”. In: *Microwave and Optical Technology Letters* 50.2 (2008), pp. 350–354.

